

**HIGH PERFORMANCE DISULFONATED
POLY(ARYLENE SULFONE) CO- AND TERPOLYMERS
FOR PROTON EXCHANGE MEMBRANES FOR FUEL
CELL AND TRANSDUCER APPLICATIONS: SYNTHESIS,
CHARACTERIZATION AND FABRICATION OF ION
CONDUCTING MEMBRANES**

by

Kenton Broyhill Wiles

Dissertation Submitted to the Faculty of the
Virginia Polytechnic Institute and State University
in partial fulfillment of the requirements for the degree of
Doctor of Philosophy
in
Macromolecular Science and Engineering

APPROVED:

Dr. James E. McGrath, Chairman

Dr. Garth L. Wilkes

Dr. Judy S. Riffle

Dr. Timothy E. Long

Dr. Donald G. Baird

April 15, 2005

Blacksburg, Virginia

Keywords: Fuel Cell, Proton Exchange Membrane, Transducer

Copyright 2005, Kenton B. Wiles

HIGH PERFORMANCE DISULFONATED POLY(ARYLENE SULFONE) CO- AND TERPOLYMERS FOR PROTON EXCHANGE MEMBRANES FOR FUEL CELL AND TRANSDUCER APPLICATIONS: SYNTHESIS, CHARACTERIZATION AND FABRICATION OF ION CONDUCTING MEMBRANES

Kenton B. Wiles

ABSTRACT

The results described in this dissertation have demonstrated several alternative proton exchange membranes (PEM) for hydrogen-air and direct methanol fuel cells (DMFC) that perform as well or better than the state of the art Nafion perfluorosulfonic acid membrane. Direct aromatic nucleophilic substitution polycondensations of disodium 3,3'-disulfonate-4,4'-difluorodiphenylsulfone (SDFDPS), 4,4'-difluorodiphenylsulfone (DFDPS) (or their chlorinated analogs, SDCDPS, DCDPS) and 4,4'-thiobisbenzenethiol (TBBT) in the presence of potassium carbonate were investigated. Electrophilic aromatic substitution was employed to synthesize the SDFDPS or SDCDPS comonomers in high yields and purity. High molecular weight disulfonated poly(arylene thioether sulfone) (PATS) copolymers were easily obtained using the SDFDPS monomers, but in general, slower rates and a lower molecular weight copolymer was obtained using the analogous chlorinated monomers. Tough and ductile membranes were solution cast from N,N-dimethylacetamide for both series of copolymers. The degrees of disulfonation (20-50%, PATS 20-50) were controlled by varying the ratio of disulfonated to unsulfonated comonomers. Composite membranes were prepared by homogeneous solution blending the copolymers with phosphotungstic acid (PTA) in dimethylacetamide (DMAc). The composite PATS membranes exhibited moderate PTA molecule water extraction after acidification treatments performed at either room or boiling temperatures. The membranes containing HPA showed improved conductivity at high temperatures (120 °C) and low relative humidities when compared to the pure copolymers.

Molecular weight of the copolymers plays a critical role in the overall copolymer physical behavior. It is well known that molecular weight has an enormous impact on practically all of the physical properties of polymeric systems. This dissertation discusses the influence of molecular weight on the characteristics of a specific family of PEM PATS copolymers. This study elucidated that the lower molecular weight materials did indeed behave differently than the higher molecular weight copolymers. Specifically, the water uptake and permeability to methanol decreased with increasing molecular weight. Furthermore, the fully hydrated mechanical properties also improved with molecular weight.

The synthesis and fabrication of 45 mole percent disulfonated poly(arylene ether phenyl phosphine oxide diphenyl sulfone) terpolymer-heteropolyacid (HPA) composite membranes and membrane electrode assemblies were chosen for detailed investigation. A series of 45 mole percent disulfonated biphenol-based poly(arylene ether phenyl

phosphine oxide diphenyl sulfone) terpolymers (BPSH45-PPO) were also synthesized by nucleophilic aromatic substitution polymerizations. The level of disulfonation was constant at 45 mole percent providing a compromise between high conductivity at low humidity and reasonable mechanical properties in liquid water. The amounts of 4,4'-difluorodiphenyl phenyl phosphine oxide comonomer incorporated into the terpolymer backbone were precisely controlled from 0-50 mole percent relative to the 4,4'-dihalodiphenyl sulfone. Phosphine oxide moieties were employed to enhance the interactions with the PTA relative to the pure copolymer. The composite BPSH45-PPO membranes exhibited lower HPA molecule water extraction after acidification at room and boiling temperatures, which was ascribed to the strong hydrogen and polar interactions between the phosphine oxide moiety and functional groups on the HPA. The membranes containing HPA displayed improved conductivity at high temperatures and low relative humidities when compared to the pure terpolymer samples. The increase of proton conductivity was attributed to the water retention characteristics of the HPA molecules, which allowed enhanced mobility of the protons even at lower humidification levels, providing superior hydrogen-air fuel cell performance.

The effect of hexafluoroisopropylidene bisphenol (6FBP) incorporation into 45 mole percent disulfonated poly(arylene ether sulfone) copolymers was investigated. This novel series of directly disulfonated poly(arylene ether sulfone) copolymers with various mole ratios of the 6FBP were synthesized in high molecular weight. The levels of fluorination within the statistically random copolymer architecture were varied from 0-100 mole percent using 6FBP and the correct stoichiometric amount of 4,4'-biphenol. The 6FBP monomer was introduced to decrease the water swelling and improve bonding characteristics with Nafion-bonded electrodes. Indeed, water uptake decreased with increasing incorporation of the 6FBP monomer into the terpolymer. This suggested that the hydrophobic fluorinated material aided in water repulsion of the system. Proton conductivity decreased slightly as the amount of fluorination increased, which was interpreted to be due to the decrease in the ion-exchange capacity. High temperature hydrogen/air fuel cell experiments indicated better Nafion-bonded electrode adhesion for the partially fluorinated materials, as depicted by high temperature (120 °C) and low humidity (50% RH) hydrogen-air fuel cell performance.

Investigations into polymeric electromechanical transducers were based on poly(arylene sulfone) ion-exchange membranes bonded between two conductive metal layer electrodes. Imposed deformations and small electric fields allowed similar explorations of both sensing and actuation applications. These copolymers produced larger sensitivities than the benchmark Nafion systems, which was interpreted as being due to their higher hydrated moduli. Methodologies for better defining the morphology of the electrodes were identified to enhance the capacitance and effective interfacial area of the conductive electrodes. The new procedures afforded major improvements to performance and transduction. Transducer actuation at lower frequencies was improved by employing a new direct assembly electrode fabrication technique that suggested a strong correlation between the capacitance and charge motion.

Acknowledgements

I would like to express my gratitude to my principle advisor, Professor Jim McGrath, for his encouragement, support and guidance throughout my graduate career. His teachings and expertise have allowed me to grow as a person and a professional. I am grateful for all the years that I have shared with him.

I would also like to extend my thanks to the rest of my advisory committee, Dr. J. S. Riffle, Dr. Garth L. Wilkes, Dr. Tim E. Long, Dr. Don G. Baird and the late Dr. Allan R. Shultz, for their helpful suggestions and technical guidance. This committee has provided me with a broad knowledge of both synthetic polymer chemistry and engineering.

I send my thanks to Sandia National Labs and United Technology Corporation Fuel Cells for the time they spent with me during my internships. My knowledge of fuel cell testing and membrane electrode fabrication and electrochemical testing has grown due to the assistance of Dr. Mike Hickner and Dr. Andrew Haug. Thank you.

My comprehension of electromechanical transducers for actuators and sensor applications has been realized thanks to the assistance of Professor Don Leo and his students Barbar Akle and Matt Bennett. I am grateful for the times, knowledge and insight that you have shared with me.

I would like to express a special thanks to my wife, Natasha, for all of her moral support throughout both of our graduate careers. Natasha had her own set of obstacles as she was writing her dissertation for a Ph. D. in Biology. I thank her for making the many hours it took to prepare this work for publication all the better as she sat across from me during this unique time in our life. I could not have succeeded without her love and understanding.

This doctorate degree began many years ago with my family, Don, Jeanette, Brad, Greg, Megan, Garrett, Grace, Thelma and Ray. I thank my parents, Don and Jeanette, for all the headaches that they endured raising me and my two brothers. Mom and Dad, you have taught me more than anyone else in my life. Thank you. My brothers, Brad and Greg, have supported me throughout all of my decisions and my life is better for it. Thank you.

Table of Contents

CHAPTER 1 Introduction	1
CHAPTER 2 Literature Review.....	8
2.1 Introduction to Ion Containing Polymers.....	8
2.2 Structure and Ionic Association.....	13
2.3 Properties and Application of Ionomers.....	19
2.4 Fuel Cells.....	23
2.5 General Processes and Functionality of Fuel Cells.....	24
2.6 Types of Fuel Cells for Electricity Production.....	40
2.7 Protonically Conductive Ion Exchange Membranes.....	48
2.8 Post-Sulfonation of Polymeric Membranes.....	48
2.9 Post-Sulfonation of Poly(arylene ether)s.....	49
2.10 Post-Sulfonation of Poly(arylene ether ketone)s.....	52
2.11 Post-Sulfonated Polystyrene.....	54
2.12 Various Polyperfluorinated Copolymers.....	56
2.13 Other Commercially Available Proton Exchange Membranes.....	60
2.14 Novel Research on Proton Exchange Membranes.....	62
2.15 Direct Polymerization of Sulfonated Monomers Via Step-Growth Techniques.....	63
2.16 Directly Polymerized Disulfonated Polyimide Copolymers.....	69
2.17 Synthesis of Disulfonated Poly(arylene ether sulfone) Copolymers Via Disulfonated Monomers.....	74
2.18 Synthesis of Disulfonated Poly(arylene ether ketone) Copolymers Via Disulfonated Monomers.....	77
2.19 Synthesis of Disulfonated Poly(arylene ether phosphine oxide) Copolymers Via Disulfonated Monomers.....	78
2.20 Synthesis of Disulfonated Poly(arylene thioether sulfone) Copolymers Via Disulfonated Monomers.....	83
2.21 Composite Membranes Based on Blends and Nanocomposites.....	88

2.22	Organic/Inorganic Composite Membranes.....	90
2.23	Poly(arylene sulfide sulfone), Poly(arylene ether phosphine oxide) and Poly(arylene ether sulfone) Synthesis.....	95
2.24	Electrophilic Aromatic Substitution Polymerization Via Friedel-Crafts Reactions.....	95
2.25	The Ullman Reaction for Synthesis of Poly(arylene ether)s and Poly(arylene thioether)s.....	97
2.26	Metal Coupling Polymerizations.....	98
2.27	Nucleophilic Aromatic Substitution Polymerizations.....	100
2.28	Polymeric Transducers Based on Ion-Exchange Membrane Electrode Assemblies.....	108
2.29	Understanding ‘Smart Materials’.....	110
2.30	Creating Capacitance Through The Electric Double Layer.....	115

CHAPTER 3 Directly Copolymerized Poly(arylene sulfide sulfone)

	Disulfonated Copolymers for PEM-Based Fuel Cell Systems: Synthesis and Characterization.....	123
3.1	Introduction.....	125
3.2	Experimental.....	129
3.2.1	Materials.....	129
3.2.2	Synthesis of the 3,3'-disulfonated 4,4'-difluorodiphenyl sulfone and 3,3'-disulfonated 4,4'-dichlorodiphenyl sulfone monomers.....	130
3.2.3	Synthesis of the Dithiol Sulfone Monomer.....	131
3.2.4	Synthesis of the Poly(arylene thioether sulfone) Copolymers....	131
3.2.5	Membrane Preparation.....	132
3.2.6	Acidification.....	132
3.2.7	Characterization.....	134
3.3	Results and Discussion.....	136
3.3.1	Disulfonated monomer synthesis.....	138
3.3.2	Proton NMR and elemental analysis of disulfonated monomer..	139

3.3.3	Synthesis of disulfonated poly(arylene thioether sulfone) copolymers.....	140
3.3.4	Acidification of salt form copolymers.....	141
3.3.5	Characterization of the disulfonated copolymers.....	143
3.3.6	Conclusions.....	151

CHAPTER 4 Directly Copolymerized Poly(arylene sulfide sulfone) Disulfonated Copolymers for PEM-Based Fuel Cell Systems: Effect of Molecular Weight on Transport and Mechanical Properties.....153

4.1	Introduction.....	153
4.2	Experimental.....	159
4.2.1	Materials.....	159
4.2.2	Membrane Preparation.....	160
4.2.3	Acidification.....	160
4.2.4	Characterization of Molecular Weight.....	161
4.2.5	Hydrated Dynamic Tensile Modulus.....	161
4.2.6	Water Uptake.....	162
4.2.7	Ion Exchange Capacity and Lambda Value.....	162
4.2.8	Proton Conductivity.....	163
4.2.9	Methanol Permeability.....	164
4.2.10	Relative Selectivity.....	167
4.3	Results and Discussion.....	168
4.4	Conclusions.....	177

CHAPTER 5 Directly Copolymerized Poly(arylene sulfide sulfone) Disulfonated Copolymers for PEM-Based Fuel Cell Systems: Fabrication and Characterization of Heteropolyacid Composite Films for High Temperature Applications.....180

5.1	Introduction.....	182
5.2	Experimental.....	187

5.2.1	Disulfonated copolymer synthesis.....	187
5.2.2	Membrane Preparation.....	188
5.2.3	Composite Membrane Fabrication.....	189
5.2.4	Acidification and HPA Extraction of Composite Membranes...	190
5.2.5	Fourier Transform Infrared Spectroscopy (FTIR).....	190
5.2.6	Morphology Using Transmission Electron Microscopy (TEM)..	191
5.2.7	Thermogravimetric Analysis of Neat & Composite Membranes	191
5.2.8	Water Uptake.....	192
5.2.9	Oxidation of Sulfide Moieties to Aid HPA Retention.....	193
5.2.10	Intrinsic Viscosity (IV) Measurements.....	193
5.2.11	Ion Exchange Capacity.....	193
5.2.12	Proton Conductivity at Low and High Temperatures and Humidities.....	194
5.2.13	Hydrogen/Air Fuel Cell Performance.....	195
5.3	Results and Discussion.....	196
5.3.1	Specific Interactions of PTA with PATS Copolymers.....	196
5.3.2	Dehydration of PATS 30 and PATS 30 + 30 wt% PTA Using FTIR.....	201
5.3.3	PTA Dispersion and Morphology of Composite Membranes Using Transmission Electron Microscopy (TEM).....	203
5.3.4	Thermogravimetric Analysis of Composite Membrane, PATS 30 and PATS 00 Control.....	205
5.3.5	Water Uptake of Neat Copolymer Films and Composite Membranes Using Various Acidification Techniques.....	206
5.3.6	Extraction of the PTA in Composite Membranes.....	207
5.3.7	Proton Conductivity in Liquid Water and at 120 °C in 45% Relative Humidity for Composite Membranes and Pure PATS Copolymers.....	209
5.3.8	Hydrogen Peroxide Oxidation of PATS 30 to Create Sulfoxide Groups to Aid in PTA Retention.....	212

5.3.9	Hydrogen/Air Fuel Cell Performance Using Platinum Loadings of 0.2 mg/cm ²	216
5.4	Conclusions.....	220

CHAPTER 6 Directly Copolymerized Poly(arylene sulfide sulfone) and Poly(arylene ether sulfone) Disulfonated Copolymers for Use in Ionic Polymer Transducers.....		225
6.1	Introduction.....	227
6.2	Experimental.....	231
6.2.1	Copolymer Synthesis.....	231
6.2.2	Membrane Preparation.....	232
6.2.3	Impregnation-Reduction Electrodes.....	233
6.2.4	Direct Electrode Assembly Technique Based on Hot Pressed Decals.....	233
6.2.5	Sample Preparation and Mounting.....	235
6.2.6	Measurements of Electromechanical Activity.....	235
6.2.7	Scanning Electron Microscopy (SEM) of Membrane Electrode Assemblies.....	241
6.3	Results and Discussion.....	242
6.4	Conclusions.....	257

CHAPTER 7 Directly Copolymerized 45 Mole Percent Disulfonated Poly(arylene ether phenyl phosphine oxide sulfone) Terpolymers for PEM Fuel Cell Systems: Synthesis, Fabrication and Characterization of Heteropolyacid Composite Membranes for Higher Temperature Fuel Cell Applications.....		259
7.1	Introduction.....	262
7.2	Experimental.....	273
7.2.1	Materials.....	273

7.2.2	Synthesis of Disulfonated Poly(arylene ether phenyl phosphine oxide sulfone) Terpolymers.....	274
7.2.3	Membrane Preparation.....	275
7.2.4	Composite Membrane Fabrication.....	276
7.2.5	Acidification and HPA Extraction of Composite Membranes...	277
7.2.6	Fourier Transform Infrared Spectroscopy (FTIR) and Proton/Phosphorous Nuclear Magnetic Resonance (NMR).....	277
7.2.7	Water Uptake.....	278
7.2.8	Intrinsic Viscosity (IV) Measurements.....	278
7.2.9	Gel Permeation Chromatography (GPC).....	279
7.2.10	Ion Conductivity at High Temperatures and Low Humidities...	279
7.2.11	Hydrogen/Air Fuel Cell Performance.....	280
7.3	Results and Discussion.....	281
7.3.1	Synthesis and Characterization of Phosphine Oxide Containing Terpolymers.....	281
7.3.2	Monitoring Polymerizations Using FTIR and NMR.....	283
7.3.3	Water Uptake of BFPPPO Containing Terpolymers.....	285
7.3.4	Specific Interactions of Phosphine Oxide and Heteropolyacid...	287
7.3.5	Water Uptake of Composite Membranes Using Various Acidification Techniques.....	290
7.3.6	Extraction of the PTA in Composite Membranes.....	292
7.3.7	Proton Conductivity at 120 °C in 45% Relative Humidity.....	294
7.3.8	Hydrogen/Air Fuel Cell Performance.....	295
7.4	Conclusions.....	301

CHAPTER 8 Directly Copolymerized 45 Mole Percent Partially Fluorinated Disulfonated Poly(arylene ether sulfone) Copolymers for PEM Fuel Cell Systems: Synthesis, Fabrication and Characterization of Membranes and Membrane Electrode Assemblies for Fuel Cell Applications.....		305
8.1	Introduction.....	308

8.2	Experimental.....	313
8.2.1	Materials.....	313
8.2.2	Synthesis of 45 Mole Percent Disulfonated Partially Fluorinated Poly(arylene ether sulfone) Co- and Terpolymers.....	313
8.2.3	Membrane Preparation.....	315
8.2.4	Characterization.....	315
8.2.5	Hydrogen/Air Fuel Cell Performance.....	317
8.3	Results and Discussion.....	319
8.3.1	Synthesis and Characterization of Partially Fluorinated 45 Mole Percent Co- and Terpolymers.....	319
8.3.2	X-Ray Photoelectron Spectroscopy (XPS) Surface Analysis of 6FBP Containing Polymers.....	323
8.3.3	Percent Water Uptake of Salt and Acid Form Membranes as a Function of Fluorine Content.....	324
8.3.4	Proton Conductivity at Room Temperature and 80 °C in Liquid Water.....	327
8.3.5	Hydrogen/Air Fuel Cell Performance as Measured by Polarization Curves and High Frequency Resistances.....	328
8.4	Conclusions.....	331
	CHAPTER 9 Overall Conclusions.....	333
	VITAE.....	337

List of Figures

Figure 1.1 Wholly aromatic random (statistical) poly(arylene) / poly(arylene disulfonated) copolymers via direct copolymerization.....	3
Figure 1.2 Copolymerization of TBBT with DCDPS and SDCDPS.....	4
Figure 2.1 Grotthuss Proton Hopping Mechanism.....	9
Figure 2.2 Chemical Structure of Ethylene-Propylene-Diene Rubber.....	12
Figure 2.3. Possible Structures of Ionomers.....	14
Figure 2.4. Possible random and comb structures of ionomers.....	14
Figure 2.5 EHM model of the area of restricted mobility of ionomeric material.....	17
Figure 2.6 Possible structure of ion channels.....	19
Figure 2.7. Hydrogen fuel cell general processes.....	25
Figure 2.8 William R. Grove (1811-1896) demonstrated in 1839 that electricity can be generated from hydrogen and oxygen in contact with platinum strips, which extend into dilute sulfuric acid functioning as a diaphragm.....	26
Figure 2.9 Membrane electrode assembly and electrochemistry for H ₂ /Air and methanol fuel cells.....	34
Figure 2.10 Bipolar plate showing pattern of gas flow channels.....	36
Figure 2.11 Schematic of a fuel cell stack consisting of the bipolar plate and MEA repeat units.....	37
Figure 2.12 Plot of voltage vs. current density of a hydrogen/air PEMFC using Nafion [®]	40
Figure 2.13 Chemical structure of Nafion [®] by DuPont.....	44
Figure 2.14 Post-sulfonation of Udel [®] polyether sulfone using chlorosulfonic acid.....	49
Figure 2.15 Sulfonated styrene-co-ethylene-co-butylene (SEB) post-sulfonated materials.....	55
Figure 2.16 Ballard Advanced Materials, BAM3G, reported chemical structure.....	56
Figure 2.17 Proposed structure of Dow XUS [®] perfluorinated copolymer.....	59

Figure 2.18 Disulfonation of DCDPS monomer for use in step-growth polymerizations.....	65
Figure 2.19 Mechanism for Electrophilic Aromatic Sulfonation.....	66
Figure 2.20 Acid-base reaction followed by titration to measure IEC.....	69
Figure 2.21 Sulfonated diamines used to produce sulfonated polyimides.....	72
Figure 2.22 Polymerization scheme for the synthesis of a BDSA based polyimide.....	73
Figure 2.23 Activated versus deactivated positions of sulfonate moieties	75
Figure 2.24 Typical synthetic procedure for disulfonated poly(ether sulfone) copolymers.....	76
Figure 2.25 Disulfonated poly(arylene ether sulfone) copolymers.....	77
Figure 2.26 Disulfonated ketone monomer used to synthesize poly(ether ketone)s.....	78
Figure 2.27 Chemical structure of 4,4'-bis(fluorophenyl) phenyl phosphine oxide.....	79
Figure 2.28 Mono-sulfonated BFPPO.....	81
Figure 2.29 Bis(4-mercaptophenyl) sulfone.....	84
Figure 2.30 Synthesis of disulfonated poly(arylene thioether sulfone) copolymers.....	85
Figure 2.31 Chemical structure of 4,4'-thiobisbenzenethiol.....	86
Figure 2.32 ¹ H NMR to determine extent of sulfonation.....	87
Figure 2.33 Primary Keggin and secondary hydrated structures of semicrystalline phosphotungstic acid.....	92
Figure 2.34 Friedel-Crafts electrophilic aromatic substitution reaction using a sulfonylium cation.....	96
Figure 2.35 The Ullman reaction to produce poly(arylene ether)s.....	97
Figure 2.36 Synthesis of poly(2,5-substituted benzophenone) using nickel coupling polymerization techniques.....	99
Figure 2.37. Nucleophilic aromatic substitution reaction to form resonance stabilized intermediate and further aromatic products of an activated phenyl ring.....	102

Figure 2.38 Strong base synthesis to produce poly(ether sulfone) based on bisphenol A.....	104
Figure 2.39 Weak base nucleophilic aromatic substitution scheme to synthesize high molecular weight poly(arylene ether)s.....	105
Figure 2.40 Production of water during decomposition of potassium carbonate.....	106
Figure 2.41 Conductive metal electrodes plated on an ion-exchange membrane.....	108
Figure 2.42 Piezo-electric strain occurring by application of electric field.....	112
Figure 2.43 Dielectric elastomer deformation by electrostatic attraction of the electrodes.....	113
Figure 2.44 Helmholtz model indicating the electric double layer present at electrolyte-electrode interface.....	119
Figure 2.45 Gouy-Chapman model indicating concentration gradient of ions in electrolyte.....	120
Figure 2.46 Stern and Grahame model indicating finite sized ions adsorbed and diffuse.....	121
Figure 2.47 Brockris, Devanathan and Muller model employing hydration shells on ions.....	122
Figure 3.1 Repeat unit of a random copolymer that contains hydrophobic repeating sulfide-sulfone moieties and hydrophilic disulfonated units randomly placed along the copolymer backbone.....	127
Figure 3.2 Activated versus deactivated positions of sulfonate moieties due to electron donation of the sulfide linkage and electron withdrawal of the sulfone linkage.....	129
Figure 3.3 Acid-base reaction followed by titration to measure IEC.....	134
Figure 3.4 Schematic and Equation of Conductivity Cell.....	136
Figure 3.5 Synthesis of Bis(4-mercaptophenyl) sulfone.....	137
Figure 3.6 Chemical structure of 4,4'-thiobisbenzenethiol.....	138
Figure 3.7 Disulfonation of DFDPS monomer for use in step-growth polymerizations.....	139

Figure 3.8 ^1H NMR of DFDPS and SFDPS.....	140
Figure 3.9 Copolymerization of TBBT with DCDPS and SDCDPS.....	141
Figure 3.10 ^1H NMR of 40% Disulfonated Copolymer Using Difluorinated Monomers to Calculate Copolymer Composition	143
Figure 3.11 Infrared Spectroscopy Indicating Increasing Incorporation of Sulfonate Moieties.....	146
Figure 3.12 Thermal Gravimetric Analysis of PATS control polymer and PATS 30 Copolymer (10 °C/minute in Air).....	147
Figure 3.13 Tapping mode AFM phase images of (a)Nafion 117, (b) PATS 30, (c) PATS 35 and (d) PATS 40. The scan area for Nafion 117 is 350nm x 350nm and the scan area for all PATS is 1 μm x 1 μm all with a phase scale of 10°.....	148
Figure 3.14 Influence of the disulfonation level on water uptake of acid form poly(arylene thioether sulfone) copolymers based on TBBT, DCDPS and SDCDPS...	150
Figure 3.15 Proton conductivity of disulfonated membranes in water at 30 °C for PATS based on TBBT, DCDPS and SDCDPS.....	151
Figure 4.1 Disulfonated PATS-XX copolymer structure indicating thioether and sulfone linkages.....	160
Figure 4.2 Glass diffusion cell and differential refractometer	165
Figure 4.3. Proton conductance of low MW and high MW acid form PATS membranes immersed in liquid water at room temperature.....	170
Figure 4.4. Water uptake of low MW and high MW acid form PATS membranes.....	170
Figure 4.5 Methanol Permeability Versus Ion-Exchange Capacity of Hydrated PATS Copolymers	174
Figure 4.6 Selectivity of Both Low MW and High MW Series of PATS Copolymers Relative to Nafion [®]	175
Figure 4.7 Hydrated Dynamic Tensile Modulus Versus Ion Exchange Capacity for High and Low MW Series PATS Copolymers.....	176
Figure 5.1 Primary Keggin and Secondary Hydrated Structures of Semicrystalline Phosphotungstic Acid.....	184

Figure 5.2 Synthesis of High Molecular Weight Disulfonated Poly(arylene thioether sulfone) Copolymers.....	188
Figure 5.3 Schematic of Conductivity Measurement Apparatus for use at Elevated Temperature and Reduced Relative Humidity at Atmospheric Pressure.....	195
Figure 5.4 Proposed Specific Interactions Between the Protonated Bridging and Terminal Oxygens on the PTA Molecule and the Sulfonate and Sulfide Moieties on the PATS Copolymer Backbone.....	198
Figure 5.5 Symmetric and Asymmetric Stretching of the SO ₃ Moieties and the Sulfonated Aryl Rings on the PATS Copolymer Backbone.....	199
Figure 5.6 Effect of PTA Incorporation on FTIR Band Shifts of PTA Oxygen Atoms.....	200
Figure 5.7 Dehydration of Pure PATS-30 and PATS-30 + 30 wt% HPA at Increasing Temperatures	202
Figure 5.8 Observed Dispersion of PTA Particles in PATS 20 + 30 wt% PTA and PATS 40 + 30 wt% PTA Composite Membranes.....	204
Figure 5.9 Observed Dynamic Weight Loss of PATS 00, PATS 30 and PATS 30 + 30 wt% PTA.....	206
Figure 5.10 Influence of Disulfonation Degree and Acidification Technique on the pure Copolymers and Composite Membranes.....	207
Figure 5.11 Influence of the Degree of Disulfonation and Reacidification Technique on PTA Extraction of Composite Films Using 30 wt% Filled Materials.....	208
Figure 5.12 Proton Conductivity at 25 °C in Liquid Water at Atmospheric Pressure for M2 Acidified PATS Copolymers and M1 and M2 Acidified Composite Membranes...	210
Figure 5.13 Proton Conductivity at 80 °C in Liquid Water at Atmospheric Pressure for M2 Acidified PATS Copolymers and M1 and M2 Acidified Composite Membranes...	211
Figure 5.14 Proton Conductivity at 120 °C in 45% Relative Humidity at Atmospheric Pressure for M2 Acidified PATS Copolymers and M1 and M2 Acidified Composite Membranes.....	212
Figure 5.15 FTIR Band Shifts Indicating Sulfoxide and Sulfone Formation Along With Sulfide Degradation.....	213
Figure 5.16 FTIR Spectra of Controlled Sulfoxide Formation at Increasing Exposure Times to 3% H ₂ O ₂ in Water.....	214

Figure 5.17 Voltage-Current Performance Curve for PATS 30 and PATS 30 + 30 wt% PTA at 80 °C, 100%RH and 20 psig.....	219
Figure 5.18 Voltage-Current Performance Curve for PATS 30 and PATS 30 + 30 wt% PTA at 120 °C, 50%RH and 20 psig.....	220
Figure 6.1. Conductive Metal Electrodes Plated on an Ion-Exchange Membrane.....	227
Figure 6.2 (a) Disulfonated PATS-XX, (b) Disulfonated BPSH-XX and (c) Nafion 117 Copolymer Structures.....	232
Figure 6.3 Free Displacement Experimental Apparatus	236
Figure 6.4 Blocked Force Experimental Apparatus.....	237
Figure 6.5 Sensing and Modulus Experimental Apparatus.....	239
Figure 6.6 Nafion 117 with Impregnation-Reduction Electrodes at (a)750x and (b)1000x Magnifications.....	246
Figure 6.7 Impregnation-Reduction Electrode with Gold Electroplated Layer.....	246
Figure 6.8 SEM Cross Section Indicating the Direct Assembly Process Electrodes Using Nafion 117 Membranes with Ratios of (a) 4:1 and (b) 2:1 Platinum to Nafion 1100....	247
Figure 6.9 SEM Showing Cross Section of (a) BPS 35 Membrane Hot Pressed with Decals Having 6 layers of RuO ₂ Electrode Ink and (b) Nafion 117 Membrane Hot Pressed with 9 Layers of Electrode Ink Both with Ratios of 2.5:1 RuO ₂ :Nafion.....	248
Figure 6.10 Frequency Versus Normalized μ Strain for Nafion 117, BPSH30, BPSH35, BPSH40, PATS30 and PATS40.....	249
Figure 6.11 Blocked Force Produced Using PATS, BPSH and Nafion Copolymers with Impregnation-Reduction Electrodes.....	251
Figure 6.12 BPSH 35 Copolymers with Novel Electrodes Containing Platinum (Pt) or Ruthenium Dioxide (RuO ₂) in the Proton (H ⁺) and Lithium (Li ⁺) Forms.....	252
Figure 6.13 Capacitance of BPSH35 Using Platinum and Ruthenium Dioxide Metals along with Proton and Lithium Cations.....	253
Figure 6.14 Normalized Strain and Displacement for Nafion 117 and 112 MEAs Using 3 and 6 Layers of RuO ₂ Ink Painted onto Decals and Hot Pressed.....	254

Figure 6.15 Strain (a), Force (b), Capacitance (c) and Modulus (d) Plotted Against Frequency for BPSH35, PATS30 and Nafion 117 Using Impregnation-Reduction and RuO ₂ Based Direct Assembly Electrodes.....	255
Figure 7.1. Chemical Structure of 4,4'-bis(fluorophenyl) phenyl phosphine oxide.....	263
Figure 7.2. Mono-Sulfonated BFPPPO.....	265
Figure 7.3 Primary Keggin and Secondary Hydrated Structures of Semicrystalline Phosphotungstic Acid.....	269
Figure 7.4 Possible Interactions of HPA with Sulfonate and Phosphine Oxide Moieties.....	273
Figure 7.5 Synthesis of Disulfonated Poly(arylene phenyl phosphine oxide ether sulfone) Terpolymers.....	275
Figure 7.6 Schematic of Conductivity Measurement Apparatus for use at Elevated Temperature and Reduced Relative Humidity at Atmospheric Pressure.....	280
Figure 7.7 Thin Film FTIR of Poly(arylene ether phenyl phosphine oxide sulfone) Terpolymers and BPSH45.....	284
Figure 7.8 Proton NMR of Poly(arylene ether phenyl phosphine oxide sulfone) Terpolymers and BPSH45.....	285
Figure 7.9 Water Uptake of M1 and M2 Series of PPO Containing Terpolymers.....	287
Figure 7.10 FTIR Spectra Indicating Band Shifts Associated with Sulfonate-PTA Complex.....	289
Figure 7.11 Phosphorous 31 NMR Indicating Peak Shift of Backbone Phosphorous Moiety with 30, 45 and 60 wt% PTA Inorganic Additive.....	290
Figure 7.12 Influences of PPO Content and PTA Inorganic Filler on Water Uptake of Composite Membranes.....	292
Figure 7.13 Extraction of Phosphotungstic Acid as a Function of Reacidification Technique and BFPPPO Content.....	294
Figure 7.14 Fuel Cell Performance at 80 °C in 100% RH and 20 psig for Neat Polymer Membrane Electrode Assemblies.....	297
Figure 7.15 Voltage Current Curve at 80 °C in 100% RH and 20 psig for 30 wt% PTA Composite Membrane Electrode Assemblies.....	299

Figure 7.16 Fuel Cell Performance at 120 °C in 50% RH and 20 psig for BPSH45+20%PPO Neat and 30 wt% PTA Composite Terpolymer.....	300
Figure 8.1 Chemical Structure of Biphenol Based Poly(arylene ether sulfone) Copolymers (BPSH) and Hexafluoroisopropylidene Bisphenol Based Poly(arylene ether sulfone) Copolymers (6FSH).....	312
Figure 8.2 Synthesis of 45 Mole Percent Disulfonated Partially Fluorinated Poly(arylene ether sulfone) Co- and Terpolymers.....	314
Figure 8.3 Effect of 6FBP Incorporation on ¹ H NMR Peaks.....	321
Figure 8.4 FTIR Spectra of Salt Form Thin Films Indicating the Incorporation of 6FBP Monomer Into the Copolymer Backbone.....	322
Figure 8.5 Percent Water Uptake of Potassium Salt Form Membranes as a Function of Fluorine Content.....	326
Figure 8.6 Water Uptake of Acid Form Membranes as a Function of 6FBP Content Measured at Room Temperature in Liquid Water.....	326
Figure 8.7 Voltage-Current Curves and High Frequency Resistances at 80 °C and 100% Relative Humidity at 20 psig for BPSH45 and 6F30BPSH45 Co- and Terpolymers ...	329
Figure 8.8 Fuel Cell Performance of BPSH45 and 6F30BPSH45 at 120 °C and 50% Relative Humidity at 20 psig.....	330

List of Tables

Table 2.1 Various dielectric materials and their corresponding dielectric constants....	116
Table 3.1 Characterization of TBBT Based Copolymers Using <u>Difluorinated</u> Comonomers	144
Table 3.2 Characterization of TBBT Based Copolymers Using <u>Dichlorinated</u> Comonomers.....	144
Table 4.1 Ion exchange capacities, intrinsic viscosities, number average molecular weights and weight average molecular weights for low MW and high MW PATS copolymers.....	169
Table 4.2 Calculated lambda values for low MW and high MW PATS copolymers	172
Table 5.1 Characterization of DFDPS, SDFDPS and TBBT Copolymers.....	197
Table 6.1 Various Dielectric Materials and Their Corresponding Dielectric Constants.....	242
Table 6.2 Physical Properties of Various Disulfonated Copolymers and Nafion 117....	245
Table 7.1 Molecular Weight Characterization of BPSH45 and BFPPPO Containing Analogs.....	283
Table 7.2 Conductivity at 120°C and 45% R.H. and Water Uptake of Neat and Composite Membranes as Compared to 45mol% Copolymer Control Containing No PPO Moieties.....	295
Table 8.1 Calculated Ion Exchange Capacity and Molecular Weight Characterization of BPSH45 and Partially Fluorinated BPSH45 Co- and Terpolymers.....	320
Table 8.2 Calculated Bulk Fluorine and Experimental Surface Fluorine Percentages Measured at Depths of Less Than 1 nm.....	324
Table 8.3 Ionic Conductivity at Room Temperature and 80 °C for Partially Fluorinated and BPSH45 Co- and Terpolymers.....	327

CHAPTER 1

Introduction

Polymer electrolyte fuel cell systems include several components such as end plates that encapsulate the current collectors, bipolar plates, gas diffusion layers, catalysts and the proton exchange membranes (PEM). The membrane electrode assembly (MEA), including the PEM and catalyst electrodes, is the essence of the fuel cell and is responsible for the proton transport from the anode to the cathode, thereby directly creating electricity from chemical energy. PEMs must have good mechanical, thermal, and chemical stabilities and still have high proton conductivity. Engineering thermoplastics based on wholly aromatic poly(arylene thioether sulfone)s, poly(arylene ether phosphine oxide)s and poly(arylene ether sulfone)s have been modified for use as proton exchange membranes for fuel cells by directly copolymerizing up to two pendent sulfonate groups per repeat unit.^{1,2,3,4,5} Mechanical, chemical and thermal resistance are inherent properties of most types of poly(arylene)s⁶ and high proton conductivity can, in

¹ M. A. Hickner, H. Ghassemi, Y. S. Kim, B. R. Einsla and J. E. McGrath, *Chem. Rev.* 2004, 104, 4587-4612.

² Wiles, K. B.; Bhanu, V. A.; Wang, F. and McGrath, J. E. *Polymer Preprints* 2002, 43(2), 993.

³ Wiles, K. B.; Bhanu, V. A.; Wang, F.; Hickner, M. A. and McGrath, J. E. *Polymer Preprints*, 2002, 44(1), 1089.

⁴ Shobha H.K.; Smalley, G.R.; Sankarapandian, M. and McGrath, J.E. *ACS Polymer Preprints* 2000, 41(1), 180.

⁵ Wang, F.; Hickner, M.; Ji, Q.; Harrison, W.; Mecham, J.B.; Zawodzinski, T.A.; McGrath, J.E. *J Membr. Sci.* **2002**. 197, 231.

⁶ Liu, Y.; Bhatnagar, A.; Ji, Q.; Riffle, J. S.; McGrath, J. E.; Gebel, J. F. and Kashiwagi, T. *Polymer*, 2000, 41, 5137-5146.

principle, be obtained by either post sulfonation or direct copolymerization using disulfonated monomers. In the current study, sulfonate groups were incorporated into the copolymer structure by direct aromatic nucleophilic substitution polycondensation of disodium 3,3'-disulfonate-4,4'-difluorodiphenylsulfone (SDFDPS), 4,4'-difluorodiphenylsulfone (DFDPS) and 4,4'-thiobisbenzenethiol in the presence of potassium carbonate. In a similar fashion, bis(4-fluorophenyl phenyl) phosphine oxide moieties were incorporated into a poly(arylene ether) backbone so as to increase the polar functionality of the overall polymer architecture, therefore, enhancing the ability to interact with other polar groups such as heteropolyacids. Recently, directly copolymerized sulfonated poly(arylene sulfone)s have shown comparable or better proton conductivity than state of the art Nafion[®] based PEMs.⁷ Precise control of the ionic concentration, well-defined ionic locations and enhanced stability due to the deactivated position of the -SO₃H group are some of the advantages of direct copolymerization of sulfonated monomers.

Previous research has focused primarily on direct copolymerization of sulfonated poly(arylene ether sulfone) copolymers, which show good mechanical and thermal stability with high proton conductivity.⁸ However, a fundamental comparison of poly(arylene ether sulfone)s to poly(arylene thioether sulfone)s and poly(arylene ether phosphine oxide)s has not previously been investigated and one anticipates differences in many properties such as proton conductivity, water swelling, mechanical strength, thermal degradation, chemical resistance, heteropolyacid retention and methanol

⁷ Wang, F.; Hickner, M.; Ji, Q.; Harrison, W.; Mecham, J.B.; Zawodzinski, T.A.; McGrath, J.E., *Macromol. Symp* 2001, 175 (1), 387.

⁸ Harrison, W. L.; Wang, F.; Mecham, J. B.; Bhanu, V. A.; Hill, M.; Kim, Y. S. and McGrath, J. E. *J. Polym. Sci.: Part A: Polym. Chem.*, 2003, 41, 2264.

permeability. As Figure 1.1 indicates, many molecular structures are of interest for higher temperature (120-150 °C) PEMs. The hydrophobic portion of the membranes allows for good mechanical strength and the hydrophilic units permit the transport of protons by specific water transport mechanisms.

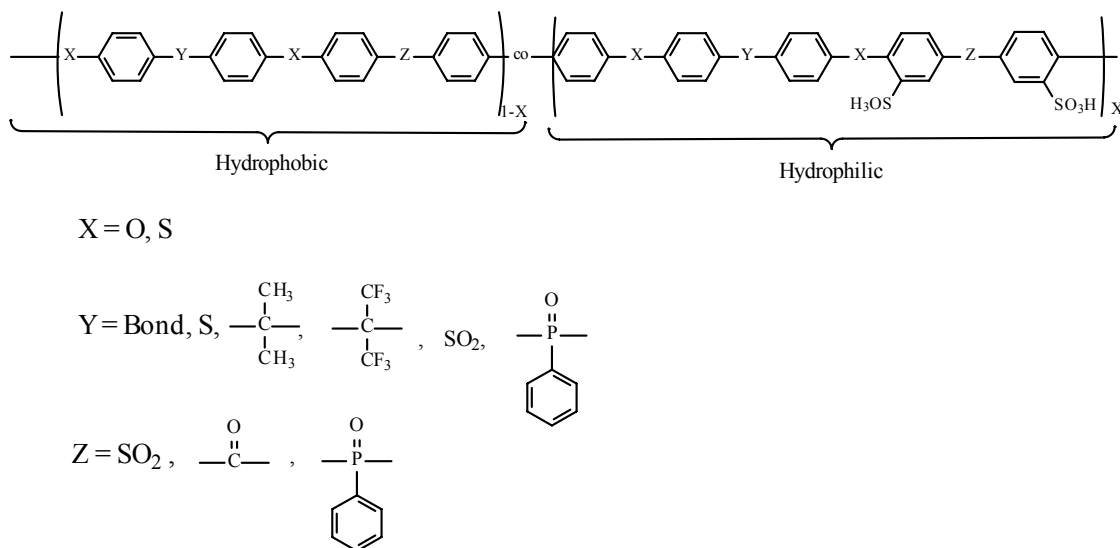


Figure 1.1 Wholly aromatic random (statistical) poly(arylene) / poly(arylene disulfonated) copolymers via direct copolymerization

Oxygen versus sulfur versus phenyl phosphine oxide as a variable in the molecular design of the copolymers is an important characteristic of these PEM materials. The synthesis of poly(arylene thioether sulfone)s has previously been

investigated^{9,10,11,12}, however, the transformation of these materials into proton exchange membranes had not yet been conducted. The successful synthesis route for producing these new materials is shown in Figure 1.2. Although the 4,4'-dichlorinated aryl sulfone monomer or the 4,4'-difluoronated aryl sulfone monomer can be used to synthesize the poly(arylene sulfide sulfone) copolymer, the chlorinated monomer is less reactive, although it would be commercially more feasible.

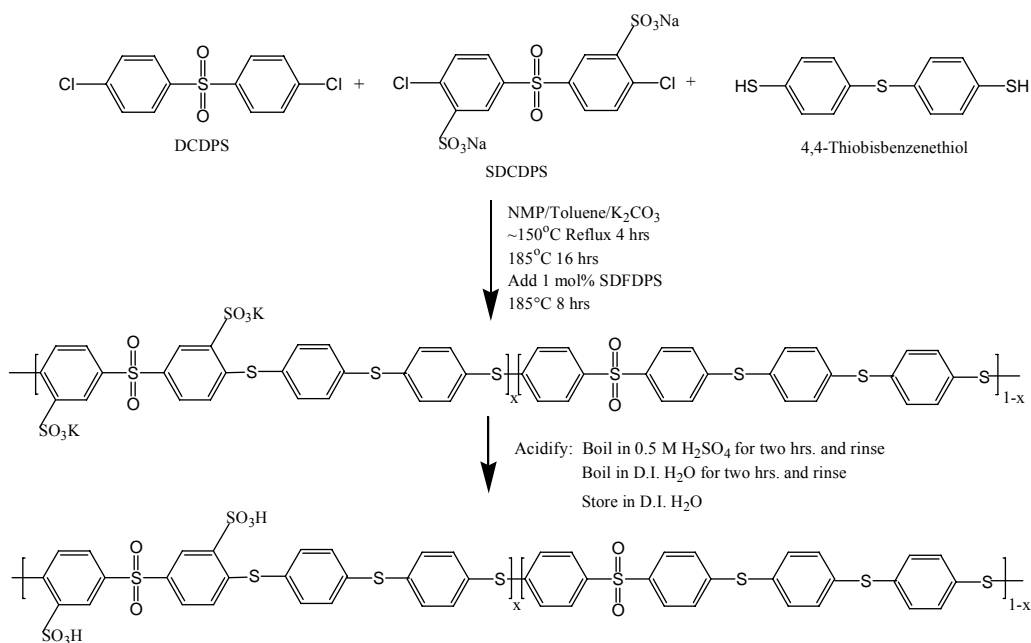


Figure 1.2 Copolymerization of TBBT with DCDPS and SDCDPS

⁹ Liu, Y. *Ph.D. Thesis*, VPI & SU, 1999.

¹⁰ Allam, C.; Liu, K. J.; McGrath, J. E. and Mohanty, D. K. *Macromol. Chem. Phys.*, 1999, 200,1854.

¹¹ Liu, Y., Bhatnager, A., Ji, Q., Riffle, J., McGrath, J. E., Geibel, J. and Kashiwagi, T. *Polymer* 42, 13, 5137, 2000.

¹² Geibel, J. F. and Campbell, R. W. In *Comprehensive Polymer Science, vol. 5: Step Polymerization*, Eastmond, G. C.; Ledwith, A.; Russo, S.; Sigwalt, P., Eds., Oxford: Pergamon Press, 1989.

The synthesis and characterization of sulfonated poly(arylene thioether sulfone), poly(arylene ether phenyl phosphine oxide) and poly(arylene ether sulfone) copolymers are the focus of this study. Polymerizations using 4,4'-dichlorodiphenylsulfone monomers relative to 4,4'-difluorodiphenylsulfone monomers have revealed differences in membrane characteristics. Furthermore, composite membranes containing inorganic additives, such as heteropolyacids ($\text{H}_3\text{PW}_{12}\text{O}_{40}$),¹³ for use in proton exchange membranes could help water retention at elevated temperatures, from 100 °C to 120 °C, and would reduce CO poisoning of the platinum electrocatalyst and increase the reaction kinetics during the electrochemical reactions to produce electricity.

Proton conductivity has been measured as a function of the mole percent disulfonation level using impedance spectroscopy.¹⁴ The values obtained for all the experimental membranes were found to be comparable the state-of-the-art Nafion[®] membranes (*i. e.* 0.1 S/cm) and other materials in the fully hydrated form. Membrane electrode assemblies (MEA) have also been successfully prepared by laminating the films to Nafion[®] electrodes. Performance voltage-current curves have been obtained for some membranes in question and show very attractive performance characteristics. It was proposed in this study to obtain a synthetic strategy to obtain high molecular weight copolymers using chemistry that can be reproduced and to continue to characterize the experimental membranes using engineering methodologies that will help in understanding the morphology and proton exchanging nature due to specific water transport mechanisms. Furthermore, this study was intended to incorporate synthetic

¹³ Kim, Y. S.; Wang, F.; Hickner, M.; Zawodzinski, T. A. and McGrath, J. E. *J. Membr. Sci.*, 2003, 212, 263-282.

¹⁴ Zawodzinski, T. A.; Neeman, M.; Sillerud, L. O. and Gottesfeld, S. *J. Phys. Chem.*, 1991, 95,6040.

chemistry with mechanical and chemical engineering to successfully produce membranes that will perform well in fuel cell environments at elevated temperatures.

Similar materials have also been used in ionic polymer transducers that show mechanical movement when small voltages (1-3 Volts) are applied across the membrane electrode assembly. Polymeric electromechanical transducers are based on an ion-exchange membrane between two conductive metal layer electrodes. Imposed deformations and small electric fields allow both sensing and actuation applications. Relative to piezoelectric electromechanical transducers, soft polymeric transducers give enhanced strain output (>1% possible), produce strain at low voltage operation (below 5V) and give high-sensitivity to small deformations in the charge-sensing mode.

The motion of charges from one pole to the other is produced by the electromechanical coupling effects in the ionic materials. By increasing the surface area of the electrodes, thereby increasing the capacitance, it has been shown that the motion of charges and actuator performance increases, thus indicating a strong correlation between the capacitance and charge motion/performance. The large capacitance in these ionomeric materials is mainly due to the electric double layer that is formed by the electrode and mobile ions.¹⁵

Manipulating the morphology of the electrodes by enhancing the capacitance and effective interfacial area of the conductive electrodes has major effects on performance and transduction. Therefore, employing novel electrode techniques that not only increase performance, but increase the capacitance and interfacial area of the active conductive electrodes can, in principle, enhance both actuation and sensing. The current state-of-the-

¹⁵ Shahinpoor, M. and Kim, K. J. *Applied Physics Letters* 80(18), 91-94, 2002.

art electrode technique employs an impregnation-reduction method.¹⁶ This technique uses a platinum salt solution, PtNH_3Cl_2 , that must diffuse into the ionic membrane and then be reduced by sodium borohydrate, NaBH_4 , to form Pt^0 . However, a novel method employing knowledge based on the use of dispersions to form membrane electrode assemblies for use in fuel cells was introduced in this thesis. This technique allowed various metal powders, such as RuO_4 , Pt/C , as well as Pt , to be incorporated into the electrodes by mixing with aqueous alcohol dispersions of the ionic polymeric materials. Enhanced surface area of the metal-polymer interface produced higher capacitance and better specific performance.

¹⁶ Shahinpoor, M. and Kim, K. J. *Applied Physics Letters* 80(18), 91-94, 2002.

CHAPTER 2: LITERATURE REVIEW

2.1 Introduction to Ion Containing Polymers - Ionomers

The understanding of ionomers has increased exponentially over the past few decades and the experimental outcomes can now be theoretically predicted for certain ionomer systems.¹⁷ Many bulk properties of the polymer system are due to the ionic interactions in minute regions of the material.^{18,19} Therefore, the composition of the ions is not the major component of the system, as is the case with electrolytes, rather the macromolecular properties of the system are the critical characteristics. However, historically ionomeric systems have been defined to be 15 mole percent or less of ion content, but that value can be and has been exceeded in many cases.²⁰ The materials that are used to produce ionomeric materials are most often copolymers with low dielectric constants and ionic side groups. The well studied ethylene and styrene systems that contain ion groups based on sulfonic acid, carboxylic acid or quaternary amines are the main focus of many papers.^{21,22} Furthermore, the number and knowledge base of ionomers are extremely large as nonionic polymeric materials could be transformed into a wide range of ionomeric materials by reaction after polymerization (post-ionization). These polymeric architectures can be different by the position, type and concentration of the ion particles on the polymer backbone, therefore, producing a large amount of potential systems to study.

¹⁷ Rees, R.W. and D.J. Vaughan, *Polymer Prepr. Am. Chem. Soc. Div. Polym. Chem.*, 1965, 6, 287.

¹⁸ Eisenberg, A. and M. Rinaudo, *Polymer Bull.*, 1990, 24, 671.

¹⁹ Lundberg, R.D. and H.S. Makowski, *A Comparison of Sulfonate and Carboxylate Ionomers*. In *Ions in Polymers*, *Adv. Chem. Ser. 187*, Eisenberg, A, Ed., 1980, pp. 21, American Chemical Society: Washington D. C.

²⁰ *Ionomers: Synthesis, Structure, Properties and Applications*, Tant, M. R., Mauritz, K. A. and Wilkes, G. L., Eds.; 1997, Chapman and Hall: New York.

²¹ Farrell, K.V. and B.P Grady, *Macromolecules*, 2000, 33, 7122.

²² Mandal, U.K., *Polymer International*, 2000, 49, 1653.

Ionomers have been studied in great lengths due to the properties that can be influenced by the incorporation of ionic moieties into a system. The glass transition temperature (T_g), modulus, fatigue, viscosity, melt strength and transport can be purposefully changed by ion incorporation. Previous industrial interests included the strength of the columbic interactions, which could account for ionomers being used as tie coats between two layers that are not compatible with each other, solubility enhancement of two non-soluble polymers and additives for uses in composite matrices.²³ Furthermore, rheology can be manipulated and enhancement of the proton conductivity of the material can be obtained. The enhanced conductive materials can be used for solid-state electrolyte applications employing the Grotthuss²⁴ proton hopping mechanism (Figure 2.1).

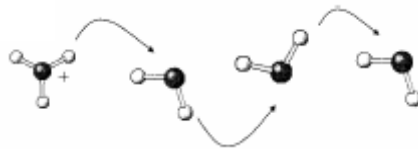


Figure 2.1 Grotthuss Proton Hopping Mechanism

Most carboxylate ionomers contain ionic carboxylate functional groups that are attached to a nonionic hydrocarbon backbone. Thermoplastic and elastomeric ionomers are the two main types of carboxylate ionomers used. The difference between the two is the backbones that are used, where thermoplastic backbones consist of structures like ethylene or styrene and elastomeric backbones consist mainly of ethylene-propylene copolymers or dienes. Thermoplastic carboxylate ionomers can be produced by

²³ Eisenberg, A. and J.-S. Kim, *Introduction to Ionomers*, 1998, Wiley: New York.

²⁴ Li, T., Wlaschin, A. and Balbuena, P. *Ind. Eng. Chem. Res.* 40, 4789, 2001.

copolymerizing acrylic acid or methacrylic acid using free radical initiators at high pressure in order to make low-density polyethylene containing carboxylate groups. Usually, the amount of acidic monomers that are used is below 7%. The films that are produced can have better toughness, transparency and lower melting points than the homopolymer backbone structure. When the acidic copolymers are neutralized with a counter ion (i. e. Zn^{++} or Na^+), the properties of the system become much different. Neutralization can be conducted in the melt, in aqueous media or in solution. Furthermore, incorporating carboxy groups into an elastomeric backbone like a diene can produce carboxylated rubbers. The ions that have been incorporated can act as a method of curing by the association of ions to form physical crosslinks. Most of these carboxylate elastomers are synthesized using free-radical initiators in commercial sized quantities. The acid monomers need special polymerization processes that may entail the use of emulsifiers.²²

Copolymers and polymers that contain a higher amount of acidic ion groups can be water-soluble products that are usually insoluble in the monomers that they are derived. Therefore, these polymerizations need to be performed in an aqueous dispersion or solution using free radical initiators that are water soluble, (i. e. sulfonates). Furthermore, polymerizations that are homogeneous in an aqueous system can be used, but the resulting solution has a higher viscosity, which can lead to a gel. Therefore, an inverse suspension or emulsion can be employed so that water-in-oil is present in the reaction.²⁵ Direct polymerization to compare the copolymers or modification of the preformed polymers can give rise to totally different compound characteristics. The

²⁵ *Advances in Polymer Synthesis*, Culbertson, B. M. and McGrath, J. E., Eds.; 1985, Plenum Press: New York.

modification of the polymer that has already been formed by adding carboxyl groups to it can be quite difficult because of intrinsic limitations due to the kinetics of hydrolysis of different systems. Tacticity and neighboring groups may give products that change with concentration. Reproducibility is always a concern when post-reacting polymeric materials with ion containing compounds.

As compared to the synthesis of carboxylate ionomers, which are mostly made by direct copolymerization techniques, the majority of sulfonated ionomers have in the past been produced by post sulfonation reactions on the preformed polymers using sulfuric acid or sulfur trioxide complexes.²⁶ Modification of the polymers result in random ions that are incorporated into the backbone polymer. Post-sulfonation techniques are difficult and time-consuming reactions and, therefore, the process of direct copolymerization of sulfonated monomers has also been of interest. Random copolymers can be prepared using styrene sulfonic acid copolymerizations to produce random copolymers that contain both styrene and sulfonated styrene structures. Free-radical initiated polymerization using redox or thermally sensitive compounds is the most common way to produce sulfonated ionic polymers. The large differences in the solubility of the non-polar and polar monomers means that the reaction must be carried out in emulsion systems rather than solution systems. Usually, instead of a traditional surfactant, a comonomer like potassium styrene sulfonate may be used to act as an emulsifier. Due to the strongly

²⁶ Lundberg, R.D. and H.S. Makowski, *A Comparison of Sulfonate and Carboxylate Ionomers*. In *Ions in Polymers*, *Adv. Chem. Ser. 187*, Eisenberg, A, Ed., 1980, pp. 21, American Chemical Society: Washington D. C.

acidic monomers, the pH of the reaction media is not tested because the monomers remain ionized throughout the reaction therefore the pH is kept fairly acidic.²⁷

One important type of well studied sulfonated ionomer is the elastomers that are produced from ethylene, propylene, diene monomers (EPDM). These rubbers (Figure 2.2) are transformed into an ionomer by the reaction of the residual unsaturation and neutralization of the diene units along the backbone. However, the use of some types of metals with EPDM systems does not show very good compatibility due to non-miscibility of the counterion. When using Na^+ and Zn^{++} as the counterions, it was found that zinc had better miscibility with the EPDM than the sodium counterion.²⁸

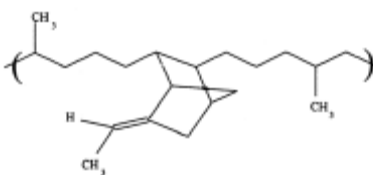


Figure 2.2 Chemical Structure of Ethylene-Propylene-Diene Rubber

Ammonium cationomers contain quaternary ammonium polymers that can be synthesized by the use of monomers that have been transformed into the cationic form before polymerization. The cationic monomers are usually in the salt form and can be polymerized with styrene by free radical or possibly ionic techniques. The polymerization is carried out in organic or aqueous media, but the pH of the reaction must be monitored and kept low to help the protonated form be soluble and produce high molecular weight.²⁹

²⁷ *Ions in Polymers*, Eisenberg, A., Ed.; *Adv. Chem. Ser. 187*, 1980, American Chemical Society: Washinton D. C.

²⁸ Ha, C.S., *Polymer Advanced Technology*, 1991, 2, 31.

²⁹ Brenner, D. and Oswald A.A. In *Ions in Polymers*, *Adv. Chem. Ser.187*, Eisenberg, A., Ed. 1980, pp. 53, American Chemical Society: Washington D. C.

2.2 Structure and Ionic Association

Many possible architectures and structures can be produced synthetically by using different techniques during synthesis. Random copolymers, block copolymers and telechelics are the main types of structures that are used for ionomeric materials. Styrene based polymers can be used to form all of these architectures, and these basic concepts can then be used on other types of polymer systems.

The use of a single ion at only one of the chain ends is termed monochelics (Figure 2.3a, where the black dots are the counterions).³⁰ Anionic polymerization can be used to prepare this type of ionomer. For example, alkyllithium initiators could be used to start the reaction and when the polymer reaches the desired length, the anion is terminated with CO₂.^{31,32} Furthermore, block copolymers could be synthesized where only one side of the block contains an ion (Figure 2.3b). When a polymer chain has a functional group including an ion on each end, it is termed a telechelic (Figure 2.3c). Telechelics can be synthesized by using sodium naphthalenide as the anionic initiator where the chain grows in two directions. Again, termination can be carried out by using CO₂ as an end capper, enabling both ends to have ionic moieties. Furthermore, telechelic ionomers can be made to produce an anion on one end and a cation on the other (Figure 2.3d). Three or more armed stars could be synthesized to produce ions on the end of every arm of the star, where, for example, sulfonic acid groups could be the terminal units of the arms (Figure 2.3e). AB block copolymers where one of the blocks is nonionic, like polystyrene, and the other block is ionic, like sulfonated polystyrene, can

³⁰ *Ionomers: Synthesis, Structure, Properties and Applications*, Tant, M. R., Mauritz, K. A. and Wilkes, G. L., Eds.; 1997, Chapman and Hall: New York.

³¹ Allen, R. D. and McGrath, J. E. In: *Coulombic Interactions in Macromolecular Systems*, Eisenberg, A. and Bailey, F. Eds.; 1986, American Chemical Society: Washington D. C.

³² Horrion, J., Jerome, R. and P. Teyssie, *J. Polymer Sci. C. Polymer Lett.*, 1986, 24, 69.

be synthesized by anionic polymerization using alkyl lithium as the initiator (Figure 2.3f). Triblocks or multiblock ionomers are synthesized using naphthalenide anionic initiators where each block is either ionic or nonionic (Figures 2.3g-h). Star block copolymers can also be synthesized to produce star type ionomeric architectures (Figure 2.3i). Diblock, triblock or multiblock ionomers where one block is totally nonionic and the other block is only partially ionic can also be formed (Figure 2.3j). An example of this type of ionomer uses hydrogenated butadiene as one block and styrene as the other block where the styrene block is partially sulfonated. Furthermore, a block copolymer that contains a block of polystyrene with an acid functionalized dendrimer at one end can be produced to form ionomeric dendritic architectures (Figure 2.3k).²³

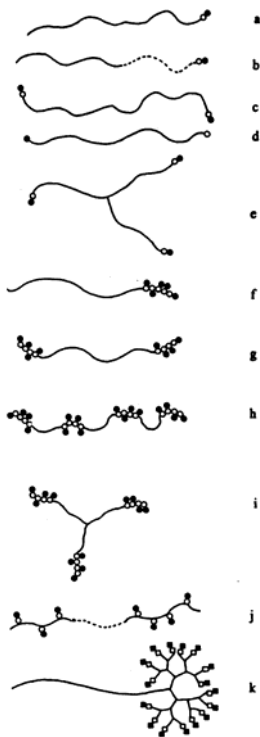


Figure 2.3. Possible Structures of Ionomers

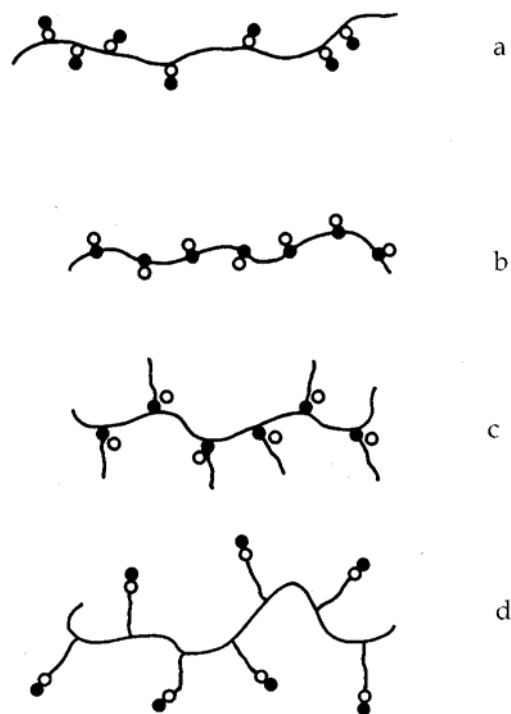


Figure 2.4. Possible random and comb structures

Random copolymers consist of a material that has random incorporation of ions along a nonionic backbone. The backbone can be made of styrene where sulfonic acid, carboxylic acid or quaternary ammonia ions could be attached randomly to aromatic rings (Figure 2.4a). Comb ionomers contain side chains that contain the ion group (Figures 2.4c,d) giving rise to many different physical properties relative to the non-ionic containing analog. The side groups can have the ions either at the end or at the beginning of the side chains. If the ions are located at the beginning of the side chain, then the counter ion will be close to the nonionic backbone. All of the architectures that have been described can, in principle, be made with polystyrene based systems. The ionomer architectures can vary from system to system, but the general structures give good insight into the field of ionomers.

The use of different counter ions in order to neutralize the system can be used with all the materials mentioned thus far. The different types of counterions can range a great deal. The use of metal ions like alkali metals, transition metals, alkaline earth metals or organic cations, such as pyridinium or ammonium could be used to neutralize cationic systems. These include such groups as Li^+ , Na^+ , K^+ , Mg^{2+} , Ca^{2+} , and Zn^{2+} to only name a few. The cations that contain multivalent charges are a bit more complicated to incorporate into the systems than the cations that contain only a single charge. The cationic polymers that need an anionic counterion can use organic anions or halides. Some of the halides that could be used include F^- , Cl^- , I^- or Br^- . Examples of organic anions are triflates, fluoroborates and tosylates.³⁰

Many properties and morphology of the ionomers in the solid state are usually influenced by the aggregates of the ionic groups in the material. When a low dielectric constant media is employed as a matrix for the ionomers, the association of the ion-counterion driving force is high. Furthermore, the association of ion pair-ion pair aggregation is high where even higher aggregate association can be achieved. The formation of the ion aggregates known as multiplets is a primary structure of ionomers and then these multiplets can form into higher agglomerations to form spheres, clusters and channels.

The multiplets that form from the ionic polymer systems that contain both ions in the polymer and counter ions in the solution could be in the form of spheres. The size of the multiplets can change as a function of the energy balance that is dependent on the electrostatic energies and the relative size of the ions. This can make the structure be in the form of a cone that is between the ion pair and the polymer chain segment that the ionic group is attached. Therefore, the type of backbone that is used in the system is an important factor when trying to determine the shape of the multiplet. If the backbone is rigid, then the multiplets will be smaller relative to a flexible backbone due to the decreased mobility of the backbone to form the multiplets.²³

The restricted mobility model that was published in 1990 by Eisenberg-Herd-Moore was termed the EHM model (Figure 2.5).³³ This model describes the mobility of the surrounding polymer chains that contain the random ions. The mobility of the material is reduced due to factors such as the anchoring of the chain to the multiplet, crowding of the chains around the multiplet and elongation of the chains due to the crowding. The mobility of the chains as they are anchored to the multiplet is a function

³³ Eisenberg, A., Hird, B. and R.B. Moore, *Macromolecules*, 1990, 23, 4098.

of the molecular weight. If the chains are anchored to each other, then the effect is an increase in molecular weight. This is a direct reason for the reduced mobility of the chains around the multiplet. Furthermore, the crowding of the chains as they are anchored to the multiplet during the formation releases electrostatic energy, which is the driving force for multiplet formation, and the surface energies help to play a role in the crowding in the immediate area of the multiplet that decreases the mobility of the chains. The chain extensions of each chain in the multiplet help the formation create more room around the multiplet so that more chains can be incorporated. Furthermore, the distribution of the sizes of the multiplets in the system as a whole will not be uniform throughout, but will consist of many different sizes of the structures. Therefore, the size of the multiplet containing the reduced mobility area will be a factor when determining the crowding correlations.

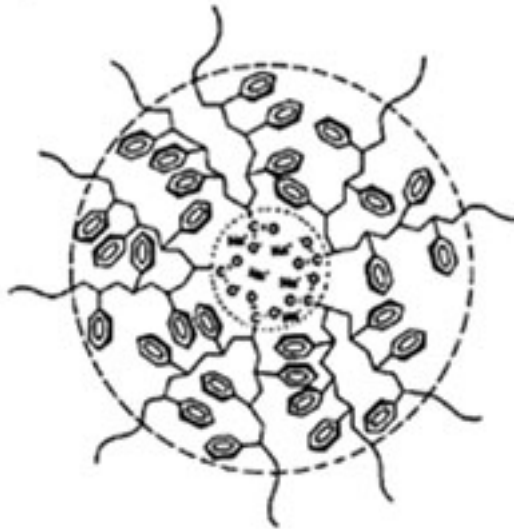


Figure 2.5 EHM model of the area of restricted mobility of ionomeric material.

For ionomer systems that contain polystyrene and another comonomers like methacrylic acid, the multiplets only consist of a few ion pairs. When these multiplets are isolated and include the chain layer that has reduced mobility, the multiplets are too small to show their own T_g , therefore, there is only one T_g present in the material. This indicates that the multiplet by itself acts as a cross linked material and is similar to single-phase structures. When the number of multiplets increases to a larger value to where the polymer chains in the reduced mobility area overlap, some of the regions of large overlap exceed the concentration needed for independent phase behavior and form a cluster. Therefore, the material starts to show two relaxations. The second phase that is seen as the concentration of the multiplets increase shows its own T_g and reflects the clustering of the multiplets.³³

Multiplets can also combine to form channels of ions through a system (Figure 2.6). Microphase separation occurs above a certain concentration of multiplets and by increasing the ion content on the polymer backbone, which decreases the chain segment length between the ions, a decrease in the distance between the ionic lamellae develops. Therefore, there is a direct correlation of the thickness of the ionic lamellae spacing on the segment length between ions of the polymer system.



Figure 2.6 Possible structure of ion channels

2.3 Properties and Applications of Ionomers

Ionomers can be used for a wide variety of applications that range from use in golf balls^{34,35} to the production of electricity produced from the transport of a proton to react with oxygen to form water.³⁶ Membranes are the largest used forms of ionomer systems in the world today. This is due to many different characteristics that ionomer films have, which include superpermeability, grease resistance, puncture resistance, clarity, thermoformability, flexibility, melt strength, hot tacking and ionomer films even have the ability to seal through contaminated areas. Perfluorosulfonates and perfluorocarboxylates are ionomeric materials that have very good stability to both heat and chemically harsh environments. Superpermeability, which slows the passage of anions to very low levels and allows the transport of cations at a much faster rate through the membrane, make electrochemical applications possible. The small conductive

³⁴ Takesue, T., Ichikawa, Y. and S. Kashiwagi, *Jpn. Kokai Tokkyo Koho*, 2000, Japanese Patent.

³⁵ Rajagopalan, M., 2001, U.S. Patent.

³⁶ *Ionomers: Characterization, Theory, and Applications*, Schlick, S., Ed., 1996, CRC: Boca Raton, FL.

channels of the ionomeric materials allow for the superpermselectivity to occur, which is directly related to the structure and morphology of the ionic film.

Two major uses of ionomeric films are in the chloro-alkali industry and the fuel cell industry. Perfluoronated ionomer membranes are used in the chloro-alkali industry to produce chlorine, Cl_2 , as a pure substance.³⁷ The starting material uses NaCl where the chlorine and hydrogen gases are produced at the anode and cathode respectively. The ionomeric membrane is in between the two gases, but allows sodium hydroxide to accumulate at the cathode side in high purity. The diffusion coefficient for the Cl^- anion is very low through the membrane and thus the production of chlorine is achieved. This process is done at high temperatures and in strongly oxidizing media, but the perfluoro ionomer membranes can hold up to these types of environments very well. Since chlorine is used in very large volumes in the industry, this process costs much less than other ways of producing chlorine and does not require the use of toxic mercury (Hg).

Membranes of perfluorosulfonated ionomers can also be used in fuel cell applications.³⁶ These solid polymer electrolytes work in the opposite way of the chloro-alkali process with respect to the power use. For chloro-alkali processes, power must be put into the system and in the fuel cell process power is generated from the system. The fuel cell membrane keeps the hydrogen and oxygen separated and helps to convert these gases to water to produce electricity as will be discussed in subsequent sections.

The use of ionomers for packaging has also been a major application of them due to their specific characteristics such as high melt strength.³⁸ Ethylene ionomers, such as SURLYN[®], used in the packaging industry have many advantages over other packaging

³⁷ Risen, W.M.Jr., In *Ionomers: Characterization, Theory, and Applications*, Schlick, S., Ed., 1996, CRC: Boca Raton, FL.

³⁸ Statz, R.J., *Polymer Prepr. Am. Chem. Soc. Div. Polymer Chem.*, 1989, 29, 435.

films because of their flex resistance, oil and chemical resistance and resistance to impact. Furthermore, the ability to heat seal the material under many different conditions, adhere to substrates that contain impurities due to the hydrophilic and hydrophobic segments, display good optical properties due to the decrease in the spherulite size in the presence of ionic groups and the ability of their high melt strength to hold things in place make them good packaging materials.

The use of ionomeric materials for elastomers is achieved by using ethylene-propylene-diene monomer (EPDM) systems that may be derivatized with ionic sulfonate groups. The ionic interactions at room temperature are strong and produce a physically cross-linked material that gives good rubber-like thermoplastic elastomer properties. When the temperature is raised, the interactions of the ions in the aggregations tend to dissociate the multiplets allowing thermoplastic processability. The physical cross links of the material do show considerable creep.³⁹ When compared to chemical cross links that break under large strains, the physical cross links may afford ion hopping, where the ion association of one chain in a multiplet breaks and reforms in another multiplet which allows the physical network to relax.

The field of ionomeric materials is extremely vast and applications range widely. The properties of certain materials can be changed by not only adding ions to the system, but by increasing the concentration of ions in the system. The T_g , modulus, viscosity, melt strength and transport behavior can be changed in ways that other comparable systems cannot compete with, making ionomers quite important. The morphology of the ionomeric systems changes dramatically with certain variables of the materials, but the basic concepts give good insight into the association and architectures of ionomer

³⁹ Ghosh, S.K. *J. Appl. Polym. Sci.*, 2000, 78, 743.

systems. Complete understanding of the entire system of ionomers is still in progress, but further research will help describe the story of ionomers in more detail and could also possibly disprove some of the models that are currently accepted.

2.4 Fuel Cells

Environmentally friendly energy sources for generation of electricity and heat are of great importance in this world of diminishing natural resources and proposed global warming. The world energy needs are growing rapidly and, to meet these needs, novel energy sources must be investigated. The current sources of energy are being depleted over time especially where petroleum is the world's most sought after fuel. The combustion of non-renewable fossil fuels produces most of the world energy and transportation needs, but produces harmful emissions, e. g. acid rain from sulfur compounds and photo chemical smog from nitrogen compound combustion, that pollute air and water. Engineering marvels based on hydropower, wind power and solar power are becoming more important for renewable and environmentally friendly energy sources, however, the cost associated with such systems is still high due to the large earth surface area that must be used to create ample power supplies. As population increases, non-renewable energy sources, such as petroleum, will diminish and the harmful greenhouse gases that they emit may deplete the health of humankind. Therefore, renewable energy sources based on the world's most abundant compounds is of extreme importance. Thus, novel engineering technology based on proton exchange membrane fuel cells (PEMFC) as an alternate energy source is becoming very attractive. The world's most prevalent compound, hydrogen (H_2), can be used to produce energy by combining with oxygen to produce direct current electricity, water and heat. The DC current can be used to run anything from a watch to entire cities. The water produced is

pure enough to drink and the heat can be used as a source of warmth in cold winter months.⁴⁰

2.5 General Processes and Functionality of the Fuel Cells

Fuel cells produce electrical energy via electrochemical reactions by delivering fuel (H_2) to the anode and an oxidizer (O_2 or Air) to the cathode. The general process has some similarity to batteries, however, fuel cells use external sources of fuel and oxidizers, whereas batteries use sealed case fuel and oxidizers as one unit.⁴¹ Furthermore, batteries will eventually run out of fuel and ‘die’; fuel cells, in principle, will only need to be re-fueled to generate power⁴² and produce continuous electricity.⁴³ In a hydrogen fuel cell, H_2 is delivered to the anode where it is oxidized with an electrocatalytic material that is usually based on the precious metal platinum. Thus, the oxidation of hydrogen produces protons and electrons. Only the protons (H^+ or H_3O^+) are transported across the proton exchange membrane. The electrons, electrical energy, are conducted away from the fuel cell to an external circuit where they could produce light, electric motor movement, etc.⁴⁴ The protons and the electrons meet at the cathode and react with the oxidizer, oxygen, to produce heat and water (Figure 2.7).⁴⁵

⁴⁰ Jacoby, M. *Chemical & Engineering News*, 1999, 77, 31.

⁴¹ Hirschenhofer, J.H.; Stauffer, D.B.; Engleman, R.R. *Fuel Cells: A Handbook* for the Department of Energy; B/T Books: Orinda, CA, 1996.

⁴² Liebhafsky, H.A.; Cairns, E.J., *Fuel Cells and Fuel Batteries*, John Wiley and Sons, Inc., New York 1968.

⁴³ Zalowitz, M.; Thomas, S. "Fuel Cells: Green Power," Department of Energy, 1999 LA-UR-99-3231.

⁴⁴ 3M's Fuel Cell Vision - http://www.3m.com/us/mfg_industrial/fuelcells/overview/pemfc.jhtml

⁴⁵ Appleby, A. J., Ed. *Fuel Cells: Trends in Research and Applications*; 1987, Hemisphere Publishing Corp.: New York; p. 281.

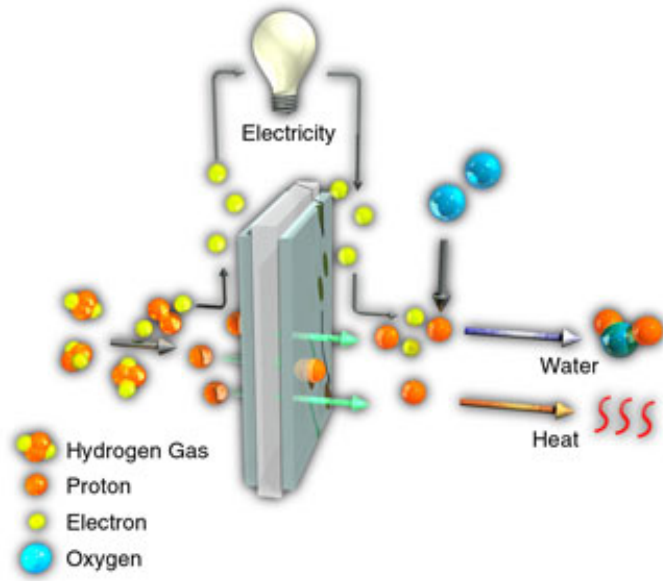


Figure 2.7. Hydrogen fuel cell general processes

The history of the fuel cell dates back to 1839 when William Grove, a British amateur physicist, first discovered the fuel cell principle.⁴⁶ He used four large cells that contained both hydrogen and oxygen to produce electricity that was then used to split the water in the upper cell into hydrogen and oxygen (Figure 2.8).

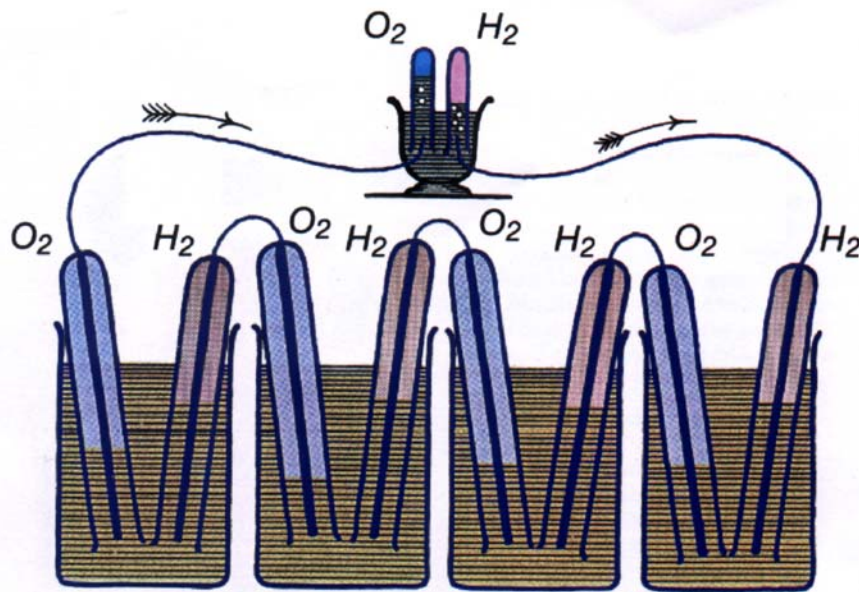


Figure 2.8 William R. Grove (1811-1896) demonstrated in 1839 that electricity can be generated from hydrogen and oxygen in contact with platinum strips, which extend into dilute sulfuric acid functioning as a diaphragm.

⁴⁶ (a) William Grove writing to Michael Faraday, October 22, 1842. (b) Zalbowitz, M.; Thomas, S. "Fuel Cells: Green Power," Department of Energy, 1999 LA-UR-99-3231.

Over 120 years later NASA began to apply this technology to provide power during space flight.⁴⁷ However, due to the technical and economical barriers of the new technology, full commercialization has not yet occurred. Today, companies, government labs and universities are trying to understand phenomena, boost performance, efficiency, reliability while minimizing weight, size and cost.

Nearly every major automobile manufacturer in the world is developing fuel cells to power vehicles. However, even though internal combustion engines are over 100 years old they are still being improved. The engine and automobile has had global impact giving reliability in transport and revolutionizing the industrial era. However, the gasoline and the tailpipe exhaust that comes from the burning of it, have contributed to our water and air pollution. Furthermore, our reliance on foreign oil from the Middle East has triggered trade imbalances and even wars. Therefore, the big picture is to develop a commercializable technology that innovates the global environment and revolutionizes a cleaner and friendlier world.

Internal combustion engines, batteries and fuel cells have one thing in common, the end product: energy. The internal combustion engine runs at high temperature and use noisy explosions that power almost all autos on the road. The energy is produced from the release of thermal energy by burning fuel with oxygen from air to produce mechanical and eventually electrical energy. Using the Carnot cycle as a model of efficiency for a heat engine, conversion of all the heat energy into mechanical energy has limitations. Much of the combustion energy is lost due to a low temperature heat sink. Internal combustion engines produce mechanical energy by accepting high temperature combustion heat (T_1) that produces mechanical work, where the rest of the heat energy is

⁴⁷ Scott, D. S. and Hafele, W. J. *Hydrogen Energy*, 1990, 15, 10.

transferred to the heat sink at low temperatures (T_2). To increase the efficiency, the difference between the high temperature combustion heat and the low temperature heat sink must be maximized.

$$(T_1 - T_2) / T_1 = \text{Maximum Efficiency}$$

However, the material limitations that occur in the internal combustion engines raw materials decrease maximum efficiency. Fuel cells, interestingly, convert chemical energy directly to electrical energy, which is the final product. No other conversions of energy are needed, *i. e.* combustion heat converted to mechanical energy. Thus, efficiencies of the fuel cells have been proposed to surpass the Carnot cycle limit even at low temperatures, *e. g.* 80 °C.⁴⁸

Limitations of the fuel cell include usable temperature ranges, hydrogen storage, fuel efficiency and cost. Solid-state polymer electrolyte membrane fuel cells are limited by the liquid water temperature range. The hydrogen ions must be transported across the membranes by specific water assisted mechanisms, thus, when water is not present in the membranes, hydrogen ions cannot be carried from the anode to the cathode. The alternative to temperature ranges below 100 °C is to use pressurized cell conditions. The pressure would help to keep the water in the liquid form so as not to vaporize and dehumidify the membrane. However, this is expensive and reduces efficiency.

Solid-state PEMs hold the negatively charged ions rigidly in place even in the presence of water. This is due to the covalent bonds that attach the anionic group to the polymer backbone. In the fuel cell, only the positive ions in the membrane move from the anode to the cathode. This process is essential for fuel cell performance. If no movement of positive ions occurred, the ionic charge in the cell would build up and the

⁴⁸ Appleby, A.J.; Foulks, F.R. *Fuel Cell Handbook*, Van Nostrand Reinhold, New York, 1989.

circuit that is defined by the wires and load would remain open where current would not flow.

Gas and liquid separation is also a characteristic of solid state PEMs. Even though the film is thin, 50-180 microns, the PEM essentially keeps the hydrogen or methanol fuel separate from the oxidant air. The PEMs are good proton conductors, however, they do not conduct electrons.⁴⁹ Ordinary electrolytes are materials that separate negatively charged ions and positively charged ions when water is present. Thus the solution of water and electrolyte is electrically conducting. In a PEM fuel cell the electrolyte is a 'solid' polymer film that is protonically conducting. Even though they are good ionic conductors, they do not conduct electrons. In fact, they are electronic insulators, thereby separating the anode electrons from the cathode electrons. Therefore, the electrons are conducted away from the membrane by electronic conductors, like carbon black or platinum, to an external circuit. The electrons are then routed to the cathode side of the cell to complete the circuit. Electrical power to run a light or a car is produced by this external circuitry that use the electrons produced at the anode side of the fuel cell.

The electrodes, located on each side of the membrane, are where the physical and electrochemical processes occur. For a hydrogen fuel cell, at the anode, H₂ gas diffuses through the polymer electrolyte that encases the platinum on carbon black. When contact of the gas and platinum occurs, the Pt catalyzes the oxidation of the H₂ compound into two hydrogen protons.⁵⁰ The two hydrogen atoms may then bond to two Pt atoms, which catalyze the release of two electrons to produce hydrogen protons, H⁺. The electrons are

⁴⁹ Fernandez, R. E. In: *Polymer Data Handbook*, Mark, J. E., Ed., Oxford University Press: New York, 1999, 233.

⁵⁰ Savinell, R. F.; Wainright, J. S. and Litt, M. in *Proton Conduction Fuel Cells II*, 1998, Pennington, NJ.

conducted away from the anode by the electron conductive carbon black and platinum atoms to the outer circuit and then to the cathode side of the cell. The protons are conducted away from the anode by the proton conducting membrane and transported to the cathode side of the membrane thereby allowing current flow in the circuit. At the cathode, an oxygen molecule, O_2 diffuses through the polymer to the platinum on carbon black and undergoes a four-electron reduction process. The slow rate of the O_2 reduction half reaction, which is about 100 times slower than the H_2 oxidation half reaction, seems to determine the overall performance of the PEM fuel cell.⁵¹ High rates of O_2 reduction are possible using relatively expensive platinum or other noble based catalysts, which reduce O_2 at relatively low temperatures, 80 °C, at which PEM fuel cells operate.

Two separate reactions occur during the electrochemical processes in a fuel cell. The oxidation half reaction occurs at the anode and the reduction half reaction occurs at the cathode. During the oxidation half-reaction, hydrogen gas is consumed and produces hydrogen ions that are transported across the protonically conductive membrane to the cathode. The electrons that are produced are conducted away from the fuel cell to an external circuit and then travel to the cathode. During the reduction half-reaction, oxygen supplied from the air-flow past the cathode combines with the protons and electrons to form water and heat. The water is transported out of the cell by the airflow in both liquid and vapor form. The excess heat must be managed by cooling of the cell stack to maintain the operating temperature at about 80 °C. At low operating temperatures, the reactions would occur very slowly, however, platinum catalysts are used on both the

⁵¹ Gottesfeld, S. and Zawodzinski, T. A. *Polymer Electrolyte Fuel Cells*, In: *Advances in Electrochem. Sci. and Eng.*, Alkire, R. C.; Gerischer, H.; Kolb, D. M. and Tobias, C. W., Eds., 1993, Vol. 5, 187.

anode and cathode electrodes so as to increase the rates of each half-reactions. Therefore, the reactions produce electricity in the form of direct current, water and heat.⁵²

The Pt catalyst has been shown to be a good catalyst for both the anode and cathode half-reactions because it optimizes the bonding of the H atoms that are not too strong and not too weak. Decreasing the loading of Pt catalyst is an ongoing effort because the precious metal is expensive (about two times gold in 2005). Construction of the catalyst layer with the highest surface area seems to be one of the best ways to decrease the amount of Pt needed for efficient half-reactions. Therefore, dispersing very small Pt particles, around 2 nanometers in diameter, on porous carbon black increases the total surface area of the active Pt catalyst. Although the total amount of Pt in the electrodes is small, the very large surface area allows electrode half-reactions to occur at many sites simultaneously. The electrodes are both designed to be porous to gases and both the Pt and carbon are good electron conductors, therefore, gases and electrons are free to move through both electrodes.

Management of the water by product in the PEM cell must be controlled and understood for the cell to operate in an efficient and effective way. Even though water is produced in the fuel cell and transported away by the airflow stream, both the fuel and the air entering the cell must be humidified before entering the cell. Hydration of the membrane must be accomplished for transportation of the hydrogen ions through specific water transport mechanisms. If the hydration of the membrane is not enough, the H⁺ ions will not be transported across the membrane and the total current of the cell will decrease. Too high hydration occurs by low flow of the air past the cathode, which cannot remove all the produced water. Therefore, flooding of the cathode occurs and cell performance

⁵² Mukerjee, S.; Lee, S. J.; Ticianelli, E. A. and McBreen, J. *Electrochim Acta*, 1999, 44, 3283.

decreases due to lack of oxygen, which must diffuse through the excess water to the Pt catalysis sites.

The membrane electrode assembly (Figure 2.9) consists of the anode adhered to the proton conducting membrane which is then adhered to the cathode.⁵³ Pt loading of the electrodes was originally as high as 4 milligrams of Pt per square centimeter. During the Gemini space program in the 1960s, this loading amount produced 0.5 amperes/milligram of Pt.⁵⁴ However, current state of the art electrodes for hydrogen fuel cells has decreased the Pt loading to 0.2 mg/cm². Even though less Pt is being used, overall performance has increased dramatically to 15 amperes per milligram of Pt. The electrodes consist of Pt on carbon black in a matrix of proton exchange membrane polymer. This matrix permits access to the catalyst sites, proton conduction and electronic conduction through the Pt/C. The interface of the electrode to membrane has been and still is fundamental and on-going research that needs to be further understood to produce more efficient proton transport from the electrodes across the membrane. The simplest procedure for producing membrane electrode assemblies is to paint catalyst ‘ink’ onto a dry proton exchange membrane. The catalyst ‘ink’ is first prepared by putting the correct amount of Pt dispersed on carbon, or other catalyst compounds, into a dispersion of membrane material in relatively low boiling point alcohols or alcohol water mixtures. The viscosity of this dispersion is usually very low and glycerol can be added to increase the viscosity to aid in enhanced painting of each layer. After thorough mixing, the ‘ink’ is applied to the surface of the dry membrane by a simple painting technique. After heating of the ‘ink’ on the membrane to dry the wet catalyst layer, further painting is

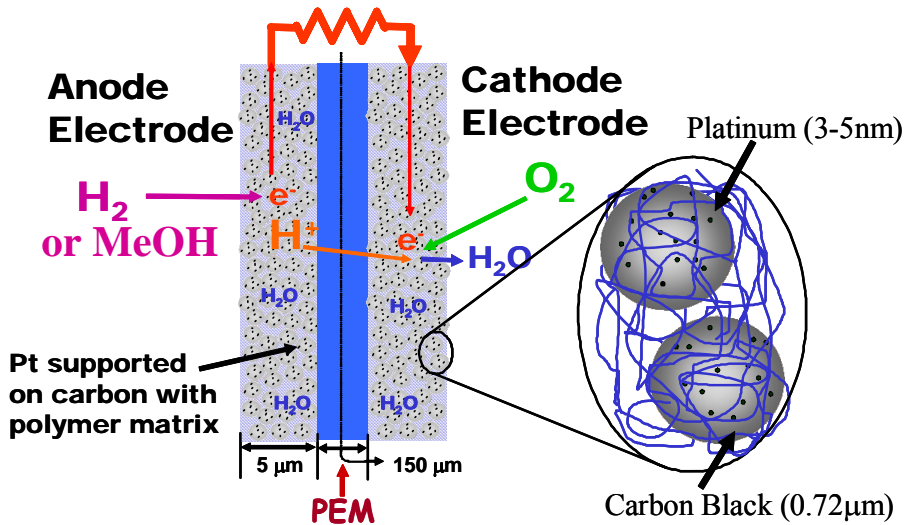
⁵³ Hickner, M. A. *PhD. Thesis*, VPI & SU, 2003.

⁵⁴ Appelby, A., *Scientific American* 1999, 74-79.

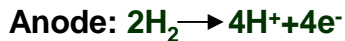
performed to obtain the correct amount of catalyst necessary for good fuel cell performance. The membrane is then turned over and the same procedure is repeated to the other side of the membrane. Rehydration and boiling in a dilute acid solution are the final steps in the production of the membrane electrode assembly, MEA.⁵⁵ After thorough rinsing in deionized water, the membrane electrode assembly is ready for fuel cell use. Another, more technologically based, process to produce MEAs is to use a hot press to aid in the adhesion of the electrode to the membrane. The first step in this technique is to prepare the ink as previously described for the painting technique. The ink is then painted onto a Teflon[®] - glass fiber reinforced decal and dried around 130 °C for ten minutes. Another coat of the ink is then painted in the opposite direction on the Teflon[®] decal. After the proper Pt loading is obtained (usually 6-8 coats), the decal electrodes are allowed to fully dry overnight at 130 °C. A pre-heated (210 °C) hot press is then used to adhere the electrodes to the membrane. When using Nafion[®] as the membrane, it must be transformed into the salt form by boiling in 1.0 M NaOH for one hour so as to increase the thermal stability. The MEA is assembled on backing plates and hot pressed for roughly 5 minutes at 200 psi. It is then removed from the hot press, allowed to cool and placed in water to fully rehydrate. The decals are then carefully removed. Reacidification is then performed to obtain the acid form MEA.⁵⁶

⁵⁵ Ren, X. and Gottesfeld, S., To The Regents of the University of California, U.S. 6,296,964, 1999.

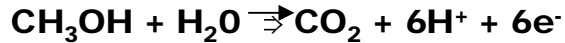
⁵⁶ M. A. Hickner, H. Ghassemi, Y. S. Kim, B. R. Einsla and J. E. McGrath, Chem. Rev. 2004, 104, 4587-4612.



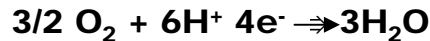
Electrochemistry



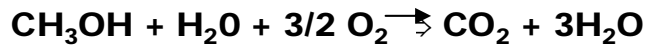
Anode Reaction



Cathode Reaction



Overall Reaction



Energy Source

H_2 from hydrocarbon fuel

O_2 from air

* Product: H_2O

Pt Catalyst



Figure 2.9 Membrane electrode assembly and electrochemistry for H_2/Air and methanol fuel cells

The backing layers, located next to both the anode and cathode, are made of a porous material that also conducts electrons away from the anode and back to the cathode. Carbon cloth about 100 to 300 microns in thickness is typically used as backing layers. In order to maximize the current that can be obtained from the MEA, the backing material must effectively and efficiently diffuse both the reactive gases to the

catalyst layers. The high concentration of gas that is present in the outer shell of the backing layer must be free to flow to the inner shell through the flow fields to a region of low concentration where the gas can then be consumed by the reaction with the Pt catalyst. The extremely porous nature of the backing material permits the gas to have intimate contact with the entire surface area of the anode and cathode parts of the membrane. Furthermore, the management of water during fuel cell operation is accomplished by the porous structure of the backing layers. The carbon cloth allows for the correct amount of water vapor to reach the MEA and regulate the correct state of hydration so that proton transport occurs efficiently. It also helps to remove the liquid water that is produced at the cathode so that the cell will not flood. In some instances, doping of the carbon cloth with Teflon is employed to provide a very slight hydrophobicity that ensures the pores will not be clogged with water.

Next to the backing layers are the current collectors, that also act as gas flow fields due to the flow channels that are machined or molded into the electron conducting material. The current collector/flow field plates are pressed tightly to the exterior surface of the backing layers. The plates are made of light but strong gas impermeable materials that help conduct the electrons away from the cell and allow for gas to flow freely to the backing layers. Historically, graphite or metal plates have been used as current collectors, but recently, graphite/polymer composites have been shown to have potentially better performance.⁵⁷ As can be observed in Figure 2.10, milled or molded flow fields provide gas to each MEA by systematically directing the gas through specific patterns. It has been observed that the type of pattern, including depth and width, account for large variations on the effectiveness of the reactant gas distribution.⁴⁸ Furthermore,

⁵⁷ Baird, D. G. *J. Power Sources*, Accepted, 2005.

the humidified gas must be evenly distributed to help humidification of the MEA and possibly dehumidification on the cathode side. The electrons that are produced by the cell must also be conducted away from the anode, therefore, as hydrogen reacts to form electrons and protons at the catalyst layer, they must pass through the anode, backing layer and current collector plate. The electrons are then conducted through an external circuit to re-enter the cell at the cathode plate, then through the backing layer and finally to the cathode catalyst sites for reaction with protons and oxygen. For single cell fuel cells, the two current collector plates are the final components that make up the cell. For cell stacks, bipolar plates and MEAs with backing layers are the repeat units so as to produce more electricity than a single fuel cell (Figure 2.11).

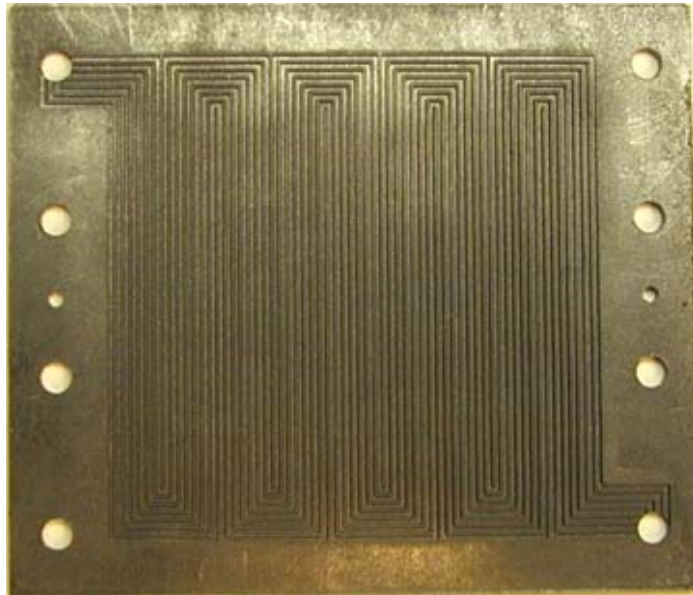


Figure 2.10 Bipolar plate showing pattern of gas flow channels

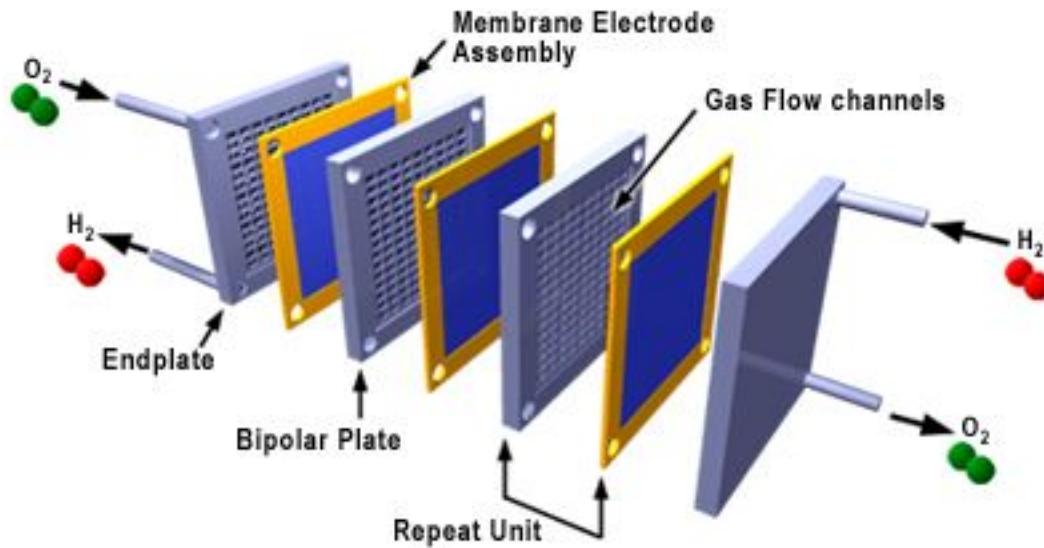


Figure 2.11 Schematic of a fuel cell stack consisting of the bipolar plate and MEA repeat units

Maximum available voltage that is possible from an H₂/air fuel cell can be expressed by determining energy differences between the initial and final state of the reactants, H₂+1/2 O₂ and H₂O respectively. The Gibbs free energy (ΔG) can be used to evaluate the thermodynamic functions of state that are associated with the energy differences. For an H₂/air fuel cell reaction (H₂ + 1/2 O₂ → H₂O), the maximum cell voltage (ΔE) at a determined temperature and pressure can be obtained [$\Delta E = - \Delta G/nF$], where n is the number of moles of electrons given off in the reaction per mole of H₂ gas and F is Faraday's constant (96,487 joules/volt (coulombs)), which is the transferred charge per mole of electrons. For example, the Gibbs free energy change, at 1 atmosphere of pressure, in a fuel cell process per mole of H₂ can be calculated using the reaction temperature, T, and changes in the reaction entropy (ΔS) and enthalpy (ΔH). If

the change in entropy and enthalpy is defined as $-285,800 \text{ J}$ and -163.2 J/K ,⁴³ respectively at 25°C , then:

$$\begin{aligned}\Delta G &= \Delta H - T\Delta S \\ &= -285,800 \text{ J} - (298\text{K})(-163.2 \text{ J/K}) \\ &= -237,200 \text{ J}\end{aligned}$$

The cell voltage, ΔE , can then be calculated at 1 atmosphere pressure and 298K.

$$\begin{aligned}\Delta E &= \Delta G/nF \\ &= (-237,200 \text{ J}/2 \times 96,487 \text{ J/V}) \\ &= 1.23\text{V}\end{aligned}$$

Increasing the temperature to 353K, 80°C , the values of ΔS and ΔH do not change much.

The only major change is the temperature. Therefore, assuming no change in ΔS and ΔH , ΔG decreases.

$$\begin{aligned}\Delta G &= -285,800 \text{ J/mol} - (353\text{K})(-163.2 \text{ J/molK}) \\ &= -228,200 \text{ J/mol}\end{aligned}$$

The cell voltage at the increased temperature can then be calculated.

$$\begin{aligned}\Delta E &= -(-228,200 \text{ J}/2 \times 96,487 \text{ J/V}) \\ &= 1.18\text{V}\end{aligned}$$

As can be observed, the cell voltage dropped with increasing temperature. Furthermore, a correction for air instead of pure oxygen must be taken into account and using humidified air and humidified hydrogen, not dry gases, decreases the maximum cell voltage to 1.16V at 80°C and 1 atm pressure in a hydrogen/air fuel cell.

The power (watts) that is produced by a cell can be calculated by multiplying the current drawn (I) by the terminal voltage (V) at that current.

$$P = I V$$

Furthermore, power can be expressed as the available energy per unit time, or rate of power available. For example, energy per unit time is the power in watt-hours.

$$P = E/t$$

The weight of the entire fuel cell also plays an important role in performance characteristics like specific power and power density.⁵⁸ The ratio of the amount of power produced to the mass of the cell is the specific power and the ratio of the power produced to the volume of the cell is the power density. Therefore, to maximize the specific power and power density, minimization of the weight and volume of the fuel cell must be accomplished.

Using the ideal fuel cell voltage of 1.16 volts at 1 atm pressure and 80 °C with zero current in as H₂/air cell, the energy conversion is that of chemical energy being transformed into both electrical energy and heat energy. Measurement of the efficiency of the energy conversion is the ratio of the experimental voltage to the theoretical voltage. If the cell is operating at 0.6 V, it is producing only 52% of electric energy and 48% of non-useful heat energy. However, when it is operating at 1.0 V, the fuel cell is 86% efficient and only 14% of the energy is lost due to heat. The voltage-current curve, or performance curve (Figure 2.12), represents the direct current (DC) voltage that is delivered to the cell terminals as a function of current density that is being drawn from the cell by a load in an external circuit.⁵⁹ The current density is expressed as the total current divided by the area of the membrane.

⁵⁸ Gottesfeld, S. *Polymer Electrolyte Fuel Cells*, Vol. 5, Wiley-VCH, 1997.

⁵⁹ Lakshmanan, B.; Huang, W.; Olmeijer, D. and Weidner, J. W. *Electrochemical and Solid State Letters*, 2003, 6(12), A282-A285.

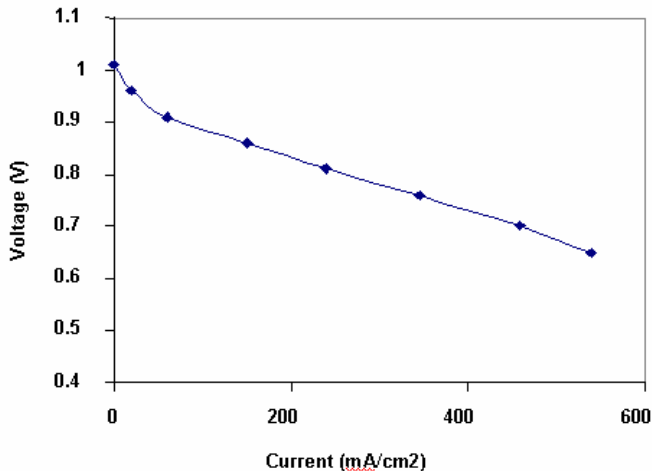


Figure 2.12 Plot of voltage vs. current density of a hydrogen/air PEMFC using Nafion[®]

2.6 Types of Fuel Cells for Electricity Production

Many types of fuel cells exist and are mainly classified by the electrolyte that is used. In general, five different types of fuel cells produce electricity through specific operation conditions and electrochemical reactions. Alkaline fuel cells, molten carbonate fuel cells, solid oxide fuel cells, phosphoric acid fuel cells and proton exchange membrane fuel cells are the five main types of devices that convert chemical energy to electrical energy.

Alkaline fuel cells^{60,61} employ an electrolyte that is a solution of water and potassium hydroxide (KOH) held in a porous stabilized matrix for use in specialized applications such as non-mobile power generation substations. The aqueous concentration of KOH can vary with the operating temperature, which ranges from 65 °C to 220 °C. The hydroxide (OH⁻) is the charge carrier, which migrates from the cathode to the anode where they react with hydrogen to produce water and electrons. The water that

⁶⁰ Appleby, A.J., *Energy* 1986, 11, 13.

⁶¹ Carrette, L.; Friedrich, K.A.; Stimming, U. *ChemPhysChem* 2000, 1,162.

is formed at the anode diffuses back to the cathode to regenerate the needed hydroxyl ions. The pressure inside the system⁶² is directly associated with the hydroxide concentration and the required temperature. The use of precious metals, like platinum, have been used and have shown to be influenced by the operating temperatures that dictate kinetics and possible poisoning. As is not the case with other types of fuel cells, carbon dioxide (CO₂), not carbon monoxide, reduces the electrolyte, hydroxide ion, concentration in the system thereby reducing the electrolyte conductivity.

The high-temperature molten carbonate fuel cells use higher operating temperatures to allow the use of natural gas directly without needing a fuel processor. Molten carbonate fuel cells use highly conductive molten salts and very high operating temperatures of 600 °C to 700 °C.^{63,64} The electrolyte is typically composed of a molten mixture of carbonate salts. The two mixtures that are currently used are lithium carbonate and potassium carbonate, and lithium carbonate and sodium carbonate. When these mixtures of carbonate salts are heated to a temperature of around 650°C, they melt and become conductive to carbonate ions (CO₃²⁻). The ions form water, carbon dioxide and electrons by flowing from the cathode to the anode where they combine with hydrogen. The electrons are then conducted through an external circuit back to the cathode, generating electricity and heat. The mixture of carbonates is retained inside the cell by employing a ceramic matrix of lithium aluminum oxide (LiAlO₂). At these high temperatures, electrocatalyst reactions can be obtained by using a less expensive nickel

⁶² Bockris, J. O'M.; Appleby, A.J., *Energy* 1986, 11, 95.

⁶³ Minh, N, in *High Temperature Fuel Cells*, *Chemtech* 1991, 21 (1), 32-37.

⁶⁴ Selman, R.J, *Energy* 1986, 11, 153.

catalyst. However, loss of efficiency can occur even at these high temperatures due to contamination of the nickel from compounds such as HCl, H₂S, H₂Se and As.⁶⁵

Solid oxide fuel cells are typically used for stationary power production at generation and co-generation facilities including industrial and large-scale central-electricity generating-stations. They conduct protons by employing oxygen ions at an extremely high temperature range of 650 °C – 1000 °C, which allows a number of fuels to be used. The electrolyte is a solid, thin ceramic material (solid oxide) that is conductive only to oxygen ions (O²⁻) and is typically made of yttrium oxide (Y₂O₃) with zirconium oxide (ZrO₂) alloys.⁶⁶ The oxygen molecules from the air stream are split into oxygen ions at the cathode with the addition of four electrons. The oxygen ions are conducted through the solid, ceramic electrolyte and combine with hydrogen at the anode, which releases four electrons. The electrons travel through an external circuit providing electric power and producing heat. A Co-ZrO₂ or Ni-ZrO₂ cement is generally used as the anode and a Sr-doped LaMnO₃⁵ is used as the cathode.⁶¹ Because of the high temperatures, fast kinetics of the half reactions occur without precious metal catalysts.⁶⁷ Limitations include the high temperature requirements and the brittle mechanical properties of the materials.

Phosphoric acid fuel cells are used for applications like stationary and utility power devices that could be used to power houses and buildings. The phosphoric acid fuel cell was the first energy producing fuel cell to be commercialized. The development in the mid-1960s and field-testing since the 1970s have improved the overall performance and has significantly enhanced the stability, while attaining a relatively low cost.

⁶⁵ Kinoshita, K.; McLarnon, F.; Cairns, E., *Fuel Cells, A Handbook*, Lawrence Berkeley Laboratory, 1988.

⁶⁶ Carrette, L.; Friedrich, K.A.; Stimming, U. *Fuel Cells* 2001, 1(1), 5.

⁶⁷ Minh, N. *J. Am. Ceram. Soc.* 1993, 76(3) 563-588.

Phosphoric acid fuel cells use a silicon carbide matrix that contains concentrated phosphoric acid (H_3PO_4), which can reach 100%, as the electrolyte. Temperature ranges of 150 °C to 220 °C are the typical use temperatures for phosphoric acid fuel cells.⁴⁵ The proton conductivity of phosphoric acid is decreased dramatically at temperatures below this range; furthermore, poisoning of the platinum electrocatalyst⁶⁸ by carbon monoxide (CO) occurs below 110°C. Using alloys of platinum, such as ruthenium-platinum, as the electrochemical catalyst has been investigated and has shown increased tolerance to CO poisoning. The major hurdle of the phosphoric acid fuel cell in application is the gradual leakage of the phosphoric acid in the system components.⁶⁹

The proton exchange membrane fuel cell (PEMFC) has recently been shown to be the most promising of all the fuel cell types for applications such as automobiles, stationary power and power for small electronics such as laptop computers and cell phones.⁷⁰ Also known as the polymer electrolyte fuel cell, PEMFCs can be adapted to specific sizes, weights, operating temperatures and power generation. A solid polymeric membrane containing ionic groups is responsible for the proton transport from the anode to the cathode. The state-of- art proton exchange membrane (PEM) is a product of DuPont and is termed Nafion[®] (Figure 2.13), which is a poly(perfluorosulfonic acid) copolymer.⁷¹

⁶⁸ Beard, B.C.; Ross, P.N., *J. Electrochem. Soc.* 1986, 133, 1839.

⁶⁹ Glass, J.T.; Cahen, G.L.; Stoner, G.E.; Taylor, E.J., *J. Electrochem. Soc.* 1987, 134, 58.

⁷⁰ Korgesch, K.; Simader, G., *Fuel Cells and Their Applications*, Wiley-VCH, Weinheim, 1996.

⁷¹ Grot, W., To E.I. du Pont de Nemours and Company, U.S. 3,718,627, 1968.

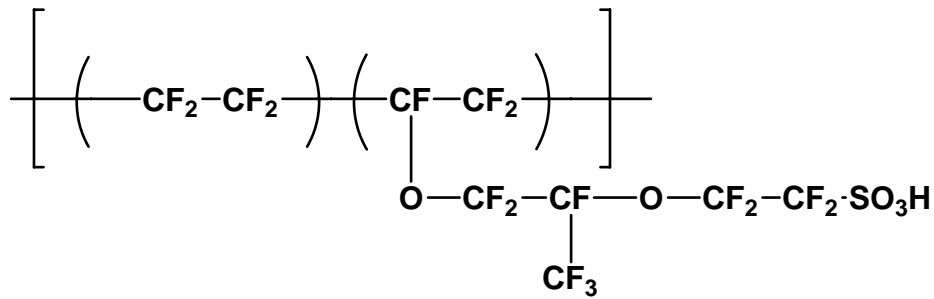
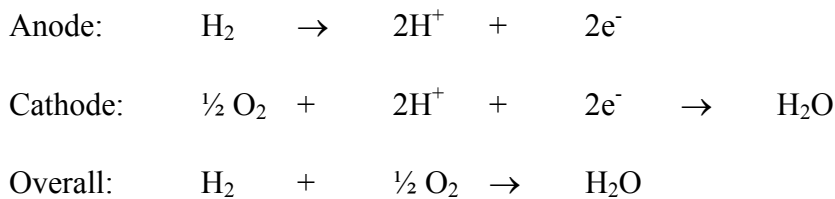


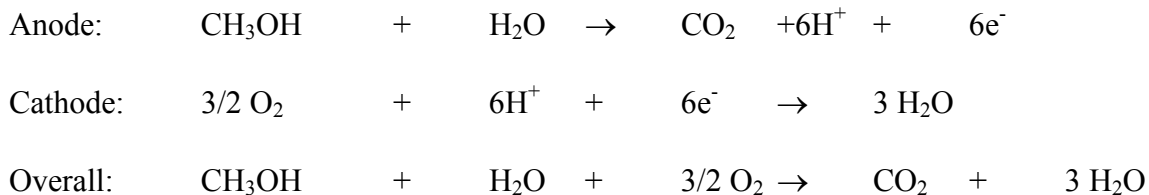
Figure 2.13 Chemical structure of Nafion[®] by DuPont

Specific water transport mechanisms are responsible for the proton transport, which indicates that the membranes must be humidified for good fuel cell performance. Operation temperatures are currently ranging from 30 °C to 100 °C.⁶⁶ The upper limiting temperature is a result of the mechanical characteristics of the Nafion[®] type membrane and the associated water loss that occurs at temperatures above 100 °C.⁷² As is similar to the phosphoric acid type fuel cells, the half reactions of the PEMFCs are as follows when using hydrogen and oxygen as the fuel oxidant, termed hydrogen/air PEMFC.



When using aqueous methanol as the fuel, the direct methanol fuel cell (DMFC) uses different electrochemical reactions that include the oxidation of the aqueous methanol fuel.

⁷² Savadogo, O., *J. New Mat. Electrochim. Sys.* 1998, 1, 47.

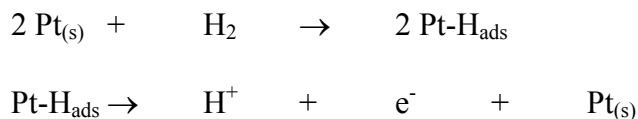


Many advantages exist for the direct methanol fuel cell (DMFC). Modifying or building a new infrastructure would be much easier relative to hydrogen gas storage where the liquid nature of methanol can be easily handled. Exceedingly, systems employing the direct methanol fuel cell do not require the large and expensive hydrogen storage or reforming subsystems. Furthermore, the oxidation of methanol at the anode is a facile process from the methanol/water solution (0.5 – 2 M) that is fed to the anode. The low concentration of methanol that is fed to the anode is directly related to the methanol permeation of the PEM. When the concentration of methanol is relatively low at the anode, unoxidized methanol is less likely to diffuse to the cathode and create a backflux of protons by oxidation at the cathode. The current state-of-the-art Nafion[®] membrane has extremely high methanol permeability⁷³, which decreases the overall efficiency of the fuel cell. Therefore, intense investigations have begun to develop a membrane that can withstand the methanol PEMFC environment, have good proton conductivity and have very low methanol permeability.

Reduction and oxidation reactions at the anode and cathode must be efficient in the cell to have overall efficiency that produces maximum power. These efficient redox reactions in the fuel cell require the use of precious metals, like platinum, and its alloys,

⁷³ Wasmus, S.; Kuever, A. J. *Electroanal. Chem.*, 1999, 461, 14.

such as platinum/ruthenium, as catalysts. A rate constant of 10^{-5} s^{-1} has been reported for the oxidation of hydrogen using platinum.⁷⁴ As can be seen below, proficient hydrogen oxidation reactions can be obtained by using solid platinum catalysts, $\text{Pt}_{(s)}$, and adsorbed hydrogen, H_{ads} .



Using platinum as the electrocatalyst has one major drawback besides cost; the active sites are readily poisoned with carbon monoxide.⁷⁵ A temperature dependant poisoning of the solid catalyst has been observed in previous research. By reducing the number of active sites on the surface of the platinum, hydrogen gas cannot be oxidized in an efficient manner, thereby reducing the efficiency of the overall cell. As was stated earlier, alloys of platinum have been investigated. These types of solid electrocatalysts, platinum-molybdenum, platinum-ruthenium, Pt-nickel, Pt-cobalt and Pt-alumina, have shown to be much more resistant to carbon monoxide poisoning.^{76,77} The use of some of the alloys at low temperatures can aid in oxidation of the carbon monoxide to carbon dioxide, thereby producing a lower adsorption energy for carbon dioxide relative to carbon monoxide and successfully removing the carbon monoxide from the system. Due to the temperature dependant nature of the poisoning of Pt by CO, increasing the operating temperature of the fuel cell to temperatures above 100 °C can reverse the CO

⁷⁴ Barber, J.; Morin, S.; Conway, B.E., *Electrochem. Soc. Proc.* 1997, 97, 101.

⁷⁵ Oetjen, H.-F.; Schmidt, V.M.; Stimming, U.; Trila, F., *J. Electrochem. Soc.* 1996, 143, 3838.

⁷⁶ Watanabe, M.; Uchida, M.; Motoo, S., *J. Electroanal. Chem.* 1987, 229, 395.

⁷⁷ Ley, K.L.; Liu, R.; Pu, C.; Fan, Q.; Leyarovska, N.; Segre, C.; Smotkin, E.S., *J. Electrochem. Soc.* 1997, 144, 1543.

binding. At these high temperatures, the rate at which CO adsorbs is slower than the rate at which it desorbs.⁷⁸ However, at these high temperatures, the state-of-the-art Nafion[®] membrane loses its mechanical properties and thus the efficiency of the fuel cell drops off dramatically. Furthermore, above the boiling point of water, the humidity in the cell decreases to less than 100% at atmospheric pressure and the water transport mechanisms that are responsible for the proton transport across the membrane are greatly decreased due to a lower humidification in the membrane. The proton conductivity of the negatively charged polymer electrolyte membranes, that are poor proton conductors unless water is absorbed, increases with water content from values of 10^{-4} S/cm to values of 10^{-1} S/cm. Therefore, concentrated investigations in producing alternative membranes for use in hydrogen/air PEMFCs that can operate at high temperatures, above 100 °C, has recently been a major thrust on the forefront of fuel cell research.^{8,5,8}

As is the case with the methanol fuel cell membrane, the hydrogen fuel cell membrane has specific hurdles to overcome before mass production. For the direct methanol fuel cell, the membrane must be mechanically robust at 80 °C, have high proton conductivity, no electronic conductivity (insulator) and must be methanol impermeable to a point. The hydrogen fuel cell membrane must be able to perform well at temperatures above 100 °C where little water is present and carbon monoxide does not poison the Pt catalyst. Furthermore, the current high cost (\$800/m²) of the state-of-the-art Nafion[®] membrane does not permit low cost production of the fuel cell system. Therefore, the investigation to produce less expensive materials for use in both methanol and hydrogen/air PEMFCs has been at the forefront of polymer fuel cell research.

⁷⁸ Kerres, J.A., *J. Membr. Sci.* 2001, 185 (1), 3.

2.7 Protonically Conductive Ion Exchange Membranes

The PEM membrane must have specific characteristics that will allow proton transport in an acidic fuel cell environment. Some of these characteristics are: good mechanical, chemical, thermal and electrochemical stability at elevated temperatures; compatibility with interfacial components like the electrodes; low permeability and high proton conductivity while being humidified and a relatively low cost. Many research groups across the world are working to develop such membranes that could replace the expensive perfluoro sulfonated copolymers, Nafion[®], and this section will describe some proposed copolymers that could be used as proton exchange membranes in fuel cells.

2.8 Post-Sulfonation of Polymeric Materials

Polymers based on aromatic backbones that contain specific linkages like sulfones, thioethers, ethers and ketones can be generally characterized by having good thermal, mechanical and chemical properties and allow for tough ductile films to be cast from high molecular weight polymers. These engineering thermoplastics can be used for applications such as electronics, coatings and films. Polymers based on polyimides, poly(arylene thioethers), poly(arylene ethers) and polyarylates allow sulfonation to occur on the aromatic rings of the backbone through electrophilic aromatic substitution. These sulfonate moieties can then be used in ion transport applications. Therefore, industrially available materials (e. g. Udel[®]) can be functionalized for other applications than was originally proposed.^{79,80} The post sulfonation reaction of various materials will be discussed in the next section.

⁷⁹ Kerres, D.; Cui, W.; Reichle, S. *J. Polym. Sci.: Part A*, 1996, 34, 2421.

⁸⁰ Kreuer, K. D. *J. Membr. Sci.*, 2001, 185, 29.

2.9 Post-Sulfonation of Poly(arylene ether)s

Polyethers have become less and less expensive as the uses and volumes of production increase. The low cost and ease of processing have permitted many research groups all over the globe to focus on their properties and characteristics.^{81,82} Although many other structures of polyethers are available, two major types of poly(arylene ether)s exist. The first is the commercially available poly(ether sulfone), termed Udel[®], and the second is the commercially available wholly aromatic, poly(ether ether ketone) or PEEK. The use of partially aliphatic Udel[®] as ion exchange film was first reported used for desalination after the post-sulfonation reaction.⁸³ One of the early sulfonation techniques used chlorosulfonic acid at room temperature in an electrophilic aromatic substitution reaction that produced ionic groups along the backbone of Udel[®] (Figure 2.14).⁸⁴

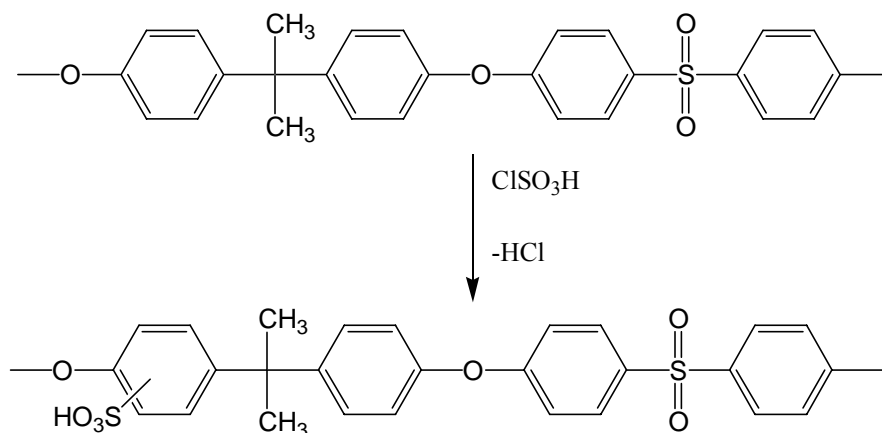


Figure 2.14 Post-sulfonation of Udel[®] polyether sulfone using chlorosulfonic acid

⁸¹ Hasiotis, C.; Deimede, V.; Kontoyannis, C. *Electrochim. Acta*, 2001, 46, 2401.

⁸² Genova-Dimitrova, P.; Baradie, B.; Foscallo, D.; Poinsignon, C. and Sanchez, J. Y. *J. Membr. Sci.*, 2001, 185, 59.

⁸³ Brousse, C.L.; Cheapurlet, R. and Quentin, J.P., *Desalination* 1976, 18, 137.

⁸⁴ Bailly, C.; Williams, D. J.; Karasz, F. E. and MacKnight, W. J. *Polymer*, 1987, 28, 1009.

The level of sulfonation was controlled by varying the time of reaction where the longer reaction time yielded a higher degree of sulfonation. This relatively harsh method of sulfonation had side reactions that produced chain scission, chain branching and cross-linking partially due to the unstable nature of the isopropylidene moiety of the bisphenol based polymer in these types of environments. A milder sulfonation technique was developed that incorporated sulfur trioxide and triethyl phosphate.^{85,86} This technique has proven to mostly eliminate the detrimental side reactions that were observed using chlorosulfonic acid. The use of sulfur trioxide in an organosulfur reaction to sulfonate organic molecules has aided in the functionalization of macromolecules.⁸⁷ Because sulfur trioxide contains three oxygen molecules double-bonded to a sulfur atom, its reactivity during electrophilic aromatic substitution reactions has been observed to be better than that of concentrated sulfuric acid.⁸⁸ When sulfonating a polymer chain, it was found that clustering of the ionic groups occurred. Therefore, sulfur trioxide and triethyl phosphate complex was developed to produce a lower clustering effect of ionic groups on the polymer structure by helping to shield the sulfonate moieties during post-sulfonation reactions.

Another method of post sulfonation was developed that incorporated chlorotrimethylsilyl sulfonate that was produced from the insitu reaction of chlorosulfonic acid with trimethyl chlorosilane in 1,2-dichloromethane at 22 °C.⁸⁹ This

⁸⁵ Johnson, B. C.; Yilgor, I.; Tran, C.; Iqbal, M.; Wightman, J. P.; Lloyd, D. R. and McGrath, J. E. *J. Appl. Polym. Sci.*, 1984, 22, 721.

⁸⁶ Noshay, A. and Robeson, L. M. *J. Appl. Poly. Sci.* 1976, 20, 1885.

⁸⁷ Cremllyn, R.J., In *An Introduction to Organosulfur Chemistry*, John Wiley & Sons: New York, 1996.

⁸⁸ Litter, M. I. and Marvel, C. S. *J. Polym. Sci.*, 1985, 23, 2205.

⁸⁹ Nolte, R.; Ledjeff, K.; Bauer, M. and Mulhaupt, R. *J. Membr. Sci.*, 1993, 83, 211.

was first reported in the patent literature by Kelsey.⁹⁰ These researchers used the commercially available Udel[®], poly(arylene ether sulfone), material and varied the time of reaction and concentration of sulfonating agent to polymer in order to control the degree of sulfonation. At high degrees of sulfonation, a large amount of swelling in water was observed. Therefore, using the sulfonic acid moieties to crosslink the polymer chains (in unknown ways) was performed to produce films that had lower water swelling but also lower proton conductivity. Reaction of the pendant sulfonic acid groups with 1,1'-carbonyl diimidazole produced an activated N-sulfonyl imidazole moiety. This functional group was then reacted with aliphatic diamines to produce the crosslinked polymer structure. The decreased degree of sulfonation by using the -SO₃ groups for crosslinking was the reason for the decreased conductivity; however, the conductivity was reported to be at appreciable levels for use as PEMs in fuel cells.

All of the described post-sulfonation processes have produced sulfonic acid functionalized polymers, but they also lack control and reproducibility. The use of chlorosulfonic acid and sulfur trioxide complexed with triethylphosphate were found to sulfonate the activated ring of the poly(arylene ether sulfone) polymers on the bisphenol A ring. This position is ortho- to the ether linkage, which is electron donating. Furthermore, the post-sulfonation was found to mono-substitute each repeat unit. The main problem with this type of sulfonated polymer is that in strong acid environments, the sulfonic acid attached to the activated isopropylidene containing bisphenol A ring can have a lower hydrolytic stability and possibly also desulfonate. Therefore, research was performed to produce a post-sulfonation reaction that placed the sulfonic acid group on

⁹⁰ Chao, H. S.; Kelsey, D. R., Process for preparing sulfonated poly(arylether) resins, U.S. 4,625,000 to Union Carbide, November 25, 1986.

the deactivated ring ortho- to the sulfone moiety.⁷⁹ The process started with the cryogenic deprotonation of Udel[®] using n-butyllithium. The lithiated product was then reacted with sulfur dioxide and further oxidation/hydrolysis to produce the sulfonic acid on the deactivated aryl ring ortho- to the electron withdrawing sulfone group. However, as with the other post-sulfonation routes, this process was also difficult to control the degree of sulfonation in reproducible conditions.

The addition of pendant phenyl rings on the backbone of poly(arylene ether sulfones)s has recently shown sulfonation or phosphonation to occur on the pendant ring and not the backbone.⁹¹ Under fuel cell conditions, these pendant ring sulfonic acid moieties were found to be more stable than the main chain sulfonic acid moieties that were located on the activated backbone ring next to the ether linkage. The pendant rings were sulfonated with chlorosulfonic acid in methylene chloride at 25 °C for varying times to control the extent of sulfonation.

2.10 Post-Sulfonation of Poly(arylene ether ketone)s

Poly(arylene ether ketone)s based on hydroquinone are used for extremely diverse applications due to the semi-crystallinity of the processed polymer. Due to the crystal structure, insolubility in polar solvents makes post-sulfonation relatively difficult and heterogeneous. However, post-sulfonation of poly(arylene ether ketone)s has been performed and has been reported to produce sulfonated polymers that may still contain some crystallinity.⁹² PEEK has great thermal stability, chemical resistance and mechanical properties and post-sulfonation reactions produce a film for use in a fuel cell

⁹¹ Miyatake, K. and Hay, A. S. *J. Polym. Sci.: Part A: Polym. Chem.*, 2001, 39, 1854.

⁹² Trotta, F.; Drioli, E.; Moraglio, G. and Poma, E. B. *J. Polym. Sci.*, 1998, 70, 477.

has been of great interest.^{93,94} It was reported that concentrated sulfuric acid is the best sulfonation agent for PEEK because fuming sulfuric acid and chlorosulfonic acid degrade the polymer backbone.⁹⁵ After the sulfonic acid moieties have been added to the polymer backbone, the crystallinity decreases and the solubility increases, therefore allowing further characterization. The degree of sulfonation can be controlled by varying the time of reaction, temperature of reaction and concentration of sulfuric acid in water. Sulfonated PEEK (SPEEK) has been synthesized at sulfonation levels of 30 – 100 mol %.⁹⁶ However, the heterogeneity of the reaction in sulfuric acid causes difficulty in the reproducibility from one experiment to another. The rate of post-sulfonation of semi-crystalline polymers is directly related to the dissolution of the crystalline phase.

When comparing the poly(perfluorosulfonic acid) PEMs with sulfonated poly(ether ether ketone) PEMs, two major differences are observed. The first is the differences of the specific sulfonic acid groups. Membranes such as Nafion[®] have a stronger acid than SPEEK due to the electron withdrawing effects of the fluorine groups adjacent to the SO₃ groups. The pK_a of the poly(perfluorosulfonic acid) membranes has been reported to be about -6, while an aromatic sulfonic acid in polymers such as SPEEK is about -1.⁹⁷ Therefore, membranes such as Nafion[®] can have a lower concentration of sulfonic acid moieties relative to membranes similar to SPEEK and possibly still have the same conductivity under similar conditions. The second difference between sulfonated poly(fluorosulfonic acid) membranes and sulfonated poly(arylene ether) membranes is

⁹³ Bishop, M.T.; Karasz, F.E., Russo, P.S., *Macromolecules* 1985, 18, 86.

⁹⁴ Devaux, J.; Delimov, D.; Daousti, D.; Legras, R.; Mercier, J.P.; Strazielle, C.; Nield, E., *Polymer* 1985, 26, 1994.

⁹⁵ Kobayashi, T.; Rikukawa, M.; Sanui, K.; Ogata, N. *Solid State Ionics*, 1998, 106, 219.

⁹⁶ Shibuya, N. and Porter, R. S. *Macromolecules*, 1992, 25, 6495.

⁹⁷ Li, Q.; He, R.; Jensen, J. E. and Bjerrum, N. J. *Chem. Mater.*, 2003, 15, 4896.

the microstructural characteristics of the hydrophobic and hydrophilic domains. Perhaps because of a stiffer polymer backbone and decreased polarity between the acid group and the backbone of the SPEEK membranes relative to the Nafion[®] type membranes, the hydrophilic domains are smaller in the SPEEK membranes.⁸⁰

2.11 Post-Sulfonated Polystyrene

One of the earliest uses of PEM fuel cell technology was the Gemini space program that incorporated crosslinked polystyrene sulfonic acid membranes.⁹⁸ Previous to this use, sulfonated crosslinked polystyrene was used for ion exchange columns and water purification membranes.⁹⁹ Durability of the sulfonated polystyrene became an issue when fuel cell performance decreased as operating times became longer on the Gemini space craft. The suspected degradation mechanism was the attack of the tertiary aromatic carbon by hydroxy radicals.¹⁰⁰ It has been proposed that the hydroxy radicals are produced by the reaction of a hydrogen atom from the fuel with oxygen in the oxidizer.¹⁰¹ Since polystyrene is relatively inexpensive and widely studied, many researchers have devised novel methods for producing sulfonated polystyrene that could withstand the fuel cell environment for longer periods of time.¹⁰² One technique is to induce cross-linking or grafting on unsulfonated polystyrene with sulfonated polystyrene.¹⁰³ The use of these ionomers to induce phase separation with ionizable groups has been studied for decades and is the rationalization for using sulfonate

⁹⁸ Scott, D. S. and Hafele, W. *J. Hydrogen Energy*, 1990, 15, 10.

⁹⁹ Wiley, R. H.; Venkatachalam, T. K. *J. Polym. Sci.: Part A*, 1966, 4, 1892.

¹⁰⁰ Okada, O.; Yokoyama, K. *Fuel Cells*, 2001, 1, 72.

¹⁰¹ Wiley, R. H.; Venkatachalam, T. K. *J. Polym. Sci.: Part A*, 1965, 3, 1063.

¹⁰² Hong, L.; Chen, N. *J. Polym. Sci.: Part B*, 2000, 38, 1530.

¹⁰³ Glipa, X.; Haddad, M. E.; Jones, D. J.; Rozier, J. *Solid State Ionics*, 1997, 97, 323.

containing moieties.^{104,105} Random and block copolymers, such as tri-block copolymers based on sulfonated styrene-co-ethylene-co-butylene (SEB) post-sulfonated materials (Figure 2.15), have shown high conductivities and perhaps acceptable fuel cell characteristics.^{106,107,108} Therefore, the SEB materials can be reacted with a sulfonate containing material through electrophilic aromatic substitution to produce the sulfonated form of the tri-block copolymer. As has been previously discussed, decreased stability of these post-sulfonated materials can be attributed to the sulfonic acid groups being in the activated, electronegative, site on the phenyl ring. Therefore, loss of the sulfonic acid groups has been proposed to occur during increased temperatures in the fuel cell environment.

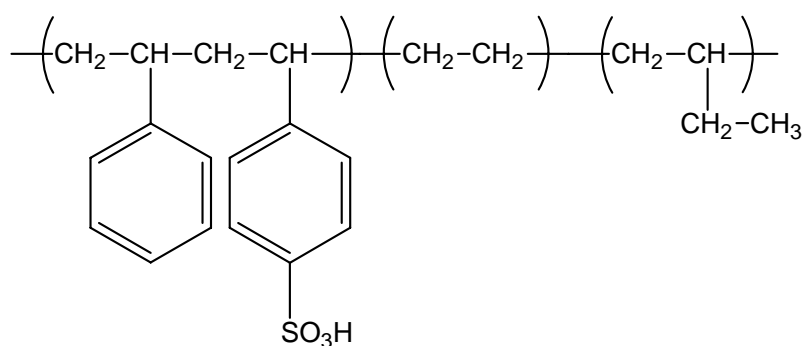


Figure 2.15 sulfonated styrene-co-ethylene-co-butylene (SEB) post-sulfonated materials

Ballard Advanced Materials Corp. has reportedly developed a polystyrene analogue that shows good stability relative to the state of the art Nafion[®] type

¹⁰⁴ Gupta, B.; Scherer, G. G. *J. Appl. Polym. Sci.*, 1993, 50, 2129.

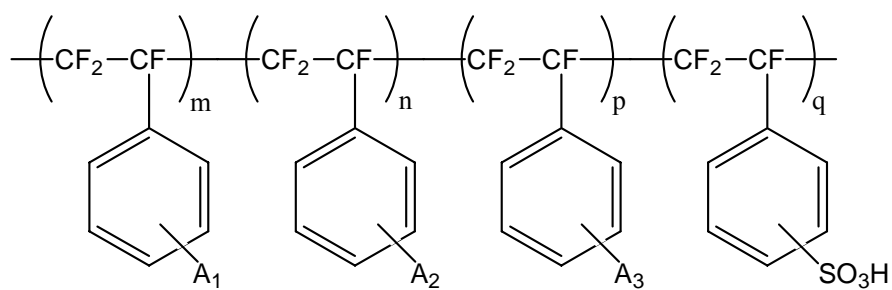
¹⁰⁵ Gupta, B.; Schere, G. G. *Chimia*, 1994, 48, 127.

¹⁰⁶ Gupta, B.; Buechi, F. N.; Scherer, G. G. Chapiro, A. *Polym. Adv. Technol.*, 1994, 5, 493.

¹⁰⁷ Ehrenberg, S. G.; Serpico, J. M.; Sheikh, B. M.; Tangredi, T. N.; Zador, E. and Wnek, G. E. *2nd International Symposium Proceedings on New Materials for Fuel Cells*, Montreal, Canada, 1997, 224.

¹⁰⁸ Serpico, J. M., Ehrenberg, S. G., Fontanella, J. J., Jiano, X., Perahia, D., McGrady, K. A., Sanders, E. H., Kellog, G. E. and Wnek, G. E. *Macromolecules*, 2002, 35, 5916.

membrane.¹⁰⁹ The membrane is composed of a perfluorosulfonic acid system that uses α , β , β -trifluorostyrene monomers with different pendent groups on the phenyl ring (Figure 2.16). This third generation Ballard Advanced Material membrane has shown good proton conductivity (0.079 S/cm) and prolonged stability of over 100,000 hours. Mechanical properties have not been reported.



at least 2 of m, n, p, q, are integers > 0

$A_1, A_2, A_3 =$ alkyls, halogens, O-R, $\text{CF}=\text{CF}_2$, CN, NO_2 , OH

Figure 2.16 Ballard Advanced Materials, BAM3G, reported chemical structure

2.12 Various Polyperfluorinated Copolymers

Nafion[®] (Figure 13) was developed by E. I. Dupont de Nemours in 1966 for the space program and has apparently undergone very little change over the past four decades. The polymer has a fluoro aliphatic Teflon[®]-like backbone that can resist chemically active and thermally unstable environments. The $-\text{CF}_2-\text{SO}_3\text{H}$ acid site is considered to be a super acid due to the pendent group being bonded to a carbon atom

¹⁰⁹ Wei, J.; Stone, C.; Steck, A.E., Issued to Ballard Inc., *US Patent 5,422,411* (1995).

that is bound to the electronegative fluorine atom.¹¹⁰ High stability of the CF groups has been confirmed in strong acids, strong oxidizers and strong reducers. Lifetime tests in the fuel cell environment of the Nafion[®] copolymer has indicated a lifetime of over 50,000 hours at 80 °C at 100 %RH, which has led researchers and the world to have increased confidence in the PEM fuel cell for alternative energy sources.¹¹¹ The base polymer of most commercially available PEMs and membrane electrode assemblies incorporate the current state-of-the-art Nafion[®] membrane copolymers. A large amount of literature and research in the fuel cell research population has been devoted to Nafion[®], including published papers, reviews and books.^{112,113,114} Furthermore, composites of Nafion[®] with inert PTFE matrices like Gore membranes or inorganic additives like heteropolyacids have been shown to improve the physical and electrochemical characteristics. Reinforcing the Nafion[®] membranes with Teflon[®] or Gore-Tex[®] fabric has produced thinner films that have increased conductivity and mechanical properties.¹¹⁵ However, it has also increased permeability to methanol, which decreases fuel efficiency and overall performance in a direct methanol fuel cell.

There are three specific drawbacks to Nafion[®]. The first is the cost to the consumer, which is about \$700-\$800 per square meter, the second is its performance at temperatures above 100 °C where it dehumidifies and the third is the methanol permeability. By increasing the fuel cell temperatures, reaction kinetics and carbon monoxide poisoning

¹¹⁰ Gottesfeld, S.; Zawodzinski, T. A.; In *Advances in Electrochemical Science and Engineering*; Alkire, R. C.; Gerischer, H.; Kolb, D. M.; Tobias, C. W., Eds.; Wiley-VCH; Weinheim Germany, 1997, 5, 195.

¹¹¹ Costamagna, P. and Srinivasan, S. *J. Power Sources*, 2001, 102, 242.

¹¹² Pourcelly, G.; Gavach, C. *Proton Conductors, Solids, Membranes and Gels-Materials and Devices*, Colomban, P., Ed.; Cambridge University Press: New York, 1992.

¹¹³ Heitner-Wirguim, C. *J. Membr. Sci.*, 1996, 120, 1.

¹¹⁴ Grot, W. G. *Macromol. Symp.*, 1994, 82, 161.

¹¹⁵ Doyle, M. and Rajendran, G. In *Handbook of Fuel Cells*, Vielstich, W.; Lamm, A. and Gasteiger, H. A., Eds.; John Wiley & Sons Ltd.: New York, 2003, 3.

can be improved. The high cost of the perfluorosulfonic acid copolymer is mainly due to the relatively expensive fluorination process. The specialty co-monomers that are needed in such a copolymer are, in general, the main reason for the high cost. Literature observed in the patent material for both Dow XUS[®] (Figure 17) and Nafion[®] suggest that perfluorinated copolymers are synthesized in the sulfonyl fluoride form and then converted into the acid form after processing into membranes.⁷² The synthesis of the copolymer can be generalized into four different steps.

1. Reaction of tetrafluoroethylene with SO₃ (fuming sulfuric acid) to form the cyclic sulfone.
2. Condensation of the products with sodium carbonate followed by free radical copolymerization with tetrafluoroethylene, which forms an insoluble semi-crystalline but melt extrudable resin.
3. Alkaline hydrolysis of the extruded film to produce a perfluorosulfonic copolymer
4. Counterion exchange of sodium to form the proton form of the salt copolymer.

The equivalent weights (EWs) of Nafion[®] can be varied by changing the ratio of the unsulfonated repeat unit (tetrafluoroethylene) with the sulfonated repeat unit. Therefore, presumably statistical copolymers with varying EWs (800-1500) have been synthesized. The equivalent weight is measured by defining the grams of polymer per mole of fixed SO₃ groups. Therefore, Nafion[®] 112 is defined as 1100 equivalent weight (milli-equivalents of sulfonic acid per gram of polymer) and 2 mil thick (~51 microns).

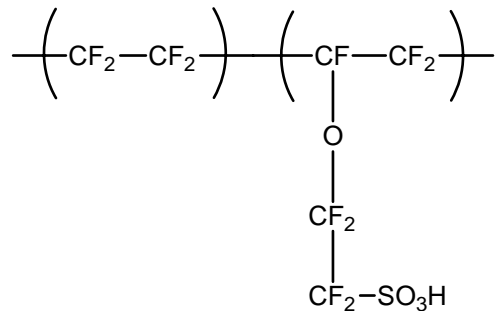


Figure 2.17 Proposed structure of Dow XUS[®] perfluorinated copolymer

Other perfluorinated copolymers have been at times produced by Dow Chemical, Aciplex and Asahi Chemical. The Dow material (Figure 2.17) has been termed Dow XUS[®] and was sold as 2 mil thick membranes with lower equivalent weights than that of Nafion[®].¹¹⁶ Therefore, it has more pendant sulfonic acid groups per gram of polymer. The Nafion[®] membranes can be obtained in varying thickness (2 mil, 3.5 mil, 7 mil and 10 mil) and is available mainly in 1100 EW, which corresponds to about 13 mole percent of sulfonated comonomer. The Dow XUS[®] membrane could have better performance in various fuel cell tests due to its higher concentration of proton exchange sites in a thinner membrane. These types of perfluorinated copolymers can be melt processed in the sulfonyl fluoride form and then hydrolyzed and acidified by sulfuric acid techniques.

Nafion[®] and similar polyperfluorinated membranes have semi-crystallinity, which can be related to the relatively low water swelling (20-30%) and water insolubility.¹¹⁷ Equivalent weights of 1000 or higher contain crystalline domains that are a product of the tetrafluoroethylene sequences similar to that of Teflon[®]. The ratio of the sulfonated comonomer to the unsulfonated tetrafluoroethylene comonomer is directly responsible

¹¹⁶ Ezzell, B.R.; Carl, W.P.; Mod, W.A., *US Patent 4,358,412*, 1982.

¹¹⁷ Gierke, T.D.; Munn, G.E.; Wilson, F.C., *J. Polym. Sci., Polym. Phys. Ed.*, 1981, 19, 1687.

for the amount of crystallinity. At equivalent weights of less than 1000, the amount of crystallinity decreases to almost zero and hydrophilicity increases. Ionic domain and phase separation are other important characteristics of Nafion[®] and the other perfluorinated membranes. Due to the flexible backbone of the polymer and the hydrophobicity of the fluorine atoms, aggregation of the sulfonic acid side chains, which are hydrophilic, is achieved.^{118,119}

2.13 Other Commercially Available Proton Exchange Membranes

Commercial alternatives to the state-of-the-art Nafion[®] membranes are few, but some do exist. Ballard Advanced Materials, Dias Analytical and W. L. Gore & Associates have all produced commercial PEMs.

W. L. Gore and Associates produce both membranes and MEAs for commercial resale.¹²⁰ The GORE-SELECT[®] membranes are reportedly based on Nafion[®] membranes but the membranes are supported with porous GORE-TEX[®] material making them thinner and mechanically stronger.¹²¹ Since GORE-TEX[®] and Nafion[®] are both fluorinated polymers, the compatibility of the two materials is probably relatively good.¹²² However, Nafion[®] swells in aqueous environments and GORE-TEX[®] does not. This could cause delamination of the Nafion[®] from the GORE-TEX[®] and increase the resistance of the ions of the composite material. Because the Nafion[®] material is used in only minimal quantities, the cost and thickness of the membranes decreases. However,

¹¹⁸ Zawodinski, T.; Springer, T.E.; Uribe, F.; Gottesfield, S., *Solid State Ionics* 1993, 60, 199.

¹¹⁹ Srinivasan, S.; Manko, D.J.; Koch, H.; Enayetullah, M.A.; Appleby, J.A., *J. Power Sources* 1990, 29 (3-4), 367.

¹²⁰ Bahar, B.; Cavalca, C.; Cleghorn, S.; Kolde, J.; Lane, D.; Murthy, M. and Rusch, G. *J. of New Matl. for Electrochem. Syst.*, 1999, 2(3), 179.

¹²¹ Bahar, B.; Hobson, A. R.; Kolde, J. A. and Zuckerbrod, D. *U. S. Patent*, 5, 547, 551, 1996.

¹²² Penner, R. and Martin, C. *J. Electrochem. Soc.* 1985, 132, 514.

thinner membranes have higher permeability and increased fuel crossover. Therefore, as the membranes reach thicknesses as thin as 20 micrometers, fuel crossover results in low open circuit voltage and low fuel efficiency. Furthermore, GORE-SELECT[®] membranes and PRIMEA[®] MEAs use Nafion[®] as the poly electrolyte membrane, which is only morphologically stable at temperatures less than 100 °C at high relative humidity, therefore, resulting in similar drawbacks as the pure Nafion[®] membranes.

Dias Analytic has produced sulfonated membranes from the well known Kraton-G[®] styrene-b-ethylene/butylene-b-styrene copolymers.¹²³ These hydrocarbon backbone polymers are of interest for low cost, low temperature and low current density arrangements. Dais membranes have proven to have similar conductivities at a given water-sulfonate ratio, but higher water uptake than that of Nafion[®] for a given ion exchange capacity. The targeted area of use for these membranes is for low cost applications that are used at room temperature environments for short periods of time since oxidative stability is limited.¹²⁴

Ballard Advanced Materials has produced a series of polymer electrolyte membranes that are based on post-sulfonation of engineering thermoplastics like poly(styrene), poly-2,6-disubstituted(phenylene oxide) and poly(trifluoro styrene). Generation one (BAMG1) of the Ballard Advanced Material team focused on poly(phenylquinoxaline) polymer membranes.¹²⁵ This polymer was sulfonated using the

¹²³ Edmonson, C. A.; Fontanella, J. J.; Chung, S.H.; Greenbaum, S.G. and Wnek, G.E. *Electrochemical Acta* 2001, 46, 1623.

¹²⁴ Serpico, J. M.; Ehrenberg, S. G.; Fontanella, J. J.; Jiao, X.; Perahia, D.; McGrady, K. A.; Sanders, E. H.; Kellogg, G. E. and Wnek, G.E. *Macromolecules* 2002, 35(15), 5916.

¹²⁵ (a) Steck, A.E., C. Stone, Membrane materials in fuel cells, 2nd Int. Symp. on New Materials for Fuel Cells and Modern Battery Systems, Montreal, Canada, July 1997, 792. (b) Harris, F. W., *Abstract of Inaugural Asilomar Conference on Advanced Materials for PEMFC*, Feb., 2003.

chlorosulfonic acid method described previously.¹²⁶ The membrane was soluble in organic solvents and cast from solution. The goal of the research was to produce a PEM that had similar hydrophobic and hydrophilic characteristics to that of Nafion[®]. However, the rigidity of the backbone of poly(phenylquinoxaline)s reportedly produced ionic clusters that were much smaller than that of Nafion[®]. In the early stages of development, the fuel cell performance was similar to that of Nafion[®], but during the lifetime tests failure of the membrane was observed early in the testing, no other information was provided. Generation two of Ballard Advanced Materials (BAMG2) was based on the thermoplastic poly(2,6-diphenyl-1,4-phenylene oxide) polymer. The availability of this high T_g, semicrystalline thermoplastic polymer made it an attractive material for post-sulfonation. As with generation one by Ballard Advanced Materials, BAMG2 had sufficient conductivity but had a short lifetime in the fuel cell testing. No details of the failure mechanisms were reported. Therefore, Ballard directed its research to a more costly starting material for post-sulfonation. As was discussed earlier, Ballard Advanced Materials generation three (BAMG3) polymer was based on poly(trifluorostyrene). The chemical stability of the fluorinated styrene-type backbone produced a sulfonated copolymer by using sulfur trioxide with triethylphosphate complex. The third generation of post-sulfonated membranes based on trifluorostyrene was reported to have a longer lifetime, 15,000 hours, relative to the first two generations, but is considerably more expensive due to the fluorinated starting material. Also no mechanical properties have ever been reported and it would be expected to be quite brittle when dry.

¹²⁶ Johnson, B.C.; Yilgor, I.; Tran, C.; Iqbal, M.; Wightman, J. P.; Lloyd, D.R. and McGrath, J. E. *J. Poly. Sci.: Part A* 1984, 22(3), 721.

2.14 Novel Research on Proton Exchange Membranes

New and alternative membrane research for fuel cells has emphasized three major topics. For industrial applications, the first topic is to produce PEMs at a low cost. This could allow mass production of fuel cell stacks for automotive and stationary power applications, not just space and aircraft applications. Due to the government funded grants and contracts, fuel cells and hydrogen storage research for automotive applications has grown dramatically over the last five years. The second objective of the fuel cell initiative is to produce a membrane that could produce high conductivity at low relative humidities and temperatures above 100 °C. As described previously, this would help to minimize the carbon monoxide poisoning of the catalyst and increase the reaction kinetics of the overall cell. It has been proposed that the state-of-the-art Nafion[®] membrane loses performance at temperatures above 100 °C because of the physical transition that occurs due to a hydrated glass transition temperature close to 100 °C. Thirdly, loss of fuel and reverse flux of protons has been at the forefront of proton exchange membrane research. In a hydrogen fuel cell, hydrogen and air must be separated so that proper catalysis occurs and short circuits or explosions do not. In a direct methanol fuel cell (DMFC), methanol crossover is a major problem with Nafion[®] membranes and causes loss of performance due to a back flux of protons that are produced at the cathode. Back flux protons work against the true direction of protons that are produced at the anode and thus decrease the overall performance of the cell and produce a crossover current. Furthermore, when methanol is not reacted at either the anode or the cathode, but still permeates through the membrane, fuel efficiency

decreases, therefore, making the overall cell have low efficiency. As the next section will discuss, novel technologies based on fuel cell membranes has emphasized copolymerization of monomers that directly contain ion-conducting sites to produce ion-exchange membranes and polymer composites that are based on polymer-polymer interactions or polymer-inorganic filler interactions.

2.15 Direct Polymerization of Sulfonated Monomers Via Step Growth Techniques

With respect to post-sulfonation techniques, direct polymerization of sulfonated monomers can produce enhanced thermal stability with reproducible results.¹²⁷ By using ion-containing monomers, different molecular architectures can be formed to control the structure-property relationships of the PEM. Furthermore, post-sulfonation techniques place only one sulfonic acid moiety per repeat unit on the activated phenyl ring and direct sulfonation of disulfonated monomers can easily and reproducibly place up to two sulfonic acid moieties per repeat unit on the deactivated phenyl ring. This direct copolymerization of sulfonated monomers produces polymer architectures that have sulfonic acid moieties that are less susceptible to hydrolyzation because of the difficulty in generating the required carbocation intermediate and thus make a thermally more stable polymer chain. Furthermore, the acidity of the sulfonic acid moieties increase due to the second sulfonation and electron withdrawing nature of the sulfone or ketone moieties. Only two approaches have been reported which place the sulfonic acid groups on the deactivated phenyl ring. The first technique, which was described previously, involves metalation of the phenyl ring followed by sulfination and subsequent oxidation

¹²⁷ Genies, C.; Mercier, R.; Sillion, B.; Cornet, N.; Gebel, G. and Pineri, M. *Polymer* 2001, 42, 359.

of preformed polymers (post-sulfonation). However, as with the other post-sulfonation techniques, this process is difficult to control and reproduce.

A novel approach has been described by Robeson and Matzner¹²⁸ and Ueda et al¹²⁹ where direct polymerization of preformed sulfonated monomers based on the reaction of 4,4'-dichlorodiphenylsulfone (DCDPS) with fuming sulfuric acid to produce 3,3'-disulfonate-4,4'-dichlorodiphenylsulfone, Figure 2.18 (SDCDPS). The electrophilic aromatic substitution¹³⁰ mechanism is reviewed in Figure 2.19.

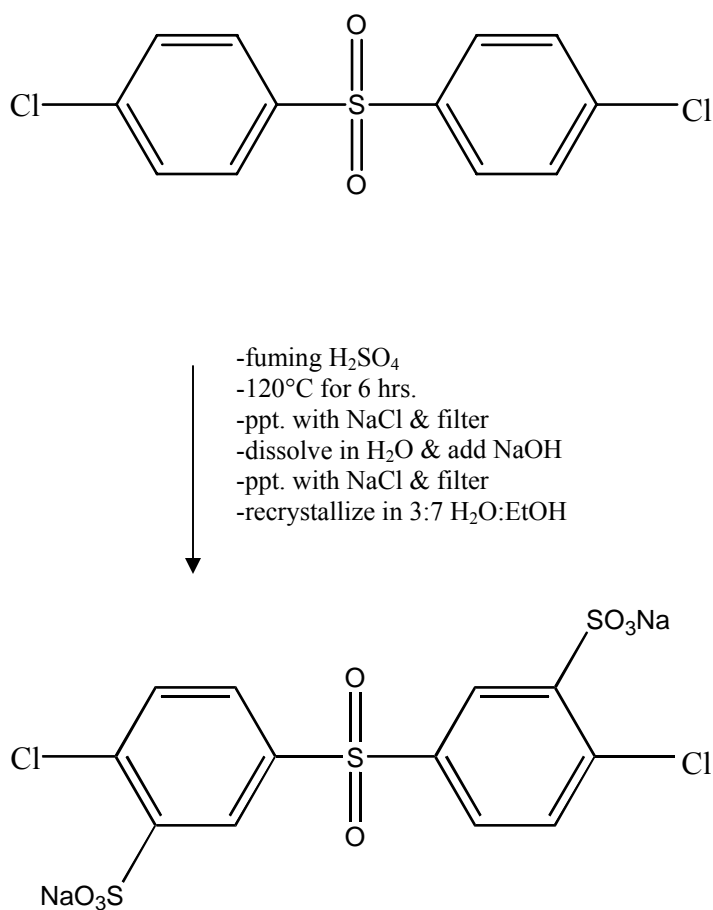


Figure 2.18 Disulfonation of DCDPS monomer for use in step-growth polymerizations

¹²⁸ Robeson, L.M., Matzner, M., Flame retardant polyarylate compositions, US Patent 4,380,598 (1983), to Union Carbide.

¹²⁹ Ueda, M.; Toyota, H.; Ouchi, T.; Sugiyama, J.; Yonetake, K.; Masuko, T.; Teramoto, T. *J. Polym. Sci.: Part A: Polym. Chem.* 1993, 31(4), 853.

¹³⁰ Vallard, K. P. C. and Schore, N. E. *Organic Chemistry, Structure and Function, 3rd Ed.*, W. H. Freeman and Company: New York, 1999, 668.

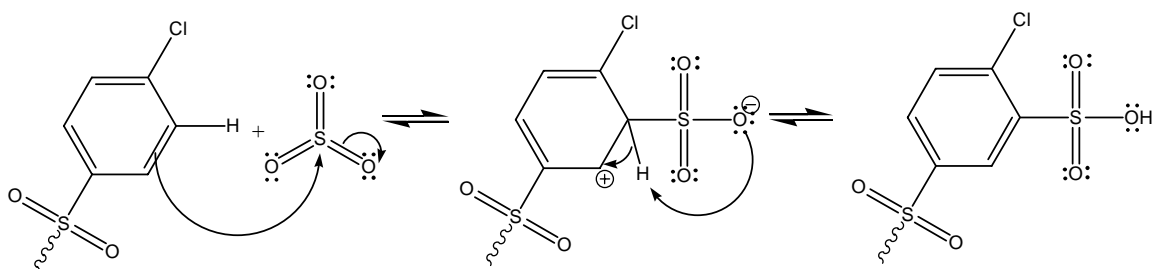


Figure 2.19 Mechanism for Electrophilic Aromatic Sulfonation

The disulfonated monomer (SDCDPS) can then be used in a step or condensation copolymerization with non-sulfonated monomers to produce polymer architectures that contain random or statistical incorporations of the disulfonated monomers. Some of the first reports of this process were developed by the McGrath group at Virginia Tech who have successfully copolymerized 3,3'-disulfonate-4,4'-dichlorodiphenylsulfone with DCDPS and 4,4'-biphenol in the presence of potassium carbonate to synthesize high molecular weight film forming poly(arylene ether sulfone) copolymers.⁷ Similarly, 4,4'-difluorodiphenylsulfone can be reacted with fuming sulfuric acid to produce 3,3'-disulfonate-4,4'-difluorodiphenylsulfone (SDFDPS) as a disulfonated monomer.¹ Fluorine has the highest electronegativity of all the possible leaving groups and although more expensive is therefore a better atom to displace relative to chlorine. Thus, decreased temperatures can be used in the polymerization to synthesize high molecular weight copolymers based on fluorine as the leaving group during the displacement reaction.

Modification of the monomers before polymerization ascertains a high degree of control of the molecular architecture that results in the copolymer structure.

Characteristic physical differences that are based on the amount of sulfonated monomers that are incorporated into the polymer structure, however subtle, can be dramatically controlled. By varying the ratio of unsulfonated monomer to sulfonated monomer, the degree of sulfonation can be easily controlled. For example, poly(arylene ether sulfone)s that are polymerized by nucleophilic aromatic substitution reactions at high temperatures using SDFDPS, DFDPS, bisphenol and potassium carbonate as the base that deprotonates the bisphenol can produce high molecular weight copolymers.¹³¹ By using the salt form of the sulfonated comonomers, the salt form of the copolymer is formed. However, during the polymerization of the sodium salt form of SDFDPS, ion exchange occurs and the resulting copolymers are in the potassium salt form due to the excess potassium carbonate base that is used in the reaction. The potassium salt form copolymers are soluble in N,N-methyl pyrrolidinone during the copolymerization, are then precipitated in an excess of isopropanol and dried in a vacuum oven. Redissolution of the polymer in DMAC or NMP and subsequent casting onto a glass substrate produces the purified potassium salt form membrane.

The salt form membrane can then be transformed into the acid form in one of two methods.¹³² Room temperature acidification can be carried out using a 1.5 M sulfuric acid in water solution. The polymer membranes are submersed in the solution for 24 hours and then rinsed with D. I. water. This process transforms the sulfonate salts to sulfonic acid moieties. Residual sulfuric acid can be removed from the membranes by allowing them to be submersed in D. I. water for another 24 hours. This room

¹³¹ Mecham, J.B., *Ph.D. Thesis*, VPI & SU, December 2001.

¹³² Kim, Y. S.; Dong, L.; Hickner, M. A.; Pivovar, B. S. and McGrath, J. E. *Polymer*, 2003, 44, 5729.

temperature acidification has been termed Method 1.¹³³ Method 2 acidification uses 0.5 M sulfuric acid in water. The films are boiled (~100 °C) in this sulfuric acid solution for two hours and again rinsed well. The residual sulfuric acid is removed by boiling in water for another 2 hours. This high temperature acidification treatment has been shown to change the morphological characteristics of the resulting acidified membranes.¹³⁴ No side reactions were observed by FT-IR, NMR and IEC during the acidification. Therefore, the incorporation of the sulfonic acid containing monomers was successful.

Introduction of the acid groups into any polymer can be classified using the ion exchange capacity (IEC). When determining the theoretical amount of acid equivalents per gram of polymer, the calculations involve the following for disulfonated copolymers:

$$\text{IEC} = \frac{(2 * \text{mol fraction of disulfonation})}{((\text{MW}_{\text{repeat}} * \text{mol fraction } y) + (\text{MW}_{\text{sulf. repeat}} * \text{mol fraction } z))}$$

Where the value 2 in the numerator corresponds to two sulfonate moieties on the sulfonated repeat unit, y is the mole fraction of the unsulfonated monomer/repeat unit, z is the mole fraction of the sulfonated monomer/repeat unit, MW_{repeat} is the molecular weight of the unsulfonated repeat unit and MW_{sulf. repeat} is the molecular weight of the sulfonated repeat unit. This equation gives the equivalents of acid moieties per gram of polymer. In order to increase the IEC value, more acid groups and less repeat units of

¹³³ Kim, Y. S.; Wang, F.; Hickner, M. A.; McCartney, S.; Hong, Y. T.; Harrison, W. L.; Zowadzinski, T. A. and McGrath, J. E. *J. Polym. Sci.: Part B: Polym. Phys.*, 2003, 41, 2816.

¹³⁴ Harrison, W. L., *Ph.D. Thesis*, VPI & SU, December, 2002.

non-sulfonated groups can be used. The experimental IEC can be determined by titrating either the dissolved polymer in solution or by first exchanging the hydrogen ions with a metal (*i. e.* sodium) to form the salt form polymer and an acid form, water soluble compound (*i. e.* sodium hydrogen sulfate). The aqueous titrations use sodium sulfate as the water-soluble ion exchange compound that produces sodium hydrogen sulfate during an equilibration reaction. The chemistry of this type of process is shown in Figure 2.20.

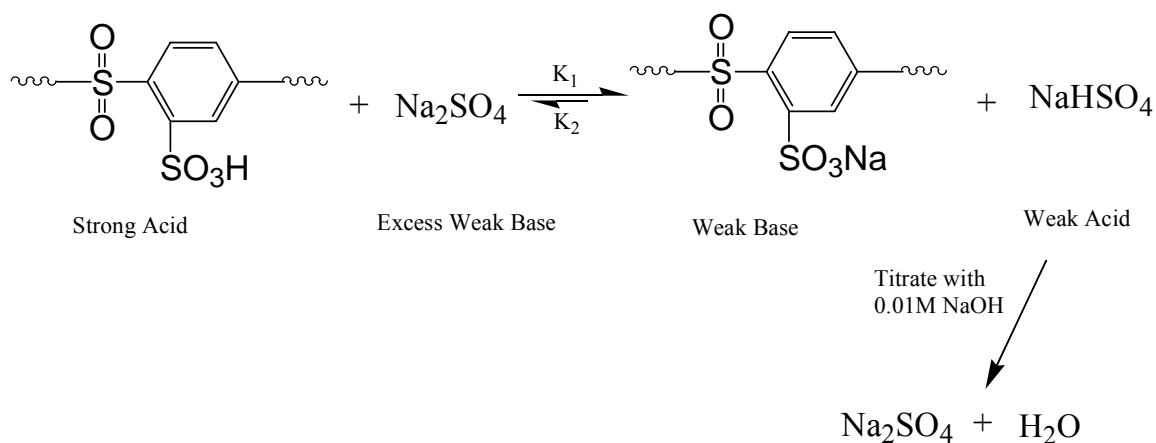


Figure 2.20 Acid-base reaction followed by titration to measure IEC

2.16 Directly Polymerized Disulfonated Polyimide Copolymers

The heterocyclic high T_g nature and semi-crystallinity of some polyimides produce polymers that are rigid and robust with excellent thermomechanical properties.¹³⁵ For some applications, more flexibility and less crystallinity is desired, therefore, pendant groups can be used to disrupt the long-range order and minimize the rigidity of the polyimide. Directly copolymerizing the polyimide monomers with a sulfonated comonomer has recently been shown to produce polymers that have proton

¹³⁵ Guo, X.; Fang, J.; Watari, T.; Tanaka, K.; Kita, H. and Okamoto, K. I. *Macromolecules*, 2002, 35, 6707.

conductivity and a decrease in crystallinity.¹³⁶ French scientists have recently used a sulfonated monomer based on 4,4'-diaminobiphenyl.¹³⁷ The commercially available sulfonated analog, 4,4'-diamino-2,2'-biphenyldisulfonic acid (BDSA), has been shown to produce sulfonated polyimide copolymers that produce thin films for potential use as proton exchange membranes.¹³⁸ Pineri et al concluded that five member ring polyimides, based on 4,4'-oxydiphthalic anhydride, quickly degrade and become brittle, whereas the six member ring polyimides, based on naphthalene tetracarboxylic dianhydride are much more stable. It was shown that the five member ring phthalic sulfonated polyimides failed during the fourth day of fuel cell testing. The proposed degradation of the five member ring polyimides was due to hydrolysis of the phthalic imide structure that led to chain scission and brittleness. The sulfonated six-member ring polyimides, based on sulfonated naphthalic repeat units, showed better longevity in the fuel cell environment (125 days at 60 °C) and better stability to hydrolysis.

Synthesis of sulfonated six-member ring polyimides has been performed by the direct polymerization procedure of sulfonated monomers.^{139,140,141} Using stoichiometric amounts of sulfonated diamine to unsulfonated diamine and a dianhydride (i. e. naphthalene tetracarboxylic dianhydride), direct synthesis of sulfonated polyimides can be done in a one-step, high temperature polycondensation reaction using m-cresol as the organic solvent. Changing the charging ratio of the unsulfonated diamine to the sulfonated diamine can easily vary the degree of sulfonation. However, solubility of the

¹³⁶ Gunduz, N. and McGrath, J. E. *Polymer Preprints*, 2000, 41(1), 182.

¹³⁷ Genies, C.; Mercier, R.; Sillion, B.; Cornet, N.; Gebel, G.; Pineri, M., *Polymer* 2001, 42, 359.

¹³⁸ Vallejo, E.; Gavach, C and Pineri, M. *J. Power Sources*, 1999, 160, 127.

¹³⁹ Hong, Y. T., Einsla, B.; Kim, Y. S. and McGrath, J. E. *Polymer Preprints*, 2002, 43(1), 667.

¹⁴⁰ Einsla, B., Y.T. Hong, Y.S. Kim, F. Wang, N. Gunduz and J.E. McGrath, *J. Poly. Sci., Part A: Polymer Chemistry* 44, 862-874, 2004.

¹⁴¹ Einsla, B. and McGrath J. E. *J. Membr. Sci.* 2005, Accepted.

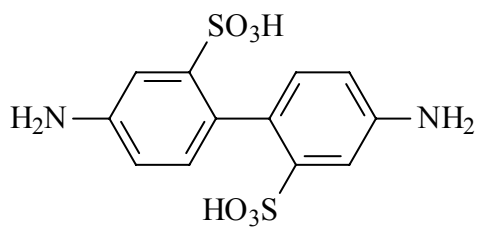
acid and sodium salt forms of the diamines becomes a major issue. In order for the sulfonated monomer to be soluble in m-cresol, the triethylammonium salt form is employed. The first step of the synthesis is to add triethylamine to the sulfonated diamine in m-cresol.¹⁴² After about 4 hours, the triethylammonium salt form of the sulfonated diamine is produced allowing solubility in m-cresol and a homogeneous reaction to occur with the dianhydride. Acid catalysis is employed by adding benzoic acid to the reaction media that initiates *trans*-isoimide formation. The final step in the synthesis is to add a basic catalyst, isoquinoline that transforms the isoimide to the imide form.

Gunduz et al^{143,144} have produced five-member ring polyimides that incorporated a large amount of different sulfonated monomers. Figure 2.21 below shows the sulfonated diamines that were employed in the research and produced soluble sulfonated polyimides with film forming characteristics. In solution as well as the solid state, these diamines would exist in the zwitterion form, which produces a salt of the acid, -SOO_3^- , and base, NH_3^+ by transference of the proton on the acid moiety to the amine to create a neutral entity.

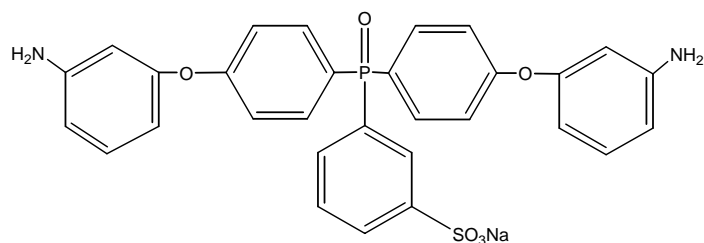
¹⁴² Vallejo, E.; Pourcelly, G.; Gavach, C.; Mercier, R. and Pineri, M., *J. Membr. Sci.*, 1999, 160, 127.

¹⁴³ Gunduz, N.; McGrath, J.E., *Polymer Preprints* 2000, 41(2), 1565.

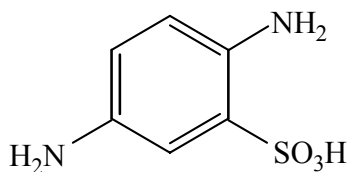
¹⁴⁴ Gunduz, N. *Ph.D. Dissertation*, Virginia Polytechnic Institute and State University, 2001.



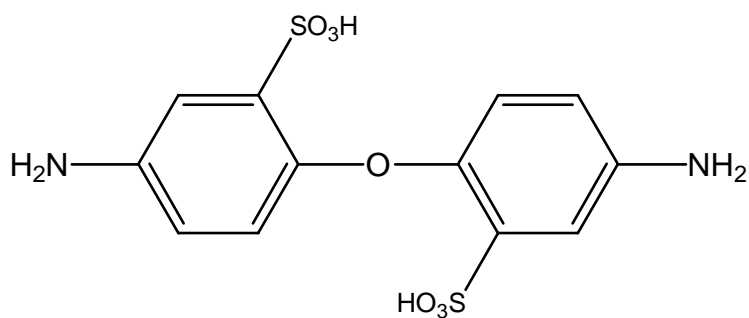
4,4' – Diamino – 2,2' – biphenyl disulfonic acid (BDSA)



3-Sulfo-4',4''-bis(3-aminophenoxy)triphenyl phosphine oxide sodium salt (SA-DADPS)



2,5-Diaminobenzenesulfonic acid (DAB)



4,4' – Diaminodiphenylether – 2,2' – disulfonic acid (ODADS)

Figure 2.21 Sulfonated diamines used to produce sulfonated polyimides

The different structures of the sulfonated monomers allowed for increased solubility characteristics and improved membrane properties. Figure 2.22 below indicates a successful polymerization that incorporated the reaction steps aforementioned using BDSA.

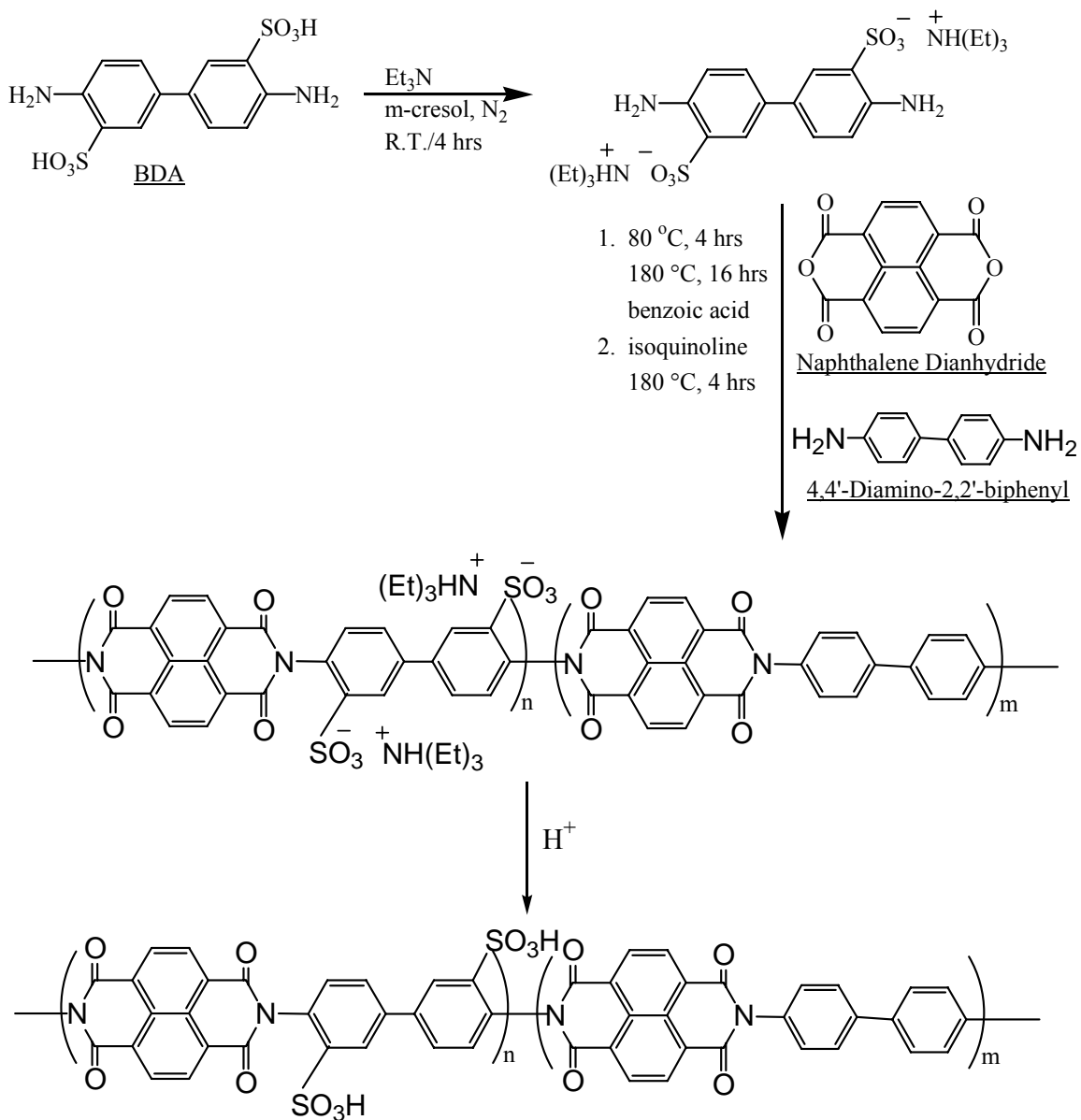
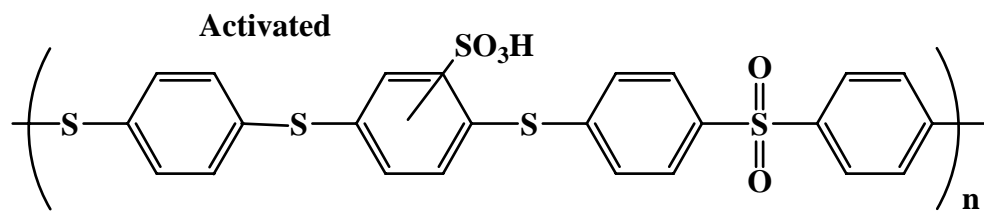


Figure 2.22 Polymerization scheme for the synthesis of a BDSA based polyimide

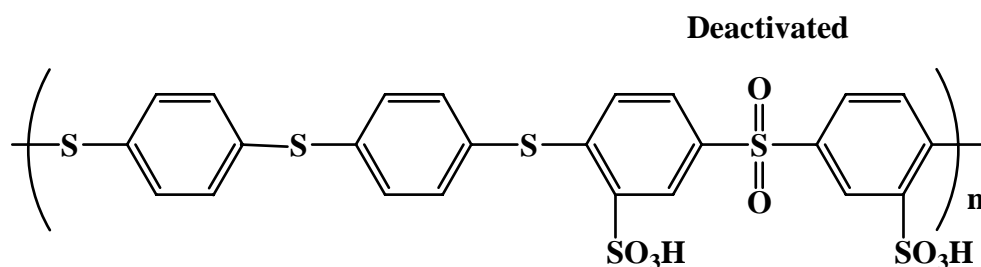
The water uptake was reportedly low(*i. e.* less than 5%) and the best proton conductivity was found to be of the order of 20 mS/cm. Einsla et al have investigated both five and six-member ring polyimides and found higher conductivities are possible, but hydrolytic stability at 80 °C is still the major issue with sulfonic acid polyimides.

2.17 Synthesis of Disulfonated Poly(arylene ether sulfone) Copolymers Via Sulfonated Monomers

As previously described, when one compares post sulfonated polymers to directly copolymerized sulfonated copolymers, it was found that post-sulfonated products generally contain only one sulfonic acid group per repeat unit on the activated phenyl ring and directly copolymerized copolymers contain two sulfonic acid moieties per repeat unit. Since the post-sulfonated polymer sulfonic acid moieties are on the activated, electron rich phenyl ring, the sulfonic acid groups could be more readily hydrolyzed. Therefore, direct polymerization of sulfonated monomers on the deactivated, (Figure 2.23) electron poor phenyl rings of a sulfone monomer has been the main focus of many research groups.



- * Post sulfonation occurs on the most reactive, but least stable, position
- * High electron density leads to relatively easy desulfonation



- * Monomer sulfonation on the deactivated position
- * Enhanced stability due to low electron density

Figure 2.23 Activated versus deactivated positions of sulfonate moieties

As discussed previously, Ueda et al¹²⁹ first described the direct synthesis of sulfonated poly(arylene ether sulfone) copolymers using a pre-sulfonated monomer. They used this sulfonated monomer, the unsulfonated monomer and bisphenol A to synthesize a disulfonated poly(arylene ether sulfone) copolymer. The yields of the disulfonated monomer was quite low (~30%). However, McGrath et al^{145,8} modified the synthetic procedures to obtain much higher yields (~80-90%). The synthesis of novel disulfonated poly(arylene ether sulfone) copolymers quickly followed and obtained

¹⁴⁵ Sankir, M.; Bhanu, V. A.; Ghassemi, H.; Wiles, K. B.; Hill, M. L.; Harrison, W.; Sumner, M.; Glass, T. E.; Riffle, J. S. and McGrath, J. E. *Polymer Preprints*, 2003, 44(1), 1079.; *J. Applied Poly. Sci.*, Accepted, 2005.

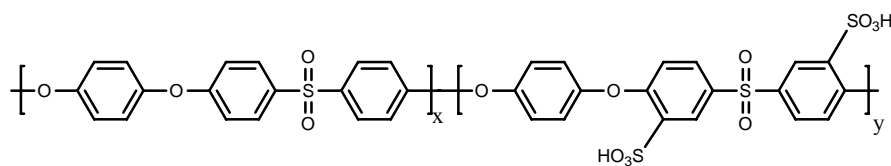
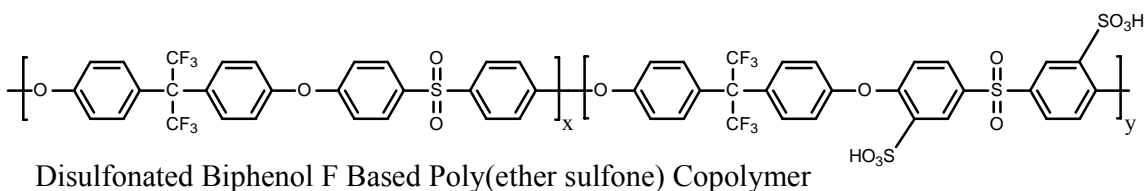
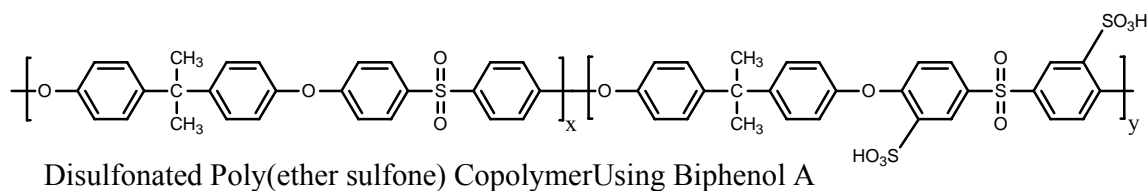
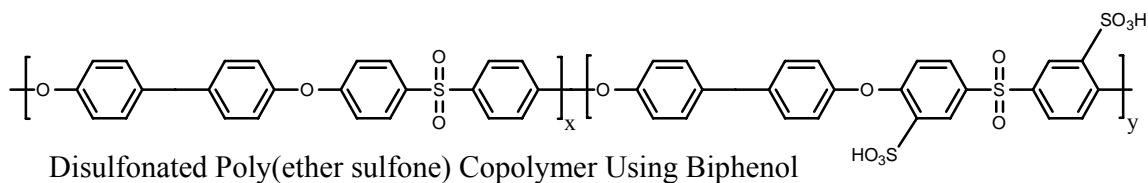


Figure 2.25 Disulfonated poly(arylene ether sulfone) copolymers

2.18 Synthesis of Disulfonated Poly(arylene ether ketone) Copolymers Via Disulfonated Monomers

Sulfonated ketone containing monomers have recently been reported using 4,4'-dichlorodiphenyl ketone to produce 3,3'-disulfonated 4,4'-dichlorodiphenyl ketone (Figure 2.26).¹⁴⁶

¹⁴⁶ Wang, F.; Li, J.; Chen, T. and Xu, J., *Polymer*, 1999, 40, 795.

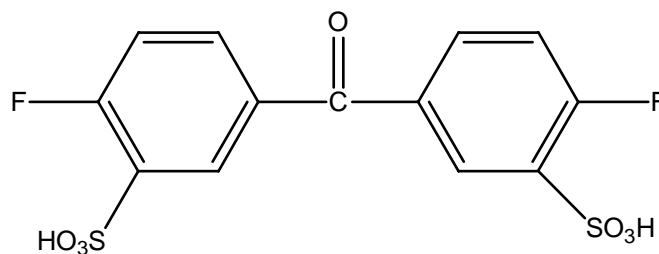


Figure 2.26 Disulfonated ketone monomer used to synthesize poly(ether ketone)s

This disulfonated monomer was then reacted with the unsulfonated monomer and bisphenol A to produce a series of disulfonated poly(arylene ether ketone) copolymers. Similar reaction conditions, relative to the poly(arylene ether sulfone) copolymers, were used and produced relatively high yield and high molecular weight copolymers. It was reported that the thermal stabilities of the ketone containing polymers was good using the salt form copolymer. However, the acid form seemed to suffer from lower thermal stability and lower proton conductivity relative to the sulfone based analogs.

2.19 Synthesis of Disulfonated Poly(arylene ether phosphine oxide) Copolymers Via Disulfonated Monomers

Phosphine oxide containing polymers based on poly(arylene ether)s and poly(arylene thioether)s have been reported to be stable at high temperatures while being flame retardant and plasma resistant.^{147,148,149,150} Generally these high performance

¹⁴⁷ Smith, C.D.; Grubbs, H.J.; Webster, H.F.; Gungor, A.; Wightman, J.P. and McGrath, J.E., *High Perform. Polym.*, 1991, 4, 211.

¹⁴⁸ Bhatnager, A.; Liu, Y. N.; Geibel, J. F. and McGrath, J. E. *Polymer Preprints*, 1997, 38(2), 227.

polymers are used as flame retardant materials that also complex with certain metals to help in dispersion and retention of inorganic/organic additives.¹⁵¹ Furthermore, reports on phosphine oxide containing poly(arylene ether)s that have good interactions with a wide variety of thermoplastics and thermosets like phenoxy, epoxy and vinylester resins has recently been described.¹⁵² It has been proposed that these phosphine oxide containing materials could have an increased interaction with functionalized carbon fibers, glass fibers or inorganic additives due to the very polar phosphine oxide groups. Synthetic procedures to produce phosphine oxide containing polymers has mainly incorporated 4,4'-bis(fluorophenyl) phenyl phosphine oxide (BFPPPO)¹⁵³, Figure 27, as the electrophile and bisphenols or thiobisphenols as the nucleophilic containing monomers.

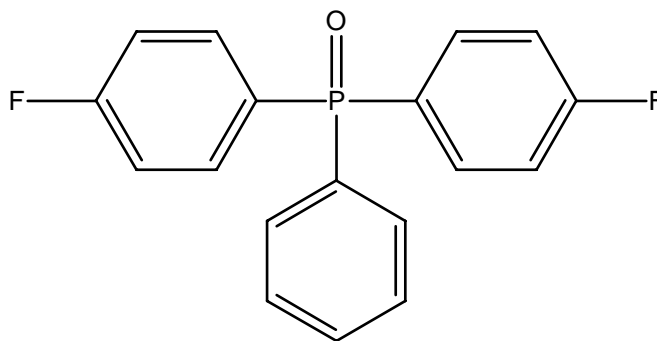


Figure 2.27 Chemical structure of 4,4'-bis(fluorophenyl) phenyl phosphine oxide

¹⁴⁹ Riley, D.J.; Gungor, A.; Srinivasan, S.A.; Sankarapandian, M.; Tchatchoua, C.; Muggli, M.W.; Ward, T.C. and McGrath, J.E., *Polym Eng. Sci.*, 1997, 37(9), 1501.

¹⁵⁰ Ding, Y. and Hay, A. S. *J. Polym. Sci.: Part A: Poly. Chem.*, 1998, 36, 519.

¹⁵¹ Hergenrother, P.M., *Angew Chem. Int. Ed. Engl.* 1990, 29, 34.

¹⁵² Wang, S., Zhuang, H., Shobha, H. K., Glass, T. E., Sankarapandian, M., Ji, Q., Shultz, A. R., McGrath, J. E. *Macromolecules* 34(23), 8051-8063, 2001.

¹⁵³ Wang, S., *Ph. D. Dissertation*, Virginia Polytechnic and State University, 2000.

The polymerizations can be carried out in solution or in the melt. The melt polymerizations have been shown to follow the silylation route invented by Kricheldorf.¹⁵⁴ These solventless reactions produce polymers that are free of inorganic salt byproducts and can be used for reactive extrusion techniques due to low viscosity in the melt even at high molecular weights (30,000 g/mol). The solution polymerization technique follows the same synthetic procedures as has been described for nucleophilic aromatic substitution reactions using potassium carbonate as the base that abstracts the proton from the nucleophilic monomer.

An early report of poly(arylene ether phosphine oxide) was published by Hashimoto et al¹⁵⁵, who obtained only low molecular weight polymeric material. They reacted 4,4'-bis(chlorophenyl) phenyl phosphine oxide (BCPPO) with various bisphenols in different aprotic dipolar solvents. The strong base approach (NaOH) was used because the phosphonyl moiety was described as being less of an electron-withdrawing group as compared to the corresponding sulfone group. Smith et al¹⁵⁶ showed that high molecular weight could be obtained from the use of bis(4-fluorophenyl)phenyl phosphine oxide (BFPPPO) due to the higher reactivity of the fluoro compounds as compared to the chloro compounds. More recently, McGrath et al¹⁵⁷ have incorporated various architectures into the polymer backbone, such as sulfonyl and carbonyl. The resulting polymeric materials based on BFPPPO monomers were observed to be amorphous, non-coplanar polymers with high T_g s and high thermal stabilities.

¹⁵⁴ Kricheldorf, H. R. and Bier, G. *Polymer*, 1984, 25, 1151.

¹⁵⁵ Hashimoto, S.; Furukawa, I. and Ueyama, K. *J. Macromol. Sci. Chem*, 1977, A11, 2167.

¹⁵⁶ Smith, C.D.; Grubbs, H.J.; Webster, H.F.; Gungor, A.; Wightman, J.P. and McGrath, J.E., *High Perform. Polym.*, 1991, 4, 211.

¹⁵⁷ McGrath, J. E.; Mecham, S. J.; Hickner, M. A.; Wang, S.; Shobha, H. B.; Oishi, Y. and Sankarpandian, M. *Polymer Preprints*, 1999, 40(2), 1291.

Sulfonating the phosphine oxide containing monomer has been reported¹⁵⁸, but produces a polymer that contains only one sulfonic acid moiety per repeat unit (Figure 2.28).

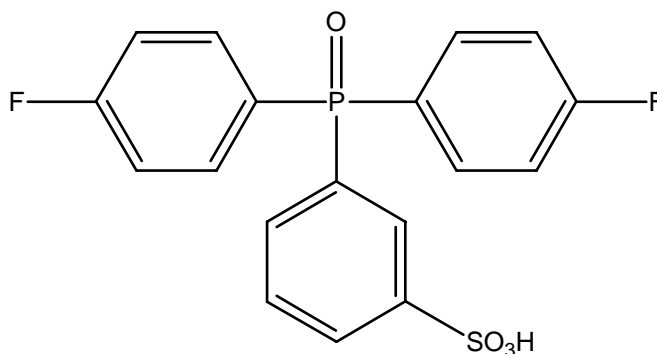


Figure 2.28 Mono-sulfonated BFPPO

The phosphine oxide containing monomer, BFPPO, can be reacted with SO₃ in fuming sulfuric acid to produce a mono-sulfonated pendant phenyl ring. Minor products of di- and tri- substituted monomers are also formed in the reaction, therefore, the mono-substituted species must be isolated from the reaction mixture using different recrystallization techniques. The nucleophilic monomer used was 4,4'-biphenol, which gave a wholly aromatic sulfonated copolymer by direct polymerization. Proton conductivity measurements indicated a lower conductivity relative to the sulfonated sulfone analog due to the lower degree of sulfonation per repeat unit and strong hydrogen bonding between the phosphine oxide moiety and sulfuric acid moiety. The thermalgravimetry data indicated a decrease in the 10% weight loss as more of the

¹⁵⁸ Shobha H.K.; Smalley, G.R.; Sankarapandian, M. and McGrath, J.E. *Polymer Preprints*, 2000, 41(1), 180.

sulfonated monomer was added probably due to the loss of more sulfonic acid groups as the sulfonation level increased. The differential scanning calorimetry data indicated an increase in the T_g with increasing sulfonation levels due to the ionomeric effect of the sulfonate group and the bulky sulfonate substituent. The ionomeric effect was also noted in the increase in intrinsic viscosity as the sulfonation level increased. The ionomeric effect is described as the association or aggregation of the ionic sulfonate groups to produce multiplet structures that can also form higher agglomerations like spheres, clusters and channels.

As has been noted above, PEMs based on Nafion[®] are limited to membrane performance below 80 °C presumably due to a thermal transition of the hydrated form and loss of water, dehydration. A novel approach could involve the use of heteropolyacids (HPA) as an additive for compatible sulfonated hydrocarbon polymers. Many HPAs have high proton conductivities but are also water-soluble. HPA composite membranes based on polymers that have a high affinity for the HPA additive can, in principle, make the HPA complex insoluble in water while still retaining high proton conductivity at elevated temperatures. Therefore, a brief study of HPA containing phosphine oxide terpolymers has been reported by Kim et al^{159,160} that described the extraction of HPA in water at elevated temperatures. It was concluded that interactions with the phosphine oxide moieties and sulfonate moieties retained the HPA additive at 80 °C in water better than the control copolymer that contained no phosphine oxide groups. Further research must be performed to understand the interactions and associated with

¹⁵⁹ Kim, Y. S.; Wang, F.; Hickner, M. A.; Zawodzinski, T. A. and McGrath, J. E. *Polymer Preprints*, 2002, 43(1), 342.

¹⁶⁰ Kim, Y. S., Wang, F., Hickner, M., Zawodzinski, T. A. and McGrath, J. E. *J. Membr. Sci.*, 212, 263-282, 2003.

such a system. Moreover, proton conductivities and fuel cell performance studies need to be performed on phosphine oxide containing sulfonated polymers.

2.20 Synthesis of Disulfonated Poly(arylene thioether sulfone) Copolymers Via Disulfonated Monomers

Poly(phenylene sulfide sulfone) and poly(phenylene sulfide) polymers have historically been interesting engineering thermoplastic materials due to high glass transition temperatures, good mechanical and electrical properties, and good chemical resistance.^{161,162,163,164,165} Liu et al⁶ reported a novel approach to synthesizing poly(arylene sulfide sulfone) polymers via A-A or A-B type thiol-functional monomers, such as 4-chloro-4-mercaptodiphenyl sulfone and bis(4-mercaptophenyl sulfone). This novel synthetic approach uses a simplified nucleophilic aromatic substitution process rather than the traditional high pressure route for synthesis of poly(arylene sulfide sulfone) polymers. As described by Wang et al¹⁶⁶, synthesis of a new monomer that contains two thiol groups and a sulfone group can be polymerized with 4,4'-difluorodiphenyl sulfone and 3,3'-disulfonated-4,4'-difluorodiphenyl sulfone to produce a copolymer that has repeating sulfide-sulfone moieties in the polymer backbone.

The synthesis of the bis(4-mercaptophenyl) sulfone monomer (BMPS) is shown in Figure 2.29 and is based on a sulfone activated chloro-displacement by hydrosulfide via an aromatic nucleophilic substitution reaction.

¹⁶¹ Fahey, D. R. and Ash, C. E. *Macromolecules*, 1991, 24, 4242.

¹⁶² Geibel, J. F. and Campbell, R. W. In *Comprehensive Polymer Science*, vol. 5: *Step Polymerization*, Eastmond, G. C.; Ledwith, A.; Russo, S.; Sigwalt, P., Eds., Oxford: Pergamon Press, 1989.

¹⁶³ Hill Jr., H. W. and Brady, D. G. In *Kirk-Othmer Encyclopedia of Chemical Technology*, Grayson, M., Ed., 18, New York: Wiley, 1982.

¹⁶⁴ Campbell, R. W. *U. S. Patent 4,125,525*, to Phillips Petroleum Company, 1978.

¹⁶⁵ Campbell, R. W. *U. S. Patent 4,016,145*, to Phillips Petroleum Company, 1997.

¹⁶⁶ Wang, F.; Mecham, J. B.; Harrison, W. and McGrath, J. E. *Polymer Preprints* 2000, 41(2), 1401.

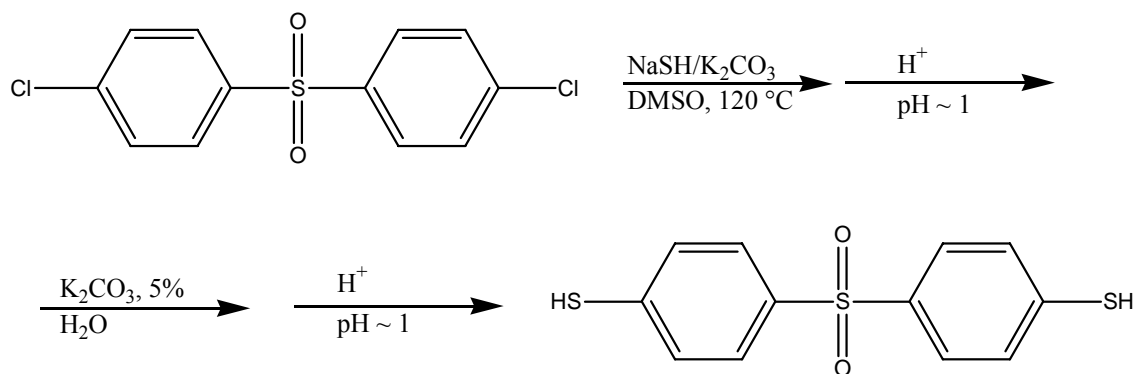


Figure 2.29 Bis(4-mercaptophenyl) sulfone

The dithiol monomer was obtained by reacting recrystallized 4,4'-dichlorodiphenyl sulfone with an excess of sodium hydrosulfide in DMSO in the presence of potassium carbonate. Disulfonated difluorodiphenyl sulfone monomer (SDFDPS) was prepared using fuming sulfuric acid as discussed previously and neutralized with sodium hydroxide. Due to the strong electron-withdrawing effect of the sulfone group and the fluorine groups, disulfonation occurred readily. As described by the electron theory of orientation in electrophilic substitution reactions, the most favorable sulfonation positions are ortho to the fluorine group and meta to the sulfonyl group.¹⁶⁷

As observed in Figure 2.30, the copolymer synthesis involves condensing a specific amount of sulfonated activated dihalide, non-sulfonated activated dihalide and BMPS in DMAc and toluene, which was used as an azeotroping agent to remove any water.

¹⁶⁷ Schmid, G. H., In: *Organic Chemistry*, Black, L. W., Ed., St. Louis: Mosby-Year Book, Inc., 1996.

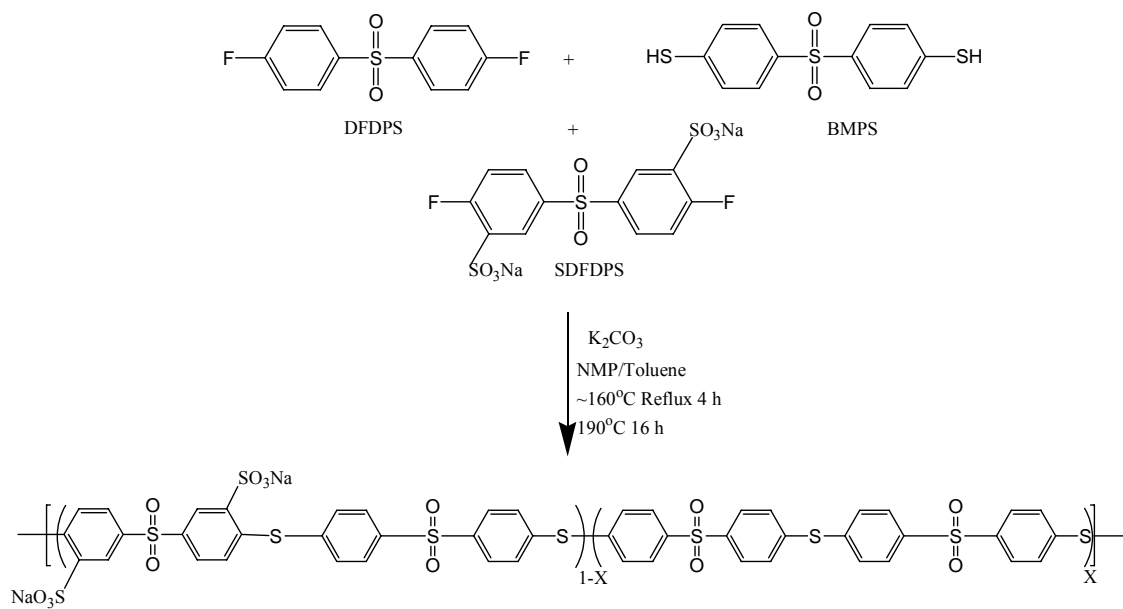


Figure 2.30 Synthesis of disulfonated poly(arylene thioether sulfone) copolymers

Stability of the disulfonated monomer is enhanced in the sodium salt form, so polymerizations were carried out using the disulfonated salt form of the SDFDPS. The disulfonated sodium salt form polymers were then transformed into the acid form by using the boiling technique described previously. As was observed with other sulfonated poly(arylene) copolymers, a significant increase in water sorption was noticed relative to the unsulfonated control type polymers. Very little characterization was performed on these copolymers and further work needs to be performed so as to determine if these materials, and similar sulfide sulfone polymers, are candidates for proton exchange membranes.

Similar to the sulfide sulfone copolymers that Wang et al have produced, Wiles et al¹ have synthesized a novel sulfonated poly(arylene thioether sulfone) copolymer (PATs) for use as proton exchange membranes. This copolymer is based on similar

nucleophilic aromatic substitution reactions but incorporates a thiol containing monomer termed 4,4'-thiobisbenzenethiol (TBBT), Figure 2.31.

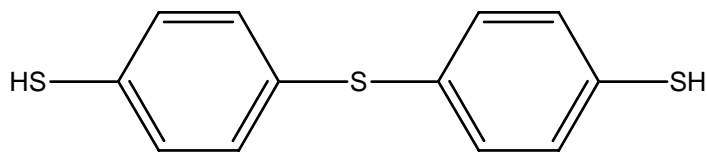


Figure 2.31 Chemical structure of 4,4'-thiobisbenzenethiol

Successful polymerizations were conducted in NMP and the sulfonated copolymers were characterized by NMR, intrinsic viscosity, TGA weight loss, water sorption, ion exchange capacity calculations and proton conductivity. The extent of sulfonation in the copolymers was calculated from the observed concentration of specific protons in the ^1H NMR spectra (Figure 2.32). As was observed, the degree of disulfonation matched well with the targeted feed values of 30 and 40 mol% for the two disulfonated copolymers studied thus far.

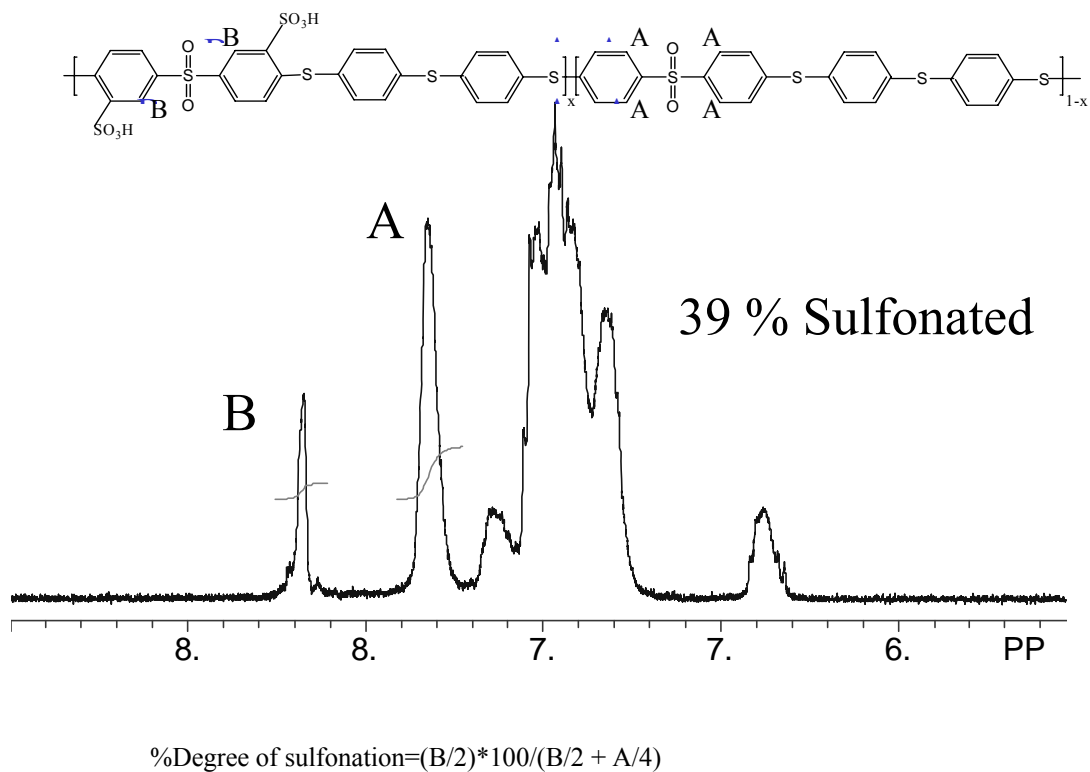


Figure 2.32 ^1H NMR Analysis of the Extent of Disulfonation

The water uptake value of the 40% disulfonated copolymer was much higher than the 30% disulfonated copolymer presumably due to its higher polarity and the plausible morphological change similar to that observed for the disulfonated poly(arylene ether sulfone) copolymers (BPSH).³ The morphological change that was observed for the BPSH materials was based on a phase inversion from a mostly hydrophobic matrix to a mostly hydrophilic matrix. The TGA data suggested that both the copolymers were fairly stable with very little non-water weight loss below 300 °C and char yields of greater than

40% in nitrogen. The reported proton conductivity values were reasonably high at 0.06 and 0.1 S/cm in water at 30 °C for the 30% and 40% disulfonated PATS copolymers respectively (Nafion = 0.1 S/cm). Further research must be conducted to fully understand the oxidation characteristics and fuel cell performance properties so as to successfully develop a membrane electrode assembly based on poly(arylene thioether sulfone) copolymers.

2.21 Composite Membranes Based on Polymer Blends and Nanocomposites

Improvement of proton conductivity and membrane properties, especially at elevated temperatures, has been a high priority research goal of university and industrial investigators. Blending of different polymers by physical techniques is a straightforward technique to modify characteristics and properties of polymer materials.¹⁶⁸ However, polymer-polymer miscibility is difficult to achieve because most polymers are known to be incompatible.¹⁶⁹ When no specific interactions, like acid-base or hydrogen bonding, between two polymer materials exist, microscopic and macroscopic phase separation is usually observed, which is usually a negative characteristic, but can still alter polymer properties.¹⁷⁰ In the case of fuel cell membranes, improving membrane properties in the areas of proton conductivity, mechanical strength and water swelling is of utmost importance. For example, many researchers are blending non-sulfonated materials with sulfonated materials in order to produce a membrane that has significantly better mechanical strength and lower water swelling, which is obtained from the non-sulfonated

¹⁶⁸ Paul, D.R. and Bucknall, C. *Polymer Blends Vol.I. Formulation and Performance*, Wiley & Sons: New York, 2000.

¹⁶⁹ Paul, D. R. and Newman, S., Eds. *Polymer Blends*, Academic Press: New York, 1978.

¹⁷⁰ Robeson, L. M., Shaw, M. T. and Olabisi, O. *Polymer-Polymer Miscibility*, Academic Press: New York, 1979.

polymer, and proton conductivity from the sulfonated polymer.^{171,172,173} As described earlier, Gore and Associates membranes are composite membranes that are based on Nafion[®] copolymers using GORE TEX[®] as a support.¹²¹ The main advantage of the micro-reinforced Gore-Select membranes was observed in the mechanical strength of very thin films. The thickness of the membrane can be decreased to values that the non-supported membranes cannot, and yet have mechanical durability for PEM applications. Therefore, the polymer-polymer blends could be good candidates for alternative PEMFCs, however, it still has the limitations associated with Nafion[®] type membranes at elevated temperatures and in direct methanol fuel cells. Furthermore, the interfacial issues of the different polymers have not been fully investigated or understood, but could be problematic.

Polymers containing a high levels of acidification usually show excellent conductivity, but often suffer from high water swelling, which produces decreased mechanical strength that makes them useless for hydrated fuel cells. Therefore, in order to resolve this problem, polymers with high concentrations of ionic groups can be reinforced with a compatible polymer that does not swell and has good mechanical strength. Kerres et al¹⁷² incorporated this idea when they blended sulfonic acid containing polymers with a polymer that contained a basic nitrogen moiety. These two functional groups would help to make two different polymers compatible through acid-base interactions. The sulfonated polymers employed in this study were post-sulfonated poly(ether sulfone) and post-sulfonated poly(ether ether ketone). The basic polymers

¹⁷¹ Wilhelm, F.G.; Punt, I.G.M.; van der Vegt, N.F.; Strathmann, H. and Wessling, M. *J. Membr. Sci.*, 2001, 1, 5138.

¹⁷² Kerres, J.; Ullrich, A., Meier, F. and Haring, T. *Solid State Ionics*, 1999, 125, 243.

¹⁷³ Deimede, V.; Voyiatzis, G.A.; Kallitsis, J.K.; Qingfeng, L. and Bjerrum, N.J. *Macromolecules*, 2000, 33, 7610.

used were poly(benzimidazole), poly(ethyleneimine) and poly(4-vinylpyridine). First dissolving the polymers separately in NMP and then adding one polymer solution to the other while stirring at a high rate produced good blending of the polymer solutions. Solution casting onto glass substrates showed no visible separation, as would be the case with incompatible polymers. As the authors described, high proton conductivity was obtained by blending sulfonated poly(sulfone) with diaminated poly(sulfone) to produce a tough ductile film with a conductivity similar to that of Nafion[®] 112. Furthermore, low methanol permeation was observed relative to Nafion[®], which was proposed to be due to the specific interactions between the basic amine groups and the acidic sulfonic groups to produce a membrane with higher acid strength.

2.22 Organic/Inorganic Composite Membranes

Investigations to find PEMs that can be used at temperatures above 100 °C is currently a major thrust in the field of proton exchange membrane hydrogen/air fuel cells. The performance barriers of pure ion containing membranes and polymer/polymer blends may be overcome by the incorporation of inorganic fillers that also are protonically conductive. These inorganic fillers can aid in the enhancement of mechanical properties and water retention at high temperatures. Furthermore, polymers that do not have any proton conductivity could, in principle, be used as a matrix for ionically conductive inorganic additives that are stable at fuel cell use temperatures for high temperature conductivity. The state-of-the-art perfluorinated membranes perform poorly at elevated temperatures (>80 °C) as reviewed earlier. At temperatures above the boiling point of water, dehydration of the membranes under ambient conditions occurs dramatically (120

°C @ 45% relative humidity) when a 100% hydrated hydrogen fuel is fed into the cell. Therefore, difficulties in high temperature fuel cell usage at ambient pressure are compounded by dehydration and decreased fuel cell performance. The overall ambition of this type of research is to find a membrane that could be used at temperatures above 100 °C and conducts protons at ambient pressure with little water. Therefore, nanocomposite PEMs have developed into a new field of macromolecular science and engineering.

Crystalline forms of inorganic heteropolyacids (HPA) have recently been used for additives in PEMs by blending with dissolved ionic polymeric materials.¹⁷⁴ The HPAs, in the crystalline form, used in this type of research are protonically conductive inorganic fillers that usually have a strong interaction with specific functional groups in the polymeric material. Many HPA possibilities exist, but only a few have been studied. Some of these are phosphotungstic acid, zirconium phosphate and silicotungstic acid. All of these examples contain multiple acid moieties with relatively high proton conduction as compared to other inorganic fillers. It has been hypothesized that the HPA in PEMs may afford alternative mechanisms to proton transport at temperatures above 100 °C where very little water is present.

Composite membranes based on phosphotungstic acid have recently been shown to have higher conductivities and lower water swelling at elevated temperatures as compared to the pure copolymer membranes. Kim et al¹³ described the solution blending and film casting using commercially available phosphotungstic acid hydrate (Figure 2.33) and poly(arylene ether sulfone), BPSH.

¹⁷⁴ Zaidi, S.M.J.; Mikhailenko, S.D.; Robertson, G.P.; Guiver, M.D. and Kaliaguine, S.J. *J. Membr. Sci.*, 2000, 173, 17.

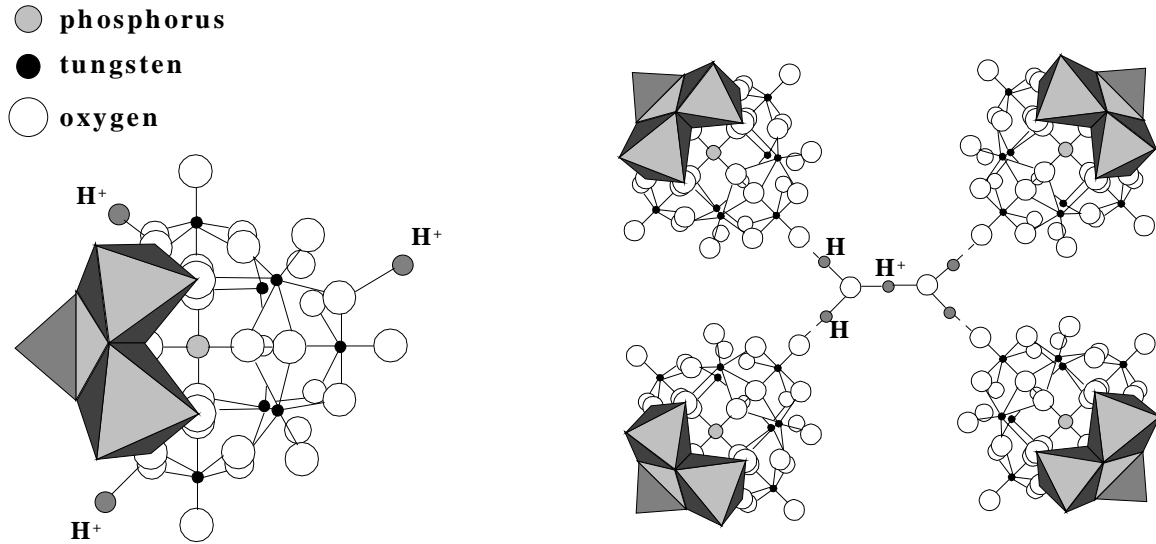


Figure 2.33 Primary Keggin and secondary hydrated structures of semicrystalline phosphotungstic acid

The composite membranes showed little initial water extraction of the HPA, which is water soluble, after water vapor treatment. Thermogravimetry data suggested enhanced stability of the sulfonate groups and better mechanical strength with lower water absorption relative to the non-composite membranes. This data, coupled with the FTIR band shifts of the sulfonic groups and tungstic oxide groups, indicate a strong specific interaction between the HPA molecules and the sulfonic acid moieties. An increase in proton conductivity for the composite membranes was also observed at elevated temperatures under pressure. A BPSH membrane with 40% disulfonation and 30 weight percent HPA additive produced conductivities of 0.08 S/cm at room temperature and 0.15 S/cm at 130 °C under pressure at 100% relative humidity. For comparison, the unfilled membranes showed conductivities of 0.07 S/cm at room

temperature and only 0.09 S/cm at 130 °C in similar conditions. Furthermore, FTIR was used to observe the dehydration of the pure membranes and the composite membranes dynamically at increasing temperatures. It was noted that the composite membranes had an increase in water retention at temperatures from 100 °C to 280 °C. These results suggested that the HPA composite membranes would be good PEMs for high temperature fuel cells operating at 120 °C by aiding in water retention, which is directly responsible for proton conductivity through specific water transport mechanisms.

Polybenzimidazole (PBI) has also been used as the matrix material for phosphotungstic acid filled membranes.¹⁷⁵ In this research, the PBI was not sulfonated and served primarily as the film-forming host for a PEM. Therefore, the only protonically conductive material in the membrane was the HPA. Since HPA and PBI are soluble in DMAc, solution cast films were produced that had 60 weight percent of HPA. Thermogravimetry indicated very good thermal stability reaching temperatures of 400 °C. The conductivity values were relatively low at 0.0014 S/cm at 150 °C in 100% relative humidity. This low conductivity could be due to a decrease in proton movement across the membrane from HPA to HPA molecule. If the membrane was sulfonated, proton movement might be increased, however, degradation of the PBI might occur due to hydrolysis from the sulfonic acid moieties.

Layered zirconium hydrogen phosphonates incorporated into ionic containing polymers have recently been investigated by Alberti et al¹⁷⁶ in Italy. They have used both sulfonated PEEK and Nafion[®] as the ionically conductive matrix for composite MEAs. These types of inorganic fillers are themselves protonically conductive and are

¹⁷⁵ Staiti, P.; Minutoli, M.; Hocevar, S. *J. Power Sources*, 2000, 90, 231.

¹⁷⁶ Alberti, G.; Casciola, M. and Palombari, R. *J. Membr. Sci.*, 2000, 172, 233.

not water soluble as is not the case for the aforementioned HPAs. Therefore, the leaching out of the inorganic filler might be decreased in hydrated environments, which would afford better stability and longevity in the fuel cell environment. This research group has also used an inorganic material based on titanium phosphate that has recently been shown to have the highest proton conductivity of all the studied layered phosphonates.^{177,178} It was noted that the incorporation of the inorganic filler showed heterogeneity at values above 20 weight percent filler in Nafion[®] recast membranes. Therefore, lower weight percents of the layered titanium fillers were used and showed increased conductivities relative to the unfilled polymers. Further collaboration with Prof. Alberti has been initiated so as to use sulfonated poly(arylene ether sulfone) copolymers as the matrix polymeric material. It is believed that using the BPSH material or a phosphine oxide containing material could help to increase inorganic filler loadings and proton conductivity with little water swelling at temperatures above 100 °C.

2.23 Poly(arylene sulfide sulfone), Poly(arylene ether phosphine oxide sulfone) and Poly(arylene ether sulfone) Synthesis

There are many specific synthetic mechanisms to synthesize substituted poly(arylene)s, poly(arylene ether)s and poly(arylene thioether)s. Some of the reactions employed are Friedel-Crafts electrophilic substitution, metal coupling, The Ullman reaction, and nucleophilic aromatic substitution. The synthetic approaches to

¹⁷⁷ Alberti, G.; Constantino, U.; Casciola, M.; Ferroni, S.; Massinelli, L. and Staiti, P. *Solid State Ionics* 2001, 145, 249.

¹⁷⁸ Alberti, G. and Casciola, M. *Annu. Rev. Mater. Res.*, 2003, 33, 129-154.

poly(arylene thioether sulfones)s, poly(arylene ether ketone)s and poly(arylene ether sulfones)s are relatively similar because the polymers are usually amorphous with no semicrystallinity. On the other hand, poly(arylene ether)s can be semicrystalline, which allows changes in the reaction parameters.

2.24 Electrophilic Aromatic Substitution Polymerization Via Friedel-Crafts Reactions

Electrophilic aromatic substitution following the Friedel-Crafts sulfonylation and acylation mechanism can produce both poly(arylene sulfone)s and poly(arylene ketone)s depending on the starting materials.^{179,180} Poly(arylene sulfone)s are prepared by first forming the sulfonylium cation, ArSO_2^+ , then electrophilic cation attack on the aromatic carbon occurs to form an intermediate complex that decomposes by losing a proton to form a new sulfone linkage.¹⁸¹ A Lewis-acid catalyst is used on the sulfonyl halide to produce the sulfonylium cation. Therefore, the sulfone linkages are prepared by the reaction of aromatic sulfonyl chlorides with specific aromatic compounds that produce the desired polymeric architecture (Figure 2.34).

¹⁷⁹ Roberts, R. M., In: *Friedel-Crafts Alkylation Chemistry: A Century of Discovery*, Khala, A. A., Ed., New York: M. Dekker, 1984.

¹⁸⁰ Schimid, G. H., In: *Organic Chemistry*, Black, L. W., Ed., St.Louis: Mosby-Year Book, Inc., 1996.

¹⁸¹ Ivin, K.J. and Rose, J.B., *Advances in Macromolecular Chemistry*, W.M. Pasika, Ed., Academic Press: London, 1, 1968.

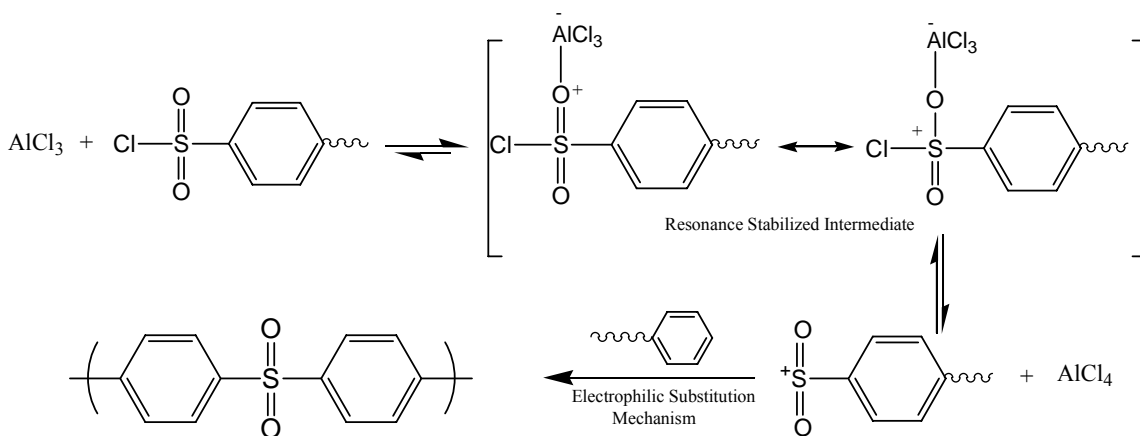


Figure 2.34 Friedel-Crafts electrophilic aromatic substitution reaction using a sulfonyl cation

Catalysis during Friedel-Crafts reactions is typically carried out by AlCl_3 , FeCl_3 or BF_3 , which proficiently sulfonylate by arenesulfonyl halides. Sulfonylation can be activated at the ortho and para positions by using electron-withdrawing groups on the aromatic rings being attacked. The para position is efficiently activated due to less steric hindrance and activation by the electron-withdrawing substituent.

For reactions involving AA-BB type sulfonylation, the aromatic ring can contain two or more activated hydrogen atoms, therefore, resulting in different repeating units. Irregularities in polymer architecture could be possible due to disulfonylation on one aromatic ring, sulfonylation at different ring positions and side reactions that are directly related to Friedel-Crafts catalysts. Therefore, since high catalyst concentrations promote side reactions that produce branched or crosslinked materials, the best methodology to decrease them was to employ the minimum amount of Friedel-Crafts catalysts (*i.e.* 0.1

wt%). The major disadvantage of both bulk and solution reactions is that metal–halide catalysts are impurities and hard to remove, contributing to deteriorating thermal stability and electrical conductance.

2.25 The Ullman Reaction to Synthesize Poly(arylene ether)s and Poly(arylene thioether)s

Synthesis of poly(aromatic ether)s can be carried out by reacting a phenol with an aromatic halide by using a copper complex as the catalyst.¹⁸² The Ullman reaction is a variation of the nucleophilic substitution reaction because of the phenolic salt reacting with the aromatic halide (Figure 2.35).¹⁸³

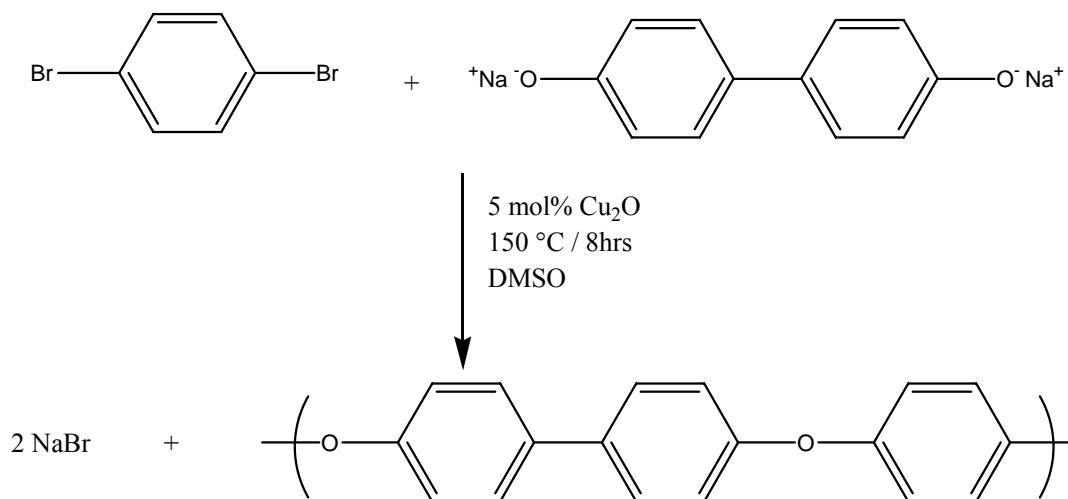


Figure 2.35 The Ullman reaction to produce poly(arylene ether)s

¹⁸² Farnham, A.G.; Robeson, L.M. and McGrath, J.E. *J. Appl. Polym. Sci.*, 1975, 26, 373.

¹⁸³ Badea, F., In: *Reaction Mechanisms in Organic Chemistry*, Turnbridge Wells, Kent: Abacus Press, 1977.

What makes this reaction unique, besides the copper catalyst, is nonactivated aromatic halides are able to be employed to produce polymeric architectures that are not possible with the classical nucleophilic substitution reactions. The difficulty of halogen displacement was determined to be opposite of that observed for the classical aromatic nucleophilic substitution reaction. Therefore, instead of using fluorine or chlorine as the halogen-leaving group, iodine or bromine was used and found to be more facile under the Ullman reaction conditions. The rate-determining step of the aryl-halide bond breakage has been shown to occur most efficiently with dibromo-monomers. Typical polymerization conditions use a cuprous chloride-pyridine complex catalyst with benzophenone solvent. Ullman coupling of bisphenols and dibromoarylenes using the copper catalyst has been shown to prepare high molecular weight poly(arylene ether)s.¹⁸⁴ However, this approach to poly(arylene ether)s synthesis has been distinguished by poor reproducibility, special brominated monomers and copper catalyst salt residues that decrease thermal stability and increase electrical conductance.

2.26 Metal Coupling Polymerizations

This novel approach to poly(arylene ether sulfone) synthesis employs Ni⁰ to form a new carbon-carbon bond from halogenated aromatic compounds.¹⁸⁵ Compared to the Ullman reaction, metal-coupling reactions using Ni⁰ catalyst provides high molecular weight polymers with chloro and fluoro compounds where unactivated or activated dihalides can be used. Furthermore, typical polymerization temperatures of 60-80 °C afford milder conditions when polymerized in aprotic solvents. As noted in the literature,

¹⁸⁴ Wang, S. and McGrath, J. E. In: *Polyarylene Ethers: A Review*, In: *Step Polymerization*, Rogers, M. and Long, T.E., Eds., Wiley, 2002.

¹⁸⁵ Ghassemi, H.; Ndip, G. and McGrath, J. E. *Polymer Preprints*, 2003, 44(1), 814.

monomers that contain only one phenyl ring can form biphenyls, triphenyls and so on, therefore, removing the need for biphenyl monomers.¹⁸⁶ Generally, a zero-valent nickel-triphenylphosphine complex is employed as the catalyst that is formed from zinc metal and nickel chloride. For example, Ghassami and McGrath¹⁸⁷ used nickel-catalyzed polymerizations to synthesize high molecular weight substituted poly(p-phenylene)s and copoly(p-phenylene)s using various dichloro monomers¹⁸⁸ including 2,5-dichlorobenzophenone (Figure 2.36).

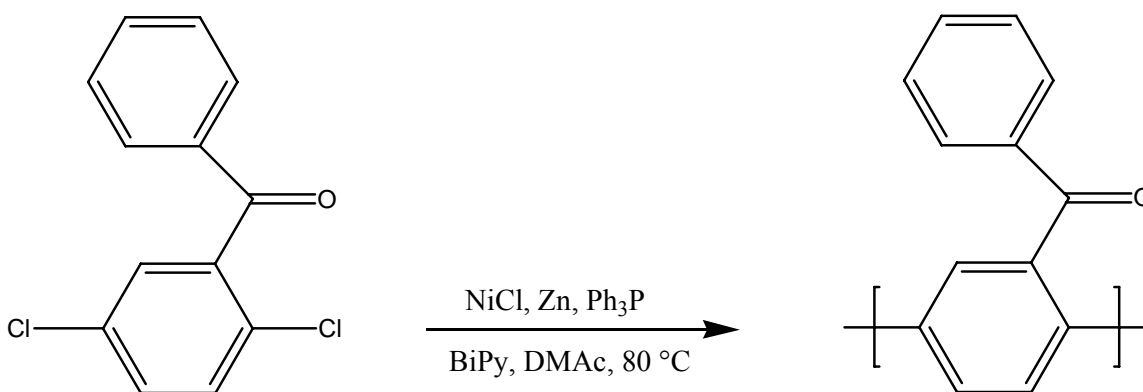


Figure 2.36 Synthesis of poly(2,5-benzophenone) using nickel coupling polymerization techniques

The carbon-carbon bonds were formed between the halogenated aromatic carbons to produce polymers with intrinsic viscosities of 0.6-1.0 dL/g. It was found that after only 40 minutes of polymerization time, the viscosity of the reaction media became very high

¹⁸⁶ Colon, I. and Kwiatkowski, G.T. *J. Polym. Sci.: Part A: Polym. Chem.* 1990, 28, 367.

¹⁸⁷ Ghassemi, H. and McGrath, J.E. *Polymer* 1997, 38, 3139.

¹⁸⁸ Ghassemi, H. and McGrath, J. E. *Polymer Preprints*, 2002, 43(2), 1021.

and after three hours, a thick paste-like material was formed. The polymeric material was precipitated into a mixture of methanol and hydrochloric acid. As indicated by the thermalgravimetry data, the poly(p-substituted-phenylene)s show high thermo-oxidative stabilities with a 5% weight loss of 480 °C or higher in air. For use as PEMs, the materials were sulfonated with fuming sulfuric acid at 25 °C for various times. As observed in previous studies, post-sulfonation was hard to control, but afforded polymers with high degrees of sulfonation as noted by the titrated IEC values. Polymers that were post-sulfonated for more than 60 minutes in H₂SO₄/SO₃ were water-soluble. In order to test the proton conductivity of the material, films must be cast, however, a major drawback of the material is its inability to produce tough, flexible films, probably due to the rigid architecture of the polymer. Previous research has shown that amorphous, high molecular weight poly(2,5-benzophenone) must be cast by composite techniques from a piece of glass fabric and dissolved polymer solution. Using this technique, conductivity values were similar to the Nafion[®] control at 0.09 S/cm.

2.27 Nucleophilic Aromatic Substitution Polymerizations

Efficiency and practicality are the major advantages of polymers derived from nucleophilic aromatic substitution reactions. Specifically, poly(arylene thioether sulfone)s and poly(arylene ether sulfone)s are most commonly formed via the strong or weak base approach of nucleophilic aromatic substitution (S_NAr). However, unactivated halide monomers cannot be used due to the low reactivity of resonance-stabilized aromatic leaving groups.¹⁸⁹ When non-activated aromatic halide molecules are used,

¹⁸⁹ Cotter, R.J. *Engineering Plastics: Handbook of Polyarylethers*, Gordon and Breach Publishers: Basel, Switzerland, 1995.

high temperatures only allow the reactions to proceed relatively slowly. As is the case with fluorobenzene, three out of the four resonance structures contain double bonds between the negative aromatic ring and the positive fluorine. Therefore, bond length would be decreased and stability of the C-F bond would be much greater than that of an activated alkyl halide compound. As a result, reactivity of non-substituted aromatic rings during nucleophilic aromatic substitution reactions is decreased to the point that extreme high temperatures (350 °C) and pressure would be needed to react fluorobenzene with a hydroxide ion in order to form the phenol product.¹⁹⁰

By using electron-withdrawing substituents to activate the aromatic ring, gentler reaction protocols can be used. Electron- withdrawing substituents activate the ortho and para positions of the aromatic ring, but the para position is usually more reactive due to less steric hindrance. Furthermore, as more activating moieties are added to the aromatic ring (i.e. in the meta positions), the reactivity of the ortho or para positions are increased such that very little heat is needed to get over the energy barrier for the reaction to occur. As many sophomore organic chemistry books will explain, the electron withdrawing power of the different activating moieties change and are indicated by the following: $\text{NO}_2 > \text{CF}_3 > \text{CN} > \text{CHO} > \text{COC} > \text{COOH} > \text{F} > \text{Cl} > \text{Br} > \text{I}$. However, not only the electronegativity of the electron-withdrawing moiety influences the reaction rate, the solvent employed in the reaction, temperature and nucleophilicity of the nucleophile used to attack the aromatic activated carbon also change the kinetics.¹⁹¹

¹⁹⁰ Clagett, D.C. In: *Encyclopedia of Polymer Science and Engineering*, Mark, H.F.; Bikales, N.M.; Overberger, C.G. and Menges, G., Eds., 6, John Wiley and Sons: New York, 1986.

¹⁹¹ Hedrick, J. L.; Mohanty, D. K.; Johnson, B. C.; Viswanathan, R.; Hinkley, J. A. and McGrath, J. E. *J. Poly. Sci.: Part A: Polym. Chem.* 1986, 23, 287.

At the onset of the reaction, nucleophilic attack occurs on the activated halide-carbon, which produces a resonance-stabilized intermediate compound. As the reaction proceeds, the halide leaving group removes itself to reform aromaticity (Figure 2.37).

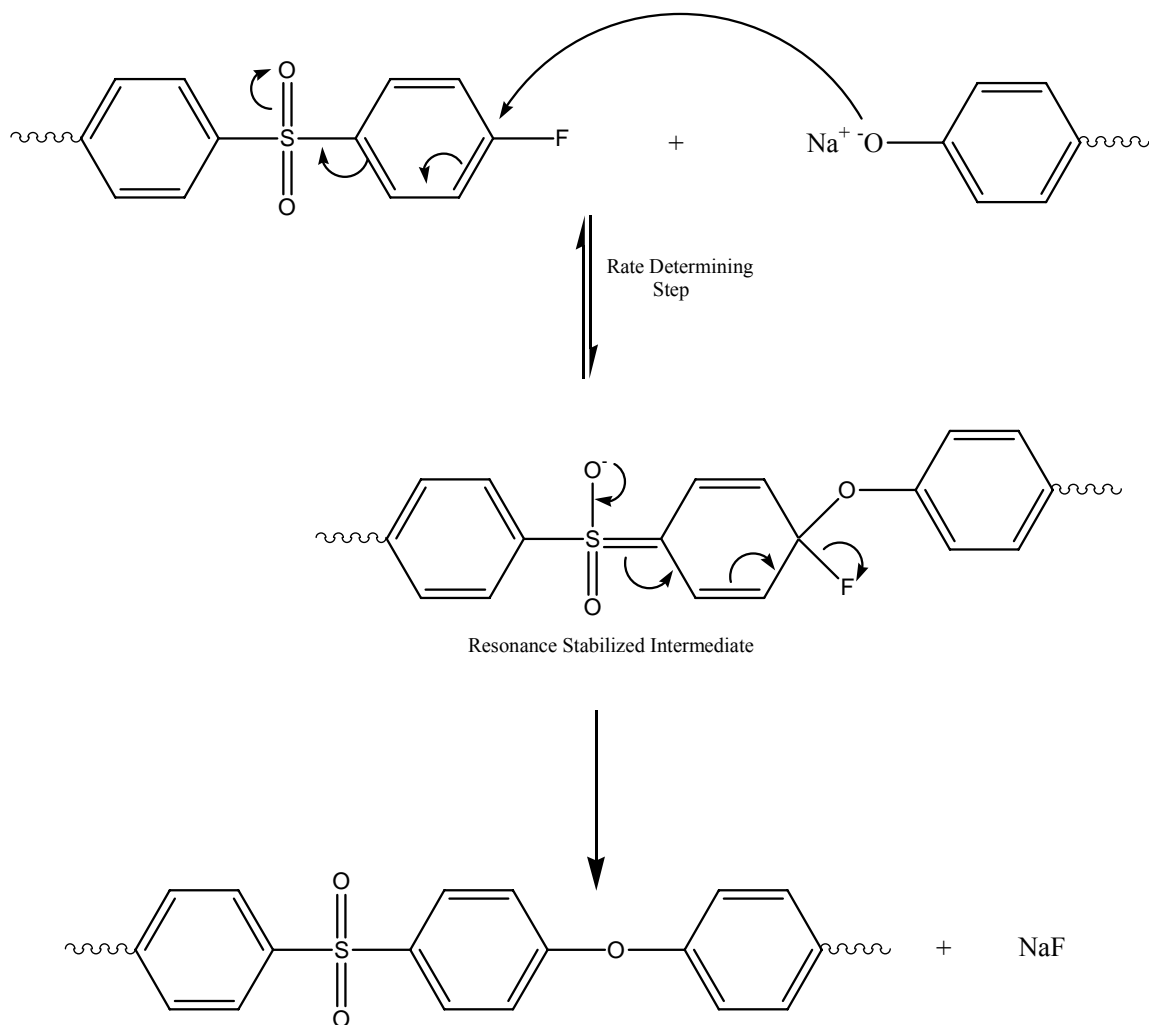


Figure 2.37. Nucleophilic aromatic substitution reaction to form resonance stabilized intermediate and further aromatic product of activated phenyl ring

The rate-determining nucleophilic attack has historically been determined by studying reaction rates of different leaving groups. Previous experiments have shown

that reactivity of halogens follows $F \gg Cl > Br > I$, which indicates that the actual departure of the halogen is not involved in the rate-determining step.¹⁹² The better reactivity of fluorine can be explained by enhanced stabilization of the intermediate by the extremely high electronegative fluorine atom using its inductive electron-withdrawing effects. Moreover, since the fluorine atom has the highest electronegativity of all the atoms, a partial positive charge will be on the attached carbon making it a much better electrophile for nucleophilic attack.

Synthesis of poly(arylene ether sulfone)s and poly(arylene thioether sulfone)s can follow two different techniques that are somewhat related, but are still experimentally different. The strong base approach uses sodium hydroxide as the base that abstracts the proton off of the hydroxyl or thiol group making it a sodium salt. The weak base approach employs potassium carbonate that abstracts the proton thereby producing a good nucleophile for nucleophilic aromatic substitution.

Johnson et al¹⁹³ first published the synthetic technique to obtain poly(arylene ether)s by step-growth nucleophilic aromatic substitution polymerization. The protocol that was used employed sodium hydroxide as the strong base, bisphenol A as the nucleophilic monomer, dichlorodiphenyl sulfone (DCDPS) as the electrophilic monomer and dimethyl sulfoxide/chlorobenzene as the solvent (Figure 2.38).

¹⁹² Miller, J.A., In *Aromatic Nucleophilic Substitution*, Elsevier: London, 1961, 61.

¹⁹³ Johnson, R.N.; Farnham, A.G.; Clendinning, R.A.; Hale, W.F. and Merriam, C.N., *J. Polym. Sci.: Part A*, 1967, 5, 2375.

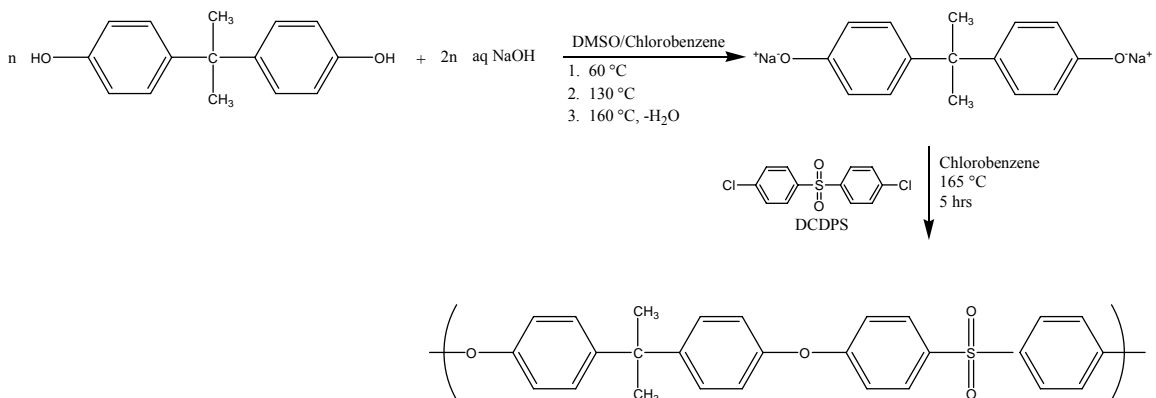


Figure 2.38 Strong base synthesis to produce poly(ether sulfone) based on bisphenol A

The mole ratio of sodium hydroxide to bisphenol A had to be an exact 2:1 ratio. An excess allows the reaction between the hydroxide ions and the activated halide (DCDPS), which would disrupt the overall stoichiometry by producing a dihydroxydiphenyl sulfone monomer. A similar reaction would occur if water was present in the reaction mixture; water could hydrolyze the activated dihalide monomer producing monohydroxy or dihydroxy sulfone monomers. Furthermore, possible chain scission could occur after polymers have been synthesized by the strong base attacking the activated aromatic ether linkages. A shortage of sodium hydroxide would not allow all the hydroxy moieties to become phenolates or good nucleophiles, thereby disturbing the 1:1 stoichiometry of the reactive phenolates. Therefore, excess sodium hydroxide or insufficient sodium hydroxide would produce low molecular weight oligomeric products and not high molecular weight polymeric materials. By preparing the phenolate salts with a strong base so they can be used for nucleophilic attack is a practical process. The phenolates will then react with the activated dihalides in either the ortho or para positions, depending

on where the halide moiety is located, relative to the electron-withdrawing group to produce a high molecular weight polymer in about five hours.

The use of potassium carbonate (K_2CO_3) or bicarbonate ($KHCO_3$) as a weak base instead of a strong base (NaOH) for nucleophilic aromatic substitution was first reported by Clendinning et al¹⁹⁴ so as to decrease the possible side reactions that could occur with sodium hydroxide. Fundamental research into the use of these weak bases for S_NAR reactions was carried out by McGrath et al¹⁹⁵ who systematically studied K_2CO_3 reactions to produce phenolate salts from bisphenol type compounds.¹⁹⁶ Figure 2.39 indicates a typical reaction scheme, which makes it relatively simple to control molecular weights and endgroup moieties.

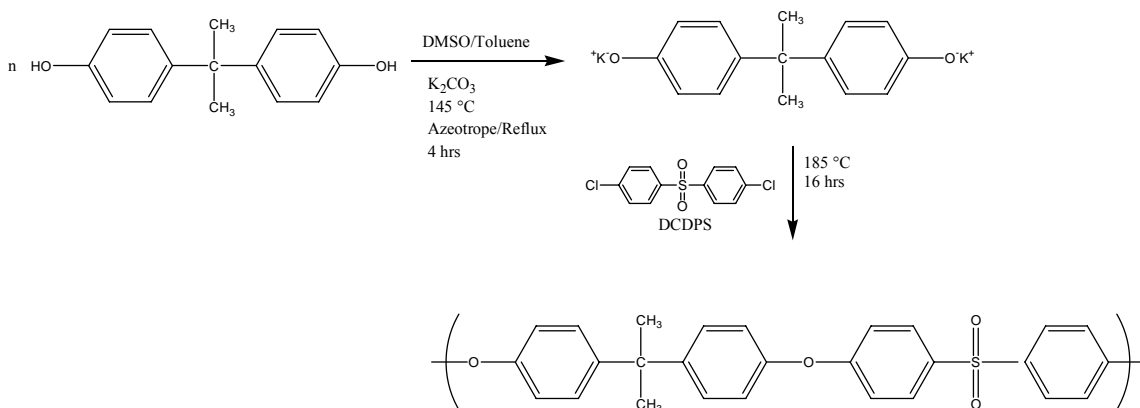


Figure 2.39 Weak base nucleophilic aromatic substitution scheme to synthesize high molecular weight poly(arylene ether)s

¹⁹⁴ Clendinning, R.A.; Farnham, A.G.; Zutty, N. L. and Priest, D.C. *Canada Patent 847,963*, 1970.

¹⁹⁵ Hedrick, J.L.; Mohanty, D.K.; Johnson, B.C.; Viswanathan, R.; Hinkley, J.A. and McGrath, J.E., *J. Polym. Sci.: Part A: Polym. Chem.*, 1986, 23, 287.

¹⁹⁶ Viswanathan, R.; Johnson, B.C.; McGrath, J.E., *Polymer* 1984, 12 (25), 1827.

Compared to the strong base approach using NaOH, stringent stoichiometry of weak base to the phenol is not needed to achieve high molecular weight polymers; in fact excess must be used. However, the disadvantage of the weak base approach as compared to the strong base approach is that the reaction rate of polymerization is, in general, slower.

Solvent choice for the weak base nucleophilic aromatic substitution reaction is critical in order to obtain high molecular weight polymers.¹⁹⁷ The solvent choice must be able to solvate both the monomers and polymers including the intermediate phenolates and Meisenheimer¹⁹⁸ complex. Aprotic polar solvents such as dimethyl sulfoxide (DMSO), N,N-dimethyl acetamide (DMAc) and N-methyl pyrrolidine (NMP) are typically employed for these high temperature reactions. However, when higher temperatures are needed, above the boiling point of the aforementioned solvents, solvents such as diphenyl sulfone and sulfolane can be used to increase reactivity of the monomers and help solubilize the resulting polymer even if it is semicrystalline (i.e. PEEK). Furthermore, as an added complication, the reaction mixture must be void of water. The presence of water be due to the sulfonated monomer absorbing it during weighing, atmospheric conditions and from the degradation of potassium carbonate as noted in Figure 2.40.



Figure 2.40 Production of water during decomposition of potassium carbonate

¹⁹⁷ Hedrick, J.L.; Dumais, J.J.; Jelinski, L.W.; Patsiga, R.A. and McGrath, J.E., *J. Polym. Sci., Polym. Chem.* 1987, 25, 2289.

¹⁹⁸ Meisenheimer, J. *Liebigs Ann. Chem.* 1902, 323, 205.

The water can hydrolyze the activated aromatic halide and upset the stoichiometry. Hence, to remove the water, an azeotroping agent must be added to the reaction mixture that will remove the water via a Dean-Stark trap. Azeotroping agents such as toluene and xylene are commonly used.

2.28 Polymeric Transducers Based on Ion-Exchange Membrane Electrode Assemblies

Ionic polymer electromechanical transducers have historically been based on the low modulus Nafion[®] materials. These transducers contain an ion-exchange membrane having conductive metal electrodes plated to the outer surfaces (Figure 2.41).

Electromechanical coupling¹⁹⁹ occurs under the submission of an electric field and physical deformations of the material produce actuation and sensing, respectively.²⁰⁰

Relative to piezoelectric materials, which have less than 1% strain and operate at 2000 Volts, polymer transducers produce a higher strain output at greater than 1%, lower voltage operation at 1-4 Volts and high sensitivity when used in charge-sensing mode.

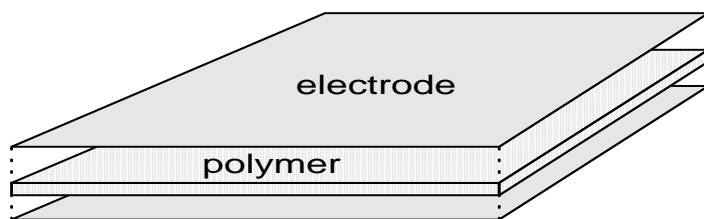


Figure 2.41 Conductive metal electrodes plated on an ion-exchange membrane

Polyelectrolyte membranes typically consist of ion containing pendent groups that are covalently bound to the polymer backbone. These pendent moieties produce phase separation and charge aggregation that allows for selective ion-exchange through ion-hopping and/or ion-host transportation. The hydrophilic clusters/channels of the ion

¹⁹⁹ Winter, M and Brodd, R. J. *Chem. Rev.* 'What Are Batteries, Fuel Cells and Supercapacitors' 2004, 104, 4245-4269.

²⁰⁰ Oguro, K., Fujiwara, N., Asaka, K., Onishi, K. and Sewa, S. *Proceedings of International Society for Optical Engineering (SPIE)*, Vol. 3669, 63-71, 1999.

containing groups allow for transport and the hydrophobic backbones allow for tough and ductile physical properties. Nafion and other alternative ion exchange membranes consist of covalently bound sulfonate moieties (anions) and very labile cations, typically protons. Therefore, the selectivity of the materials can be tailored to improve cation transport (e. g. H^+ , Li^+ , Na^+) while the anions are fixed.

The electromechanical actuation and sensing of these materials has been determined to be due to ion conduction and flux when a small electric field is applied.²⁰¹ Models have been proposed²⁰² that relate the pressures and velocities in the materials to ion flux and electric field. Similar modeling has been proposed by Newbury and Leo^{203,204,205} that employs force, displacement, charge and voltage as variables rather than only ion flux and electric field. Nemat-Nasser²⁰⁶ determined that the electric field allows an accumulation of cations on the negatively charged electrode and a depletion of cations at the positively charged electrode. Therefore, the steady-state distribution of charges during electromechanical deformation was due to ionic attraction through ionic flux. The phenomenon of relaxation when a constant electric field is applied has also been modeled by Nemat-Nasser²⁰⁷, which allowed for a prediction of low-frequency relaxation in ionic polymers. By combining the model of charge accumulation and the model of charge state within the polymer, mechanical deformation and quasi-static relaxation was predicted.

²⁰¹ Shahinpoor, M., Bar-Cohen, Y., Simpson, J. and Smith, J. *Smart Materials and Structures*, 7(6), 15-30, 1998.

²⁰² de Gennes, P., Okumura, K., Shahinpoor, M. and Kim, K. J. *Europhysics Letters*, 50(4), 513-518, 2000.

²⁰³ Newbury, K. M. and Leo, D. J. *J. of Intelligent Materials and Structures*, 13(1), 51-60, 2002.

²⁰⁴ Newbury, K. M. and Leo, D. J. *J. of Intelligent Materials and Structures*, 14(6), 333-342, 2003.

²⁰⁵ Newbury, K. M. and Leo, D. J. *J. of Intelligent Materials and Structures*, 14(6), 343-358, 2003.

²⁰⁶ Nemat-Nasser, S. and Li, J. *Proceedings of SPIE*, Vol. 3987, 82-91, 2000.

²⁰⁷ Nemat-Nasser, S. *J. of Applied Physics*, 92(5), 2899-2915, 2002.

A recent study aided in further understanding of electromechanical deformation and charge accumulation at the electrodes.²⁰⁸ By varying the molar amounts of fixed anions and the type of cations in Flemion[®] (Asahi Glass), a relationship between the motion of the tip and the total charge flow in the ionomer was apparent. They concluded that there was a linear relationship between the normalized charge, which is to say the cations versus the anions, and the normalized deflection. However, when Nafion[®] actuators were subjected to similar experiments, the material exhibited a relaxation, thereby not allowing full analysis of the normalized charge to normalized deflection. A previous study²⁰⁹, comparing Nafion[®] and Flemion[®] with various cations and induced charges, described that the ratio of the tip displacement to induced charge, charge-specific displacement, was variable for different forms of cations in both materials. The study also suggested that there was a relationship between the charge-specific tip displacement and the conductivity of the ionomer. Studying the freezable bound water in the systems and relating it to the charge deformation suggested a similar relationship.

2.29 Understanding 'Smart Materials'

Smart material applications include actuators, sensors and dampers to only name a few. These types of materials can adapt to changes in physical environments that include varied electrical charge, magnetic polarity, humidity and temperatures.

Electromechanical transducers are of utmost importance to both mechanical engineers and materials scientists. Tailoring material properties to best fit the criteria for enhanced physical performance has been a major area of research for electromechanical

²⁰⁸ Nemat-Nasser, S. and Wu, Y. *J. of Applied Physics*, 93(9), 5255-5267, 2003.

²⁰⁹ Asaka, K., Fujiwara, N., Oguro, K., Onishi, K., Sewa, S. *J. of Electroanalytical Chem.*, 505, 24-32, 2001.

transducers. Various materials have been studied that show electromechanical coupling effects such as piezo-polymers, piezo-ceramics, dielectric elastomers, shape memory polymers and alloys, conducting polymers and ionic polymers.

Piezo-electric materials, or ferro-electric materials, typically are made of ceramics, metals or polymers. High frequency transduction occurs in these materials when an electric field is applied by rotation of the dipoles that are inherently present in these materials. An example of a ceramic piezo material is Lead Zirconate Titanate (PZT), which produces very large forces but very little displacement. An example of a piezo-polymer material is poly(vinylidene fluoride trifluoroethylene), which succumbs to the same disadvantage as the piezo-ceramic materials, very little displacement. The PVDF dipoles are directly related to the electronegativity of the fluorine atoms along the polymer backbone.²¹⁰ PVDF actuators are produced by heating the material above the Currie temperature where the dipoles are allowed to randomize followed by an electric field perpendicular to the direction that the material will elongate. The material is then cooled while the electric field is still applied.²¹¹ By applying a large voltage (e. g. 1-2 kV) in the opposite direction of the dipoles, the material undergoes dipole rotation to elongate in the specific direction (Figure 2.42).

²¹⁰ Bar-Cohen, Y. *Electroactive Polymer Actuators as Artificial Muscles*, SPIE Press, Bellingham, WA, 2001.

²¹¹ Cheng, Z. Y., Bharti, V. and Zhang, Q. M. *Sensors and Actuators A-Physics*, 90, 138-147, 2001.

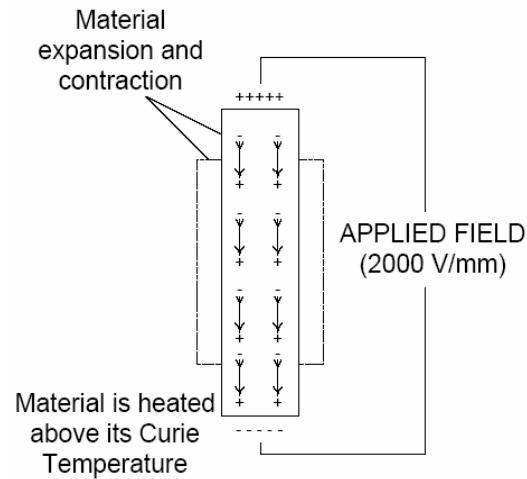


Figure 2.42 Piezo-electric strain occurring by application of electric field

Dielectric elastomer transducers are produced by plating conductive electrodes on both sides of an elastomeric polymer membrane. By applying a large voltage across the electrodes (e. g. 1-2 kV), electrostatic attraction of the electrodes produces a large pressure on the elastomeric material, thereby causing physical deformation²¹² (Figure 2.43). Ease of manufacturing, large stresses and very large displacements (i. e. up to 400%) make these materials promising, however, the disadvantages include large actuation voltages and poor durability of the membrane electrode assembly.

²¹² Kornblush, R. and Perline, R. *Int. Symp. on Smart Structures and Mat.: Electroactive Polym. Actuator Devices SPIE Proceedings*, 3669, 149-161, 1999.

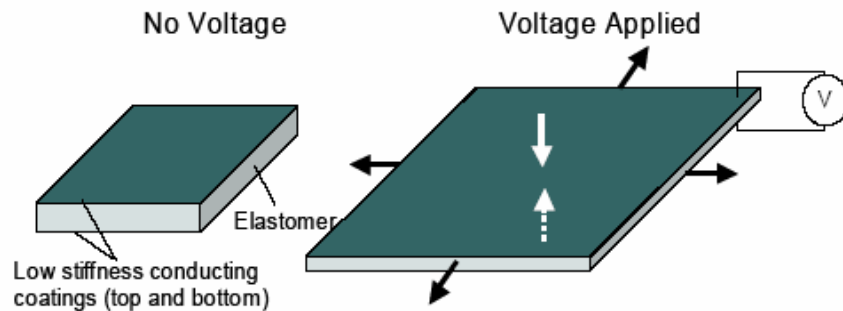


Figure 2.43 Dielectric elastomer deformation by electrostatic attraction of the electrodes

Polymer or alloys that deform when a phase transition is reached due to a change in temperature are termed shape memory materials. These thermocoupled materials remember a previous shape and can be transition between shapes through heating and cooling. Shape memory alloys (SMA) are typically made of Nickel Titanium alloys and can rearrange the molecular structure between a martensitic phase and an austenitic phase due to changes in temperature.²¹³ Material properties of SMAs consist of slow response times on the order of seconds to minutes, extreme temperature dependence, thermal conductivity of the surrounding environment dependence, good cycling ability, roughly 5-8% strain and large stresses that can be up to 200 MPa. Shape memory polymers have recently entered the field, but are limited to only one cycle life. These polymeric materials experience large physical deformations when high temperatures are applied (e. g. heat shrink wrap and tubing).²¹⁴

Electronically conductive polymers consist of conjugated structures along the backbone. The oxidation state of the material can be changed by applying an electric potential which will lead to the removal or addition of charge along the backbone.

²¹³ Funukubo, H. *Shape Memory Alloys*, Gordon and Breach Press, New York, 1987.

²¹⁴ Landlein, A. and Langer, R. *Science*, 296(5573), 1673-1676, 2002.

Therefore, to balance the charge, ions are transported through the material and inserted between the backbones to produce large deformations under small electric potentials. However, disadvantages include low charge-displacement efficiencies, slow response times and the conducting polymers must be doped with an electrolyte.

Ionic polymers, which have been previously described using sulfonate moieties as the ion conducting group, can also be based on poly(ethylene oxide) (PEO) and poly(ethylene glycol) (PEG).²¹⁵ Typically these materials are composed of a matrix of high molecular weight PEO blended with low molecular weight PEG.²¹⁶ These solvent-free transducers produce large deformations (10% strain) at low voltages (1-3V) but can only operate at low frequencies in the range of 10Hz.

The need for large displacements and low voltage operating transducers is becoming more apparent as relevant to the industries leading piezo materials. Piezo materials produce large forces but provide only micron-scale displacements. The industry has overcome some of the strain barriers by stacking the piezo materials and adding mechanical amplification devices. However, these techniques decrease energy densities where the materials still need very high voltages. Larger displacement actuators based on ionomers can be enhanced by various synthetic techniques on the molecular level which can allow high power densities and lightweight devices. Furthermore, biocompatibility and low voltages allow them to be potential candidates for artificial muscles and wearable sensors.

²¹⁵ Shahinpoor, M and Kim, K. J. *Applied Physics Letters*, 80(18), 91-94, 2002.

²¹⁶ Gray, M. *Polymer Electrolyte Reviews-1*, MacCallum, J. R. and Vincent, C. A., Eds., pg. 139, Kluwer Academic Press, Dordrecht, 1987.

2.30 Creating Capacitance Through The Electric Double Layer

Capacitance has been defined as the derivative of, or change in, charge motion divided by the derivative of voltage. This helps to understand the correlation between charge motion and displacement. Therefore, it is understood that an increase in capacitance will increase the motion of charges at constant voltage. The capacitance can further be defined as the ability of a material to store an electric charge for use at a later time. This electronic device is designed to provide energy in an electric circuit by storing electricity in an electric field that is between two separate conducting plates. Capacitors are used in many ways such as computer chip memory, camera flashes and tuned circuit radios. In their simplest form, they consist of two electronically conductive plates that are separated by an electronic insulator termed a dielectric. When applying a voltage source to a capacitor, electrons are forced onto the surface of one plate that in turn pulls electrons off the surface of the other plate. This process creates a potential between the two plates that are separated by a dielectric media. The dielectric material that is used depends on the application and includes paper, ceramic, air, mica, and electrolytic materials. Because the dielectric material between the plates act as an insulator, current does not flow until an external circuit is closed resulting in a discharge. The capacitor plates can be charged and discharged as determined by the application.

Dielectric materials serve both as an insulator to prevent current flow and as a media to support the electrostatic force of a charged capacitor. Dielectrics are rated by their ability to support the electrostatic forces by employing a number called a dielectric constant. The standard by which all other dielectric materials are measured is a vacuum, which has a dielectric constant of 1.0. The value for air is much the same at 1.00059.

However, as Table 2.1 indicates, a variety of materials can be used as dielectric materials.²¹⁷

Table 2.1 Various dielectric materials and their corresponding dielectric constants.

Material	Dielectric Constant
Vacuum	1.0
Air	1.00059
Teflon	2.1
Polyethylene	2.25
Polystyrene	2.5
Mylar	3.1
Polyvinyl Chloride	3.18
Plexiglas	3.4
Paper	3.5
Mica	3-6
Neoprene	6.7
Glass	5-10
Methyl Alcohol	35
Glycerin	42.5
Water	80.4

The measure of capacitance is the Farad (symbol F), which is named after Michael Faraday. The value of 1.0 farad is defined as 1.0 coulomb being placed on a capacitor having a potential difference between the plates of 1.0 volt, where coulomb is the amount of charge transferred by a current of 1.0 ampere in 1.0 second, which is equal to the charge of 6.25×10^{18} electrons. Therefore, 1.0 farad is a very large amount of capacitance and thus microfarads and picofarads are commonly employed. Factors that affect the value of capacitance include the area of the plates, the distance between the plates and the dielectric constant of the material between the plates. When the plates have a larger surface area, they provide a greater capacity to store a charge, thus a higher capacitance. The electrostatic force field between the plates is much stronger when they

²¹⁷ Sears, F. W., Zemansky, M. W. and Young, H. D. *University Physics, 6th Ed.*, Addison-Wesley, 1982.

are closer together and the value of capacitance is directly proportional to the amount of electrostatic force. Therefore, as the distance between the plates increases, the capacitance decreases and as the distance decreases, the capacitance increases. The third factor determining capacitance is the dielectric material. There is a direct correlation between the ability of the dielectric material that supports the electrostatic forces to the dielectric constant. Therefore, as the dielectric constant decreases, capacitance decreases. As table 1 indicates, water supports the electrostatic forces better than any other material in the table and is a very good dielectric material. The capacitance can be calculated using the following equation where C is the capacitance, k is the dielectric constant, A is the area of one plate in m², d is the distance between the plates in meters and 8.855 is a constant.

$$C = (8.855kA) / d$$

The capacitance that is present in polymeric transducers has been determined to be due to the electric double layer that forms between the interface of the electrode and dielectric polymer.²¹⁸ The electric double layer theory has been used to calculate the motion of ions and distribution of ions in an electrolyte dielectric material. The mobile ions in the electrolyte tend to adsorb onto the metal layer and also tend to be distributed away from the polymer-metal interface in such a fashion that the charge on the metal electrode is balanced. This phenomenon is termed supercapacitance and is described as having a very large capacitance per unit weight or volume.

²¹⁸ Sadeghipour, K., Salomon, R. and Neogi, S. *Smart Materials and Structures*, 1, 3445-3447, 1992.

Supercapacitors are neutral systems that contain an electric double layer at the interface of the metal electrode and electrolyte dielectric material.²¹⁹ The neutrality of the system is obtained by a diffuse layer of positive charges in the electrolyte opposing a centralized layer of negative charges in the electrode. Thus, the double layer is formed in which the separation of each layer is on the order of a few angstroms.²²⁰ The following electric double layer models have historically been proposed as a means to better understand transduction mechanisms and supercapacitor phenomenon.²²¹

In 1853 Helmholtz suggested the electric double layer (EDL) theory for metal-metal interfaces and in 1879 it was further developed for electrolyte-metal interfaces.²²² As shown in Figure 2.44, the Helmholtz model describes the interface as consisting of an arranged layer of adsorbed ions in the electrolyte and a layer of electrons at the surface of the electrode. This early account of the EDL is useful in that it describes basic supercapacitance, however, it neglects to describe the concentration gradient of ions in the electrolyte that occurs further from the electrode-electrolyte interface.

²¹⁹ Winter, M and Brodd, R. J. *Chem. Rev.* 'What Are Batteries, Fuel Cells and Supercapacitors' 2004, 104, 4245-4269.

²²⁰ Endo, M. and Ishii, K. *Carbon Science*, 1, 117-128, 2001.

²²¹ A. Kitahara 'Electrical Phenomena at Interfaces', Vol. 15, Addison-Wesley, 1984.

²²² Sparnaay, M. *The Electrical Double Layer*, Pergamon Press, Oxford, New York, 1972.

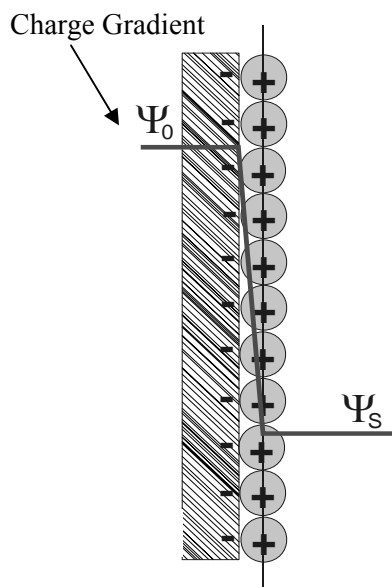


Figure 2.44 Helmholtz model indicating the electric double layer present at electrolyte-electrode interface

It was not until around 1910 that Gouy and Chapman independently described the EDL as having a diffuse layer consisting of a concentration gradient of ions at the metal-electrolyte interface. They took into account the applied voltage, electrolyte concentration and the thermal motion of the ions to create a model that influenced the capacity of the EDL. As Figure 2.45 indicates, the EDL is not as compressed as the earlier model, which produced a variation in ion density at any one point in the ion layer. It was determined that the Gouy-Chapman model calculated larger capacitances relative to the experimental results. These calculated data assumed the ions to be ‘point charges’ where there were no shells on the ions, only the charge itself. Therefore, the model did not take into account the spatial size of the ions and the correct packing at the interface.

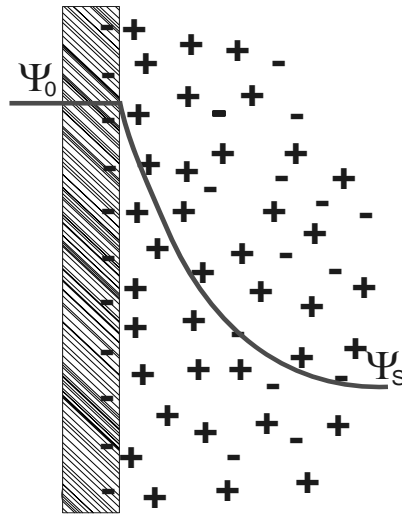


Figure 2.45 Gouy-Chapman model indicating concentration gradient of ions in electrolyte

Around 1940, Stern and Grahame developed a model that allowed for finite sized ions to contain charges at the center. Stern used both the Helmholtz model and the Gouy-Chapman model to better define the EDL using both an adsorbed layer of finite sized ions and a diffuse layer of ions in the electrolyte. Grahame used the basics of what Stern had developed and further defined it into two regions. He defined the compact layer of finite sized ions adsorbed on the electrode as the inner Helmholtz plane and the diffuse layer of ions in the electrolyte solution as the outer Helmholtz plane (Figure 2.46). The Stern and Grahame model described the capacitance in great detail, however, it failed to account for a hydration shell of the ions in solution.

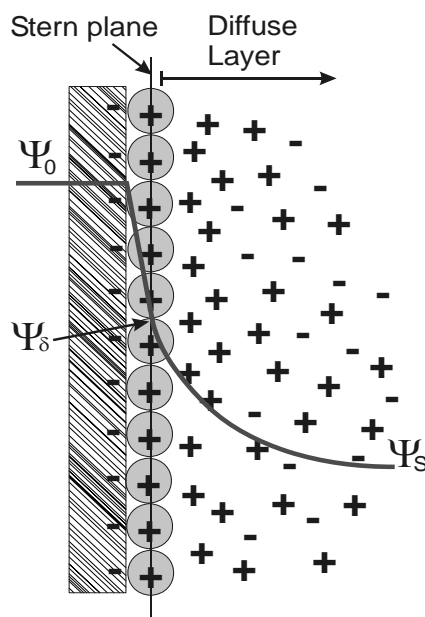


Figure 2.46 Stern and Grahame model indicating finite sized ions adsorbed and diffuse

It was not until 1963 that Bockris, Devanathan and Muller defined a model that employed the impact of solvent on ions near the metal-electrolyte interface.²²³ When hydrated with water, the model accounted for a hydration shell at the inner Helmholtz plane, which was further developed to allow for the fixed dipoles due to the charge in the electrodes. The hydration shell at the inner Helmholtz plane would be displaced due to the adsorption of ions at the electrode surface (Figure 2.47). The outer Helmholtz plane would consist of hydrated ions in a diffuse layer.

²²³ Matsumoto, M. In *Electrical Phenomena at Interfaces: Fundamentals, Measurements and Applications*, Vol. 76, 2nd Edition, Marcel Dekker Inc., New York, 1998.

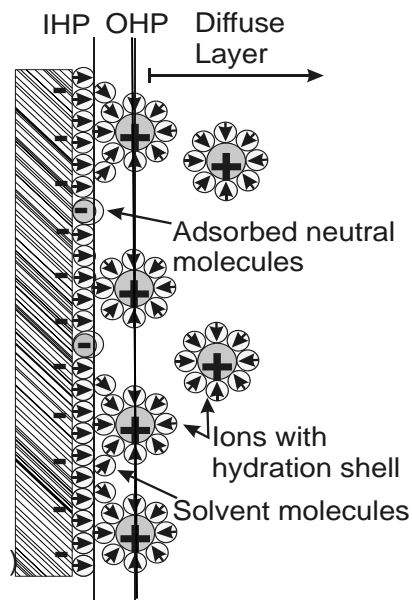


Figure 2.47 Brockris, Devanathan and Muller model employing hydration shells on ions

CHAPTER 3:

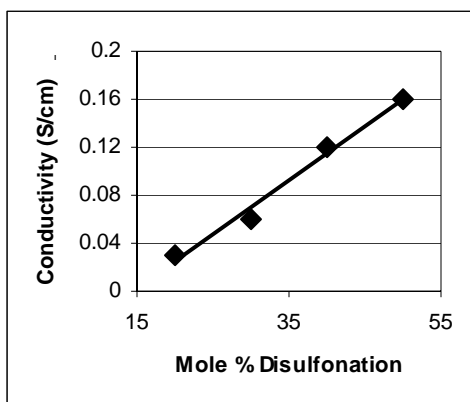
DIRECTLY COPOLYMERIZED POLY(ARYLENE SULFIDE SULFONE) DISULFONATED COPOLYMERS FOR PEM-BASED FUEL CELL SYSTEMS: SYNTHESIS AND CHARACTERIZATION

Taken From: Wiles, K. B., Wang, F. and McGrath, J. E. *J. Poly. Sci.: Part A: Poly. Chem.*, Accepted, 2005.

Graphical Abstract

Direct aromatic nucleophilic substitution polycondensations of disodium 3,3'-disulfonate-4,4'-difluorodiphenylsulfone (SDFDPS), 4,4'-difluorodiphenylsulfone (DFDPS) (or their chlorinated analogs, SDCDPS, DCDPS) and 4,4'-thiobisbenzenethiol (TBBT) in the presence of potassium carbonate were investigated. Electrophilic aromatic substitution was employed to synthesize the disodium 3,3'-disulfonate-4,4'-difluorodiphenylsulfone comonomer in high yields and purity. High molecular weight disulfonated poly(arylene thioether sulfone) (PATs) copolymers were easily obtained using the SDFDPS monomers, but in general, slower rates and a lower molecular weight copolymer was obtained using the analogous chlorinated monomers. Tough and ductile membranes were solution cast from N,N-dimethylacetamide for both series of copolymers. The degrees of disulfonation (20-50%, PATs 20-50) were controlled by varying the ratio of disulfonated to unsulfonated comonomers. Precise control of the ionic concentration, well-defined ionic locations and enhanced stability due to the deactivated position of the

-SO₃H group are some of the suggested advantages for direct copolymerization of sulfonated monomers. Proton NMR, infrared spectroscopy and ion exchange capacity experiments successfully characterized the copolymer structure as increased amounts of disulfonated monomers were used in the reaction media. Morphological studies using AFM phase imaging indicated an increase in connectivity of ionic domains from the low disulfonated copolymers to levels of full connectivity for the 40 mol% copolymer. A phase inversion from hydrophobic to hydrophilic continuity was observed in the range of 35 mol% to 40 mol% disulfonation for the PATS system. Coupling these findings with water uptake further characterizes the percolation threshold with the dramatic increase of water sorption from 35 mol% disulfonation to 40 mol% disulfonation. Enhanced proton conductivity was obtained with increasing mol% of disulfonation reaching levels of 0.16 S/cm for PATS 50.



Proton conductivity of disulfonated membranes in water at 30 °C for PATS based on TBBT, DCDPS and SDCDPS.

Key Words: sulfonated copolymer, poly(arylene thioether sulfone), poly(arylene sulfide sulfone), poly(arylene ether sulfone), proton exchange membrane, fuel cell, Nafion, morphology

3.1 Introduction

Proton exchange membrane fuel cells (PEMFC) based on polymer electrolyte membranes (PEM) are promising candidates for applications such as stationary power, low-emission vehicles and portable electronics. The membrane electrode assembly (MEA), consisting of well-bonded catalyst electrodes and proton exchange membrane (PEM), is the essence of the fuel cell and is critical for allowing proton transport from the anode to the cathode and the generation of electricity from chemical energy. PEMs must have good mechanical, thermal, and chemical stabilities and still have high proton conductivity. The polyperfluorinated sulfonic acid membranes are the state-of-the-art PEMs used for both hydrogen and methanol fuel cells.²²⁴ However, some specific limitations exist for Nafion™-type membranes, which include low conductivity at high temperatures and low humidity as well as high methanol permeability that decreases fuel efficiency.²²⁵

The bulk properties of ion-containing copolymeric systems are a function of the ionic interactions in nanometer-size regions of the material.^{226,227} For solid-state PEMs, the composition of the ions is not the major component, or the matrix, of the system, as is the case with most biological polyelectrolytes. Rather, the macromolecular properties of

²²⁴ M. A. Hickner, H. Ghassemi, Y. S. Kim, B. R. Einsla and J. E. McGrath, *Chem. Rev.* 2004, 104, 4587-4612.

²²⁵ M. Mathias, H. Gasteiger, R. Makharia, S. Kocha, T. Fuller, T. Xie and J. Pisco, *Preprints of Symposia - American Chemical Society, Division of Fuel Chemistry 2004*, 49(2), 471-474.

²²⁶ A. Eisenberg and M. Rinaudo, *Polymer Bull.* 1990, 24, 671.

²²⁷ Lundberg, R.D. and H.S. Makowski, *A Comparison of Sulfonate and Carboxylate Ionomers*. In *Ions in Polymers, Adv. Chem. Ser. 187*, Eisenberg, A, Ed., 1980, pp. 21, American Chemical Society: Washington D. C.

the system are the critical characteristics.²²⁸ The materials that are used to produce ionomeric materials are most often random copolymers in the proton form with ionic side groups. The well studied ethylene and styrene systems that contain ionic groups which may contain sulfonic acid, carboxylic acid or quaternary amines are the main focus of many papers.^{229,230} Non-ionic polymeric materials can also be transformed into a wide range of ionomeric materials by reactions after polymerization (post-ionization). The polymeric architectures can be different by the position, type and concentration of the ion moieties on the polymer backbone. However, post-ionization reactions have proven to be difficult to precisely reproduce and typically only place one ion moiety randomly on an aromatic repeat unit.

Poly(phenylene sulfide) polymers are interesting engineering thermoplastic materials due to high crystalline melting temperatures, good mechanical and electrical properties and good chemical resistance.^{231,232,233,234,235} Liu et al²³⁶ reported a novel approach to synthesizing related poly(arylene sulfide sulfone) polymers via A-A or A-B type thiol-functional monomers, such as 4-chloro-4-mercaptodiphenyl sulfone and bis(4-mercaptophenyl sulfone). This novel synthetic approach uses a simplified nucleophilic

²²⁸ Ionomers: Synthesis, Structure, Properties and Applications, M. R. Tant, K. A. Mauritz and G. L. Wilkes, Eds., 1997, Chapman and Hall: New York.

²²⁹ K.V. Farrell, and B.P Grady, *Macromolecules* 2000, 33, 7122.

²³⁰ U.K. Mandal, *Polymer International* 2000, 49, 1653.

²³¹ D. R. Fahey and C. E. Ash, *Macromolecules* 1991, 24, 4242.

²³² J. F. Geibel and R. W. Campbell, In: *Comprehensive Polymer Science*, vol. 5: Step Polymerization, G. C. Eastmond, A. Ledwith, S. Russo, P. Sigwalt, Eds., Oxford: Pergamon Press, 1989.

²³³ H. W. Hill Jr. and D. G. Brady, In: *Kirk-Othmer Encyclopedia of Chemical Technology*, M. Grayson, Ed., 18, New York: Wiley, 1982.

²³⁴ R. W. Campbell, U. S. Patent 4,125,525, to Phillips Petroleum Company, 1978.

²³⁵ R. W. Campbell, U. S. Patent 4,016,145, to Phillips Petroleum Company, 1997.

²³⁶ Y. Liu, A. Bhatnagar, Q. Ji, J. S. Riffle, J. E. McGrath, J. F. Geibel, and T. Kashiwagi, *Polymer* 2000, 41, 5137.

aromatic substitution process rather than the traditional high pressure route which is suitable for the synthesis of amorphous poly(arylene sulfide sulfone) polymers. An earlier preprint from our group²³⁷ described a synthesis of a new monomer that contains two thiol groups and a sulfone group. This dithiol was copolymerized with 4,4'-difluorodiphenyl (DFDPS) sulfone and 3,3'-disulfonated 4,4'-difluorodiphenyl sulfone (SDFDPS) to produce a random copolymer that contains hydrophobic repeating sulfide-sulfone moieties and hydrophilic disulfonated units randomly placed along the copolymer backbone (Figure 3.1).

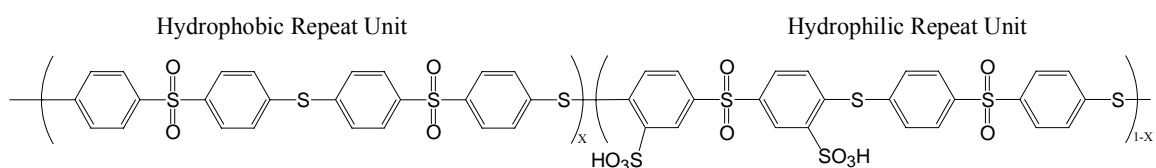


Figure 3.1 Repeat unit of a random copolymer that contains hydrophobic repeating sulfide-sulfone moieties and hydrophilic disulfonated units randomly placed along the copolymer backbone.

Our laboratory has actively investigated²³⁸ sulfonated poly(arylene ether sulfone) copolymers^{239,240,241,242} and related polyimide systems²⁴³. The similarities and

²³⁷ F. Wang, J. B. Mecham, W. Harrison, and J. E. McGrath, *Polymer Preprints* 2000, 41(2), 1401.

²³⁸ Y. S. Kim, L. Dong, M. A. Hickner, T. E. Glass, V. Webb and J. E. McGrath, *Macromolecules*, 2003, 36(17), 6281-6285.

²³⁹ F. Wang, M. Hickner, Q. Ji, W. Harrison, J.B. Mecham, T.A. Zawodzinski and J.E. McGrath, *Macromol. Symp.* 2001, 175, 387.

²⁴⁰ Y. S. Kim, L. Dong, M. A. Hickner, B. S. Pivovar, and J. E. McGrath, *Polymer* 2003, 44, 5729.

²⁴¹ F. Wang, M. A. Hickner, Y. S. Kim, T. A. Zawodzinski and J. E. McGrath, *J. Membrane Sci.* 2002, 197, 231-242.

²⁴² Y. S. Kim, F. Wang, M. A. Hickner, S. McCartney, Y. T. Hong, W. L. Harrison, T. A. Zawadzinski and J. E. McGrath, *J. Polym. Sci.: Part B: Polym. Phys.* 2003, 41, 2816.

differences of oxygen and sulfur that has previously been observed for non-sulfonated polymer architectures encouraged us to investigate thioether polymeric structures. Preliminary reports^{244,245,246,247,248} have further described how these wholly aromatic poly(arylene thioether sulfone) copolymers can be employed as proton exchange membranes for fuel cells. The cationic containing moieties that were randomly copolymerized along the backbone allow for ion-aggregation and ion-exchange through specific water transport mechanisms. In our view the direct copolymerization of disulfonated monomers affords enhanced control and stability relative to the post-sulfonation route.^{249,250} One explanation is that the proton exchange sites were introduced to the deactivated phenyl rings of the monomer, which would be expected to provide enhanced chemical stability to desulfonation (Figure 3.2). Furthermore, high molecular weight copolymers with various amounts of disulfonation were synthesized directly as a function of the molar ratios of starting monomers, which avoids several possible side reactions that can easily occur during post-sulfonation.

²⁴³ B. Einsla, Y. Hong, Y. S. Kim, F. Wang, N. Gunduz, J. E. McGrath, *J. Poly. Sci.: Part A: Polymer Chemistry* 2004, 42(4), 862-874.

²⁴⁴ K. B. Wiles, V. A. Bhanu, F. Wang and J. E. McGrath, *Polymer Preprints* 2002, 43(2) 993.

²⁴⁵ K. B. Wiles, V. A. Bhanu, F. Wang, M. A. Hickner, and J. E. McGrath, *Polymer Preprints* 2003, 44(1) 1089.

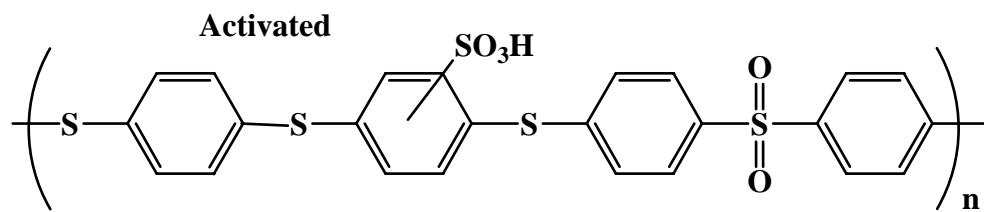
²⁴⁶ H.K. Shobha, G.R. Smalley, M. Sankarapandian, and J.E. McGrath, *Polymer Preprints* 2000, 41(1), 180.

²⁴⁷ K.B. Wiles, C. M. de Diego and J.E. McGrath, *Polymer Preprints* 2004, 45(1), 724.

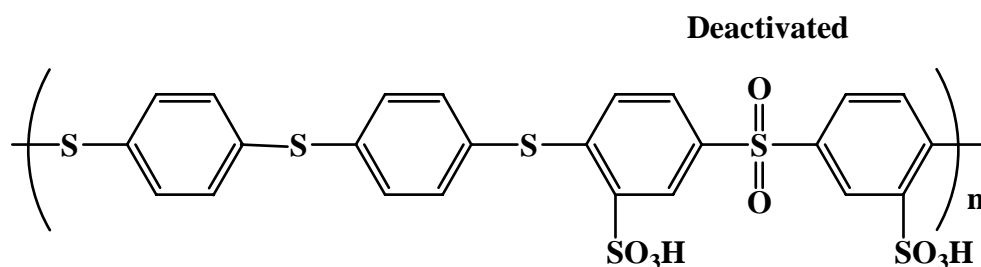
²⁴⁸ Z. Bai, L. D. Williams, M. F. Durstock and T. D. Dang, *Polymer Preprints* 2004, 45(1), 60.

²⁴⁹ B. C. Johnson, I. Yilgor, C. Tran, M. Iqbal, J. P. Wightman, D. R. Lloyd and J. E. McGrath, *J. of Polym. Sci.* 1984, 22, 721.

²⁵⁰ M. A. Dinno, Y. Kang, D. R. Lloyd, J. E. McGrath and J. P. Wightman, In: *Physicochemical Aspects of Polymer Surfaces*, Vol. 1, K. L. Mittal, Ed., Plenum Publishing Corp.: New York, p. 347-366, 1983.



- * Post sulfonation occurs on the most reactive, but least stable, position
- * High electron density leads to relatively easy desulfonation



- * Monomer sulfonation on the deactivated position
- * Enhanced stability due to low electron density

Figure 3.2 Activated versus deactivated positions of sulfonate moieties due to electron donation of the sulfide linkage and electron withdrawal of the sulfone linkage.

3.2 Experimental

3.2.1 Materials

Commercially available 4,4' dichlorodiphenyl sulfone was kindly provided by Solvay Advanced Polymers and recrystallized before use. The 4, 4' - Difluorodiphenylsulfone (DFDPS), 4,4'- thiobisbenzenethiol (TBBT), anhydrous potassium carbonate and N,N-dimethylacetamide were obtained from Aldrich. N-methyl-2-pyrrolidinone (NMP) and toluene (both from Burdick and Jackson) were dried

as follows: NMP was dried overnight over calcium hydride with a nitrogen purge and distilled at reduced pressure; toluene was dried over molecular sieves and filtered before use. N,N-dimethylacetamide (DMAc) was obtained from Burdick & Jackson and used as received.

3.2.2 *Synthesis of the 3,3'-disulfonated 4,4'-difluorodiphenyl sulfone and 3,3'-disulfonated 4,4'-dichlorodiphenyl sulfone monomers*

Both the disulfonated monomers were synthesized in a similar fashion²⁵¹ however, this discussion will focus on highly reactive 4,4'-difluorodiphenyl sulfone (DFDPS) and 3,3'-disulfonated 4,4'-difluorodiphenyl sulfone (SDFDPS). A mixture of DFDPS (25 g., 98.24 mmol) and fuming sulfuric acid (50 grams, 27% SO₃) was added to a round bottom flask fitted with a mechanical stirrer and an initial nitrogen inlet and heated to 120 °C. During the reaction, care must be taken not to seal the system but also not to allow the SO₃ to escape. This is accomplished by removing the nitrogen inlet after the initial charging and allowing a 'loose' seal at the mechanical stirrer-Teflon bearing interface. After six hours, the dark colored reaction mixture was added to deionized ice water and allowed to stir. A copious quantity of NaCl was added to the reaction mixture, thereby, precipitating the disulfonated monomer (SDFDPS) in salt solution. Neutralization to a pH of 7.0 with 10 N NaOH, filtration, drying, and recrystallizing using 7:3 ethanol:water followed the salting out process. Final drying in a vacuum oven at 150 °C for 12 hours produced the monomer grade disulfonated compound. The elemental analysis agreed well with the calculated values.

²⁵¹ M. Ueda, H. Toyota, T. Ouchi, J. Sugiyama, K. Yonetake, T. Masuko and T. Teramoto, *J. Polym. Sci.: Part A: Polym. Chem.* 1993, 31(4), 853.

3.2.3 *Synthesis of the Dithiol Sulfone Monomer*

Bis-(4-mercaptophenyl) sulfone, BMPS, was synthesized using commercially available 4,4'-dichlorodiphenyl sulfone. The synthetic approach is based on a sulfone-activated chloro-displacement by the hydrosulfide via an aromatic nucleophilic substitution reaction. A large excess of sodium hydrosulfide in dimethylsulfoxide (DMSO) was used in the presence of potassium carbonate, all obtained from Aldrich. Typical reaction conditions were 120 °C for 20 hours under a nitrogen atmosphere.

3.2.4 *Synthesis of the Poly(arylene thioether sulfone) Copolymers*

Typical copolymerizations of TBBT, SDFDPS and DFDPS were conducted in a flame dried three-necked flask. The flask was fitted with a nitrogen inlet, thermocouple sensor, over-head stirrer and Dean Stark trap fitted with a condenser. For 40 mole % disulfonation, the flask was charged with TBBT (3.8gm, 15.2 mmols), SDFDPS (3 gm, 6.07 mmols), DFDPS (2.6 gm, 9.1mmols), potassium carbonate (2.4gm, 17.5 mmoles; 15% excess), dry NMP (40ml; 20% solids) and toluene (20ml; azeotropic agent). The reaction flask was heated in an oil bath to 150 °C, and the toluene was allowed to reflux for 4 hours to remove any water present from the hydrated atmosphere or hydrated monomers. The toluene was then removed over a 60-minute time interval. The Dean Stark trap was emptied and the reaction temperature was slowly increased to 180 °C for 16 hours. By the end of the reaction, the solution media became very viscous. The

reaction mixture was hot filtered at 150 °C using a Buchner funnel to remove the by-product (salt, KF), and the isolated filtrate was slowly poured into a 50-fold excess of isopropanol to precipitate the copolymer. The fibrous precipitate was collected by filtration and washed with isopropanol and water to aid in the removal of salts. It was dried under vacuum at 80 °C for one hour, then at 100 °C for 15 hours. The degree of disulfonation was controlled by varying the charge ratios of the SFDPS to the DFDPS.

3.2.5 Membrane Preparation

The potassium salt films were prepared by redissolving the fibrous copolymer in DMAc, filtering the solution through a 0.45 µm Teflon™ syringe filter and directly casting the solution into a glass-casting tray. The glass tray had side-walls so as to aid in membrane thickness control. The copolymer solutions were dried in a vacuum oven in a nitrogen atmosphere at 50 °C for 4 hours, 80 °C for 4 hours, 100°C for 12 hours and 120 °C for 4 hours.

3.2.6. Acidification

Addition of water to the casting tray swelled the membranes and allowed them to be easily removed. The salt form membranes were then transformed into the acid form by one of two methods. Room temperature acidification employed a 1.5 M sulfuric acid in water solution. The copolymer membranes were submersed in the solution for 24 hours and then rinsed with deionized (D. I.) water. Residual sulfuric acid was removed

from the membranes by allowing them to be submersed in D. I. water for another 24 hours. Further washing with and submersion in water aids in removing the last traces on sulfuric acid. This room temperature acidification has been termed Method 1. Method 2 acidification, employed in the present study, used 0.5 M sulfuric acid in water. The films were boiled (~100 °C) in this sulfuric acid solution for two hours and rinsed well. The residual sulfuric acid was removed by boiling in water for another 2 hours. This high temperature acidification treatment has been shown to change the morphological characteristics of the resulting acidified membranes through possible reorganization of the sulfonate moieties possibly producing ion clusters and channels.²⁵²

Introduction of the acid groups into any polymer can be classified by its ion exchange capacity (IEC). When determining the theoretical amount of acid equivalents per gram of polymer, the calculations involve the following for disulfonated copolymers:

$$\text{IEC} = \frac{(2 * \text{mol fraction of disulfonation})}{((\text{MW}_{\text{repeat}} * \text{mol fraction } y) + (\text{MW}_{\text{sulf. repeat}} * \text{mol fraction } z))}$$

Where the value 2 in the numerator corresponds to two sulfonate moieties on the sulfonated repeat unit, y is the mole fraction of the unsulfonated monomer/repeat unit, z is the mole fraction of the sulfonated monomer/repeat unit, $\text{MW}_{\text{repeat}}$ is the molecular weight of the unsulfonated repeat unit and $\text{MW}_{\text{sulf. repeat}}$ is the molecular weight of the sulfonated repeat unit. This equation calculates the equivalents of acid moieties per gram of polymer.

²⁵² W. L. Harrison, , Ph.D. Thesis, Virginia Polytechnic Institute and State University, December, 2002.

The experimental IEC can be determined by titrating either the dissolved copolymer in solution or by first exchanging the hydrogen ions with a metal (*i. e.* sodium) to form the salt form polymer and an acid form, water soluble compound (*i. e.* sodium hydrogen sulfate). For this study, the aqueous titrations used sodium sulfate as the water-soluble ion exchange compound that produces sodium hydrogen sulfate during an equilibration reaction. The chemistry is summarized in Figure 3.3.

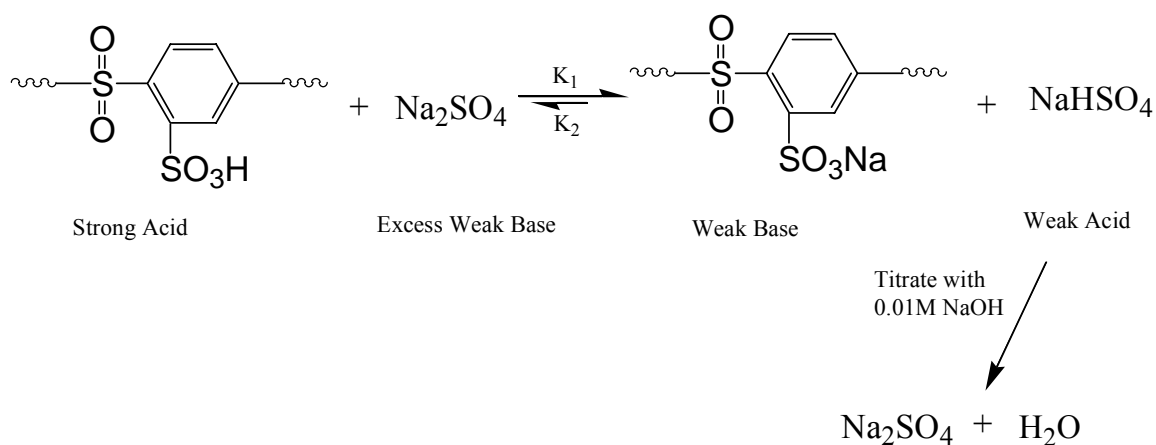


Figure 3.3 Acid-base reaction followed by titration to measure IEC

3.2.7 Characterization

Fourier Transfer-Infrared (FTIR) spectra were recorded using a Nicolet Impact 400 FT-IR spectrometer. Sample preparation for FT-IR studies included casting very thin, homogeneous, salt form films and acidifying by method 2. Proton NMR spectra were obtained with a JEOL 500 MHz spectrometer using DMSO- d_6 as solvent (5% w/v polymer solutions). Intrinsic viscosity (IV) measurements were obtained in NMP at 25 °C using a Cannon Ubbelohde viscometer. Aqueous-potentiometric titrations were

performed using a Schott TitroLine automatic titrator. Membrane water uptake was determined by a weight difference approach. The dry films were weighed and then immersed in deionized water for 24 hours at room temperature. The wet films were then blotted dry and immediately weighed. The ratio of weight gain to initial film weight was expressed as % water uptake. Proton conductivity of the membranes under fully hydrated conditions was determined at 30 °C using a Solatron 1260 Impedance/Gain-Phase Analyzer over the frequency range of 10Hz- 1 MHz following the reported procedure.²⁵³ The resistance of the films was taken at the frequency which produced the minimum imaginary response. The conductivity of the membranes was calculated from the measured resistance and the geometry of the cell (Figure 3.4). Tapping mode atomic force microscopy (TM-AFM) was performed with a microfabricated cantilever using a Digital Instruments Dimension 3000 with a force constant of approximately 40 N/m. The ratio of amplitudes used in the feedback control was adjusted to 0.75 of the free air amplitude for all the reported images. All treated samples were dried at 100 °C for 12 h followed by immersing in water at 30 °C for 1 h and were allowed to equilibrate by exposure to 50% relative humidity at 30 °C for 2 h before testing. The samples were then imaged immediately at a relative humidity of about 50%.

²⁵³ T. A. Zawodzinski, M. Neeman, L. O. Sillerud and S. J. Gottesfeld, *Phys. Chem.* 1991, 95, 6040.

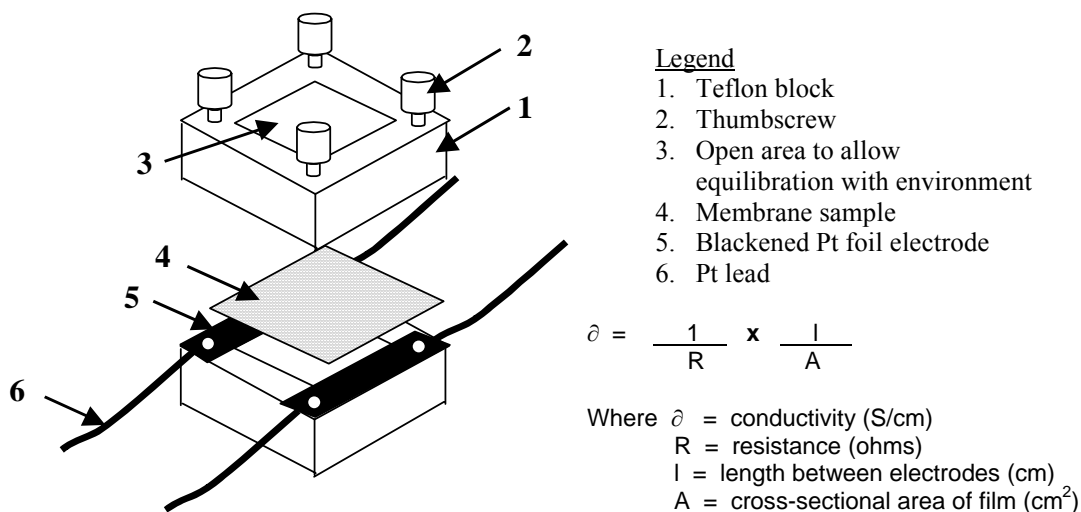


Figure 3.4 Schematic and Equation of Conductivity Cell

3.3 Results and Discussion

Wang et. al. have produced high molecular weight poly(arylene sulfide sulfone) copolymers using bis(4-mercaptophenyl) sulfone. The synthesis of the bis(4-mercaptophenyl) sulfone monomer (BMPS) is shown in Figure 3.5 and is based on a sulfone activated chloro-displacement by hydrosulfide via an aromatic nucleophilic substitution reaction. The dithiol monomer was obtained by reacting recrystallized 4,4'-dichlorodiphenyl sulfone with an excess of sodium hydrosulfide in DMSO in the presence of potassium carbonate.

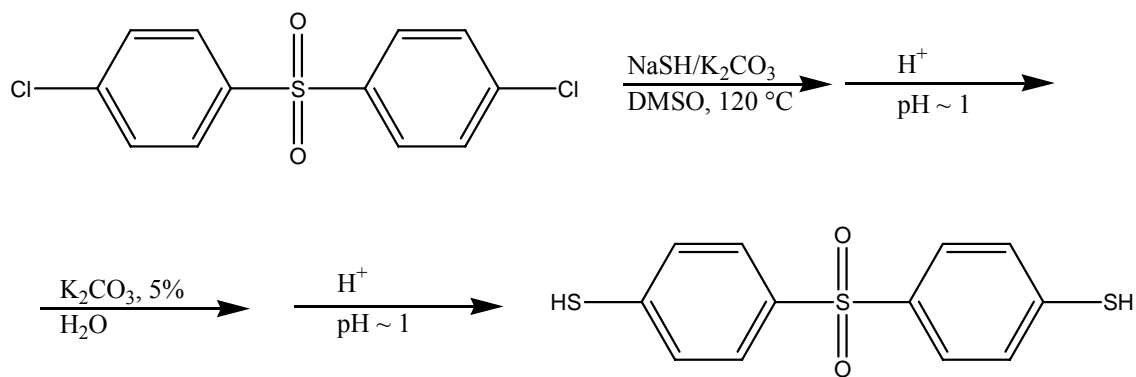


Figure 3.5 Synthesis of Bis(4-mercaptophenyl) sulfone

The copolymer synthesis involved condensing a specific amount of sulfonated activated dihalide, non-sulfonated activated dihalide and BMPS in DMAc and toluene, which was used as an azeotroping agent to remove any water. Copolymerizations were necessarily conducted using the disulfonated salt form of SDFDPS. The disulfonated potassium salt form polymers were then transformed into the acid form by using the boiling technique described in the experimental section. As expected, a significant increase in water sorption was observed relative to the unsulfonated control type polymers, especially in the acid form.

This paper builds on this knowledge and incorporates a related comonomer that contains dithiol nucleophiles and three thioether linkages. It describes the synthesis and characterization of SDFDPS monomer, SDCDPS, as well as the synthesis of two series of disulfonated poly(arylene thioether sulfone) (PATS) copolymers via direct copolymerizations. Thus the two series produce the same repeat units from different starting materials. A lower molecular weight series was synthesized using the less reactive DCDPS monomer and a higher molecular weight series was made from the

difluoro analogs. These copolymers were based on similar nucleophilic aromatic substitution reactions and incorporated a sulfide-dithiol containing monomer termed 4,4'-thiobisbenzenethiol (TBBT) (Figure 3.6).

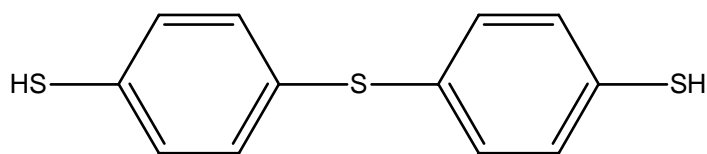


Figure 3.6 Chemical structure of 4,4'-thiobisbenzenethiol

3.3.1 Disulfonated monomer synthesis

The disulfonated monomer was synthesized using electrophilic aromatic substitution reactions as shown in Figure 3.7. The DFDPS monomer was reacted with fuming sulfuric acid containing 27% SO_3 at 120 °C for 6 hours. The ortho-para-directing fluoro atom and the deactivating sulfone linkage result in the electrophilic aromatic substitution reaction producing 3,3'-disulfonated moieties.²⁵⁴

²⁵⁴ G. H. Schmid, In: Organic Chemistry, L. W. Black, Ed., St. Louis: Mosby-Year Book Inc., 1996.

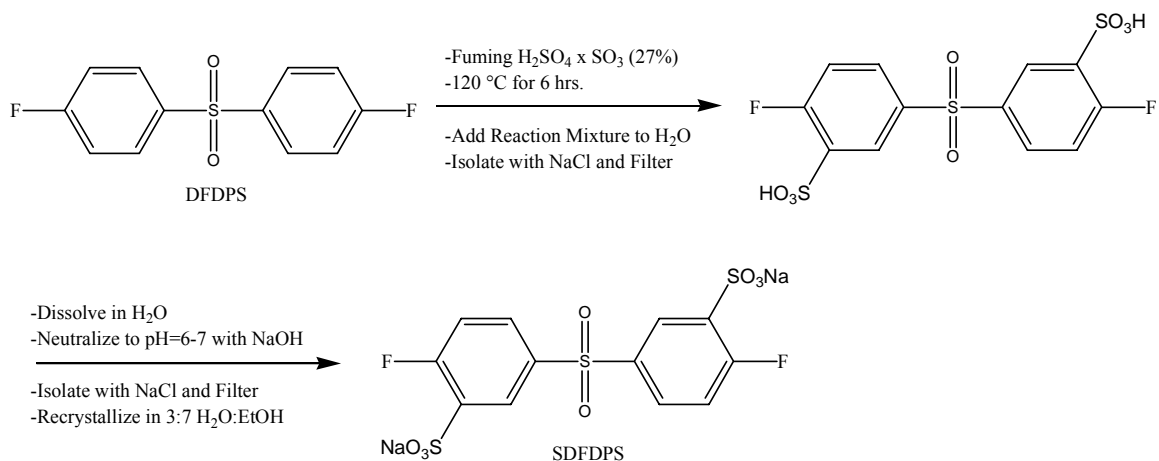


Figure 3.7 Disulfonation of DFDPS monomer for use in step-growth polymerizations

3.3.2. Proton NMR and elemental analysis of disulfonated monomer

The molecular structure of the disulfonated monomer was determined by ^1H NMR in d_6 -DMSO (Figure 3.8), infrared spectroscopy, ^{13}C NMR and elemental analysis. The DFDPS ^1H NMR spectrum indicated two different types of protons present in the starting material corresponding to the four protons ortho to both the fluorine atoms and the other four protons meta to both the fluorine atoms. After the disulfonation reaction, the ^1H NMR spectrum indicated three different types of protons present. The highest electronegative protons next to the sulfonate and sulfone moieties were observed at 8.15 ppm. Further evaluation using ^1H NMR prediction software aided in determining the proper structure of the disulfonated monomer. Elemental analysis of SDFDPS-Na indicated the calculated amounts and the experimental amounts correspond very well. The predicted disulfonated monomer was obtained in yields of 85-90%.

Elem. Anal. Calcd.: C, 31.45%; H, 1.32%; S, 20.98%; Na, 10.03%. Found: C, 30.53%; H, 1.42%; S, 20.28%; Na, 9.70.

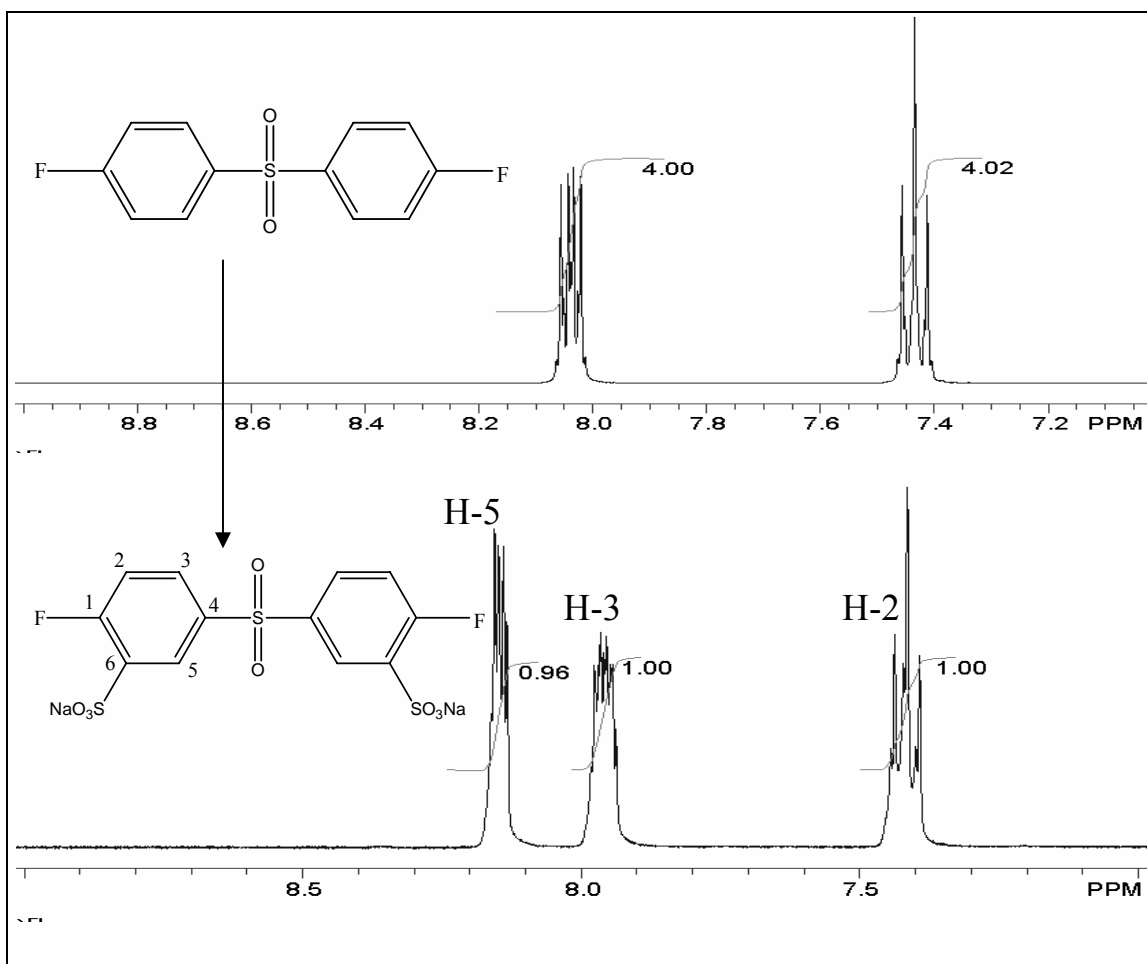


Figure 3.8 ¹H NMR of DFDPS and SDFDPS

3.3.3. Synthesis of disulfonated poly(arylene thioether sulfone) copolymers

Poly(arylene thioether sulfone) copolymerizations were conducted by condensing a varying ratio of the disulfonated activated dihalides with activated dihalides and TBBT

(Figure 3.9). The reactions were performed in NMP as the polar organic solution using toluene as a refluxing agent to aid in removal of residual water through azeotropic mechanisms. However, by using potassium carbonate as the base, ion exchange of the sodium and the potassium ions occurs, thereby producing potassium salt form copolymers.

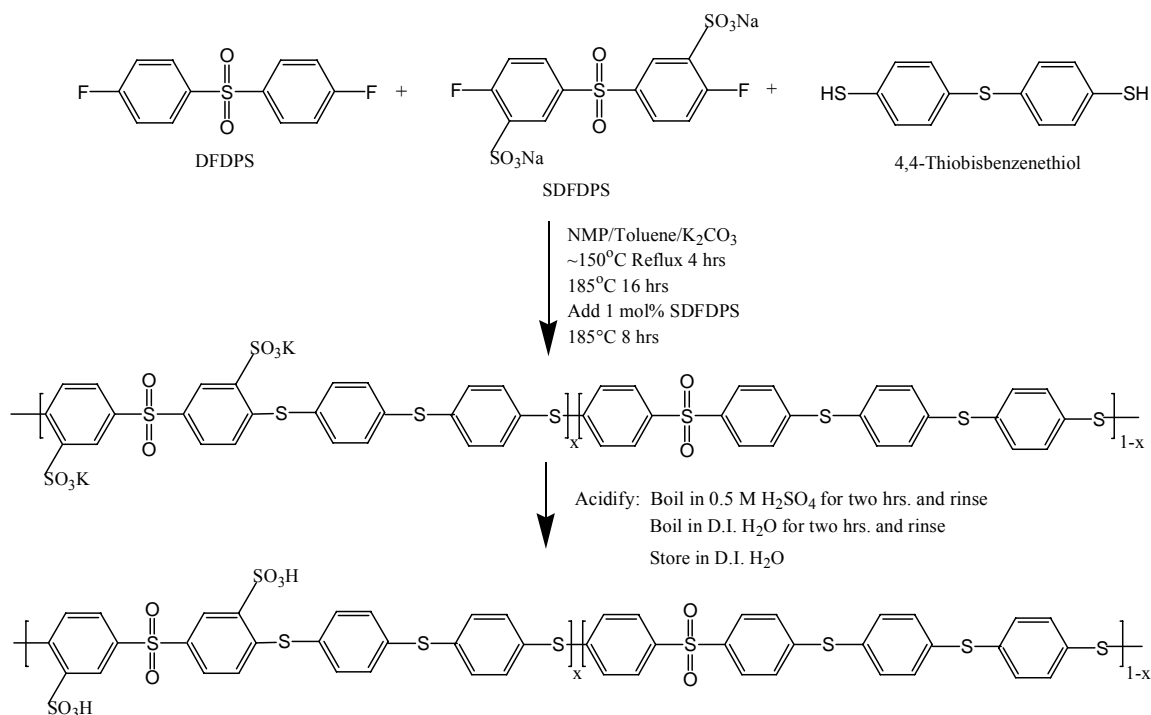


Figure 3.9 Copolymerization of TBBT with DCDPS and SDCDPS

As noted above, the activated dihalide was either 4,4'-dichloro- or 4,4'-difluoro- (DCDPS or DFDPS). Similarly, the disulfonated activated dihalide employed was either SDCDPS or SDFDPS. It is well known that halogen atoms ortho- or para- to a strongly electron-withdrawing substituent undergoes nucleophilic aromatic substitution readily. For the weak base method of nucleophilic aromatic substitution, the base (K₂CO₃)

deprotonates the –SH moiety (thiol) to form a good nucleophile ($-S:^-$), which attacks the partial positively charged aromatic carbon covalently bonded to either the chlorine or fluorine halogen. The fluorinated activated halides are well known to be more reactive.²⁵⁵ Therefore, higher reactivity in aromatic nucleophilic polycondensation is achieved by using SDFDPS and DFDPS relative to SDCDPS and DCDPS. Consequently, shorter times and/or lower reaction temperatures (160 °C) are needed to synthesize high molecular weight disulfonated poly(arylene thioether sulfone) copolymers.

3.3.4 Acidification of salt form copolymers

The salt form copolymers were cast into thin films using a 10 weight percent solution in DMAc. The solution was filtered through a 0.45 μm Teflon[®] syringe filter to remove any residual salt byproduct and cast into a glass casting tray in a vacuum oven with a very slight nitrogen purge. After careful drying, the cast membranes were transformed into the acid form by a high temperature, boiling method for two hours using 0.5 M sulfuric acid in water (Method 2). The membranes were then boiled in deionized water for two hours to remove any residual acid and rinsed thoroughly. As discussed previously, another method of acidifying could be used using a 1.5 M sulfuric acid at room temperature for 24 hours (Method 1). However, it has been observed that a morphological change, possible reorganization of the sulfonate moieties, associated with

²⁵⁵ S. Wang, J. E. McGrath, Synthesis of Poly(arylene ethers), In: Synthetic Methods in Step Growth Polymers, M. E. Rogers and T. E. Long, Eds., Wiley: New York, 2003, pp 327-374.

Method 2 accounts for an increase in conductivity of the membrane without increasing the amount of disulfonation as compared to the Method 1.

3.3.5. Characterization of the disulfonated copolymers

The extent of disulfonated comonomer that was incorporated into the copolymer architecture was calculated from the areas of specific proton peaks (marked A and B in Figure 3.10) using ^1H NMR. The degree of disulfonation matched well with the targeted feed values as observed and tabulated in both tables 3.1 and 3.2.

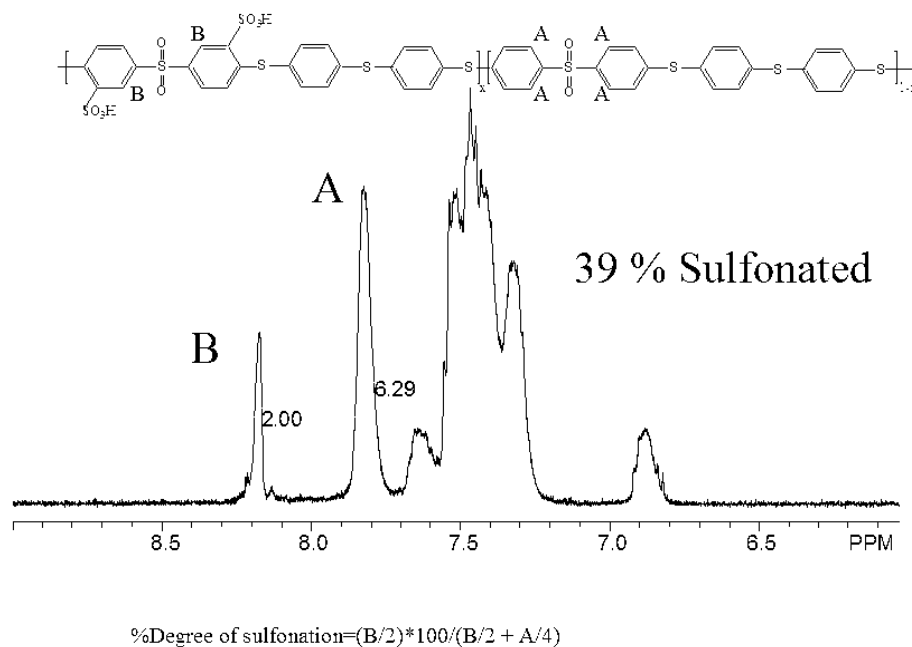


Figure 3.10 ^1H NMR of 40% Disulfonated Copolymer Using Difluorinated Monomers to Calculate Copolymer Composition

Table 3.1 Characterization of TBBT Based Copolymers Using Difluorinated Comonomers

DFDPS + TBBT +	I.V. dL/gm (NMP 25°C)	Sulfonation By ¹H NMR	Calc. Ion Exch. Capacity (IEC) (meq/gm)	Experimental IEC (meq/gm) (NafionTM 1100 = 0.91)
0% SDFDPS	0.6	0	0	0
20 mol % SDFDPS	1.0	18%	0.81	0.75
30 mol % SDFDPS	1.2	28%	1.17	1.10
40 mol % SDFDPS	1.5	39%	1.51	1.32
50 mol % SDFDPS	1.8	48%	1.83	1.65

Table 3.2 Characterization of TBBT Based Copolymers Using Dichlorinated Comonomers

DCDPS + TBBT +	I.V. dL/gm (NMP 25°C)	Sulfonation By ¹H NMR	Calc. Ion Exch. Capacity (IEC) (meq/gm)	Experimental IEC (meq/gm) (NafionTM 1100 = 0.91)
0% SDCDPS	0.49	0%	0	0
20 mol % SDCDPS	0.69	18%	0.81	0.73
30 mol % SDCDPS	0.75	29%	1.17	1.12
40 mol % SDCDPS	0.8	40%	1.51	1.35
50 mol % SDCDPS	1.0	50%	1.83	1.64

The yields obtained from the polycondensation reactions were quantitative and, as noted in table 2 and table 3, intrinsic viscosities (IV) in NMP at 30 °C were high enough to obtain tough ductile films for both series of disulfonated copolymers. The increase in IV as a function of disulfonation does not necessarily reflect higher molar mass and is likely due to the intermolecular dissociation of the sulfonate moieties. Thereby producing larger spacial sizes of molecules that are ascribed to the stronger ionic repulsion of the sulfonate groups. Current investigations, to be published soon, compare lithium bromide modified NMP which eliminates the polyelectrolyte effect to unmodified NMP.

Fourier transfer infrared spectroscopy (FTIR) was used to further verify the incorporation of the sulfonate groups and chemical architecture of the poly(arylene thioether sulfone) copolymers. As Figure 3.11 indicates, the symmetric and asymmetric stretching and corresponding wagging of the sulfonate moieties can be observed at 1060 cm^{-1} , 1215 cm^{-1} and 1250 cm^{-1} . As the mole percent of the disulfonated monomer was increased, the corresponding bands on the FTIR spectra were observed to increase in intensity for the thin film copolymers. These FTIR results aid in concluding that successful incorporation of the disulfonated monomer was achieved.

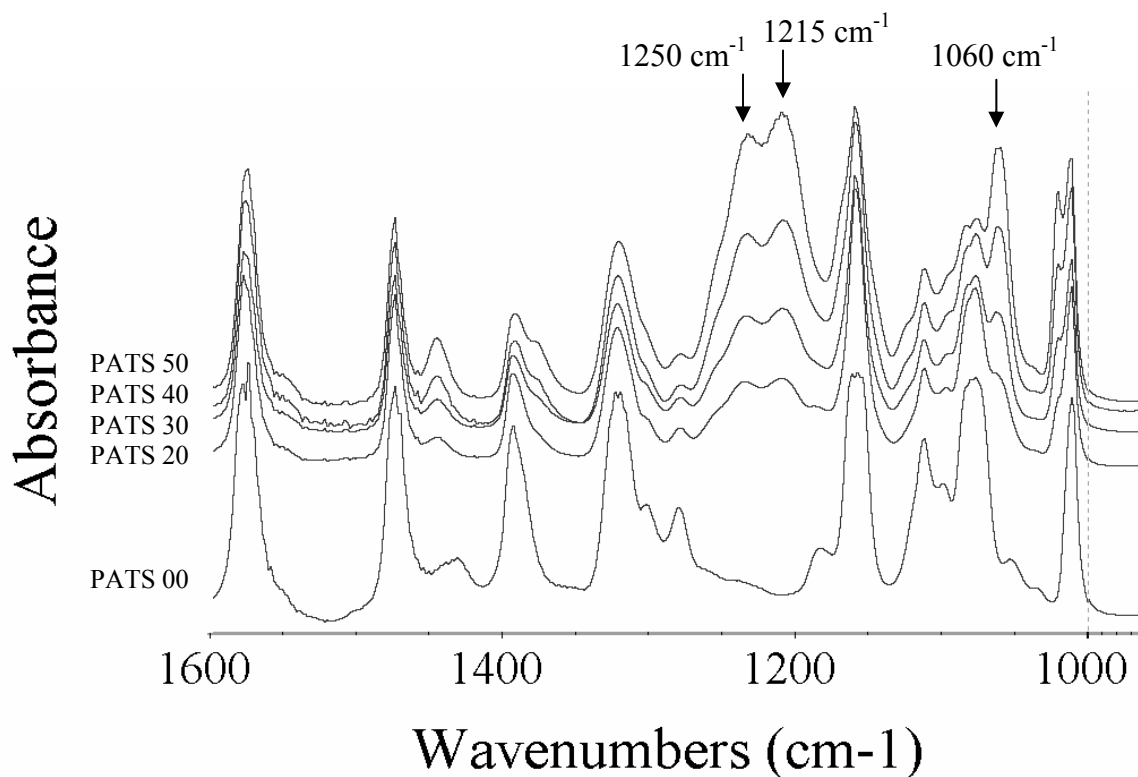


Figure 3.11 Infrared Spectroscopy Indicating Increasing Incorporation of Sulfonate Moieties

Thermal gravimetric analysis (TGA) in air operating at 10 °C/min was employed to preliminarily characterize the thermal stability of the disulfonated copolymers in the acid form, relative to the control, non-sulfonated polymer. All the TGA samples were first preheated to 150 °C for 20 minutes in the furnace to remove any moisture. Typical TGA curves from 50 °C to 800 °C for non-sulfonated PATS and 30 mole percent disulfonated PATS are given in Figure 3.12. The control polymer is well known to be thermally stable and showed a 5% weight loss at 467 °C whereas the analogous 30 mole percent acid form disulfonated copolymer showed a 5% weight loss at only 361 °C. At

temperatures below 650 °C the control only showed one weight loss step indicating the degradation of the backbone architecture. However, the disulfonated copolymer showed two weight loss steps. The initial weight loss of about 10% was assigned to the loss of the $\text{-SO}_3\text{H}$ moieties and the second degradation step was assigned to the decomposition of the copolymer backbone at a temperature around 465 °C, which is in close agreement with the backbone degradation of the control homopolymer. It was further observed that as the percent of disulfonation increased, the initial degradation temperature was constant for all levels of disulfonation (e.g. 320 °C for PATS 50 and 323°C for PATS 30). These data indicated that the addition of the sulfonate groups to the polymer backbone decreased the thermal stability. However, it is suggested that all the disulfonated copolymers would have acceptable thermal stability for use at 120 °C.

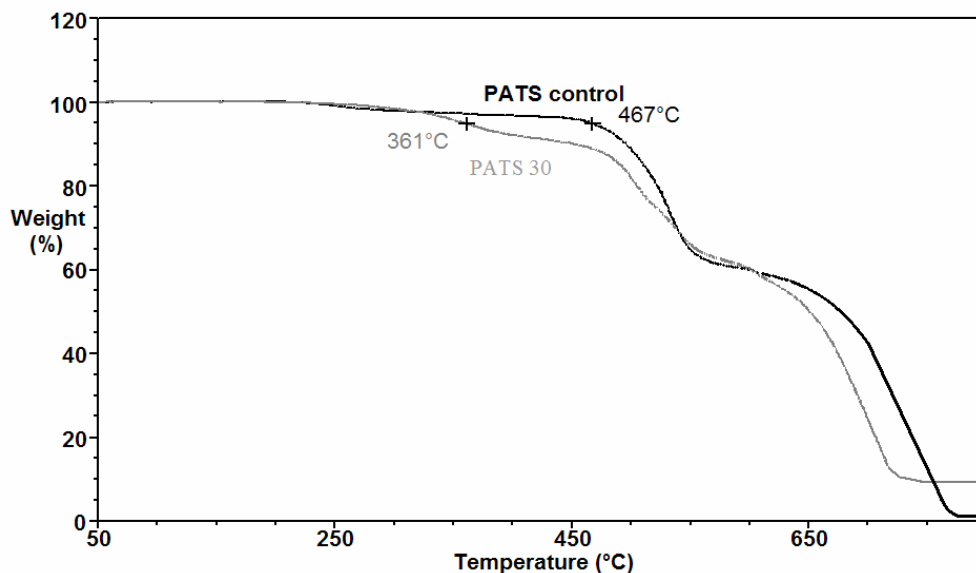


Figure 3.12 Thermal Gravimetric Analysis of PATS control polymer and PATS 30 Copolymer (10 °C/minute in Air)

Morphological understanding of the hydrophobic and hydrophilic phases of the copolymers was investigated using tapping mode atomic force microscopy (TM-AFM) employing a Digital Instruments Dimension 3000 with a microfabricated cantilever operating at a force constant of 40 N/m. Tapping mode phase images of the disulfonated PATS copolymers were recorded in ambient conditions using 1 μm x 1 μm size scale so as to investigate features such as ionic conglomerates, clusters and channels.

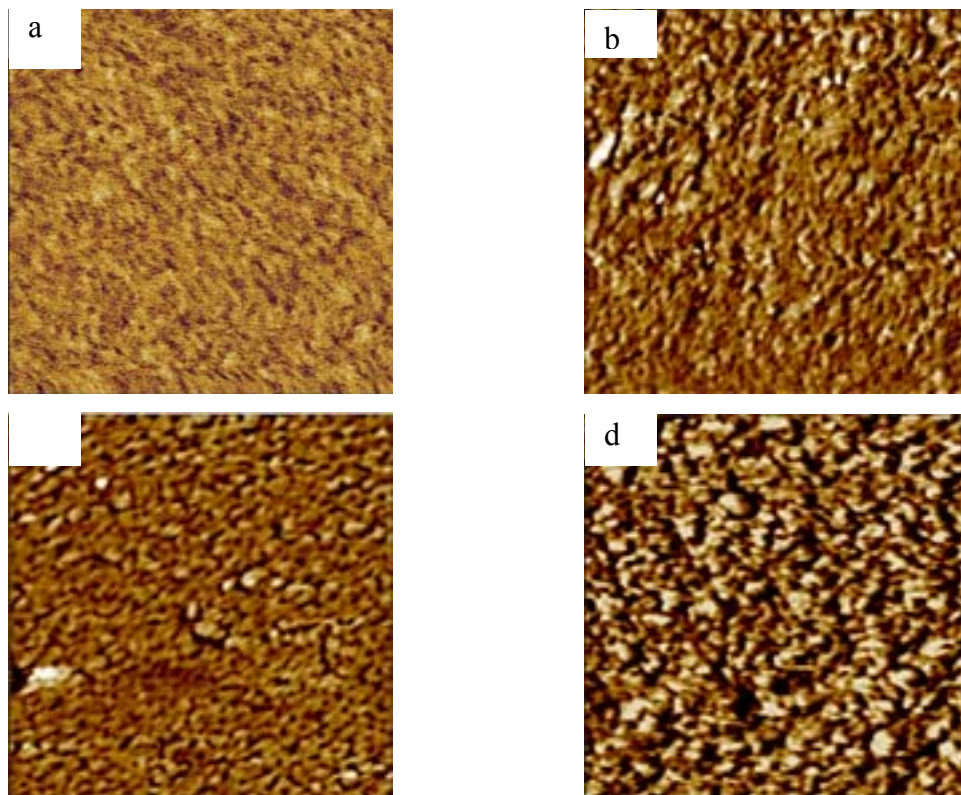


Figure 3.13 Tapping mode AFM phase images of (a) Nafion 117, (b) PATS 30, (c) PATS 35 and (d) PATS 40. The scan area for Nafion 117 is 350nm x 350nm and the scan area for all PATS is 1 μm x 1 μm all with a phase scale of 10 $^\circ$.

Tapping mode AFM, as observed in Figure 3.13, aided in identifying the hydrophilic, soft phases (dark areas) and the hydrophobic, hard phases (light areas). For

Nafion 117 (Figure 3.12a), the darker phases indicate ca. 10 nm ionic channels which is consistent with the literature.²⁵⁶ Even though these ionic channels are very small, clear connectivity was observed. For PATS 30 (Figure 3.12b), larger hydrophilic phases with cluster-like structures that had diameters of 10-20 nm were observed. When the mole percent of disulfonation was increased to 35, PATS 35 (Figure 3.12c), the ionic, hydrophilic domain size increased to 15-25 nm indicating better connectivity of the ionic phases. For PATS 30 and PATS 35, the non-ionic phase matrix allows mechanical strength and, as will be discussed, lower water sorption. By comparing the aforementioned phase images to PATS 40 (Figure 63.12d), an obvious change in ionic domains was observed. The ionic areas were not just isolated domains; but rather become the matrix. Therefore, hydrophilic ionic clusters became a continuous phase to form large channels with non-ionic domains that had sizes of 40-50 nm. Based on these phase images, it was concluded that the PATS system reaches a percolation threshold at about 40 mol% of disulfonated monomer.

This percolation threshold could also be observed by coupling the AFM images and water uptake of the PATS series of copolymers,. Figure 3.14 shows that the water sorption from 35 mol% disulfonated monomer increased dramatically when the disulfonation level increased only 5 mol% to 40 mol%. These data help to further understand the phase/matrix inversion that takes place between 35 and 40 mol% disulfonation for the PATS series of copolymers. Thus, at levels of disulfonation lower than 40 mol%, the matrix consisted of connected hydrophobic phases, but above

²⁵⁶ R. S. McLean, M. Doyle and B. B. Sauer, *Macromolecules* 2000, 33(17), 6541.

approximately 40 mol%, the matrix is transformed to hydrophilic channels with hydrophobic domains.

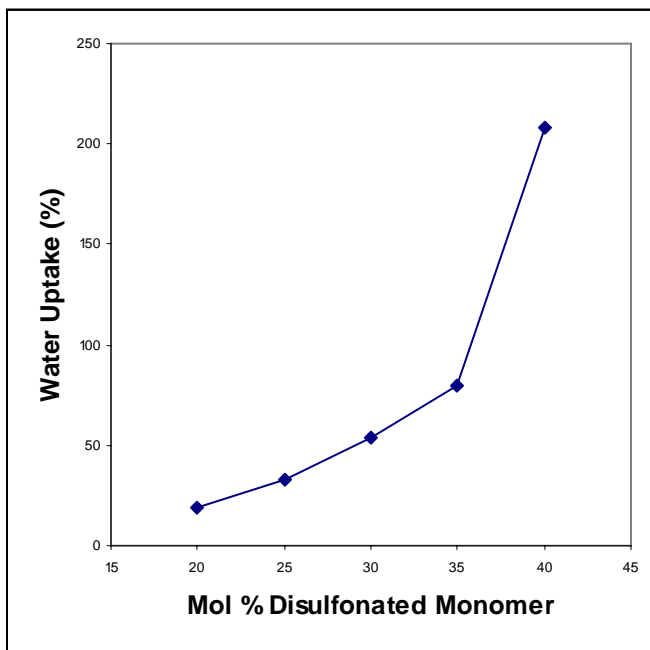


Figure 3.14 Influence of the disulfonation level on water uptake of acid form poly(arylene thioether sulfone) copolymers based on TBBT, DCDPS and SDCDPS.

The proton conductivity was measured in 30 °C in water using the aforementioned conductivity cell. The conductivity of the disulfonated membranes increases with increasing mol % disulfonation as shown in Figure 3.15. The range of conductivities for the acid form films varied from 0.03 – 0.16 S/cm for PATS 20 – PATS 50, while the conductivity of the control Nafion 117 was 0.11 S/cm under similar conditions (liquid water, 30 °C).

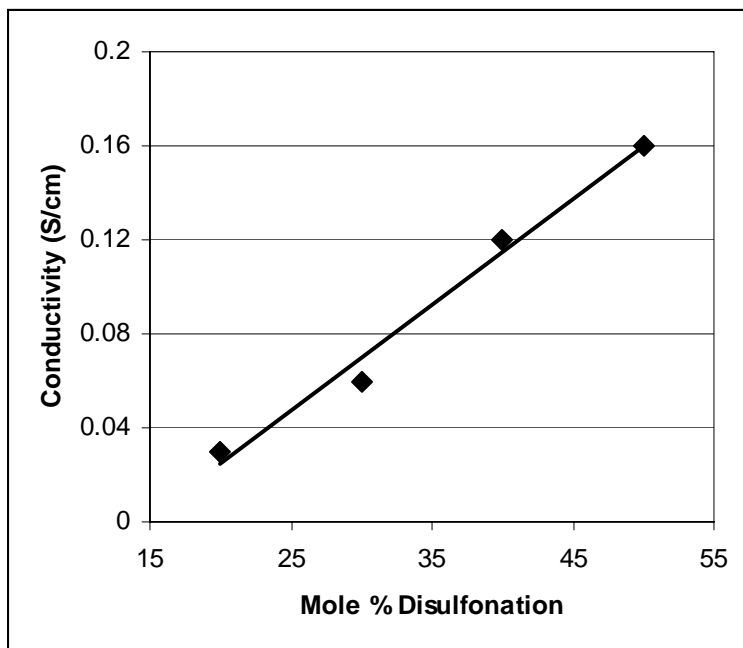


Figure 3.15 Proton conductivity of disulfonated membranes in water at 30 °C for PATS based on TBBT, DCDPS and SDCDPS

3.4 Conclusions

Successful synthesis of poly(arylene thioether sulfone) copolymers was performed by directly copolymerizing either disulfonated chloro- or fluoro- activated dihalide monomers using nucleophilic aromatic polycondensation techniques. Successful synthesis of SDFDPS was achieved using electrophilic aromatic substitution with fuming sulfuric acid. The rates of reactions were faster with the fluorinated monomer and thus it was easier to prepare high molecular weight copolymers. Solution cast, salt form membranes were transformed into the acid form at 100 °C which afforded tough and ductile films. Proton NMR, infrared spectroscopy and ion exchange capacity experiments successfully characterized the copolymer structure as increased amounts of

disulfonated monomers were used in the reaction media. Thermal gravimetric analysis indicated a decrease in thermal stability for the disulfonated copolymers relative to the non-sulfonated control copolymer, however, thermal stability was still acceptable for use in moderate temperature fuel cell environments. Morphological studies using AFM phase imaging indicated an increase in ionic domains in the low disulfonated copolymers to levels of connectivity for the 40 mol% copolymer. A phase inversion from hydrophobic to hydrophilic continuity was observed in the range of 35 mol% to 40 mol% disulfonation for the PATS system. Coupling these findings with water uptake further characterizes the percolation threshold to a dramatic increase of water sorption from 35 mol% disulfonation to 40 mol% disulfonation. Enhanced proton conductivity was obtained with increasing mol% of disulfonation reaching levels of 0.16 S/cm for PATS 50. Part II of this research will discuss further features of the copolymers that have the same repeat unit, but different molecular weights. Characterization has included methanol permeability, water uptake, proton conductivity and dynamic mechanical analysis. The fuel cell testing of these PATS materials is of high interest and further research is ongoing to produce membrane electrode assemblies for both the pure copolymer architecture and conductive inorganic-organic composites and this will be reported later.

Acknowledgements.

The authors would like to thank the Department of Energy for funding under contract #DE-FC36-01G011086 and OMNOVA Solutions Signature University Award Fellowship.

CHAPTER 4:

DIRECTLY COPOLYMERIZED POLY(ARYLENE SULFIDE SULFONE) DISULFONATED COPOLYMERS FOR PEM-BASED FUEL CELL SYSTEMS: EFFECT OF MOLECULAR WEIGHT ON TRANSPORT AND MECHANICAL PROPERTIES

Abstract

Molecular weight characterization of proton exchange membranes for fuel cells is critical for longevity and durability issues that arise during normal fuel cell cycling and operations. Synthesis of various families of ionomers has produced many alternatives to poly(perfluorosulfonic acid) copolymers as both hydrogen and methanol fuel cell membranes. Characterization of these materials typically consists of analytical techniques that are directly related to the physical properties that are needed for use as proton exchange membranes, such as proton conductivity, water uptake, gas permeability and methanol permeability. Often overlooked is the molecular weight of the co- and ter-polymers that play critical roles in the overall polymer physical properties. Historically, molecular weight has been proven to have an enormous impact on practically all of the physical properties of polymeric systems. Therefore, this report reveals the molecular weight dependence on various properties of a specific family of proton exchange

membrane, namely, disulfonated poly(arylene thioether sulfone) copolymers. This study elucidated that the lower molecular weight materials behaved differently than the higher molecular weight copolymers. Specifically, the water uptake and permeability to methanol was enhanced for the lower molecular weight copolymers as compared to the higher molecular weight materials. Furthermore, the fully hydrated mechanical properties were observed to increase as a function of molecular weight. However, at the values of molecular weight employed in this study, the proton conductivity of the disulfonated copolymers was not significantly influenced by variations in the molecular weight.

Key Words: poly(arylene thioether sulfone), poly(arylene sulfide sulfone), molecular weight affect, poly(arylene ether sulfone), proton exchange membrane, fuel cell, Nafion

4.1 Introduction

Alternative proton exchange membranes must possess properties that are, at the least, comparable to the poly(perfluorinated) copolymers that are employed as the state-of-the-art fuel cell membranes. The advantages of Nafion[®]-type membranes include good proton conductance, great durability at temperatures between 20-80 °C and good chemical resistance due to the semicrystallinity of the fluorocarbon backbone. However, these poly(perfluorinated) copolymer membranes do not possess sufficient properties for all fuel cell conditions. When employed in direct methanol fuel cells, Nafion[®] membranes suffer from high methanol permeability which leads to loss of fuel efficiency and a back-flux of protons that are produced at the cathode rather than at the anode. Furthermore, at operation temperatures above 80 °C in a hydrogen/air fuel cell, the membrane lacks physical durability that decreases long-term stability. These deficiencies have produced many alternative polyelectrolyte membranes for use in both direct methanol and hydrogen fuel cells. The majority of the successful alternative membranes are based on high performance polymeric backbones containing sulfonic acid pendant groups. The hydrophobic backbones enhance physical properties and the sulfonic acid pendent groups provide ionic conductance. Many reports have described the advances in alternative proton exchange membranes employing high performance polymer such as polysulfone,^{257,258,259,260} polyimide,^{261,262,263} polybenzimidazole²⁶⁴ and polyketone²⁶⁵.

²⁵⁷ Hickner, M. A., Ghassami, H., Kim, Y. S., Einsla B. R. and McGrath, J. E. *Chem. Rev.* 104, 4587-4612, 2004.

²⁵⁸ Wang, F., Hickner, M. A., Kim, Y., Zawadzinski, T. and McGrath, J. E. *J. Membr. Sci.* 197, 231-242, 2002.

²⁵⁹ Nolte, R., Ledjeff, K., Bauer, M. and Muhaupt, R. *J. Membr. Sci.* 83, 211, 1993.

²⁶⁰ Koter, S., Piotrowski, P. and Kerres, J. *J. Membr. Sci.* 153, 83-90, 1999.

Two different synthetic techniques have been utilized in producing ion-containing proton exchange membranes. One technique employs post-sulfonation of existing high performance homopolymers that are attained from commercial sources.. Typically, sulfonic pendant moieties are attached using either fuming sulfuric acid or chlorosulfonic acid to the arylene containing polymer backbone following electrophilic aromatic substitution processes.²⁶⁶ One specific advantage of this technique is the relative ease of producing an entire family of proton exchange membranes by averting the intricate polymerization reactions and only employing the aforementioned post-sulfonation reaction. One specific disadvantage includes the use of these commercial polymers that have relatively low molecular weights because of the processing that must be done to produce the end products. During synthesis, the molecular weights of these commercially available polymers are kept as low as possible for the projected purpose. Therefore, after post sulfonation, the proton exchange membranes contain molecular weights that correspond to injection molded-type products and not that of high performance separation membranes where extremely high molecular weights are needed.

A viable alternative to post-ionization is synthesizing ion-containing copolymers via direct polymerization of sulfonated monomers. This process produces sulfonate containing copolymers that can be synthetically tailored to produce extremely high molecular weights. However, the major disadvantage to the process lies in the synthesis of new sulfonated comonomers and successfully employing these comonomers in

²⁶¹ Einsla, B., Y.T. Hong, Y.S. Kim, F. Wang, N. Gunduz and J.E. McGrath, *J. Poly. Sci., Part A: Polymer Chemistry* 44, 862-874, 2004.

²⁶² Gunduz, N., Inan, T. Y., Yidez, E. and McGrath, J. E. *Polymeric Mat. Sci. Eng.* 84, 911, 2001.

²⁶³ Genies, C., Mercier, R., Sillion, B., Cornet, N., Gebel, G. and Pineri, M. *Polymer* 42, 359, 2001.

²⁶⁴ Einsla, B. and McGrath J. E. *J. Membr. Sci.* 2005, Accepted.

²⁶⁵ Alberti, G., Casciola, M., Massinelli, L. and Bauer, B. *J. Membr. Sci.* 185, 73, 2001.

²⁶⁶ Poppe, D., Frey, H., Kreuer, K., Heinzl, R. and Mulhaupt, R. *Macromolecules* 35, 7936, 2002.

copolymerizations. But direct copolymerization of ion-containing monomers allows enhanced control of macromolecular architecture and, importantly, molecular weight.

Molecular weight characterization of ionomers has historically been difficult to analyze due to the ‘polyelectrolyte effect.’ The polyelectrolyte effect is based on the ion moieties electrostatically repelling one another so that the size of the molecule in solution actually increases in size as the concentration decreases.²⁶⁷ As the literature base of alternative proton exchange membranes has grown in the past decade, many pertinent fuel cell properties have been investigated including proton conductivity, water uptake and voltage current studies. However, molecular weight has been largely overlooked as a basic relevant fuel cell property. Traditional characterization of molecular weight for ionomers has, thus, been problematic because of the polyelectrolyte effect. Typically, polymer molecular weights are based on the size of the molecules in dilute, non-entangled, solutions using instruments such as viscometers, gel permeation chromatographs (GPC) and light scattering that are mainly based on standard calibration curves. But the polyelectrolyte effect has hampered this type of traditional characterization. Therefore, novel methods have been developed to suppress the elongation effects of ionomers in dilute solutions. Addition of various electrolytes, such as lithium bromide (LiBr), into the mobile phase of a GPC screens the electrostatic repulsion of the sulfonate groups and decreases the ionomer interaction with the GPC column. Concentrations of LiBr in the range of 0.05M²⁶⁸ tend to repress both of these

²⁶⁷ Chakrabarty, K., Shao, L-Y. and Weiss, R. A. In: *Ionomers, Synthesis, Structure, Properties and Applications* Eds. Tant, M. R., Mauritz, K. A. and Wilkes, G. L., Blackie Academic and Professional, London, 1997.

²⁶⁸ Nefedov, P. P. *Polymer Sci. U. S. S. R.* 23, 1055, 1981.

electrolyte characteristics and allow true molecular weights to be determined for ionic polymers.

Morphologies of sulfonated copolymers that are employed as polyelectrolyte membranes develop microphase-separated phases where ion-rich domains act as the proton conductors and ion-poor domains act as mechanical ties. Therefore, in typical fuel cell conditions, the ionic domains swell with water and allow for proton, water and methanol transport from the anode to the cathode. Furthermore, the non-ionic domains confine the water-swollen material to provide for mechanical integrity and long-term durability. However, the hydrophobic, non-ionic, domains must be the bulk of the volume fraction so as to allow for a continuous hydrophobic morphology. If the ion-phase becomes the bulk of the material, the continuity of the hydrophilic morphology will allow for dramatic increases in water swelling and dimensional changes that sacrifice the mechanical integrity and durability of the membrane.

Mechanical integrity and durability have recently been proposed to be significantly affected by molecular weight of the sulfonated polymer chains.²⁶⁹ When a polyelectrolyte film is swollen with water, the chain entanglements aid in restraining the dimensional changes of the membrane. High molecular weight copolymers that contain a relatively large number of chain entanglements allow for greater repression of dimensional changes when compared to low molecular weight copolymers that contain a relatively few number of chain entanglements. Adsorption of water affects various diffusion properties such as proton conductivity and methanol permeability. In this study, two series of copolymers were investigated that contained the same chemical structure, but different molecular weights. Elucidating the effects of molecular weight

²⁶⁹ Hickner, M. A. *Ph.D. Dissertation*, Virginia Polytechnic and State University, 2003.

variations on proton exchange membrane properties will aid in understanding the importance of producing high molecular weight copolymers for fuel cell use. This report demonstrates that low molecular weight disulfonated poly(arylene thioether sulfone) copolymers yield increased water uptake which, in turn, gives increased transport characteristics and decreased mechanical properties relative to the higher molecular weight equivalent. The entire disulfonation series of PATS copolymers was synthesized, including PATS-00, PATS-10, PATS-50, PATS-60, PATS-70, PATS-80, PATS-90 and PATS-100, but this report focuses on the disulfonation degree that directly relates to proton exchange fuel cell membranes having acceptable water uptakes and conductivities.

4.2 Experimental

4.2.1 Materials

The ion-containing polymeric material utilized in this study was disulfonated poly(arylene thioether sulfone), referred to as 'PATS'. It was synthesized following the reported procedure^{270,271} by directly polymerizing sulfonated monomer using nucleophilic aromatic substitution reactions of activated dihalides and dithiol containing monomers. Various ratios of disulfonated monomer to unsulfonated monomer and bis(4-mercaptodiphenyl thioether) produced a family of copolymers having the structure shown in Figure 4.1. The PATS-XX acronym numbers indicate the molar percentage of

²⁷⁰ Wiles, K.B., Wang, F. and McGrath, J.E., 'Directly Copolymerized Poly(arylene sulfide sulfone) Disulfonated Copolymers for PEM-Based Fuel Cell Systems I: Synthesis and Characterization,' *J. of Polym. Sci.: Part A: Polym. Chem.*, Accepted, 2005.

²⁷¹ Wiles, K. B., Bhanu, V. A., Wang, F. and McGrath, J. E. *Polymer Preprints* 43(2), 993-994, 2002.

randomly polymerized disulfonated repeat units. For example, PATS-30 indicates the copolymer architecture contains 30 mole% of hydrophilic disulfonated repeat units and 70 mole% of unsulfonated hydrophobic repeat units.

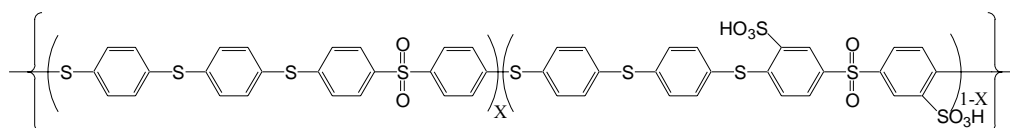


Figure 4.1 Disulfonated PATS-XX copolymer structure indicating thioether and sulfone linkages

4.2.2 Membrane Preparation

Redissolving the fibrous copolymer in N,N-dimethylacetamide (Burdick and Jackson), filtering the solution through a 0.45 μm Teflon[™] syringe filter and directly casting the solution into an aluminum-casting tray prepared tough and ductile potassium salt films. The aluminum tray had sidewalls so as to aid in membrane thickness control. The copolymer solutions were dried in a vacuum oven in a nitrogen atmosphere at 50 °C for 4 hours, 80 °C for 4 hours, 100°C for 12 hours and 120 °C for 4 hours.

4.2.3 Acidification

Addition of water to the casting tray swelled the membranes and allowed them to be easily removed. The salt form membranes were then transformed into the acid form using a boiling technique in 0.5 M sulfuric acid in deionized water. The films were boiled (\sim 100 °C) in this sulfuric acid solution for two hours and rinsed well. The residual

sulfuric acid was removed by boiling in water for another 2 hours. The acid form films were then rinsed and stored in deionized water for one week before testing.

4.2.4 Characterization of Molecular Weight

Intrinsic viscosity (IV) measurements were obtained in NMP at 25 °C using a Cannon Ubbelohde viscometer. IV data were calculated using the extrapolated values to zero concentration of the averages of the reduced and inherent viscosities. Gel permeation chromatography determined the molecular weights using a Waters 1515 isocratic HPLC pump, Waters Autosampler and Waters 2414 refractive index detector calibrated using polystyrene standards with very narrow polydispersities. The oven temperature of the column set containing two Styragel HT 6E and one Styragel HT 3 was constant at 60 °C. N-methylpyrrolidone containing 0.05 M LiBr with a 1.0 mL/min flow rate was used as the mobile phase.

4.2.5 Hydrated Dynamic Tensile Modulus

Dynamic mechanical tensile properties of the membranes submersed in deionized water were determined at room temperature using a dynamic mechanical analyzer (DMA) by TA Instruments (DMA 2980). The submersion clamp permits tensile modulus experiments in a fully immersed liquid water environment. An oscillation of 1 Hz was applied to the film while the amplitude was increased until a constant modulus plateau was achieved and allowed to equilibrate for 30 minutes.

4.2.6 Water Uptake

Membrane water uptake was determined by a weight difference methodology. The dry films were weighed and then immersed at room temperature in deionized water for one week after acidification. The wet films were then blotted dry and immediately weighed. In order to more precisely calculate the water uptake the wet films were then dried in a vacuum oven at 100 °C for 24 hours and weighed again. An average of 5 experiments of the ratio of weight gain to dry film weight was expressed as % water uptake. The equation for % water uptake is as follows:

$$\% \text{ water uptake} = \frac{\text{mass}_{\text{wet}} - \text{mass}_{\text{dry}}}{\text{mass}_{\text{dry}}} \times 100 \quad \text{Equation 4.1}$$

where mass_{wet} is the average weight of 5 wet membranes, mass_{dry} is the average weight of 5 dry membranes.

4.2.7 Ion Exchange Capacity and Lambda Value

Determination of the theoretical amount of acid equivalents per gram of polymer can be performed by calculating the ion exchange capacity:

$$\text{IEC} = \frac{(2 * \text{mol fraction of disulfonation})}{((\text{MW}_{\text{repeat}} * \text{mol fraction } y) + (\text{MW}_{\text{sulf. repeat}} * \text{mol fraction } z))} \quad \text{Equation 4.2}$$

Where the value 2 in the numerator corresponds to two sulfonate moieties on the sulfonated repeat unit, y is the mole fraction of the unsulfonated monomer/repeat unit, z is the mole fraction of the sulfonated monomer/repeat unit, MW_{repeat} is the molecular weight of the unsulfonated repeat unit and $MW_{sulf. repeat}$ is the molecular weight of the sulfonated repeat unit. This equation calculates the equivalents of acid moieties per gram of polymer.

The number of water molecules per sulfonic acid site, lambda value (λ), was calculated using the water uptake measurements and the IEC of the copolymer using the following equation where MW_{H_2O} is the molecular weight of water (18.01 g/mol) and IEC is the value of the milli-equivalents of acid groups per gram of copolymer.

$$\lambda = \frac{mass_{wet} - mass_{dry} / MW_{H_2O}}{IEC \times mass_{dry}} \quad \text{Equation 4.3}$$

4.2.8 Proton Conductivity

Proton conductivity of the membranes under fully hydrated conditions in liquid water was determined at 30 °C using a Solatron 1260 Impedance/Gain-Phase Analyzer over the frequency range of 10Hz- 1 MHz following the reported procedure.²⁷² The resistance of the films was taken at the frequency that produced the minimum imaginary response. The conductivity of the membranes was calculated from the measured resistance and the geometry of the cell. The following equation calculates the proton

²⁷² Zawodzinski, T. A., Neeman, M., Sillerud L. O., and S. Gottesfeld, *J. Phys. Chem.* 95, 6040, 1991.

conductivity (σ) using the length between the electrodes (l), the cross sectional area of the membrane (A) and the real contribution of the impedance response (Z').

$$\text{Proton Conductivity } \sigma = \frac{l}{A \cdot Z'} \quad \text{Equation 4.4}$$

4.2.9 Methanol Permeability

Acid form membranes were used to determine methanol permeability of PATS copolymers using a membrane separated diffusion cell and a recirculation pump connected to a differential refractometer²⁷³ as shown in figure 4-2. The glass diffusion cell contained water in one chamber and a water-methanol mixture in the supplementary chamber. When both chambers were filled, methanol permeated through the swollen film and into the water. Over time, the concentration of methanol would increase in the water chamber and would decrease in the methanol chamber until equilibrium was reached. The refractive index instrument monitored the change in methanol concentration in the chamber of previously pure water. Methanol permeation was determined using the rate of change in concentration for each side.²⁷⁴ There are three assumptions in the mathematical calculations to acquire methanol permeability:

²⁷³ Kim, Y. S., Hickner, M. A., Dong, L., Pivovar, B. and McGrath, J. E. *J. Membr. Sci.* 243(1-2), 317-326, 2004.

²⁷⁴ Cussler, E. L. *Diffusion Mass Transfer in Fluid Systems*, 2nd Ed., Cambridge University Press, New York, 1997.

1. No mass transfer resistance
2. No water flux occurs
3. Steady-state conditions

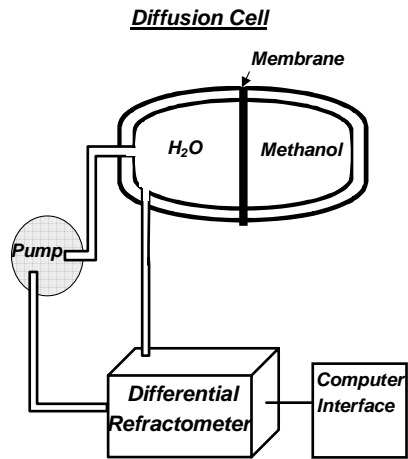


Figure 4.2 Glass diffusion cell and differential refractometer

The following equations outline the mass balance for the right and left chambers of the diffusion cell as depicted in Figure 4.2:

$$V_L \frac{dc_{\text{CH}_3\text{OH},L}}{dt} = Aj \quad \text{Equation 4.5}$$

$$V_R \frac{dc_{\text{CH}_3\text{OH},R}}{dt} = Aj \quad \text{Equation 4.6}$$

Where V_L and V_R are the volumes of the chambers, A is the area of the membrane, $dc_{\text{CH}_3\text{OH},L}$ and $dc_{\text{CH}_3\text{OH},R}$ are the change in methanol concentrations in the left and right chambers, dt is the change in time and j is the geometrical constant. Subtraction of these

two equations gives the following where D and H are the methanol diffusivity and partition coefficient, respectively:

$$\frac{d}{dt}(c_{CH_3OH,R} - c_{CH_3OH,L}) = DH\chi(c_{CH_3OH,L} - c_{CH_3OH,R}) \quad \text{Equation 4.7}$$

The geometrical dimensions of the diffusion cell are denoted as χ , which can be calculated with the following equation using l as the membrane thickness:

$$\chi = \frac{AH}{l} \left(\frac{1}{V_L} + \frac{1}{V_R} \right) \quad \text{Equation 4.8}$$

By integrating equation 4.7 using the initial conditions, the following is obtained:

$$c_{CH_3OH,R} - c_{CH_3OH,L} = c_{CH_3OH,R}^o - c_{CH_3OH,L}^o \quad \text{Equation 4.9}$$

Further rearrangement gives:

$$\frac{c_{CH_3OH,R} - c_{CH_3OH,L}}{c_{CH_3OH,R}^o - c_{CH_3OH,L}^o} = e^{-DH\chi t} \quad \text{Equation 4.10}$$

By taking the natural log of each side and solving for the change in methanol concentrations, the following equation allows methanol permeability (DH) to be obtained by plotting a straight line using $\ln[(c_{1,R} - c_{1,L})/(c_{1,R}^o - c_{1,L}^o)]$ versus time with the slope equal to $-DH \chi$.

$$-DH_{FS} \cdot \chi \cdot t = \ln \left(\frac{\Delta c_{CH_3OH}}{\Delta c_{CH_3OH}^o} \right) \quad \text{Equation 4.11}$$

4.2.10 Relative Selectivity

Relative selectivity of ion exchange membranes is described as the selectivity of the alternative membrane divided by the selectivity of Nafion[®] as shown in the following equation:

$$\text{Relative Selectivity} = \frac{\beta_{AM}}{\beta_{Nafion}} \quad \text{Equation 4.12}$$

where β_{AM} is the selectivity of the alternative membrane and β_{Nafion} is the selectivity of Nafion[®]. The selectivity is determined by dividing the proton conductivity by the methanol permeability as shown in the following equation:

$$\text{Selectivity } \beta = \frac{\sigma}{DH} \quad \text{Equation 4.13}$$

where σ is the proton conductivity and DH is the methanol permeability. A film with a higher value of selectivity displays lower electro-osmotic drag and an alternative membrane with a relative selectivity that is greater than 1 is a potentially better proton exchange membrane for direct methanol fuel cells relative to Nafion[®].

4.3 Results and Discussion

Two series of disulfonated PATS copolymers were synthesized. The solitary difference between the two series of copolymers was the activated dihalide monomer charged into the reaction thereby producing different molecular weights. One series of PATS copolymers employed activated aryl dihalides containing chlorine-leaving groups where the other series used fluorine-leaving groups as the dihalide agents. The higher electronegative, and thus more reactive monomer in a nucleophilic aromatic substitution reaction, difluoro- monomers produced a higher molecular weight series of PATS copolymers when compared to the less reactive dichloro-based copolymers. The nomenclature for the following discussion will denote the two series as either the low molecular weight (low MW) or high molecular weight (high MW) PATS series. The data in table 4-1 indicate the ion exchange capacities (IEC), intrinsic viscosities (IV), number average molecular weights (M_n) and weight average molecular weights (M_w) for both high MW and low MW series of PATS copolymers.

Table 4.1 Ion exchange capacities, intrinsic viscosities, number average molecular weights and weight average molecular weights for low MW and high MW PATS copolymers.

	IEC (meq/g)	IV (dL/g) 25 °C, NMP	M _n (kg/mol)	M _w (kg/mol)
			NMP + 0.05 M LiBr using polystyrene standards	
PATS 20 low MW	0.81	0.69	23	68
PATS 30 low MW	1.17	0.61	19	58
PATS 40 low MW	1.51	0.76	20	61
PATS 20 high MW	0.81	1.30	25	104
PATS 30 high MW	1.17	1.00	26	127
PATS 40 high MW	1.51	1.20	28	151

These data indicate that the more reactive difluoro- series of copolymers produced consistently higher intrinsic viscosities and molecular weights, specifically M_w, as compared to the less reactive dichloro- series. It is assumed that at higher molecular weights, the number of chain entanglements per unit chain will increase and the number of chain ends per volume of copolymer will decrease. Therefore, physical crosslinks (i. e. chain entanglements) and fewer dangling chain ends that are in a current state of motion should theoretically decrease the overall swollen volume of the membrane in liquid water.

Protonically conductive membranes showing enhanced conductivity allows for better performance in the fuel cell environment. However, increased water uptake typically goes hand-in-hand with increased proton conductivity. Therefore, if a membrane has extremely high proton conductance and extremely high water sorption, the electrochemical processes work well but the physical stability of the film is poor and decreases membrane durability. Without proton conductance, water uptake is typically

low but the poor conductivity does not allow efficient performance in hydrogen or methanol fuel cells. The acid form proton conductivities and water uptakes are shown in Figures 4.3 and 4.4, respectively.

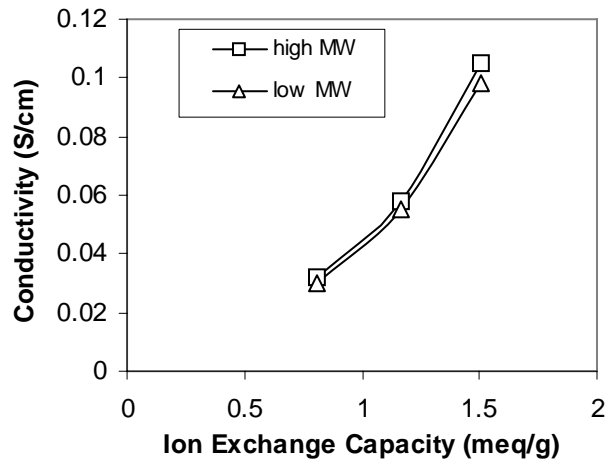


Figure 4.3. Proton conductance of low MW and high MW acid form PATS membranes immersed in liquid water at room temperature

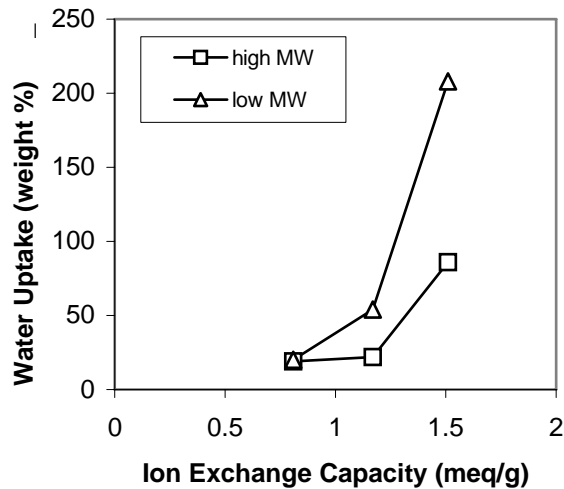


Figure 4.4. Water uptake of low MW and high MW acid form PATS membranes

The proton conductance of the copolymers increases with increasing ion exchange capacities. The conductivities of the acid form films ranged from 30 mS/cm for PATS 20 to 110 mS/cm for PATS 40. Comparable conductivities were observed for both the high MW and low MW PATS copolymer series. These results indicate that the proton conductance is fairly constant for these varying molecular weight copolymers that contain matching chemical structures and identical numbers of ion moieties along the polymer backbone.

As is typically coupled with the proton conductivity trend, the liquid water uptake at room temperature of both series of PATS copolymers increased as the ion exchange capacities and proton conductivities increased. At the lowest ion exchange capacity, the PATS 20 copolymers gave similar water uptakes at 19% and 20% for the high MW and low MW series. However, at higher degrees of sulfonation, the copolymers synthesized from the difluoro- series produced lower water uptakes. The high MW PATS 30 copolymer showed only 22% water sorption, while the low MW PATS 30 copolymer showed 54% water uptake. The low MW PATS 40 samples gave the highest water uptake of the series at 208%, while the high MW PATS 40 showed only 86% water sorption.

The proposed theory to describe the intense increase in water uptake from PATS 30 to PATS 40 for both series of copolymers points to the morphology of the materials. The lower ion exchange copolymers, PATS 20 and PATS 30, contain high volume fractions of hydrophobic, ion-poor domains that have continuity and tend to restrict the swelling of the ion-rich, hydrophilic non-continuous domains. The higher ion exchange materials, PATS 40, contain higher volume fractions of hydrophilic domains that are

described as being the co-continuous majority of the material. The minor, hydrophobic phases become secluded from each other, thus, not restricting the swelling of the ion-rich domains thereby permitting higher water sorption.

Comparison of the proton conductivities and the water sorption data indicates two significant observations. The increased water uptake of the low MW PATS 40 sample does not seem to have an appreciable effect on the conductivity. Therefore, the greater volume of water does not impede nor enhance proton conductance at a given ion exchange capacity. The PATS 20 copolymer conductivities are too low for efficient fuel cell performance and the physical water uptake properties of the low MW PATS 40 membranes are too high for adequate engineering into the membrane electrode assembly and long-term durability. Therefore, high molecular weight copolymers seem to allow the highest levels of conductivity with the lowest levels of water uptake.

Using equation 4.3, the number of water molecules per sulfonic acid site, lambda value (λ), was calculated using the water sorption measurements and the ion exchange capacities of the copolymers. Table 4.2 indicates the lambda values for both series of PATS copolymers.

Table 4.2 Calculated lambda values for both low MW and high MW PATS copolymers

	Water Uptake (wt%)	IEC (meq/g)	Lambda (N H ₂ O/SO ₃ H)
low MW PATS 20	20	0.81	13
low MW PATS 30	54	1.17	26
low MW PATS 40	208	1.51	77
high MW PATS 20	19	0.81	12
high MW PATS 30	22	1.17	11
high MW PATS 40	86	1.51	32

As the data indicate, the lambda values for both the PATS 20 samples were very similar, further characterizing that the low IEC copolymers are dominated by the hydrophobic phase. However, when comparing the lambda values of both the low MW and high MW PATS 30 and 40 samples, a large increase in the number of water molecules per sulfonic acid groups is evident. By coupling the proton conductivity and lambda values, it was observed that the conductivity does not change dramatically over a wide range of lambda values for a given ion exchange capacity. This further indicates that molecular weights of the copolymers affect not only the water uptake on a weight percent basis, but, and not surprisingly, the number of water molecules per sulfonic acid group.

Permeability to methanol of both the high and low MW series of PATS copolymers was determined using a diffusion cell (Figure 4.2) to understand the transport characteristics for varying molecular weights and ion exchange capacities. The methanol permeability data shown in Figure 4.5 indicate that at the low ion exchange capacity, the permeability of both low and high MW PATS 20 is very low and similar. Therefore, since the volume fraction of the hydrophobic phase is dominant and the ion-poor matrix restricts the swelling of the hydrophilic phase, molecular weight does not increase or decrease the transport properties. Further observations of the data indicate that as the ion-exchange capacity increases, the permeability to methanol increases. By then comparing the two series of PATS copolymers, it is deduced that higher molecular weight, at the higher ion exchange capacities, plays an intense role in transport of methanol. The high MW PATS 30 sample had 41% lower methanol permeation (3.2×10^{-7} cm²/s) relative to the low MW PATS 30 (4.6×10^{-7} cm²/s). The PATS 40 sample that

had lower molecular weight showed a 20% increase in methanol permeation (9.3×10^{-7} cm^2/s) relative to the high MW PATS 40.

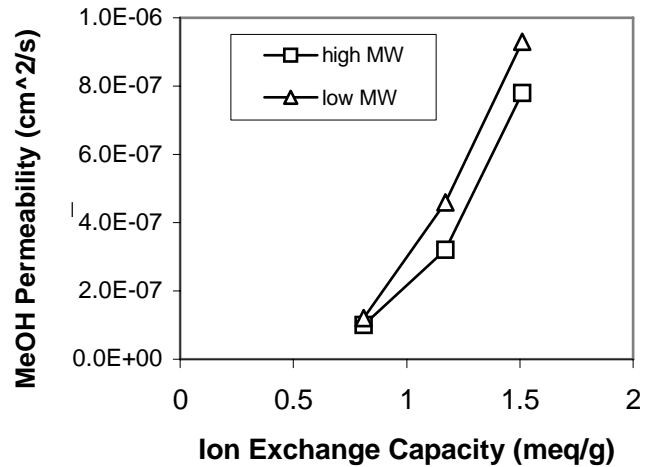


Figure 4.5 Methanol permeability versus ion-exchange capacity of hydrated PATS copolymers

By calculating the relative selectivity of the alternate membranes using the conductivities and methanol permeability values, further understanding of the molecular weight influence on transport was elucidated. Figure 4.6 indicates that even though the conductivity values are similar for a given ion exchange capacity, the selectivity relative to Nafion[®] of the high MW PATS series is higher than that of the low MW PATS series. Therefore, the lower molecular weight copolymers are not as advantageous as the higher molecular weight PATS copolymers that show enhanced selectivity at all amounts of ion exchange capacities.

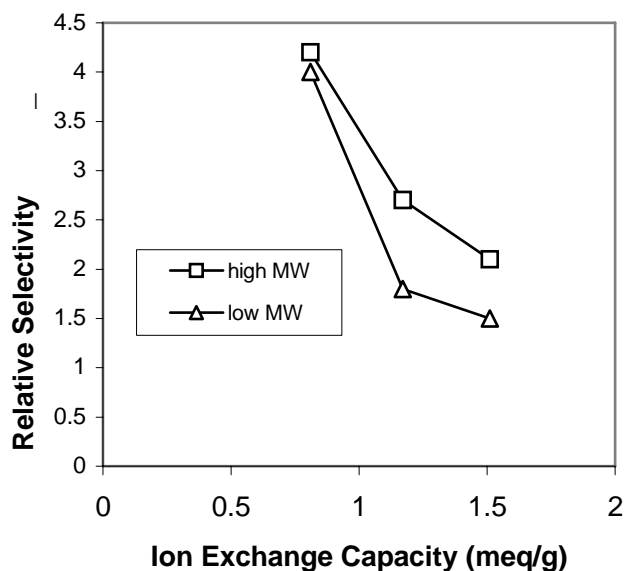


Figure 4.6 Selectivity of both low MW and high MW series of PATS Copolymers relative to Nafion[®]

Dynamic mechanical analysis (DMA) in liquid water at room temperature was performed on both series of high and low MW PATS copolymers so as to provide information on their ability to make both mechanically robust and durable membrane electrode assemblies that give extended lifetime performance. Fuel cell membranes physically, electrochemically and mechanically multitask by supporting the electrodes, separating the fuel and oxidant, mechanically sealing the gaskets and by transporting protons and insulating electrons. The film must be able to withstand large pressure gradients both in the active areas and gasket areas along with large tensions/stresses around membrane-electrode and membrane-gasket interfaces. Therefore, the strength and ductility was probed by in-situ dynamic mechanical analysis using the acid form films. The fully hydrated environment allows proper characterization in direct methanol and fully hydrated hydrogen/air fuel cell atmospheres. The results of the experiments are

shown in Figure 4.7 and provide insight into a well-known characteristic where molecular weight plays a crucial role in mechanical properties of all types of polymers.

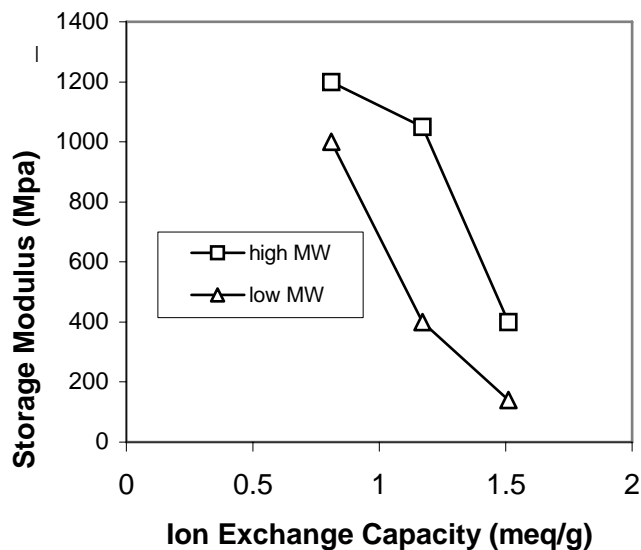


Figure 4.7 Hydrated dynamic tensile modulus versus ion exchange capacity for high and low MW series PATS copolymers

A very sharp difference was observed in the hydrated storage moduli when comparing the high MW PATS series and the low MW PATS series. As expected, the hydrated modulus of the lower ion exchange capacity copolymers was much higher due to the hydrophobic matrix resisting the swelling of the ion-rich domains producing low water uptakes and stronger films. It was deduced that at the 20% disulfonation level, the volume fraction of the hydrophobic, ion-poor domains acts as physical crosslinks that bind the hydrated membrane collectively. However, even at low ion contents, the mechanical properties were dramatically different (200 Mpa) when comparing high and low MW PATS 20 copolymers. This set of data indicates the direct correlation between mechanical properties and molecular weights. When observing the two data series

jointly, the hydrated modulus decreases with increasing disulfonation and with decreasing molecular weight. This infers that the decline in hydrophobic domains at high ion exchange capacities decreases the physical crosslinks that restrict the water sorption and decreases the mechanical properties. Furthermore, low molecular weight thereby producing fewer chain entanglements produce poor physical properties, which would decrease durability and lifetime performance in a fuel cell environment.

4.4 Conclusions

Many properties of proton exchange membranes have been determined to be directly related to molecular weight. The physical properties that were analyzed include water uptake, conductivity, methanol permeation, relative selectivity to Nafion[®] and hydrated storage modulus. A low molecular weight series of disulfonated poly(arylene ether sulfone) copolymers was synthesized using dichloro- dihalide monomers (3,3'-disulfonate 4,4'-dichlorodiphenyl sulfone and 4,4'-dichlorodiphenyl sulfone), while a higher molecular weight series of PATS was synthesized using higher reactive difluoro-dihalide monomers (3,3'-disulfonate 4,4'-difluorodiphenyl sulfone and 4,4'-difluorodiphenyl sulfone).

Assessment of proton conductivity indicated that the molecular weight range that was studied had very little effect. However, the water uptake and lambda values were determined to change drastically with changes in molecular weight. For the low MW series of PATS copolymers, the water uptake and the lambda values (number of water

molecules per sulfonic acid group) were much higher than the high MW series that showed similar conductivity values. The low MW series indicated enhanced methanol permeability, which would lead to low fuel efficiency and a reverse flux of proton transport. It was found that at the lowest degree of disulfonation, PATS 20, the methanol permeability and water uptake varied little within the range of molecular weights that was studied. The volume fraction of hydrophobic repeat units is very high in the lowest ion exchange capacity materials and, thus resisted the swelling of the hydrophilic domains. It was concluded that the ion poor domain volume fraction outweighed the molecular weight influence. However, above 20% disulfonation, the water sorption and methanol permeability increased dramatically for the low molecular weight samples. The volume fraction of the hydrophilic repeat units allowed larger water sorptions and more of an influence of lower molecular weights. The low MW samples were concluded to have fewer chain entanglements thereby allowing higher amounts of water and methanol to be adsorbed and transported into and through the membrane.

Because relative selectivity reflects on the overall methanol permeability and conductivity, the value for the selectivity relative to Nafion[®] was decreased for the low MW series of copolymers. Hydrated storage modulus experiments were performed submersed in liquid water and indicated that the entire low MW series of copolymers had poor physical mechanical properties relative to the high MW series. These conclusions signify that molecular weight has a very large impact on the relevant physical properties of proton exchange membranes at any sulfonation level. The fabrication processes to make membrane electrode assemblies can be hindered by membranes that swell dramatically upon submersion in water thereby delaminating the electrodes (i. e. low MW

series). Furthermore, durability and lifetime in a prolonged temperature and humidity cycling environment can be decreased by low MW copolymers having low hydrated modulus and fewer chain entanglements producing cracks and pinholes and little fatigue resistance.

Synthetically controlling the molecular weight of disulfonated PATS copolymers using differences in the reactivity of the monomers allowed a systematically detailed study of the effect of molecular weight on fuel cell membranes in fuel cell environments. These results and conclusions that have been drawn from the data for the PATS alternative ion exchange membranes can be extended to alternative membranes that are based on post-sulfonated materials. Typically, the molecular weight of industrially available polymers is often low because of the processing characteristics that high performance polymers must possess. However, the ease of synthetically producing ion exchange membranes by post-sulfonation would compromise the physical properties that are needed for both instantaneous and prolonged fuel cell performance. Therefore, production of the ideal copolymer membrane that characteristically attains desirable properties including methanol permeability, mechanical strength, water sorption and conductivity must include the highest molecular weights possible. This report reveals that high molecular weight is essential in a fuel cell environment that relies heavily on both electrochemical and mechanical properties.

CHAPTER 5

DIRECTLY COPOLYMERIZED POLY(ARYLENE SULFIDE SULFONE) DISULFONATED COPOLYMERS FOR PEM-BASED FUEL CELL SYSTEMS: FABRICATION AND CHARACTERIZATION OF HETEROPOLYACID COMPOSITE MEMBRANES FOR HIGHER TEMPERATURE FUEL CELL APPLICATIONS

Abstract

The fabrication and viability of producing heteropolyacid (HPA)-disulfonated poly(arylene thioether sulfone) copolymer composite membranes and membrane electrode assemblies was investigated. A series of partially disulfonated poly(arylene thioether sulfone) copolymers (PATS) was synthesized by nucleophilic aromatic substitution copolymerizations employing potassium carbonate as a weak base. Composite membranes were prepared by homogeneous solution blending and casting the copolymers with phosphotungstic acid (PTA). Fourier transfer infrared spectroscopy was used to evaluate band shifts corresponding to the sulfonic acid moieties on the copolymer backbone hydrogen bonded to the bridging tungstic oxide groups on the HPA molecule. The composite PATS membranes exhibited low HPA molecule water extraction after acidification treatments performed at room temperature and boiling temperatures. The thermal stability of the composite membranes was probed by thermogravimetric analysis

and indicated an enhanced stability of the sulfonic acid moieties presumably due the hydrogen bonding interactions between the HPA molecules and sulfonic acid groups. The membranes containing HPA indicated improved conductivity at high temperatures and low relative humidities when compared to the pure copolymer samples. For example, at 120 °C and 45% relative humidity at atmospheric pressure, the conductivity of the composite PATS 30 sample containing 30 wt% of HPA was 10 mS/cm while the conductivity of the pure PATS 30 sample was only 4 mS/cm. The increase of proton conductivity was ascribed to the water retention characteristics of the HPA molecules which allowed enhanced mobility of the protons. Alternatively, dehumidification of the pure PATS membrane decreased the maximum attainable conductivity. The dehydration process of both the composite and the pure membranes was monitored by dynamic infrared analysis by observing the decrease in the intensity of the hydroxyl vibrations as the sample was heated. By coupling the infrared results to the conductivity results, the composite membranes were determined to provide enhanced water retention at temperatures above the boiling point of water. This suggested that incorporation of phosphotungstic acid would enhance higher temperature fuel cell performance at low relative humidities.

Key Words: poly(arylene thioether sulfone), poly(arylene sulfide sulfone), poly(arylene ether sulfone), proton exchange membrane, fuel cell, Nafion, composite membrane, phosphotungstic acid, heteropolyacid

5.1 Introduction

Proton exchange membrane fuel cells (PEMFC) based on polymer electrolyte membranes (PEM) are promising candidates for applications such as stationary power, low-emission vehicles and portable electronics. The membrane electrode assembly (MEA), consisting of well-bonded catalyst electrodes and proton exchange membrane (PEM), is the foundation of the fuel cell and is critical for allowing proton transport from the anode to the cathode and the generation of electricity from chemical energy. PEMs must have good mechanical, thermal, and chemical stabilities and still have high proton conductivity. The polyperfluorinated sulfonic acid membranes are the state-of-the-art PEMs used for both hydrogen and methanol fuel cells.^{275,276} However, some specific limitations exist for Nafion™-type membranes, which include low conductivity at high temperatures and low humidity as well as high methanol permeability that decreases fuel efficiency.²⁷⁷

Operating a fuel cell at a temperature range of 100-120 °C has been shown to improve reaction kinetics, especially at the cathode, and to decrease carbon monoxide poisoning of the platinum catalyst.²⁷⁸ Both the limitations of Nafion material and the possibility for improved performance at elevated temperatures has spurred many efforts to develop alternative proton exchange materials based on various chemical structures

²⁷⁵ M. A. Hickner, H. Ghassami, Y. S. Kim, B. R. Einsla and J. E. McGrath, *Chem. Rev.* 2004, 104, 4587-4612.

²⁷⁶ Mauritz, K. A. and Moore, R. B. *Chem. Rev.* 2004, 104, 4535-4585.

²⁷⁷ M. Mathias, H. Gasteiger, R. Makharia, S. Kocha, T. Fuller, T. Xie and J. Pisco, Preprints of Symposia - American Chemical Society, Division of Fuel Chemistry 2004, 49(2), 471-474.

²⁷⁸ Malhotra, S. and Datta, R. J. *J. Electrochem. Soc.* 1997, 144, L23.

including polyimides^{279,280,281}, polyketones^{282,283}, poly(phenylene ether)s²⁸⁴ and poly(sulfone)s²⁸⁵. These aromatic polymers and copolymers may provide adequate performance while maintaining low cost and stability. Improvements including control of molecular weights and the stability of the proton conducting sites have aided in development of alternative membranes, however, conductivity performance at temperatures in excess of 100 °C is still inadequate due to dehydration and low water retention above the water boiling point. Variations of these acidic copolymers have been reported using both complexes with basic polymers based on polybenzimidazole²⁸⁶ and acidic inorganic additives based on heteropolyacids.^{287,288}

Inorganic-organic composite membranes based on heteropolyacids and sulfonated aromatic polymers are an interesting class of proton exchange membrane because of their high thermal stability, proton conductivity and water retention at elevated temperatures. The overall architecture of heteropolyacid (HPA) molecules depends primarily on the hydration state, where the dehydrated form is termed the primary Keggin unit (Figure 5.1).²⁸⁹ The primary structure contains four different types of oxygen atoms which have been denoted as the (1) central oxygen atoms, (2) bridging oxygen atoms from tungsten to tungsten, (3) bridging oxygen atoms from phosphorus to tungsten and (4) terminal

²⁷⁹ Gunduz, N. and McGrath, J. E. *Polym. Prepr.* 41, 2, 1565, 2000.

²⁸⁰ Genies, C., Mercier, R., Sillion, B., Cornet, N., Gebel, G. and Pineri, M. *Polymer* 42, 359, 2001.

²⁸¹ Einsla, B.R., Hong, Y.T., Kim, Y.S., Wang, F., Gunduz, N. and McGrath, J.E. *J. Polym. Sci., Part A: Polym. Chem.* 44, 862-874, 2004.

²⁸² Alberti, G., Casciola, M., Massinelli, L. and Bauer, B. *J. Membr. Sci.* 185, 73, 2001.

²⁸³ Zaidi, S.M.J., Mikhailenko, S. D., Robertson, G. P., Guiver, M. D. and Kaliaguine, S. *J. Membr. Sci.* 173, 17, 2000.

²⁸⁴ Wang, F., Hickner, M., Kim, Y. S., Zawodzinski, T. A. and McGrath, J. E. *J. Membr. Sci.* 197, 231, 2002.

²⁸⁵ Harrison, W. L., Wang, F., Meham, J., Bhanu, V., Hill, M., Kim, Y. S. and McGrath, J. E. *J. Polym. Sci. Part A: Polym. Chem.* 41, 2264, 2003.

²⁸⁶ Kerres, J., Ulrich, A., Meier, A. F. and Haring, T. *Solid State Ionics* 125, 243, 1999.

²⁸⁷ Kim, Y. S., Wang, F., Hickner, M., Zawodzinski, T. and McGrath, J. E. *J. Membr. Sci.* 212, 263, 2003.

²⁸⁸ Bonnet, B., Jones, D., Rozier, J., Tchicaya, L., Alberti, G., Casciola, M., Massinelli, L., Bauer, B., Peraio, A. and Ramunni, E. *J. New Mater. Electrochem. Syst.* 3, 87, 2000.

²⁸⁹ Bardin, B. B., Bordawekar, S. V., Neurock, M. and Davis, R. J. *J. Phys. Chem. B* 102, 10817, 1998.

oxygen atoms. The secondary structure, or hydrated architecture, forms hydrogen bonding bridges between four HPA molecules and hydronium ions (H_5O_2^+). Coordination of the loosely bound hydronium ions around the terminal oxygens in the HPA molecules are considered to provide high proton conductivity; however, the conductivity further depends on the hydration state and temperature of the environment. As a candidate for a solid electrolyte material, the water solubility of the HPA and the hydration dependence on conductivity prevented acceptable long-term stability. However, it has been suggested that the strong interactions between the HPA molecules and the sulfonic acid groups on suitable polymeric material may allow for greater water retention and therefore a higher level of overall hydration that produces acceptable conductivity values above the boiling point of water.²⁹⁰

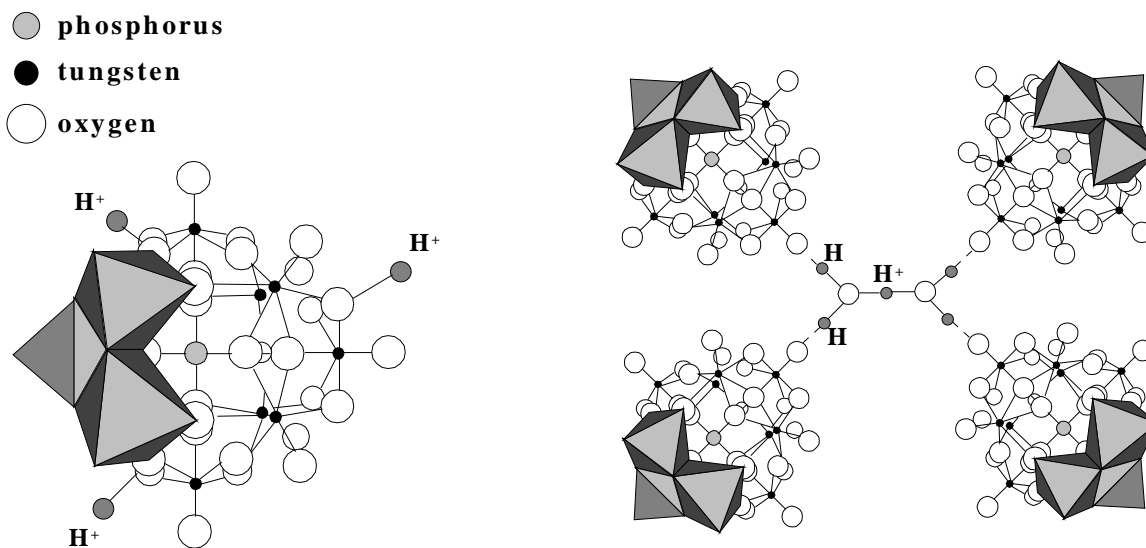


Figure 5.1 Primary Keggin and Secondary Hydrated Structures of Semicrystalline Phosphotungstic Acid

²⁹⁰ Zaidi, S., Mikhailenko, S., Robertson, G., Guiver, M., and Kaliaguine, S. *J. Membr. Sci.* 173, 17, 2000.

Synthesis of various disulfonated comonomer compositions in poly(arylene thioether sulfone) copolymers (PATS) has been recently reported by our group.^{291,292} Major advantages of the direct polycondensation reactions of disulfonated monomers can be noted relative to post-sulfonation of preformed homopolymers. These specific advantages include tailoring reaction conditions to produce precise ion concentrations and enhanced stabilities of the ions due to their location on the deactivated aryl sulfone linkage. Accurate control of disulfonation during copolymerization allowed for a family of disulfonated arylene copolymers containing sulfide and sulfone linkages to be prepared. Morphological studies of the unfilled disulfonated copolymers using atomic force microscopy indicated enhanced connectivity of hydrophilic domains as the level of disulfonation increased. A phase inversion from a hydrophobic matrix to a hydrophilic matrix was observed in the range of 35-40 mol% disulfonation. Further investigation in these findings indicated that the water uptake increases dramatically at this percolation threshold of 35-40% disulfonation. Proton conductivity values also increased with the amount of disulfonation reaching levels of 0.16 S/cm for PATS 50 in liquid water at room temperature. The ability to tailor polymer properties by varying the levels of disulfonation encouraged further characterization of the PATS copolymer family using molecular weights as a variable.²⁹³ Low molecular weight materials produced higher water swelling and methanol permeability than the higher molecular weight counterparts, presumably due the decrease in physical chain entanglements. As predicted, due to the

²⁹¹ Wiles, K.B., Bhanu, V A., Wang, F. and McGrath, J.E. *Polymer Preprints*, 2002, 43(2), 993.

²⁹² Wiles, K.B., Wang F. and McGrath, J.E. *J. of Polym. Sci.: Part A: Polym. Chem.*, Accepted, 2005.

²⁹³ Wiles, K. B., Bhanu, V.A., Wang, F., Hickner, M. A. and McGrath, J.E. *Polymer Preprints*, 2003, 44(1), 1089.

large influence of molecular weight on physical properties, the low degree of entanglements produced poor hydrated storage moduli. Therefore, the present study employed high molecular weight copolymers made from highly reactive difluoro activated halide comonomers, allowing tough ductile films to be cast from solution. These copolymers also served as host matrices for inorganic fillers that contain hydrogen bonding sites for water retention and hydronium ion transport.²⁹⁴

This dissertation chapter illustrates the composite membrane preparation and characterization of disulfonated poly(arylene thioether sulfone) copolymers with a phosphotungstic acid heteropolyacid as an inorganic filler. Solution blending and further casting well dispersed HPA composite membranes allowed for careful investigations of the specific interactions associated with the HPA molecules and the disulfonated copolymers. This was probed using infrared analysis, thermogravimetry and transmission electron microscopy. The effects of the HPA additive on the physical properties included water uptake, thermal stability, morphology, HPA extraction and conductivity at room temperature and elevated temperatures. Oxidation of the sulfide moieties to create sulfoxide and sulfone linkages to aid in HPA retention through polar-polar interactions was explored using various hydrogen peroxide concentrations and submersion times. Dehydration characteristics of the pure copolymers and the composite materials were studied by infrared analysis to further understand water retention at temperatures above the boiling point. Enhanced ionic conductivity of the composite membranes relative to the pure copolymers at elevated temperatures were observed due to greater water retention. Therefore, low relative humidity conductivity experiments and

²⁹⁴ Wiles, K. B., de Diego, C. M. and McGrath, J.E. *Polymer Preprints*, 2004, 45(1), 724.

hydrogen/air fuel cell performance at high temperatures and low levels of humidification were performed on both the neat membranes and the composite membranes.

5.2 Experimental

5.2.1 Disulfonated copolymer synthesis

Synthesis of 3,3'-disulfonated 4,4'-difluorodiphenyl sulfone (SDFDPS) and high molecular weight PATS copolymers was accomplished by following the reported procedures incorporating direct nucleophilic aromatic substitution polymerizations using disulfonated monomers.²⁹⁵ The disulfonated monomer synthesis employing electrophilic aromatic substitution reactions and was carried out in fuming sulfuric acid that provided sulfonic acid groups that were *meta* to the sulfone moiety and *ortho* to the fluorine leaving atom. Activated dihalides based on highly reactive 4,4'-difluorodiphenyl sulfone (DFDPS) as the electrophile and 4,4'-thiobisbenzenethiol (TBBT) as the nucleophile (after K₂CO₃ reaction) in a basic environment using N-methyl-2-pyrrolidinone (NMP) as an organic solvent provided high molecular weight copolymers (Figure 5.2).

²⁹⁵ Wiles, K.B., Wang F. and McGrath, J.E. 'Directly Copolymerized Poly(arylene sulfide sulfone) Disulfonated Copolymers for PEM-Based Fuel Cell Systems I: Synthesis and Characterization,' *J. of Polym. Sci.: Part A: Polym. Chem.*, Accepted, 2005.

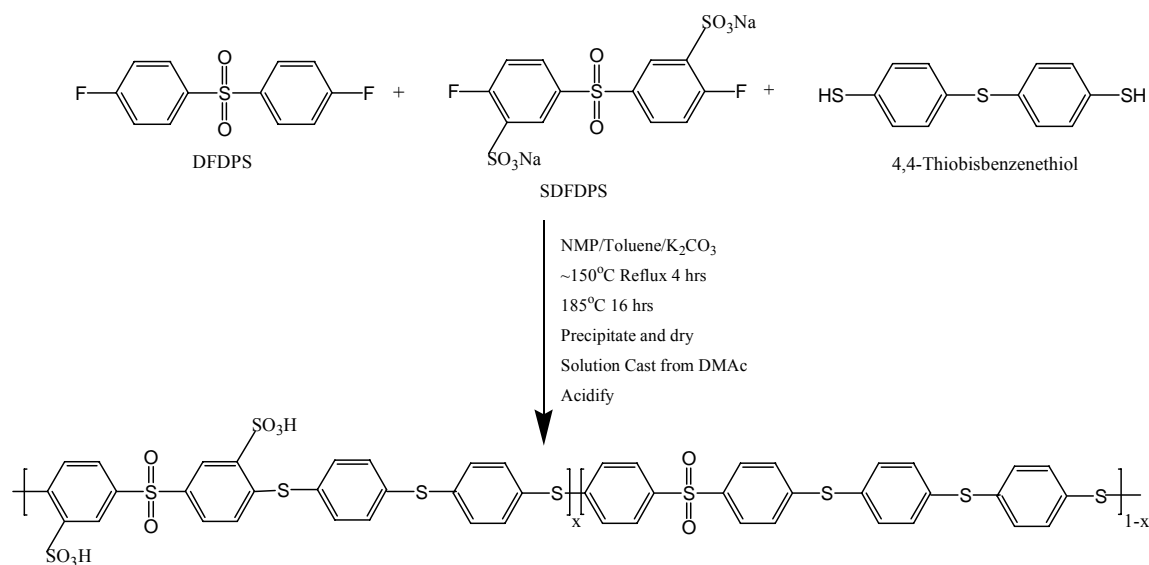


Figure 5.2 Synthesis of high molecular weight disulfonated poly(arylene thioether sulfone) copolymers

5.2.2 Membrane Preparation

The potassium salt films were prepared by first redissolving the fibrous copolymer in dimethylacetamide (DMAc) and then by filtering the solution through a 0.45 μm Teflon[™] syringe filter thereby directly casting the solution into a glass-casting tray. The glass tray had side-walls so as to aid in membrane thickness control. The copolymer solutions were dried in a vacuum oven by slowly increasing the temperature settings from 50 °C for 4 hours to 80 °C for 4 hours to 100°C for 12 hours and finally for 120 °C for 4 hours. Careful leveling of the glass casting tray provided uniform films. Addition of water to the casting tray swelled the membranes and allowed them to be easily removed. The salt form membranes were then transformed into the acid form using a boiling (~100 °C) technique in 0.5 M sulfuric acid in water for two hours. The

residual sulfuric acid was removed by boiling in water for another 2 hours. All the neat membranes tested were acidified using this high temperature acidification treatment so as to appreciably change the morphological characteristics of the resulting acidified membranes through possible reorganization of the sulfonate moieties producing ion clusters and channels.²⁹⁶

5.2.3 Composite Membrane Fabrication

Transparent, tough and ductile films were prepared by solution casting the acid form of PATS (5 wt%) and the semi-crystalline form of phosphotungstic acid (Fluka Chemicals) which were both dissolved in DMAc and mixed overnight. Prior to dissolution in DMAc, phosphotungstic acid (PTA) was dried at 100 °C in a convection oven for 16 hours (water molecules per HPA ~ 6). The casting conditions were the same as the neat membranes on glass trays as described above. Various disulfonation levels of PATS copolymers produced a family of phosphotungstic oxide containing composite membranes. The weight ratio of HPA to disulfonated PATS copolymer was held constant at 30 weight percent. All the resulting membranes were transparent with a slight orange color similar to the neat PATS membranes.

²⁹⁶ Y. S. Kim, F. Wang, M. A. Hickner, S. McCartney, Y. T. Hong, W. L. Harrison, T. A. Zowadzinski and J. E. McGrath, *J. Polym. Sci.: Part B: Polym. Phys.* 2003, 41, 2816.

5.2.4 Acidification and HPA Extraction of Composite Membranes

The composite membranes were tested either ‘Acid Cast’ or ‘reacidified’ using Method 1 or Method 2 acidification techniques. Method 1 reacidification of the composite membranes was performed at room temperature using a 1.5 M sulfuric acid solution in water. The copolymer composite membranes were submersed in the slow stirring solution for 24 hours and then rinsed with deionized (D. I.) water. Residual sulfuric acid was removed from the membranes by allowing them to be submersed in slow stirring D. I. water for another 24 hours while changing the water every 6 hours. A thorough and final rinsing removed the last traces of sulfuric acid. This room temperature reacidification produced what will now be termed Method 1 (M1) composite membranes. Method 2 reacidification of the composite films employed boiling (~100 °C) conditions in 0.5 M sulfuric acid in water for two hours. After a thorough rinsing, the residual sulfuric acid was removed by boiling in water for another 2 hours. A final rinse produced what will now be termed Method 2 (M2) composite membranes. HPA extraction was measured by the difference in weight before and after reacidification of the dry composite membranes divided by the original weight.

5.2.5 Fourier Transform Infrared Spectroscopy (FTIR)

Absorbance mode FTIR spectra of the neat and composite PATS thin films were obtained using a Nicolet Impact 400 FTIR spectrophotometer fitted with a ceramic heating cell. Peak shift experiments were performed using vacuum dried thin films at a

temperature of 120 °C. Dehydration experiments were conducted using the heating cell where membrane water loss was monitored as a function of temperature. After equilibration at 40 °C, fully hydrated FTIR spectra were recorded for PATS 30 and PATS 30 + 30 wt% PTA. A slow increase in temperature (10 °C/min) and equilibration at each temperature for five minutes for both neat and composite membranes allowed for measuring the loss in the water peak at 3500 cm⁻¹. The resolution of all the spectra was constant at 2 cm⁻¹. The average of 48 scans was reported.

5.2.6 Morphology Using Transmission Electron Microscopy (TEM)

TEM was performed on the composite membranes to understand the morphology and dispersive characteristics of the PTA additive in the PATS copolymers. The TEM was a Phillips 420T that produced bright field images taken with an accelerating voltage of 100 kV. The electron density of the PTA was high enough so that no staining was required to view the PTA particles (30 wt%) dispersed in a PATS copolymer matrix. Dry sample membranes were placed into epoxy and cured. The tip of the epoxy cube was sharpened to reveal the bulk of the composite membrane. Very thin films (70 µm) were cryogenically microtomed onto electron micrograph grids and viewed in vacuum.

5.2.7 Thermogravimetric Analysis (TGA) of Neat and Composite Membranes

Thermo-oxidative stability of the neat and composite membranes was performed dynamically on a TA Instruments TGA Q500. Sample preparation included drying a

small membrane in vacuum for 24 hrs at 100 °C. The dry film was then cut into very small pieces and loaded into a calibrated platinum TGA pan. A further drying cycle to remove any remaining water was carried out by heating the TGA furnace to 150 °C for 30 minutes. The sample was then cooled to 50 °C in the furnace at which time a heating cycle began to increase the heat to 800 °C at 10 °C/minute. The weight loss as a function of temperature was recorded in an air atmosphere.

5.2.8 Water Uptake

The water absorption of the composite membranes and neat copolymers was accomplished by using weight-difference calculations. The acidified films were dried in a vacuum oven at 100 °C for 24 hours and weighed. They were then immersed in deionized water at room temperature for 24 hours at which time they were removed from the water, blotted dry and weighed again. A final drying in vacuum at 100 °C for 24 hours was performed and the samples were then weighed. Weight gain based on the dry weight was recorded using an average of three membranes per type of film. No measurable loss was observed from the first-dry weight to the second-dry weight, thereby suggesting no PTA extraction for either of the M1 or M2 composite membrane series during water uptake experiments.

5.2.9 Oxidation of Sulfide Moieties to Aid HPA Retention

Dry solution cast membranes were submersed in 3-30% hydrogen peroxide in water for varying times at room temperature. The partially oxidized membranes were rinsed thoroughly with deionized water and dried in a vacuum oven at 100 °C for 24 hours. Infrared spectra were taken of oxidized PATS 30 (OX-PATS 30) using varying amounts of hydrogen peroxide and increasing times in 3% H₂O₂. Unfortunately, solution casting OX-PATS 30 composite membranes using a 30 wt% PTA loading provided brittle membranes.

5.2.10 Intrinsic Viscosity (IV) Measurements

IV data were calculated using the extrapolated values to zero concentration of the averages of the reduced and inherent viscosities. Characterization of molar mass after polymerizations and after the loss of molecular weight during exposure to hydrogen peroxide was monitored by intrinsic viscosity measurements using NMP at 25 °C and a Cannon Ubbelohde viscometer.

5.2.11 Ion Exchange Capacity

The experimental IEC was determined by titrating the weak acid that was formed, which was sodium hydrogen sulfate, in an aqueous solution by reacting a weak base, sodium sulfate, with the acid form membrane. Ion exchanging the hydrogen ions with a

metal (*i. e.* sodium) to form the salt form polymer and an acid form, water soluble compound (*i. e.* sodium hydrogen sulfate) allowed for potentiometric aqueous titrations. For this study, the aqueous titrations used sodium sulfate as the water-soluble ion exchange compound that produces sodium hydrogen sulfate during an equilibration reaction with the acid form membrane. The equilibrium reaction was directed to the sodium hydrogen sulfate by addition of a large excess of sodium sulfate.

5.2.12 Proton Conductivity at Low and High Temperatures and Humidities

Ionic conductivity was measured using a Hewlett Packard 4192 Impedance/Gain Phase Analyzer over a frequency range of 10Hz-1MHz.²⁹⁷ The resistance of the films was taken at the frequency which produced the minimum imaginary response. The conductivity of the membranes was calculated from the measured resistance and the geometry of the cell. Low temperature (<100 °C) conductivity values were obtained in liquid water. High temperature conductivity data was attained in a convection oven fitted with a deionized water humidification steam generator and a hygrometer to measure relative humidity on a dynamic scale (Figure 5.3). The temperature was controlled by an oven thermocouple placed directly next to the conductivity cell. The membranes were allowed to equilibrate for four hours before testing.

²⁹⁷ T. A. Zawodzinski, M. Neeman, L. O. Sillerud and S. J. Gottesfeld, *Phys. Chem.* 1991, 95, 6040.

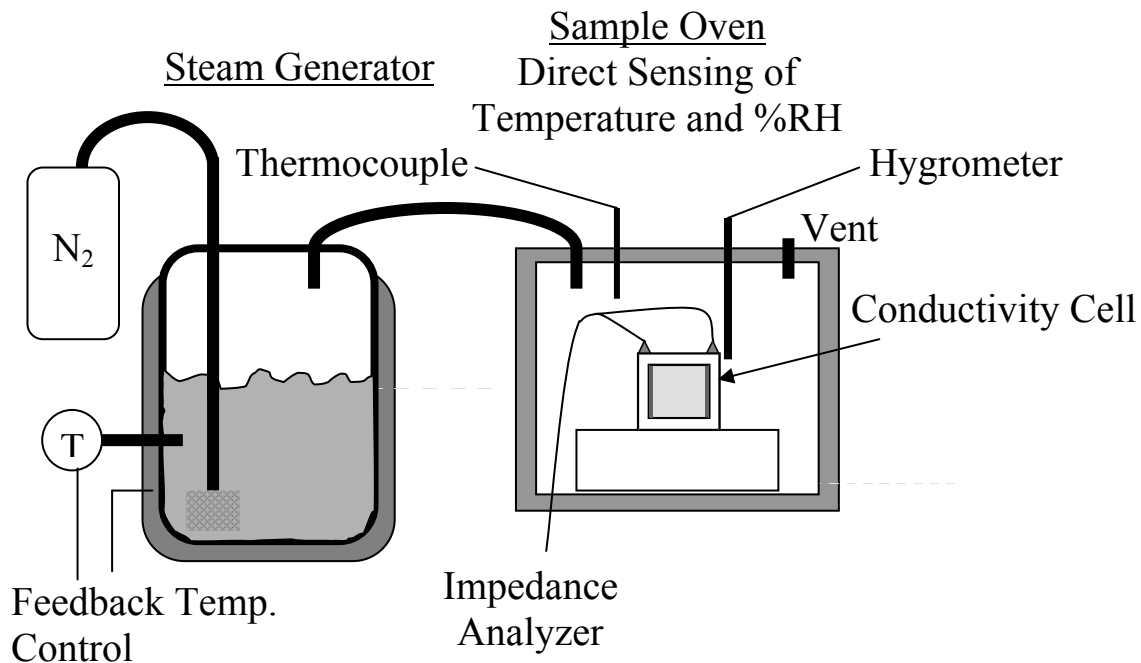


Figure 5.3 Schematic of Conductivity Measurement Apparatus for use at Elevated Temperature and Reduced Relative Humidity at Atmospheric Pressure

5.2.13 Hydrogen/Air Fuel Cell Performance

Fuel cell performance was obtained using a Fuel Cell Technologies Test Station operating up to 10 Volts at 50 Amps and 60 Watts. A Hewlett Packard load box with a computer interface was used to monitor voltage, current and resistance of 5 cm^2 membrane electrode assemblies. Catalyst loadings and weight percent of ionomer were held constant for all samples at 0.2 mg/cm^2 using 20%Pt on Vulcan carbon black and 28.5wt% N1100 in both anode and cathode electrodes respectively. Catalyst inks contained Nafion (5% dispersion in alcohols), Glycerol and 20% Pt supported on carbon black. The formulations obtained a 2.5:1 ratio of platinum catalyst to Nafion. The ink was stirred and sonicated to promote even dispersion of the Pt/C particles. The Nafion

dispersion and platinum supported on carbon were obtained from Electrochem Inc. and the glycerol from Aldrich. Electrode decals were fabricated using Teflon reinforced with glass fiber backing layers. The catalyst ink was painted layer-by-layer onto the decals using a high quality #4 camel hair brush. Uniform electrodes were dried after every coat of ink at 130 °C for ten minutes. After the correct loadings were obtained by calculating the difference between the decal backing layer and the electrode decal, the prefabricated electrodes were dried overnight at 130 °C to remove any residual glycerol and alcohols. Membrane electrode assemblies (MEAs) were produced by placing a salt form membrane between two electrode decals and hot pressing at 210 °C and 3000 psi for a total of 8 minutes. The MEAs were then acidified using either M1 or M2 acidification techniques. After constructing the single 5 cm² cell using the Fuel Cell Technologies Inc. hardware, E-Tek gas diffusion layers and Teflon gaskets, conditioning of the cell was performed using a life time test at 0.5 Volts at 80 °C and 100 %RH. After the current density reached a plateau, voltage-current-resistance experiments were conducted.

5.3 Results and Discussion

5.3.1 Specific Interactions of PTA and PATS Copolymers

Composite membranes were solution cast from high molecular weight acid form PATS copolymers and 30 weight percent of PTA inorganic filler. The acid form rather than the salt form copolymers were used to promote proper hydrogen bonding and polar interactions between the sulfonate and acid groups on the PTA molecules. Organic

homogeneous solution polymerizations produced a family of PATS copolymers that had relatively high intrinsic viscosity values (Table 5.1) that made tough and ductile films. Along with ion exchange capacity, proton nuclear magnetic resonance experiments in deuterated dimethyl sulfoxide determined that the synthetically obtained sulfonation levels were in good accord relative to the predetermined disulfonated to unsulfonated ratios. Experimental ion exchange capacity potentiometric aqueous titrations showed good agreement to the calculated IEC values of all the neat copolymers indicating good incorporation of the disulfonated repeat unit.

Table 5.1 Polymerization Characterization of DFDPS, SDFDPS and TBBT

DFDPS+ TBBT +	I.V. dL/gm (NMP 25°C)	Obtained Sulfonation By ¹ H NMR	Ion Exchange Capacity (meq/gm)	
			Calculated	Experimental
20 mol % SDFDPS	1.3	18%	0.81	0.75
30 mol % SDFDPS	1.5	28%	1.17	1.10
40 mol % SDFDPS	1.7	39%	1.51	1.32
50 mol % SDFDPS	2.0	49%	1.83	1.65

Specific interactions in the disulfonated copolymer-PTA composite membranes are extremely important so as to positively influence the dispersion and miscibility of the PTA particles in the copolymer matrix. The complex of PTA particles to the copolymer backbone aids in retaining the water soluble inorganic additive in humidified conditions. The proposed interactions are shown in Figure 5.4.



Figure 5.4 Proposed Specific Interactions Between the Protonated Bridging and Terminal Oxygens on the PTA Molecule and the Sulfonate and Sulfide Moieties on the PATS Copolymer Backbone

The proposed interactions were characterized using FTIR spectroscopy that focused on two frequency ranges. The first range contained the symmetric and asymmetric stretching regions of the SO_3 moieties and the sulfonated aryl rings respectively ($1030\text{-}1100\text{ cm}^{-1}$ and $1170\text{-}1270\text{ cm}^{-1}$) and the second was tungsten-oxygen stretching region incorporating the terminal, corner and edge shared oxygen atoms ($750\text{-}1000\text{ cm}^{-1}$). Figure 5.5 displays the spectral regions of the composite membranes using a representative unsulfonated PATS 00 control homopolymer, PATS 30 and PATS 30 containing 30wt% PTA. All of the FTIR spectra were recorded at $120\text{ }^\circ\text{C}$ after drying the films in vacuum at $100\text{ }^\circ\text{C}$ for 24 hours so as to remove the possibility of dissociated water molecules at lower temperatures affecting the characteristic bands. The region from $1100\text{-}1110\text{ cm}^{-1}$ was assigned to the unsulfonated aryl sulfone moieties, which were unaffected by the incorporation of PTA. The symmetric stretching of SO_3 was observed at 1060 cm^{-1} in pure PATS 30 and shifted to 1070 cm^{-1} for the composite blend thin films. This large shift of the sulfonate band indicated a strong interaction with PTA molecules. The affect of chain architecture on the addition of PTA was also observed from the region $1170\text{-}1270\text{ cm}^{-1}$. The slight red shift in the peak of PATS 30 at 1211 cm^{-1} to 1207

cm^{-1} in the composite membrane was assigned to the symmetric arylene ring stretches that were covalently bound to the complex sulfonate moiety, thereby affecting infrared excitement. A similar shift was observed for the asymmetric sulfonated arylene ring peak at 1235 cm^{-1} . The results indicated that the PTA particles mainly complex with the sulfonic acid groups as opposed to the other backbone functional groups including the sulfone and sulfide moieties.

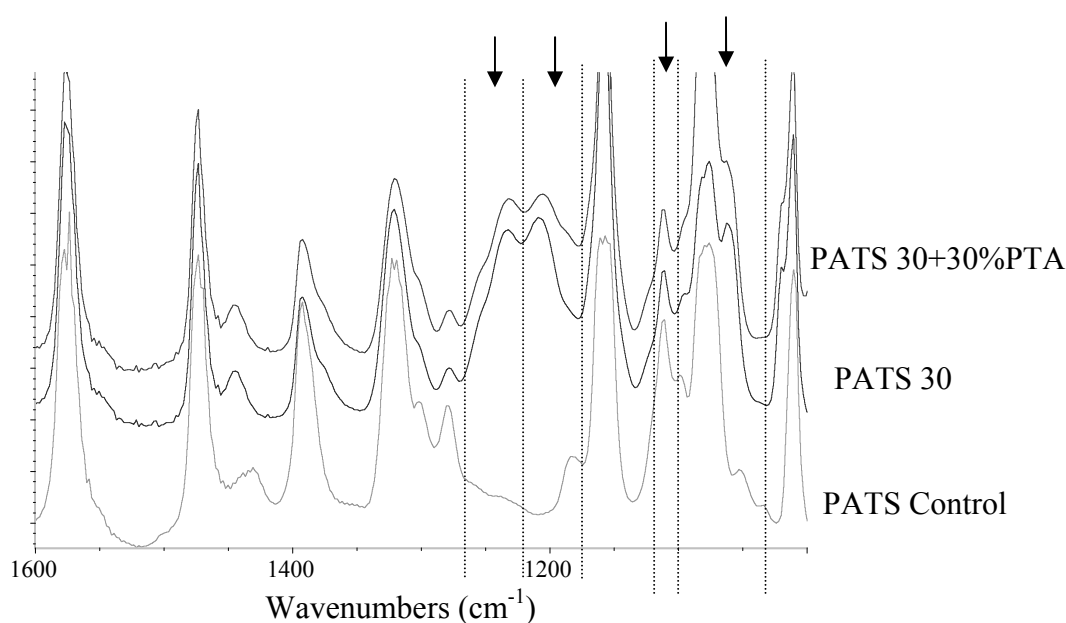


Figure 5.5 Symmetric and Asymmetric Stretching of the SO_3 Moieties and the Sulfonated Aryl Rings on the PATS Copolymer Backbone

The phosphotungstic acid region of the FTIR spectra is shown in Figure 5.6 indicating the vibrational modes of the terminal oxygen atoms ($\text{W}=\text{O}_t$), the central shared oxygen atoms ($\text{W}-\text{O}_c-\text{W}$) and the edge shared oxygen atoms ($\text{W}-\text{O}_e-\text{W}$). The representative PATS 30 spectrum, the PATS 30 + 30wt% PTA spectrum and the pure PTA ($\text{H}_3\text{PW}_{12}\text{O}_{40}\cdot 6\text{H}_2\text{O}$) spectrum indicated strong interactions of the various oxygen

atoms in the PTA molecule. The large shift of the edge shared oxygen atom when cast into the PATS 30 membrane was determined to be from 795 cm^{-1} for the pure PTA to 814 cm^{-1} for the composite membrane representing a change in architecture in the secondary structure of the PTA molecule presumably due to the interactions associated with the edge shared oxygens and the sulfonate group. The chemical shift of the central bridging oxygen atom was also large from 890 cm^{-1} to 896 cm^{-1} indicating good complex formation with the sulfonate groups. The terminal oxygen shift was very slight at 981 cm^{-1} for the partially hydrated PTA molecules and 979 cm^{-1} for the composite membrane. This indicates that the hydrogen bonding and complexation of the terminal oxygen to the hydronium ion was not interrupted and therefore allowed good complex formation with the sulfonate groups while not replacing the hydronium ions in the secondary structure. In other words, the secondary structure of the PTA molecules was not disturbed thereby retaining the state of hydration while still having complex formation with the sulfonate moieties through the central and edge shared oxygen atoms. This is presumed to help retain the water soluble PTA in hydrated environments.

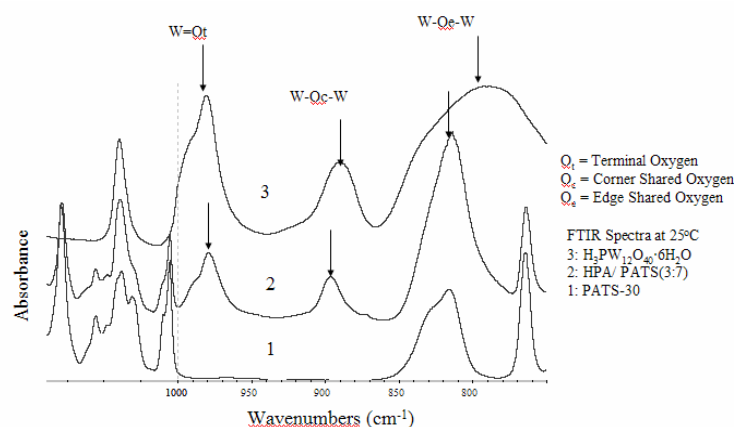


Figure 5.6 Effect of PTA Incorporation on FTIR Band Shifts of PTA Oxygen Atoms

5.3.2 Dehydration of PATS 30 and PATS 30 + 30 wt% PTA Using FTIR

Dynamic dehydration was performed to describe the water retention characteristics of the pure and composite membranes. It was hypothesized that since the hydrated PTA seems to strongly complex with hydronium ions, the water retention at temperatures above the boiling point of water should be enhanced. In turn, the proton conductivity at elevated temperatures and low relative humidities would be increased due to larger amounts of water in the composite membrane compared to the neat copolymer film. Figure 5.7 indicates the dynamic dehydration of PATS 30 and PATS 30 + 30wt% PTA membranes for temperatures ranging from 40-280 °C. The membranes were fully hydrated in liquid water and patted dry before placing in the heating cell. The two plots indicate the hydroxide stretching region of the hydrogen bonded structure for both the neat and composite membranes. For pure PATS 30, broad symmetric stretching and bending bands were observed at 3420 cm^{-1} and 1610 cm^{-1} respectively, which is associated to weak hydrogen bonding with water. It has previously been determined that the OH stretching and bending of bulk water molecules appear at 3650 cm^{-1} and 1590 cm^{-1} .²⁹⁸ If complex formation occurs creating a hydrogen bonded structure to the surrounding environment, the specific FTIR bands would shift toward lower wavenumbers, which is the case for the composite membranes at 3420 and 1610 cm^{-1} .

²⁹⁸ Pereira, M. R. and Yarwood, J. J. *Chem. Soc. Faraday Trans.* 92, 2731, 1996.

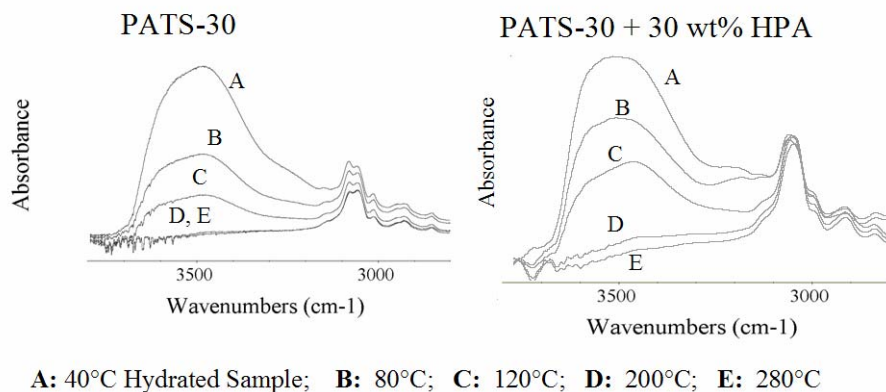


Figure 5.7 Dehydration of Pure PATS-30 and PATS-30 + 30 wt% HPA at Increasing Temperatures

The hydrogen bonding in the pure PATS copolymer was determined to be predominately weak due to the loss of all OH band intensity at 3420 cm^{-1} at temperatures above the boiling point of water ($200\text{ }^{\circ}\text{C}$). This indicated that at temperatures lower than $120\text{ }^{\circ}\text{C}$, the hydrogen bonded water was dominant in the membrane and then disappeared when the temperature reached $200\text{ }^{\circ}\text{C}$. This provided evidence that as the water was removed, the sulfonate groups directly interacted with the main chain sulfone and sulfonate groups without water or hydronium ion bridges. The hydrogen bonding in the PATS 30 + 30 wt% PTA membranes was observed to be different based on higher intensity bands at 3420 cm^{-1} for temperatures in excess of $200\text{ }^{\circ}\text{C}$. When the temperature was raised from $40\text{ }^{\circ}\text{C}$ to $120\text{ }^{\circ}\text{C}$, a large decrease in the band intensity was observed indicating that the weakly hydrogen bonded water species evaporated. As noted in the dehydration process of the composite membranes, the water molecules were retained at much higher temperatures than the pure PATS 30 membranes. Even at $280\text{ }^{\circ}\text{C}$, there is a

small curvature of the OH band in the composite membrane, thereby indicating enhanced water retention.

These FTIR and the previous FTIR results indicated many interesting phenomena that were observed in the composite membrane that was not seen in the pure PATS membrane. The PTA incorporation contained more hydrogen bonded water species at temperatures in excess of 120 °C. This indicated that the water retention in the composite system was enhanced relative to the neat copolymer. These results further deduce the strong specific interactions described previously between the PTA molecules and the sulfonic acid moieties along the polymer backbone. Since specific water transport mechanisms are responsible for proton conductivity, the PTA composite membranes should show higher conductivity values at temperatures in excess of the boiling point of water relative to the pure PATS copolymers.

5.3.3 PTA Dispersion and Morphology of Composite Membranes Using Transmission Electron Microscopy (TEM)

TEM of the composite membranes was performed to understand the morphology and dispersive characteristics of the PTA additive in two PATS copolymers, namely PATS 20 and PATS 40. The density of electrons in the PTA structure was high enough so that no staining was required to observe the PTA particles (30 wt%) dispersed in a PATS copolymer matrix. The thin films were observed to be of uniform thickness at 70 nm. The dispersive characteristics of the PTA particles are shown in Figure 5.8 and indicate two separate magnifications for each composite membrane (note the length scales).

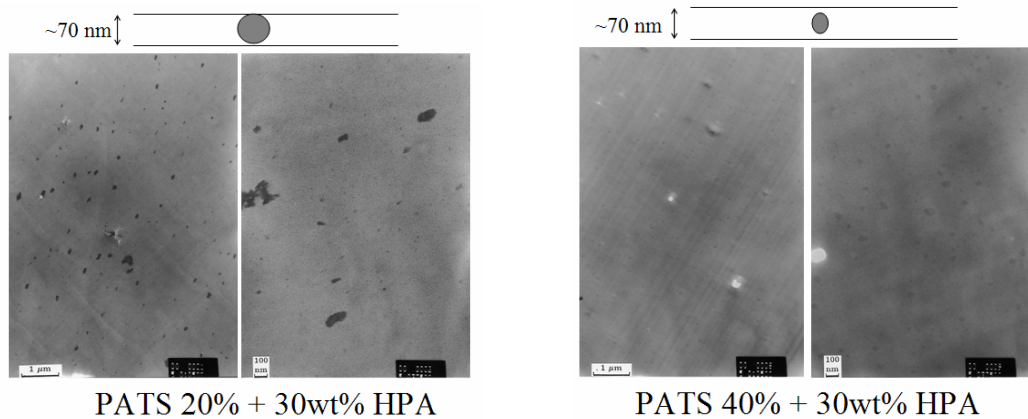


Figure 5.8 Observed Dispersion of PTA Particles in PATS 20 + 30 wt% PTA and PATS 40 + 30 wt% PTA Composite Membranes

The first two images are of a PATS 20 + 30 wt% PTA composite membrane indicating poor dispersion of the PTA particles as determined by the large inorganic phases at both magnifications (~50-200 nm). Large agglomerations were evident in the PATS 20 matrix, thereby suggesting weak dispersive qualities and the possibility of enhancement by addition of more acid groups into the polymer. It was then observed that as the percent of disulfonation increased from PATS 20 to PATS 40 (right two TEM micrographs), the dispersive characteristics increased due to an increase in the number of possible hydrogen bonding sites available in the disulfonated copolymer matrix. The inorganic phases were observed to be dispersed in a better fashion thereby creating smaller, more dispersed structures having dimensions on the order of 5-50 nm. No large agglomerations were observed for the PATS 40 matrix composite. These observations further indicate that the sulfonate moieties are primarily responsible for the specific interactions between the PTA molecules and the copolymer material.

5.3.4 Thermogravimetric Analysis of Composite Membrane, PATS 30 and PATS 00 Control

The thermal stability and the specific interactions of the PTA with the sulfonate moieties were observed using TGA in an air environment. The thermal stability of PTA was excellent showing negligible weight loss from temperature ranges of 50 °C to 800 °C except for the gradual loss of water. Figure 5.9 indicates that the 5% weight loss of the control polymer (PATS 00) containing no sulfonic acid groups was 467°C, while PATS 30 containing 30 mol % sulfonate groups was only 361°C. This reduction in degradation temperature can only be due to the loss of the sulfonate moiety from the disulfonated copolymer backbone since all other factors were held constant. The control homopolymer showed a two step weight loss where the first began around 460 °C and the second began around 600 °C. This first weight loss step was determined to be due to the degradation of the backbone forming cross links and a networked structure. The second weight loss around 600 °C was assumed to be due the carbonization of the resulting structure. The disulfonated copolymer showed similar degradation steps at those temperatures (460 °C and 600 °C), however the onset of the desulfonation reaction was observed to be at 350 °C. When PTA was incorporated into the polymer structure, the 5% weight loss increased from 361 °C for PATS 30 to 390°C for the composite PATS 30, an increase of 29°C. This increase in stability was determined to be due to the specific interactions associated with the PTA and the polymer structure, thereby thermally stabilizing the material, specifically the sulfonate moieties. These results suggest that the composite membranes are stable enough for elevated temperature operation in a fuel cell environment.

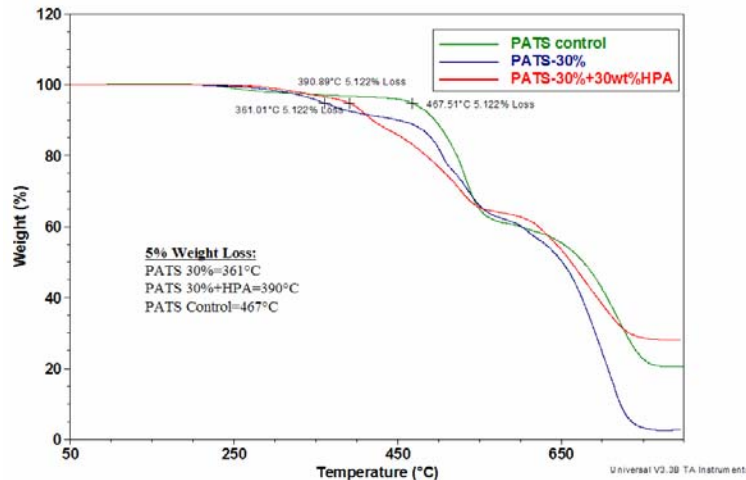


Figure 5.9 Observed Dynamic Weight Loss of PATS 00, PATS 30 and PATS 30 + 30 wt% PTA

5.3.5 Water Uptake of Neat Copolymer Films and Composite Membranes Using Various Acidification Techniques

The water uptake of disulfonated copolymers for use as proton exchange membranes is generally known to play an intense role on proton conductivity and mechanical properties.²⁹⁹ As the water uptake increases, the solvation state of the sulfonate groups also increases, which, in turn, produces high proton conductivity. However, enhanced water uptake produces poor mechanical strength materials. As can be observed in Figure 5.10 that shows water uptake versus mole percent disulfonation, water sorption of the neat PATS films using method 2 acidification obtained the highest water uptake values. The lowest water absorption was observed using the Acid Cast composites that were obtained directly out of the casting trays. The composite films that were reacidified using M1 or M2 indicated water management was enhanced in the

²⁹⁹ Zawodzinski, T. A., Springer, T. E., Davey, J., Jestel, R., Lopez, C., Valeria, J. and Gottsfeld, S. J. *Electrochem. Soc.* 140, 1981, 1993.

composite films relative to the neat PATS films. Interestingly, these results suggested that the PTA in the composite films decreased the overall water sorption. This is interpreted as being due to two different mechanisms. First, the membranes were dried in a vacuum oven after submersion in liquid water where, presumably all the water was removed. However, it is believed that the removal of the hydrogen bonded water molecules in the composite membrane was incomplete due to the strong interactions with the sulfonate and PTA complex. Second, since the number of water absorption sites decreased in the composite membranes due to the strong complex formation of sulfonic acid groups with the PTA molecules, lower water amounts were reversibly absorbed.

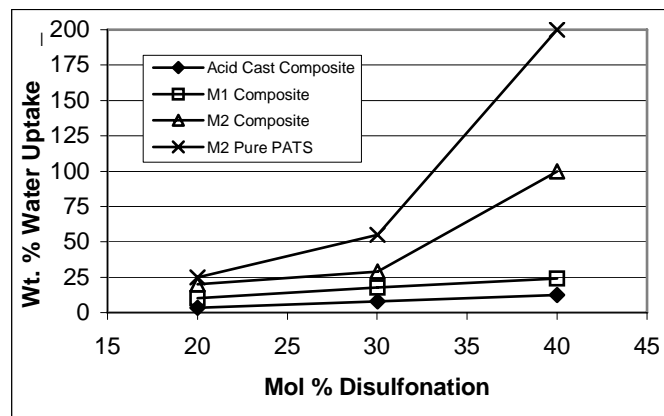


Figure 5.10 Influence of Disulfonation Degree and Acidification Technique on the pure Copolymers and Composite Membranes

5.3.6 Extraction of the PTA in Composite Membranes

Retention of the PTA inorganic particles was presumed to be one of the primary parameters that control chemical properties leading to good conductivity values and durable lifetimes. If low affinity between the PTA and disulfonated copolymers was a

characteristic of the composite membrane, the PTA material, which is water soluble, would be easily extracted from the film in the presence of water. This would undoubtedly decrease the proton conductivity and durability by creating voids and possibly pin-holes in the membrane. Figure 5.11 indicates the extraction of the inorganic filler in the composite membranes that were loaded with 30 weight % PTA. The method 2 reacidification technique extracted the largest amount of PTA and the room temperature extraction of the ‘Acid Cast’ and method 1 films indicated that very little PTA was removed. The rigorous environment at boiling temperatures and the increase in water swelling using M2 acidification were the primary reasons for the loss of PTA molecules during the M2 reacidification technique. At these temperatures, the thermal energy available for PTA dissolution from the complex with the sulfonate moieties was high enough so as to extract the water soluble additive.

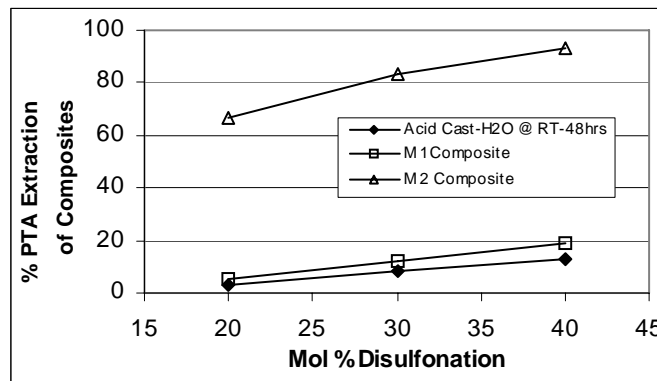


Figure 5.11 Influence of the Degree of Disulfonation and Reacidification Technique on PTA Extraction of Composite Films Using 30 wt% Filled Materials

5.3.7 Proton Conductivity in Liquid Water and at 120 °C in 45% Relative Humidity for Composite Membranes and Pure PATS Copolymers

The proton conductivity was determined at 25 °C and 80 °C in liquid water and at 120 °C in 45 % relative humidity at atmospheric pressure in the apparatus shown in Figure 5.3. By coupling the previous water uptake and extraction data with the conductivity at 25 °C (Figure 5.12), 80 °C (Figure 5.13) and 120°C 45% RH (Figure 5.14), the overall PTA extraction of composite membranes initially containing 30 weight percent PTA was determined to play an important role in the conductivity performance. The membranes that had high amounts of extraction during the reacidification, showed relatively low conductivity values as compared to the membranes with very little HPA extraction. However, comparison of the Acid Cast membrane conductivities to the reacidified conductivity values of the composite membranes suggested that the membrane performance was better when re-exposed to sulfuric acid. Furthermore, the pure PATS membranes acidified by M2 were outperformed by the composite membranes that were acidified by M1 at both 80 °C and 120 °C. Figure 5.12 indicates that the proton conductivity at 25 °C in water was the highest for the entire series of M2 neat copolymer membranes followed closely by the M1 composite materials. The weak performance of the Acid Cast materials at all temperatures was presumably due to the strong complex between the PTA and the sulfonate groups in the copolymer matrix that were formed during the casting process thereby decreasing the number of sites for proton motion. Poor performance of the M2 composite membranes at all temperatures was presumably due to possible voids in the films where the HPA filler was initially located. This would produce non-continuous phases that would prohibit proper proton transport.

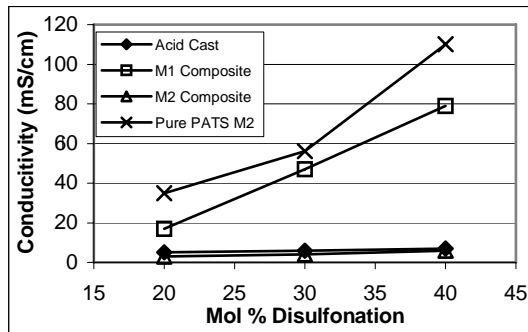


Figure 5.12 Proton Conductivity at 25 °C in Liquid Water at Atmospheric Pressure for M2 Acidified PATS Copolymers and M1 and M2 Acidified Composite Membranes

As shown in Figure 5.13, the conductivity values at 80 °C for the pure and composite membranes increased at all levels of disulfonation relative to the 25 °C values. At this higher temperature, the performance of the M1 composite materials was higher than that of the pure copolymer materials. This suggested that the PTA conductivity was increased at a faster rate as a function of temperature than the pure sulfuric acid conductivity. The activation energy for proton transport using PTA additives presumably decreased, thereby providing enhanced conductivity values at elevated temperatures. When also considering the water uptake values that showed a large decrease in the number of solvent water molecules for the PTA composites, it is suggested that the proton conductivity occurs in a more efficient method in the organic-inorganic composite membranes reacidified using M1.

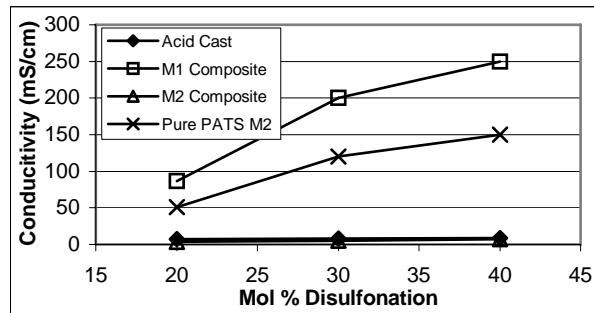


Figure 5.13 Proton Conductivity at 80 °C in Liquid Water at Atmospheric Pressure for M2 Acidified PATS Copolymers and M1 and M2 Acidified Composite Membranes

The plot in Figure 5.14 indicates the conductivity performance at 120 °C in 45% relative humidity under atmospheric pressure. This experiment was meant to imitate a fuel cell environment where humidified gases and low hydration due to atmospheric pressure and high temperatures create rigorous conditions. At all levels of disulfonation, the M1 composite membranes containing an initial charging of 30 weight percent of PTA showed enhanced proton conductivity at temperatures above the boiling point of water where little relative humidity was present. This increase in performance relative to the pure PATS copolymers suggested higher amounts of water retention at temperatures above the boiling point of water than the pure copolymers that would rapidly dehydrate, thereby decreasing proton transport characteristics. Furthermore, it was hypothesized that the PTA-PATS complex acidity was enhanced by the HPA addition resulting in the specific interactions previously observed.

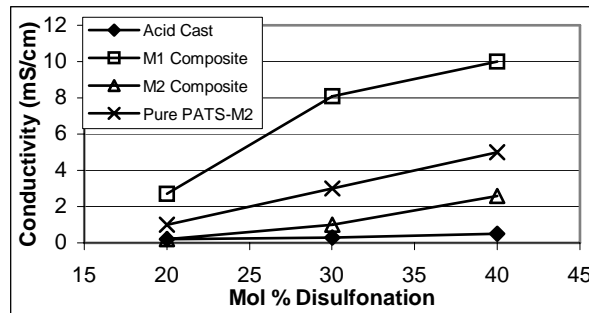


Figure 5.14 Proton Conductivity at 120 °C in 45% Relative Humidity at Atmospheric Pressure for M2 Acidified PATS Copolymers and M1 and M2 Acidified Composite Membranes

5.3.8 Oxidation of PATS 30 to Create Sulfoxide Groups Using Hydrogen Peroxide to Aid in PTA Retention

Chemical oxidation of the sulfide groups to form very polar sulfoxide moieties was conducted so as to create better polar-polar complexes with the PTA molecules, thereby retaining higher amounts of the HPA additive and possibly increase conductivity. FTIR was used to monitor the oxidation of the sulfide groups to sulfoxides and on to sulfones presumably due to hydroxyl or radical attack that occurred in the hydrogen peroxide solutions. The polarity of the three sulfur containing groups was maximized at the sulfoxide stage. The increased polarity of the sulfoxide was expected to retain larger amounts of the PTA additive during extraction experiments. All the samples examined in this oxidation study were PATS 30 solution cast thin films. Figure 5.15 shows the representative spectrum of films that were submersed in water as the control, 3 wt% H₂O₂, 15 wt% H₂O₂ and 30 wt% H₂O₂ in water for 6 hours. The films were then rinsed and dried in vacuum at 100 °C for 24 hours. The sulfide peak in the control PATS 30 sample was determined to be the broad peak from 1025-1075 cm⁻¹. As the percent of

hydrogen peroxide increased from 3-30 weight percent, the intensity of the peak at 1060 cm^{-1} decreased to lower levels indicative of the transformation into the sulfoxide. The peaks of the growing sulfoxide asymmetric and symmetric stretches were observed at 1040 cm^{-1} and 1100 cm^{-1} . Since a large sulfone peak intensity was previously present in the copolymer structure, little change was observed in the sulfone peak at 1145 cm^{-1} .

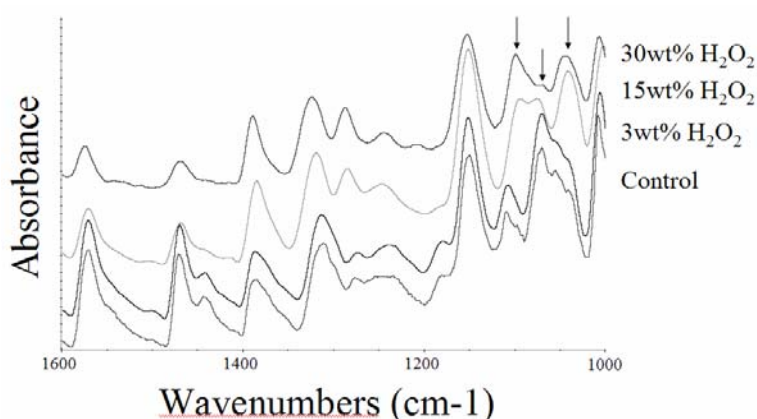


Figure 5.15 FTIR Band Shifts Indicating Sulfoxide and Sulfone Formation Along With Sulfide Degradation

This data suggested successful oxidation; however, chain scission was also proposed. Therefore, intrinsic viscosity studies using NMP as the solvent performed at 25 °C were used to study changes in molecular weight. The control PATS 30 copolymer had an IV of 1.5 dL/g. After only six hours in 30 wt% hydrogen peroxide in water, the intrinsic viscosity was lessened to 0.85 dL/g. The IV of the 15 wt% sample was 1.1 dL/g, where the 3 wt% sample was the highest at 1.41 dL/g. It was concluded that the best control over the oxidation level, while not disrupting the molecular weight, was to use the 3 weight percent hydrogen peroxide solution in water. Figure 5.16 indicates the increase in the sulfoxide peak at 1040 cm^{-1} and then the loss of the peak intensity as time

passed. The times of oxidation were increased to observe the slow increase of sulfoxide groups along the polymer backbone. A separate sample was used for each time interval, thereby allowing precise control over the times of peroxide exposure. The sulfoxide peak at 1040 cm^{-1} was observed to be at a maximum after 24 hours of exposure to 3 wt% hydrogen peroxide. After 24 hours, the sulfoxide peak decreased due to formation of sulfone groups. This indicated that the best candidate for organic-inorganic composites was the sample submersed in 3 wt% of hydrogen peroxide. This sample appeared to contain the highest amounts of the very polar sulfoxide groups.

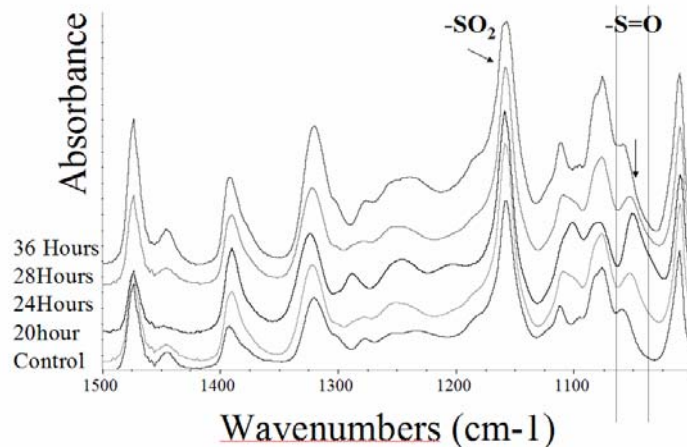


Figure 5.16 FTIR Spectra of Controlled Sulfoxide Formation at Increasing Exposure Times to 3% H₂O₂ in Water

The PATS 30 material that was submersed in 3 wt% hydrogen peroxide was redissolved and mixed with 30 wt% dissolved PTA. The mixtures were allowed to stir overnight to allow proper hydrogen and polar-polar bonding. The material was solution cast and removed from the glass plate after complete drying and weighed. These oxidized materials were termed OX-PATS 30. The composite membranes were then reacidified using either the room temperature acidification technique, M1, or the high

temperature technique, M2, and weighed. The difference in the initial weight and reacidified weight divided by the initial weight was calculated to be the extraction of PTA. When compared to the M1 extraction of the PATS 30 composite at 3.6%, the OX-PATS 30 PTA extraction was found to be almost 50% lower at 1.9%. The comparison in the M2 extraction for PATS 30 was 25 %, where the OX-PATS 30 only lost 17 %. These data indicated that more PTA was being retained in the oxidized PATS copolymers relative to the untreated material during both M1 and M2 extraction experiments.

Comparison of the proton conductivity at 80 °C and 120 °C at 45% RH was determined using the M1 oxidized composite membranes to maximize the performance based on the previous studies. The conductivity of the PATS 30 composite membrane at 80 °C in water was 200 mS/cm, where the ionic conductivity of the OX-PATS 30 composite membrane was lower at 132 mS/cm. A similar trend was observed at 120 °C in 45% RH where the PATS 30 composite material showed proton conductivities of 8 mS/cm and the OX-PATS 30 composite gave only 2 mS/cm. The decrease in the conductivity at both temperatures, even though the PTA retention was increased in the oxidized sample, was thought to be due to the extremely strong interactions and complex formation of the PTA, sulfonate and sulfoxide groups. The enhanced polarity of the copolymer backbone was found to be detrimental to the overall proton conductivity because of the increase in attraction to the acid groups thereby removing them from proton conduction mechanisms. However, a larger retention of the PTA particles using polar sulfoxide groups still suggested that conditions could be optimized for sulfoxide or even phosphine oxide groups to retain the water soluble additive but still produce similar proton conductivities in both water saturated and unsaturated environments.

5.3.9 Hydrogen/Air Fuel Cell Performance Using Platinum Loadings of 0.2 mg/cm²

Membrane electrode assemblies were made using prefabricated electrodes containing Nafion 1100 ionomer. The Pt loadings and the weight percent Nafion ionomer in the anode and cathode electrodes were held constant at 0.2 mg/cm² and 28.5% respectively. The 2 mil (50 micron) thick membranes were hot pressed at 210 °C using 3000 psi of pressure for eight minutes. The membrane electrode assemblies were then assembled into a single cell having 5 cm² of active catalyst area. Conditioning and wet-up of the cell was performed at 0.5V until the current density leveled, typically around 5 hours. Two sets of voltage- current-resistance curves were performed at 80 °C in 100 % RH and 20 psig and at 120 °C in 50% RH and 20 psig.

The fuel cell performance of both PATS 30 and PATS 30 composite membrane electrode assemblies at 80 °C, 100% RH and 20 psig are shown in Figure 5.17. These sets of experiments were designed to mimic the actual fuel cell conditions of stationary power applications used for private residence and business applications. There are three different areas of these curves to aid in the understanding of the MEA. The first area is between 1 and 0.8 volts. This area indicates the performance of the electrode area of the MEA. The PATS 30 material shows a current density of 100 mA/cm² at 0.8 volts while the composite membrane shows a decreased current density of only 25 mA/cm². This trend is indicative of two phenomena. The first is the hydrogen and air crossover that occurs with membranes that have pinholes and the second possibility is that the PTA particles or copolymer material complexes with the Pt active sites thereby removing them from the overall catalytic mechanism. The previous is most likely the case for these

materials since the equilibration time at 80 °C and 100% RH could have removed large amounts of PTA particles causing pinholes to form and hydrogen crossover to occur. The hydrogen that leaks through the membrane then reacts at the cathode and causes a back flux of protons that ultimately work against the system. The second area of the curve to identify was the membrane or ohmic region between 0.8 volts and 0.5 volts. This region of the voltage current curve has a direct relationship to the conductivity of the copolymer membrane thereby allowing direct comparison of the membranes alone. The ohmic region performance of the composite membrane at 80 °C was found to be much lower than that of the pure PATS 30 material. This could be due to loss of the inorganic, water insoluble PTA additive during break-in and equilibration. The previous conductivity data suggested that as more of the PTA was extracted, the proton transport was hindered by voids and pores that were produced. Therefore, by using these conductivity observations and comparing them to the present fuel cell performance, it was suggested that increased amounts of the additive were washed from the composite membranes, thus decreasing the ohmic region performance that is directly related to the specific proton conductivity of the copolymer membrane. Furthermore, PTA that did not wash away must have formed a very strong complex with the functional groups in the membrane. If this is correct, the conductive functional sites of the PATS 30 composite membrane would be lower than that of the pure PATS 30 membrane, thereby decreasing performance. The third region of the voltage-current curve was termed the mass transport region where the performance is restricted by water transport out of the cell. When the amount of water that is produced at the cathode is greater than the amount that is removed by the humidified air stream, flooding occurs which in turn drops the

diffusion characteristics that are needed for efficient performance. The water buildup at the cathode hinders oxygen diffusion that is needed for catalysis at the platinum sites. For the present study, the voltage was controlled to remove any possibility for cell flooding giving true performance structure-property relationships.

Another measure of fuel cell performance depends on the high frequency resistance (HFR) of the membrane electrode assembly. The HFR is a measure of how well the electrodes were adhered to the membrane. The lower the HFR, the better the interfacial properties are between the electrode and membrane. If the HFR values are too high, the interfacial resistance between the membrane and electrode create unfavorable resistances for proton transport. When the HFR is low ($\sim 0.1 \text{ ohm}\cdot\text{cm}^2$ or lower), the interfacial resistance does not interfere with the overall performance and indicates good electrode adhesion and compatibility. The HFR of the PATS 30 MEA at $80 \text{ }^\circ\text{C}$ was found to be $0.094 \text{ ohm}\cdot\text{cm}^2$ while the HFR of the PATS 30 composite MEA was found to be $0.098 \text{ ohm}\cdot\text{cm}^2$. These data indicated that the compatibility and adhesion between the pure copolymer and the electrodes was better than that of the composite membrane. This reaffirms the observations that possible voids and pinholes were present in the composite material.

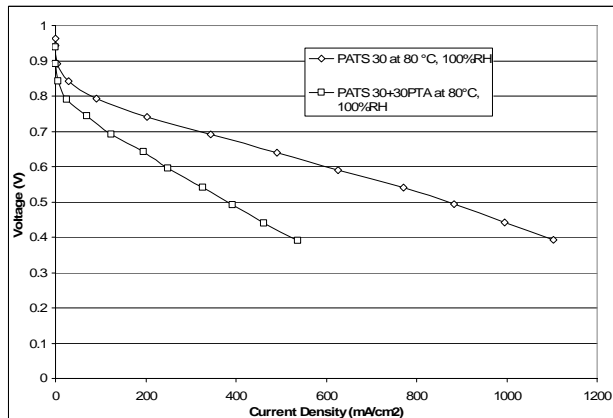


Figure 5.17 Voltage-Current Performance Curve for PATS 30 and PATS 30 + 30 wt% PTA at 80 °C, 100%RH and 20 psig

The performance of the pure PATS 30 MEA and the composite PATS 30 MEA at 120 °C, 45% RH and 20 psig was plotted in Figure 5.18. These sets of experiments were used to assess actual fuel cell conditions that have been outlined by The Department of Energy for automotive applications. Similar trends were observed relative to the 80 °C data. The performance in the electrode active area of the curves indicated a loss in performance of the composite material presumably due to pinhole formation during equilibration and break-in. The hydrogen cross over was higher in the composite materials relative to the pure PATS 30 materials. The ohmic region of the curves showed that the composite material performed closer to the pure copolymer MEA when compared to the 80 °C performance data. This indicated that although PTA was leached from the composite MEA, the water retention of the remaining PTA molecules allowed closer overall performance when compared to the pure copolymer MEA. It was suggested that if the electrode activity was equal to the pure PATS 30 MEA, the performance of the composite at this high temperature and low humidity would be shifted to values above that of the pure PATS 30 MEA. The HFR value of the PATS 30 MEA

was $3.0 \text{ ohm}\cdot\text{cm}^2$ while the HFR of the composite membrane was $1.1 \text{ ohm}\cdot\text{cm}^2$. This suggested that the interfacial resistance for the composite membrane that had a lower water swelling was much better than that of the PATS 30 material that swelled twice as much as the composite membrane. The lower water swelling allows the membrane to swell at a similar amount as that of the Nafion ionomer in the electrode (~25 weight percent). The similar water swelling characteristics promotes better adhesion and lower interfacial resistances so that the protons move in an efficient manner.

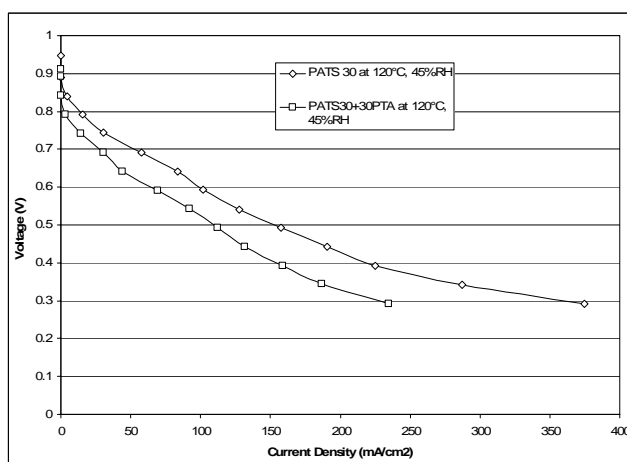


Figure 5.18 Voltage-Current Performance Curve for PATS 30 and PATS 30 + 30 wt% PTA at 120 °C, 50%RH and 20 psig

5.4 Conclusions

Specific characteristics and interactions of the PTA-PATS composite membranes was thoroughly probed using FTIR, TGA, TEM, water uptake, conductivity and fuel cell analyses. Polymer synthesis using highly reactive difluoro monomers created a family of poly(arylene thioether sulfone) copolymers having various levels of disulfonation ranging

from 0-40 mole percent. When solution mixed with PTA, composite membranes were found to be tough and transparent indicating good dispersion of the PTA molecules. The specific interactions were first observed using FTIR experiments. The data indicated strong interaction and complex formation occurring at the sulfonate on the copolymer backbone and the bridging oxygen atoms on the PTA molecules. FTIR band shifts were observed for the sulfonate moieties and the oxygen moieties in the copolymer and PTA molecules respectively. The dehydration nature of both the pure PATS 30 copolymer and the PATS 30 composite material was determined using dynamic FTIR experiments in a heated ceramic cell. It was concluded that the water retention characteristics of the composite film was enhanced due to the specific interactions with the polymer backbone and the secondary hydrated structure of the PTA molecule. The dispersive characteristics of the PTA molecules in the PATS matrix were probed using transmission electron microscopy. The images indicated that the PATS 20 material did not disperse the PTA particles as well as the PATS 40 material, thereby suggesting that the sulfonate moieties were primarily responsible for PTA dispersion and concentration uniformity. Larger agglomerations were evident when using PATS 20 material as the matrix while smaller, well dispersed phases were observed using PATS 40 copolymer. Thermogravimetric analysis indicated an enhancement in the thermal stability of the composite membrane. The 5% weight loss increased from 361 °C for pure PATS 30 copolymer to 390 °C for the composite PATS 30 material. This is indicative of strong interactions between the sulfonate moiety and the extremely stable inorganic PTA molecule. The composite complex aided in stabilizing the sulfonate group thereby increasing the thermal stability by 29 °C. The water uptake data showed further evidence of the specific interactions.

The composite membranes showed lower water uptake relative to the pure copolymer membranes suggesting better water management and smaller dimensional swelling. The materials with the highest water sorption were found to be the pure copolymers that were acidified by M2. The M1 composite membranes showed only fractional amounts of water sorption when compared to the pure copolymers. It was concluded that the specific interactions of the PTA particles with the sulfonate groups on the copolymer backbone removed the water sorption sites from the overall mechanism thus not absorbing extreme amounts of water. Extraction of the PTA particles during the reacidification was calculated with respect to the original amount of PTA molecules incorporated into the material. Thirty weight percent of PTA was used for all composite membranes. It was noted that the high temperature and harsh conditions of the M2 reacidification technique extracted most of the PTA particle. It was concluded that the specific interactions between the PTA and sulfonate groups were lost in this high energy environment thereby extracting the water soluble molecules. The extraction of the M1 composite membranes indicated very little loss of the PTA material that was possibly due to the surface particle removal. Proton conductivity was determined at 25 °C and 80 °C in water and at 120 °C in 45% relative humidity. The conductivity at 25 °C was dominated by the M2 pure PATS series of copolymers. The 80 °C and 120 °C conductivity was dominated by the composite membranes reacidified using M1. This enhancement of conductivity at elevated temperatures was presumably due to the greater water retention and increase in acidity of the composite membranes. Oxidation of PATS 30 to create sulfoxide groups using hydrogen peroxide to aid in PTA retention determined that an increase in retention was possible. However, a loss of conductivity was observed for the OX-PATS 30

composite material presumably due to the increase in polarity and in turn the increase in the affinity for PTA. The increased affinity allowed the PTA to complex with the copolymer strongly enough so as to remove even more acid sites from the conduction mechanism. Hydrogen-air fuel cell performance at both 80 °C and 120 °C was performed on a pure PATS 30 MEA and a PATS 30 composite MEA containing 30 weight percent PTA. The voltage-current curve at 80 °C indicated possible pinhole formation during equilibration that was due to the extraction of PTA particles. The ohmic region of the composite curve suggested lower conductivity which was determined to be due to loss of PTA particles and an increase in membrane voids. The HFR data suggested possible interfacial adhesion problems in the composite MEA. It was concluded that the data reaffirmed the hypothesis that PTA particles were abstracted creating voids and increasing the interfacial resistance between the membrane and electrodes. The 120 °C fuel cell data obtained at 50% relative humidity indicated that the ohmic region of the curve more closely related the pure copolymer performance. Therefore, it was presumed that if the composite material would not have lost the PTA particles thereby creating pinholes, the entire curve would be shifted up to values above that of the pure copolymer. The HFR was found to be dramatically lower for the composite membrane relative to the copolymer MEA. This is indicative of the lower water swelling and better interfacial characteristics that go along with similar dimensional changes when hydrated for the membrane and electrodes. Future research should include synthesizing highly polar phosphine oxide containing disulfonated copolymers so as to increase the affinity for the PTA molecules thereby increasing particle retention in water environments even at high temperatures. A series of

copolymers containing increasing amounts of phosphine oxide groups will be used to determine the optimal amount of chain polarity so as to retain as much PTA as possible yet still allowing free acid sites for proton transport mechanisms.

Acknowledgements

The authors would like to thank the Department of Energy and United Technologies Corporation for funding under contract # sub-56844-FMIJOBDOE-99241. Further appreciation is extended to OMNOVA Solutions for their generous fellowship that supported this work.

CHAPTER 6

DIRECTLY COPOLYMERIZED POLY(ARYLENE SULFIDE SULFONE) AND POLY(ARYLENE ETHER SULFONE) DISULFONATED COPOLYMERS FOR USE IN IONIC POLYMER TRANSDUCERS

K. B. Wiles^a, B. J. Akle^b, D. J. Leo^b and J. E. McGrath^a

^a Chemistry Department and Macromolecules and Interfaces Institute, Virginia Tech,
Blacksburg, VA 24061-0212

^b Center for Intelligent Material Systems and Structures, Mechanical Engineering
Department, Virginia Tech, Blacksburg, VA 24061-0261

Abstract

Polymeric electromechanical transducers were based on an ion-exchange membrane between two conductive metal layer electrodes. Imposed deformations and small electric fields allowed both sensing and actuation applications. Soft actuator materials produced large bending displacements when only a small voltage was applied across the membrane electrode assembly. Charge motion from one pole to the other pole

produced electromechanical coupling effects in the ionic materials through the electric double layer. By increasing the surface area of the electrodes, thereby increasing the capacitance, it was shown that the motion of charges and actuator performance increases, thus indicating a strong correlation between the capacitance and charge motion/performance. Manipulation of the morphology of the electrodes by enhancing the capacitance and effective interfacial area of the conductive electrodes produced major effects on performance and transduction. Transducer actuation/performance at lower frequencies was enhanced by employing a novel electrode fabrication technique based on RuO₂. At higher frequencies, mass transport and interfacial resistance appeared to play pivotal roles in actuator performance.

Keywords: electromechanical transducer, poly(arylene ether sulfone), poly(arylene thioether sulfone), Nafion, actuator, sensor, capacitor, transducer, electric double layer

6.1 Introduction

Interest in polymeric actuators, sensors and super capacitors has increased dramatically over the past few years because of their diverse applications that include artificial muscles, shear flow sensing and charge carrying species for electrical applications. Ionic polymer electromechanical transducers have historically been based on the low modulus Nafion[®] materials. These transducers contain the ion-exchange membrane having conductive metal electrodes plated to the outer surfaces (Figure 6.1). Electromechanical coupling occurs under the submission of an electric field where physical deformations of the material produce actuation and sensing.³⁰⁰ Relative to piezoelectric materials, which have less than 1% strain and operate at 2000 Volts, polymer transducers produce a higher strain output at greater than 1%, lower voltage operation at 1-4 Volts and high sensitivity when used in charge-sensing mode.

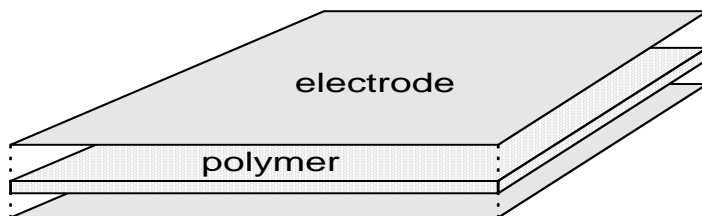


Figure 6.1. Conductive Metal Electrodes Plated on an Ion-Exchange Membrane

³⁰⁰ Oguro, K., Fujiwara, N., Asaka, K., Onishi, K. and Sewa, S. *Proceedings of International Society for Optical Engineering (SPIE)*, Vol. 3669, 63-71, 1999.

Polyelectrolyte membranes typically consist of ion containing pendent groups that are covalently bound to the polymer backbone. These pendent moieties produce phase separation and charge aggregation that allows for selective ion-exchange through ion-hopping and/or ion-host transportation. The hydrophilic clusters/channels of the ion containing groups allow for transport and the hydrophobic backbones allow for tough and ductile physical properties. Nafion and other alternative ion exchange membranes consist of covalently bound sulfonate moieties (anions) and very labile cations, typically protons. Therefore, the selectivity of the materials can be tailored to improve cation transport (e. g. H^+ , Li^+ , Na^+) while the anions are fixed.

Soft actuator materials based on ionic polymer transducers can produce large bending displacements when only a small voltage is applied across the membrane electrode assembly. The motion of charges from one pole to the other is produced by the electromechanical coupling effects in the ionic materials. By increasing the surface area of the electrodes, thereby increasing the capacitance, it has been recently shown that the motion of charges and actuator performance increases, thus indicating a strong correlation between the capacitance and charge motion/performance.³⁰¹ The large capacitance in these ionomeric materials is mainly due to the electric double layer that is formed by the electrode and mobile ions.³⁰²

Smart material applications include actuators, sensors and dampers to only name a few. These types of materials can adapt to changes in physical environments that include

³⁰¹ Akle, B. J., Hickner, M. A., McGrath, J. E. and Leo, D. J., "Electroactive Polymers Based on Novel Ionomers," in *Proceedings of 2003 ASME International Mechanical Engineering Congress & Exposition*, 2003.

³⁰² Park, K. W., Ahn, H. J. and Sung, Y. E., "All-Solid-State Supercapacitor Using a Nafion Polymer Membrane and Its Hybridization with Direct methanol Fuel Cell," *Journal of Power Sources*, 2002, 109, 500-506.

varied electrical charge, magnetic polarity, humidity and temperatures.

Electromechanical transducers are becoming more important to both materials scientists and mechanical engineers. Tailoring material properties to best fit the criteria for enhanced physical performance has been the major thrust of research. Various materials have been studied that show electromechanical coupling effects such as piezo-polymers, piezo-metals, piezo-ceramics, dielectric elastomers, shape memory polymers and alloys, conducting polymers and ionic polymers.

The need for large displacements and low voltage operating transducers is becoming more apparent when compared to the state of the art leading piezo materials. Piezo materials produce large forces but provide only micron-scale displacements. The industry has overcome some of the strain barriers by stacking the piezo materials and adding mechanical amplification devices. However, these techniques decrease energy densities where the materials still need very high voltages. Larger displacement actuators based on ionomers can be enhanced by various synthetic techniques on the molecular level which can allow high power densities and lightweight devices. Furthermore, biocompatibility and low voltages allow them to be potential candidates for artificial muscles and wearable sensors.

Three different ionomeric materials were used in the present study. The ion-containing polymers were poly(arylene thioether sulfone) and poly(arylene ether sulfone) disulfonated copolymers and Nafion. The two former copolymer materials were first developed as alternatives for use in proton exchange membrane fuel cells, where Nafion is now almost exclusively used as the base material. Synthetic variations with the starting monomers during the copolymerization process afforded two systematic series of

materials, namely poly(arylene thioether sulfone) and poly(arylene ether sulfone) termed PATS and BPSH, respectively. These materials were first characterized by the state of the art impregnation-reduction electrode process relative to Nafion. After careful analysis, novel electrode techniques based on proton exchange membrane fuel cell technology was explored. Manipulation of the morphology of the electrodes by enhancing the capacitance and effective interfacial area of the conductive electrodes afforded major effects on performance and transduction. Therefore, this research employed a novel electrode technique that not only increases performance, but increases the capacitance and interfacial area of the active conductive electrodes. The current state-of-the-art electrode technique employs an impregnation-reduction method that uses a platinum salt solution, PtNH_3Cl_2 , that must first diffuse into the ionic membrane and then be reduced by sodium borohydrate, NaBH_4 , to form Pt^0 .³⁰³ However, a novel method which is discussed herein employed a membrane electrode assembly (MEA) technique currently used in proton exchange membrane fuel cells. This new technique allows various metal powders, such as RuO_4 , Pt/C, or Pt, to be incorporated into the electrodes by mixing with dispersions of ionic copolymeric materials. By first painting decals, and then hot pressing the decals to the membrane, various electrode morphologies were produced.

³⁰³ Kim, K. J. and Shahinpoor, M., "Ionic Polymer-Metal Composites : Ii. Manufacturing Techniques," *Smart Materials and Structures*, 2003, 12, 65-79.

6.2 Experimental

6.2.1 Copolymer Synthesis

Three different membrane ionomers were used in this study, namely disulfonated poly(arylene ether sulfone) and disulfonated poly(arylene thioether sulfone) random copolymers and Nafion[®] 117. The two novel ion-containing polymeric materials were disulfonated poly(arylene thioether sulfone), referred to as 'PATS' and poly(arylene ether sulfone), referred to as BPSH. They were synthesized^{304,305} by directly copolymerizing disulfonated monomer using nucleophilic aromatic substitution reactions of activated dihalides and dithiol or di-alcohol containing monomers. Various ratios of disulfonated monomer to unsulfonated monomer produced two families of copolymers having the structures shown in Figure 6.2. PATS was synthesized using 4,4'-thiobisbenzene thiol as the nucleophile while BPSH employed 4,4'-biphenol. The PATS-XX and BPSH-XX acronym numbers indicate molar percentages of randomly copolymerized disulfonated repeat units. For example, PATS-30 indicates the copolymer architecture contains 30 mole% of hydrophilic disulfonated repeat units and 70 mole% of unsulfonated hydrophobic repeat units.

³⁰⁴ Wiles, K.B., Wang, F. and McGrath, J.E., 'Directly Copolymerized Poly(arylene sulfide sulfone) Disulfonated Copolymers for PEM-Based Fuel Cell Systems I: Synthesis and Characterization,' *J. of Polym. Sci.: Part A: Polym. Chem.*, Accepted, 2005.

³⁰⁵ Wiles, K. B., Bhanu, V. A., Wang, F. and McGrath, J. E. *Polymer Preprints* 43(2), 993-994, 2002.

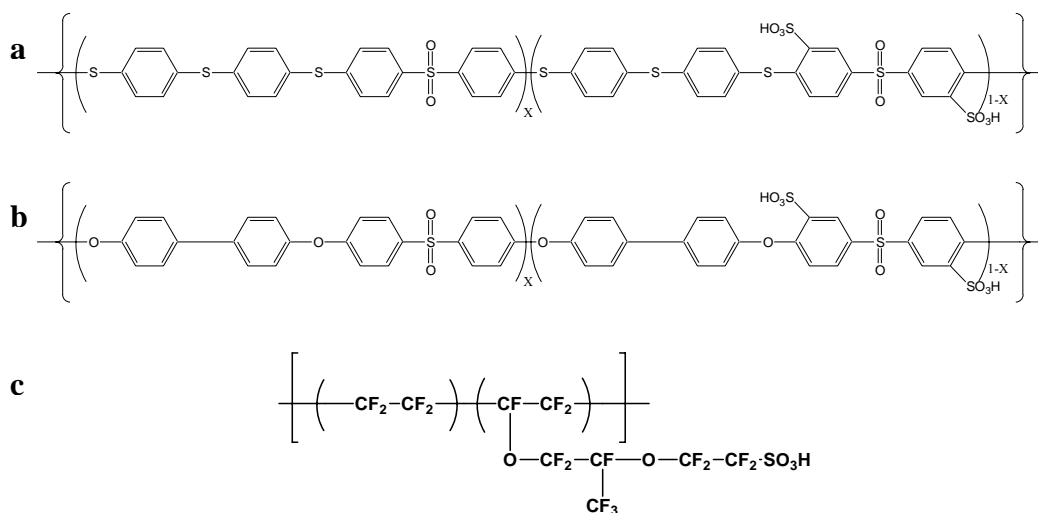


Figure 6.2 (a) Disulfonated PATS-XX, (b) Disulfonated BPSH-XX and (c) Nafion 117 Copolymer Structures

6.2.2 Membrane Preparation

Redissolving the fibrous copolymer in N,N-dimethylacetamide (Burdick and Jackson), filtering the solution through a 0.45 μm TeflonTM syringe filter and directly casting the solution into an aluminum-casting tray prepared tough and ductile potassium salt films. The aluminum tray had sidewalls thereby allowing precise control of membrane thickness to produce 7 mil membranes (7 mils \sim 178 μm thick). The copolymer solutions were dried in a vacuum oven in a nitrogen atmosphere at 50 $^{\circ}\text{C}$ for 4 hours, 80 $^{\circ}\text{C}$ for 4 hours, 100 $^{\circ}\text{C}$ for 12 hours and 120 $^{\circ}\text{C}$ for 4 hours. Nafion 117 obtained from Aldrich was 1100 equivalent weight (meq/g) and 7 mils thick.

6.2.3 Impregnation-Reduction Electrodes

The current electrode standard in electromechanical applications uses an impregnation-reduction process.³⁰⁶ The membranes were first submersed in a solution of a water soluble platinum based salt (0.01M PtNH₃Cl₂) in order to imbibe a reducible metal molecule (Pt²⁺). The metal salt was then reduced on the surface of the membrane using a reducing agent such as sodium borohydride (NaBH₄). Control of platinum metal amounts penetrating from the surface of the membrane was accomplished by tailoring the concentration of the reducing agent to allow full optimization. The concentration of NaBH₄ in water was initially a mixture of 0.05 weight percent. At thirty minute intervals, the concentration was increased by 0.05 wt %. The number of iterations of immersion in platinum salt and then immersion in the reducing agent was held constant through the study at 6 platinum layers. The final step in the impregnation-reduction electrode process was to increase the surface electrical conductivity by electroplating gold onto the surface of the transducer. After impregnation and reduction, the membrane can be put into many possible cation forms by immersion in 1.0 M solutions in water. The current study used sodium hydroxide, lithium hydroxide or sulfuric acid to tailor the cation in the membrane to either sodium (Na⁺), lithium (Li⁺) or hydrogen (H⁺).

³⁰⁶ Kim, K. J. and Shahinpoor, M., "Ionic Polymer-Metal Composites : Ii. Manufacturing Techniques," *Smart Materials and Structures*, 2003, 12, 65-79.

6.2.4 Direct Electrode Assembly Technique Based on Hot Pressed Decals

This novel method of adhesively binding electrodes to thin films allows at least two specific advantages over impregnation-reduction electrodes. First, the metal or alloy in the electrode can be varied by using prefabricated and fully reduced metals in the electrode ink thereby removing the dependence on soluble metal salts and the harsh reduction process of the salts to form metals. Second, the metal-polymer interface surface area can be tailored to produce variations in capacitance that is directly related to the electrodes ability to hold charge. Metal loadings were held constant for all samples at 0.2 mg/cm^2 using either 20%Pt on Vulcan carbon black, ruthenium dioxide or platinum black. The weight percent of the ionomer in the electrode was also held constant at 28.5wt% N1100 in both anode and cathode electrodes. Catalyst inks contained Nafion (5% dispersion in alcohols), Glycerol and the proper metal powder. The formulations obtained a 2.5:1 weight ratio of metal to Nafion. The ink was stirred for at least two hours and sonicated throughout for 60 seconds at a time to promote an even dispersion of the metal particles. Electrode decals were fabricated using Teflon reinforced with glass fiber backing layers. The electrode ink was painted layer-by-layer onto the decals using a high quality #4 camel hair brush. Uniform electrodes were dried after every coat of ink at $130 \text{ }^\circ\text{C}$ for ten minutes. After the correct loadings were obtained by calculating the difference between the decal backing layer and the electrode decal, the prefabricated electrodes were dried overnight at $130 \text{ }^\circ\text{C}$ to remove most of the residual glycerol. Membrane electrode assemblies (MEAs) were produced by placing a membrane between two electrode decals and hot pressing at $210 \text{ }^\circ\text{C}$ and 3000 psi for a total of 8 minutes. The MEAs then underwent gold electroplating and impregnation reduction to obtain

enhanced surface electrical conductivity. As in the previous method, the cation in the membrane was then exchanged with either Na^+ , Li^+ or H^+ .

6.2.5 Sample Preparation and Mounting

After proper electrode fabrication, test samples were cut into 30x5 mm rectangles. The polymers were clamped between two electrodes mounted on a testing stand. The ratio of the width to length of MEA protrusion from the mounting electrodes was held constant at 1:5. The thickness of the MEA varied slightly from 0.13-0.20 mm, however, the calculations to determine performance accounts for variations in thickness, width and length.

6.2.6 Measurements of Electromechanical Activity

Transducer characterization was performed using three different experimental techniques: maximum deflection, block force and sensing tests. The maximum deflection experiments employed an apparatus similar to the one pictured in Figure 6.3. This experiment determined the free displacement of the actuator by allowing the tip to move freely from side to side while the base was clamped between two working electrodes that applied a potential. The potential was either stepped, meaning the voltage was held constant, to provide a one sided displacement or the poles were sigmoidally changed from positive to negative to promote a flapping motion. The movement was measured by a laser vibrometer. The strain and displacement were determined using the

following equation where D is the measured tip displacement as determined from the laser vibrometer, T is the average film thickness of the membrane electrode assembly and L is free length of the material:

$$Strain(\%) = \frac{D * T}{L^2}$$

These calculations assume that the actuator bending motion was at a constant curvature and was tested in the cantilever beam configuration. The resonance frequency, which determines the maximum attainable strain at a specific frequency, was also obtainable using this apparatus; however, the resonance frequency was a function of the physical material properties such as modulus, thickness and weight.

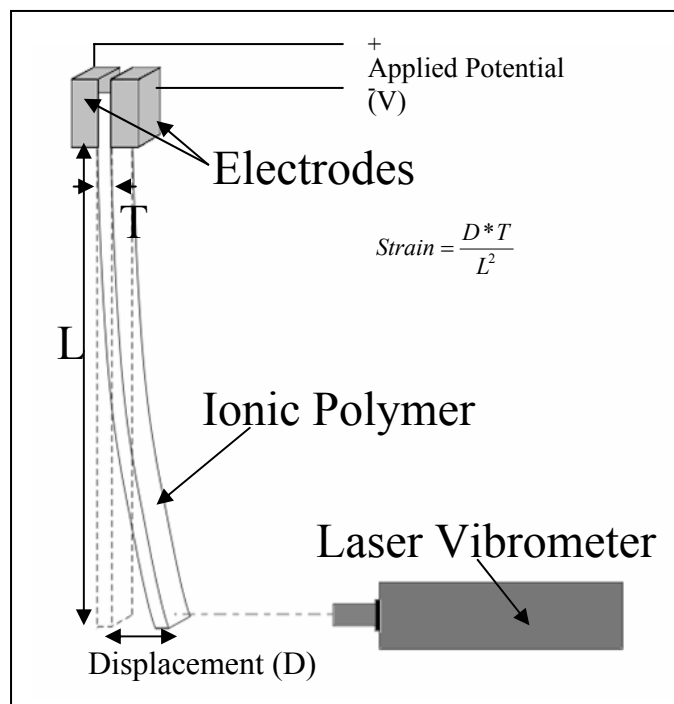


Figure 6.3 Free Displacement Experimental Apparatus

The blocked force test, as shown in Figure 6.4, was used to characterize the maximum force that an actuator could generate due to an applied voltage. This technique was similar to the maximum displacement experiment, although the tip was not allowed to move; rather it was blocked by a load cell that measured the maximum attainable force that was produced at the tip of the cantilever specimen. The blocked force and displacement tests determined the electrical impedance by measuring the actuation current and voltage flows into the material. Both of these tests were normalized to account for any variations in the geometry of the samples.

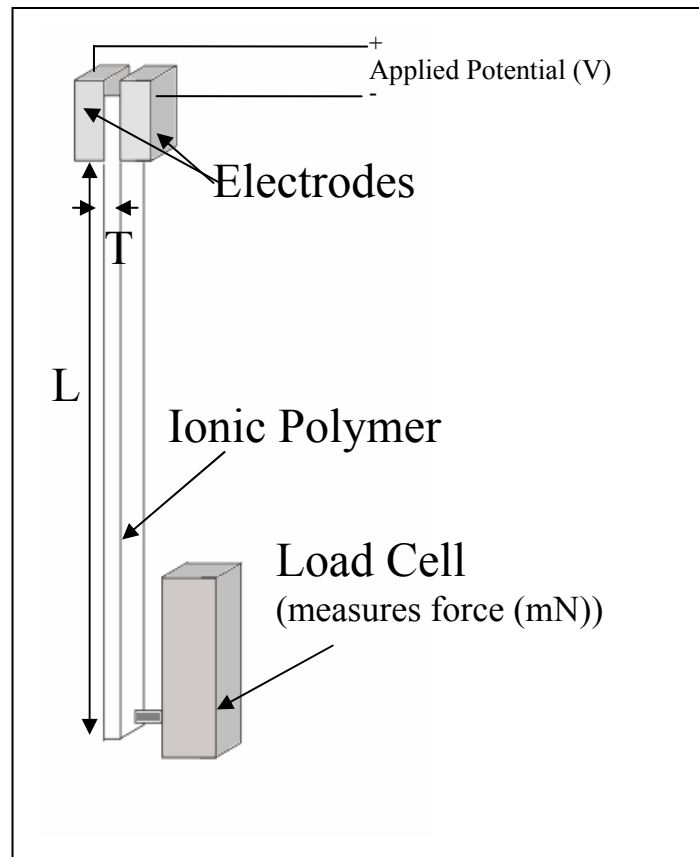


Figure 6.4 Blocked Force Experimental Apparatus

The capacitance per unit area was calculated using the measured electrical impedance of the material, which assumed that the capacitance was in a series with a resistor. The following equation was used where C is the capacitance, L_t is the total length of the membrane electrode assembly in cm, W is the width in cm, $\text{Im}(Z)$ is the imaginary part of the impedance and ω is the frequency in rad/s:

$$C = \frac{10^3}{L_t * W * \text{Im}(Z) * \omega} \left(\frac{mF}{cm^2} \right)$$

The sensing test employed the experimental apparatus shown in Figure 6.5. The external shaker clamped one end of the actuator and mechanically displaced it while the other end was blocked with a load cell. By dividing the measured force by the mechanical displacement of the sample, the measured stiffness of the membrane electrode assembly was calculated. The amount of current that was produced by mechanically displacing the material was a measure of the sensing ability of the specific ionic polymer. The sensitivity was calculated by dividing the sensing current by the velocity of displacement.

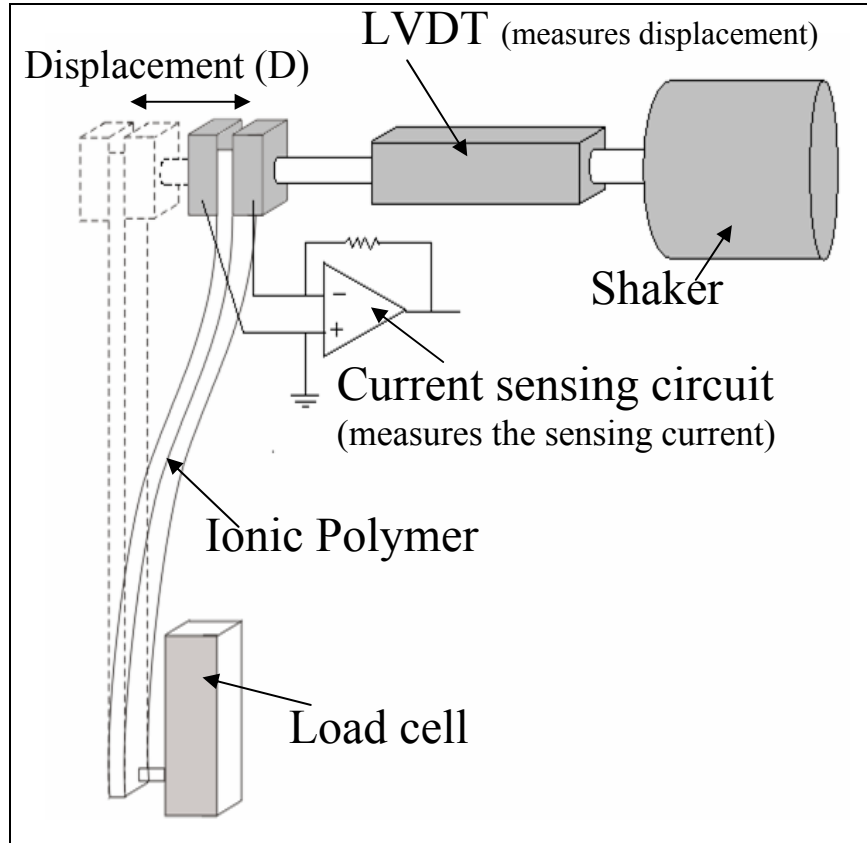


Figure 6.5 Sensing and Modulus Experimental Apparatus

The modulus of elasticity of the material was calculated using the measured stiffness of the membrane electrode assembly obtained from the sensing experiment. The following equation was used where k is the measured stiffness, L is the free length, W is the width, and T is the thickness to determine the elastic modulus E :

$$E = \frac{kL^3}{3\left(\frac{WT^3}{12}\right)}$$

The blocked force test can be related to the material parameters using the following equation where $\left(\frac{f}{v}\right)^u$ is the measured block force, d is the coefficient

describing the strain coupling, T is the thickness, W is the width, L_d is the free length of the membrane electrode assembly and E is the modulus of elasticity:

$$\left(\frac{f}{v}\right)^{\cup} = \frac{3 * d * T * W * E}{4 * L_d}$$

Normalization of the force for variations in geometric parameters of all the blocked force data was accomplished by using the following equation that couples the measured force with the geometry of the material:

$$Normalized_Force = \left(\frac{f}{v}\right)^{\cup} * \frac{4 * L_d}{3 * T * W} = dE \left(\frac{N}{Vm}\right)$$

The frequency input for these experiments was a random white noise signal over a range of 0-256 Hz. At frequencies above 200 Hz, the input signal was filtered using an anti-aliasing filter. The responses were then transformed to the correct frequency range by using Fourier Transforms of the input voltage and response. A Textronix Fourier Analyzer was used to calculate the phase and magnitude of the input-output frequency response function in real-time.

6.2.7 Scanning Electron Microscopy (SEM) of Membrane Electrode Assemblies

Field emission scanning electron microscopy (FE-SEM) was used to understand the morphology of the resulting membrane electrode assemblies. A LEO-1550 field emission SEM was operated at 5 kV at various magnifications. The MEA samples were freeze fractured after immersion in liquid nitrogen and mounted onto aluminum stubs using double sided copper tape. The samples were then coated with gold (~15 nm thick) using a sputter coater and placed in a vacuum environment for analysis.

6.2.8 Hydrated Dynamic Tensile Modulus

Dynamic mechanical tensile properties of the membranes submersed in deionized water were determined at room temperature using a dynamic mechanical analyzer (DMA) by TA Instruments (DMA 2980). The submersion clamp permits tensile modulus experiments in a fully immersed liquid water environment having a 95% confidence limit. An oscillation of 1 Hz was applied to the film while the amplitude was increased until a constant modulus plateau was achieved and allowed to equilibrate for 30 minutes.

6.3 Results and Discussion

The underlying electromechanical characteristic that permits proper transduction has been largely linked to electrical capacitance. The derivative of, or change in, charge motion divided by the derivative of voltage determines the capacitance. An increase in capacitance will increase the number and motion of charges at constant voltage. The capacitance can further be defined as the ability of a material to store an electric charge for use at a later time. Capacitors are designed to provide energy in an electric circuit by storing electricity in an electric field that is between two separate conducting plates or electrodes. When applying a voltage source to a capacitor, electrons are forced onto the surface of one electrode that in turn pulls electrons off the surface of the other. This process creates a potential between the two plates that are separated by a dielectric media. The dielectric material that can be used depends on the application and includes paper, ceramic, air, mica, and electrolytic materials. Because the dielectric material between the

plates act as an electron insulator, electrical current does not flow until an external circuit is closed resulting in a discharge. The capacitor electrodes can be either positive or negative and also can be charged and discharged as determined by the application.

Electrolyte dielectric materials serve both as an insulator to prevent current flow and as a media to support the electrostatic force of a charged capacitor electrode.

Dielectrics are rated by their ability to support the electrostatic forces by employing a number termed dielectric constant. The standard by which all other dielectric materials are measured is a vacuum, which has a dielectric constant of 1.000. The value for air is much the same at 1.001. However, as Table 6.1 indicates, a variety of materials can be used as dielectric materials.³⁰⁷

Table 6.1 Various Dielectric Materials and Their Corresponding Dielectric Constants

Material	Dielectric Constant
Vacuum	1.000
Air	1.001
Teflon	2.1
Polyethylene	2.25
Polystyrene	2.5
Mylar	3.1
Polyvinyl Chloride	3.18
Plexiglas	3.4
Paper	3.5
Mica	3-6
Neoprene	6.7
Glass	5-10
Methyl Alcohol	35
Glycerin	42.5
Water	80.4

³⁰⁷ Sears, F. W., Zemansky, M. W. and Young, H. D. *University Physics, 6th Ed.*, Addison-Wesley, 1982.

The measure of capacitance is the Farad (symbol F), which is named after Michael Faraday. The value of 1.0 Farad is defined as 1.0 coulomb being placed on a capacitor having a potential difference between the plates of 1.0 volt, where coulomb is the amount of charge transferred by a current of 1.0 ampere in 1.0 second, which is equal to the charge of 6.25×10^{18} electrons. Therefore, 1.0 Farad is a very large value for capacitance and thus microfarads and picofarads are more typical and were employed in the current study. Factors that affect the value of capacitance include the area of the plates, the distance between the plates and the dielectric constant of the material between the plates. When the plates have a larger surface area, they provide a greater capacity to store a charge, thus a higher capacitance. The electrostatic force field between the plates is much stronger when they are closer together and the value of capacitance is directly proportional to the amount of electrostatic force. Therefore, as the distance between the plates increases, the capacitance decreases and as the distance decreases, the capacitance increases. The third factor determining capacitance is the dielectric material. There is a direct correlation between the ability of the dielectric material that supports the electrostatic forces to the dielectric constant. Therefore, as the dielectric constant decreases, capacitance decreases. As table 6.1 indicates, water supports the electrostatic forces better than any other material in the table suggesting it is a very good dielectric material thereby allowing aqueous electrolytes to provide supercapacitance.

The capacitance generated in polymeric transducers has been determined to be due to the electric double layer that forms between the interface of the electrode and dielectric polymer.³⁰⁸ The electric double layer theory has been used to calculate the motion of ions and distribution of ions in an electrolyte dielectric material. The mobile

³⁰⁸ Sadeghipour, K., Salomon, R. and Neogi, S. *Smart Materials and Structures*, 1, 3445-3447, 1992.

ions in the electrolyte tend to adsorb onto the metal layer and also tend to be distributed away from the polymer-metal interface in such a fashion that the charge on the metal electrode is balanced. This phenomenon is termed supercapacitance and is described as having a very large capacitance per unit weight or volume. Supercapacitors are neutral systems that contain an electric double layer at the interface of the metal electrode and electrolyte dielectric material.³⁰⁹ The neutrality of the system is obtained by a diffuse layer of positive charges in the electrolyte opposing a centralized layer of negative charges in the electrode. Thus, the double layer is formed in which the separation of each layer is on the order of a few angstroms.³¹⁰

Specific advantages of PATS and BPSH materials as compared to Nafion are higher hydrated moduli and accurately controlled ion content during copolymer synthesis. The ability to control the amount of ion content directly polymerized into the copolymer backbone affords a systematic study of structure-property relationships and various electrolyte concentrations. More precisely, the transducer performance can be directly related to the molecular structure. As Table 6.2 indicates, the physical properties of the disulfonated copolymers change dramatically with an increase in ion exchange capacity.

³⁰⁹ Winter, M and Brodd, R. J. *Chem. Rev.* 'What Are Batteries, Fuel Cells and Supercapacitors' 2004, 104, 4245-4269.

³¹⁰ Endo, M. and Ishii, K. *Carbon Science*, 1, 117-128, 2001.

Table 6.2 Physical Properties of Various Disulfonated Copolymers and Nafion 117

	EW (g/cq)	IEC (meq/g)	Water Uptake (weight %)	Protonic Conductivity (S/cm)	Hydrated Modulus (MPa)
Nafion 117	1100	0.91	22	0.11	120
BPSH 30	1110	1.3	29	0.06	920
BPSH 35	770	1.53	40	0.08	640
BPSH 40	650	1.7	56	0.10	400
PATS 30	860	1.17	20	0.06	1040
PATS 40	660	1.51	86	0.11	400

Limitations of Nafion type transducers include low hydrated modulus (120 MPa) and hydration dependence. The hydration dependence both reduces operating environments and limits the driving voltages to values below 1.22 V. Voltage values above 1.22 V electrolyze water producing hydrogen and oxygen gases. Short electrode excursions to higher voltages has been accomplished, however, eventual dehydration due to electrolysis decreased overall performance. The limitation of a low hydrated modulus can be directly apparent during the maximum force experiments where low force can be determined. High hydrated modulus materials allow for enhanced force producing characteristics allowing better performance during the blocked force test.

Scanning electron microscopy was performed on the MEAs to determine electrode morphology and metal dispersion. Figure 6.6 shows the freeze fractured cross section of Nafion 117 having impregnation-reduction electrodes at 750x magnification on the left and 5,000x magnification on the right. The images indicated that the reduced platinum particles penetrated the material to an average depth of only 2 μm with maximum penetration at concentrated areas reaching depths of 8 μm . The branch-like structures associated with the absorption of the platinum solution and subsequent reduction with sodium borohydride provided acceptable surface area of the metal-

polymer interface. This surface interface was responsible for the electrical capacitance and double-layer properties. Further electrical conductance was produced by gold plating the platinum surface with gold. Figure 6.7 indicates the thin gold layer directly on top of the impregnated and reduced platinum electrode.

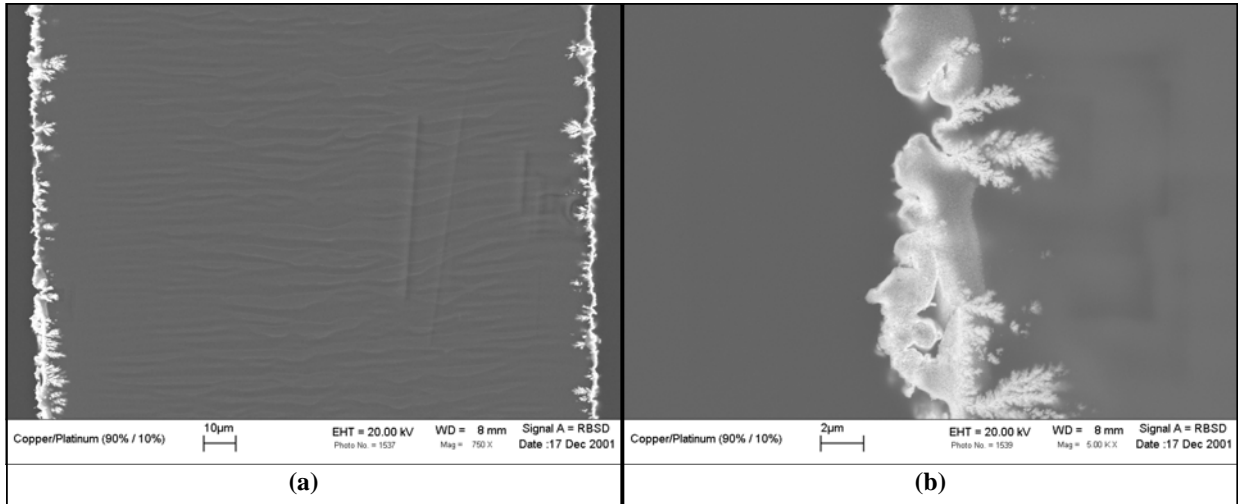


Figure 6.6 Nafion 117 with Impregnation-Reduction Electrodes at (a)750x and (b)1000x Magnifications

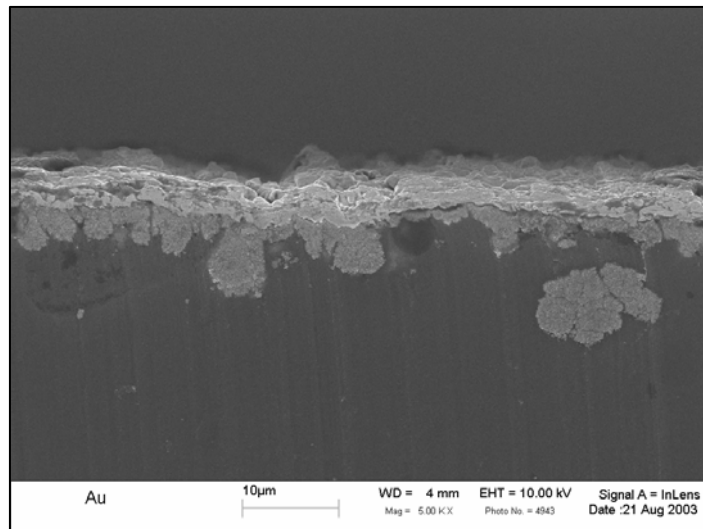


Figure 6.7 Impregnation-Reduction Electrode with Gold Electroplated Layer

The novel electrode technique, which is termed the direct assembly process, allowed for various electrode morphologies and metal powders to be used for transduction. Figure 6.8 indicates the electrode morphology of hot pressed membrane electrode assemblies showing the ionomer containing conductive powder electrodes that contain ratios of (a) 4:1 and (b) 2:1 platinum to Nafion 1100. The variations in the concentrations of the metal powder were evident and indicated that the higher loading of platinum particles increased the intensity of the image and thus increased the polymer-metal surface area. The lower loading (b) indicated more ionomer as the matrix material and less metal powder dispersed in the matrix. In both images, the final layers of impregnation-reduction platinum and electroplated gold was observed to increase the overall thickness of the membrane electrode assembly. Direct comparison of the impregnation-reduction electrodes to the direct assembly process suggests higher metal surface areas and better dispersion of the metal particles in the ionomer matrix.

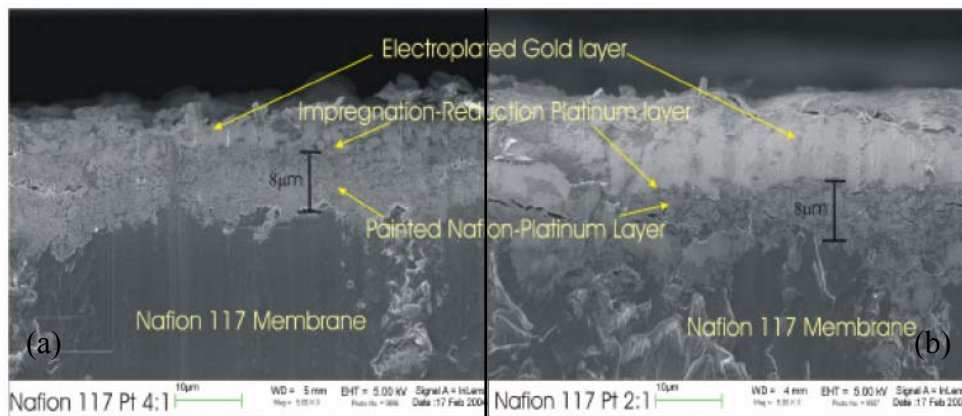


Figure 6.8 SEM Cross Section Indicating the Direct Assembly Process Electrodes Using Nafion 117 Membranes with Ratios of (a) 4:1 and (b) 2:1 Platinum to Nafion 1100

One of the advantages of the direct assembly process is that it allows different conductive materials to be dispersed throughout the electrode structure. Ruthenium dioxide (RuO_2) was incorporated into the electrode ink by simple mixing and sonicating with Nafion dispersion. The ink was then painted onto decals and then hot pressed onto proton exchange membranes. The SEMs of (a) BPS 35 and (b) Nafion 117 membranes containing RuO_2 conductive powder in a Nafion 1100 matrix are shown in Figure 6.9. The BPS 35 membrane (a) was hot pressed with an electrode decal containing 6 layers of painted ink thereby providing an electrode thickness of 6 μm . The Nafion 117 membrane (b) was directly assembled using decals that were painted with 9 layers of painted electrode thus providing a thickness of 8 μm . These SEM images also indicated the excellent connectivity between the hot pressed electrode and membrane material. These images showed that the electrode thickness and loadings were precisely controlled thereby allowing various morphologies and capacitances to be produced.

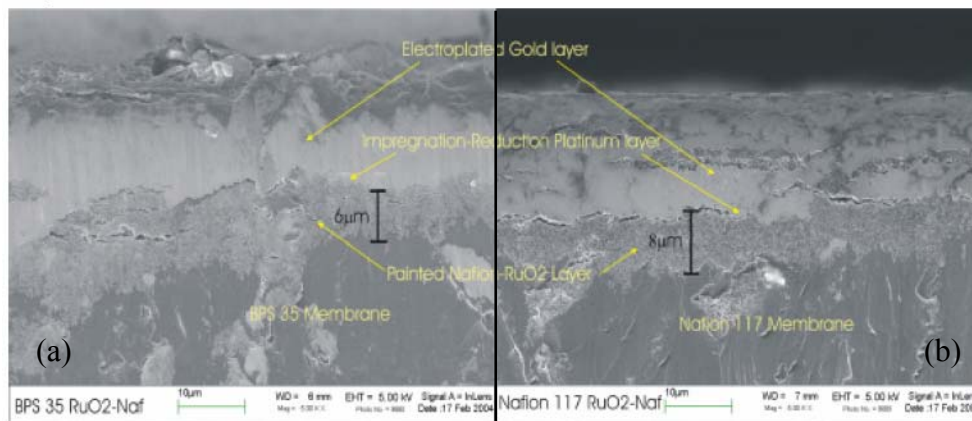


Figure 6.9 SEM Showing Cross Section of (a) BPS 35 Membrane Hot Pressed with Decals Having 6 layers of RuO_2 Electrode Ink and (b) Nafion 117 Membrane Hot Pressed with 9 Layers of Electrode Ink Both with Ratios of 2.5:1 RuO_2 :Nafion

Characterization using the previously described electromechanical experiments demonstrated that the impregnation-reduction electrodes performed poorly when compared to the direct assembly technique. As will be discussed in the following section, the novel plating technique introduced in this work outperformed the state of the art impregnation-reduction electrode technique by creating higher capacitances and enhanced strain output. However, the novel materials were first investigated using the impregnation-reduction electrodes to better understand the material properties. Fully hydrated BPSH, PATS and Nafion 117 materials were tested in actuation mode with impregnation-reduction electrodes. The results are shown in Figure 6.10 indicating frequency (cycles of pole rotation per second) on the x-axis and normalized $\mu\text{strain}/V$ (displacement/V) on the y-axis.

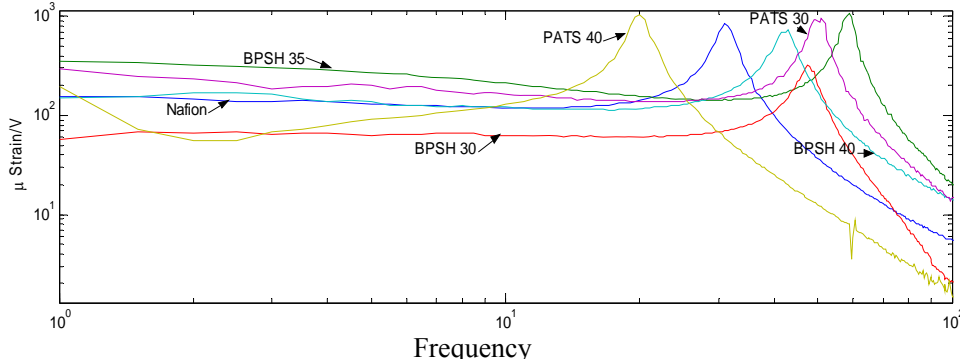


Figure 6.10 Frequency Versus Normalized $\mu\text{Strain}/V$ for Nafion 117, BPSH30, BPSH35, BPSH40, PATS30 and PATS40

The primary area of interest for artificial muscle applications in these types of plots is typically at frequencies below 10 Hz. The resonance frequency of the materials was observed at various frequencies above 10 Hz and is indicative of the physical material properties that can be tailored such as stiffness, thickness and weight of the

MEA. At the resonance frequency of a material, the ion flux is in harmony with the pole rotation from positive to negative creating the highest displacements. These values are typically used for applications such as flapping flight and micro-air vehicles. At values below the resonance frequency, various applications include biocompatible muscle, robotic muscles and vibration control to only name a few. Focusing on the displacements that were below 10 Hz, it was observed that the material properties of the BPSH and PATS materials could be tailored for enhanced performance in actuation mode. For example, BPSH 30 performed relatively poorly presumably due to low conductivity, but BPSH 35 was the best performer assumingly due to a good balance of conductivity and modulus, while the performance of BPSH 40 fell to values similar to Nafion 117 primarily due to the low hydrated modulus. The disulfonated copolymers based on thioether linkages showed similar performance relative to BPSH materials where PATS 30 produced displacements above Nafion and PATS 40 fell to values similar to BPSH 30. It was concluded that the material properties of the BPSH and PATS copolymers allowed enhanced control over actuation performance using the state of the art electrodes when compared to Nafion.

The blocked force test was also performed on BPSH, PATS and N117 samples with impregnation-reduction electrodes. The results are shown in Figure 6.11 and indicate the frequency on the x-axis and the normalized force (mN/V) on the y-axis. The force produced from the MEAs was directly related to the hydrated modulus coupled with the free displacement tests of all the materials. PATS 30 and BPSH 35 MEAs were previously shown to perform the best in the free displacement test and furthermore, the hydrated moduli of these materials were determined to be 1040 and 640 MPa

respectively. It was suggested that the enhanced performance and large hydrated modulus accounted for the increase in blocked force when compared to Nafion 117, which only had a hydrated modulus of 120 MPa. Therefore, it was concluded that BPSH 35 had the best displacement and produced the highest force of all the materials studied with impregnation-reduction electrodes.

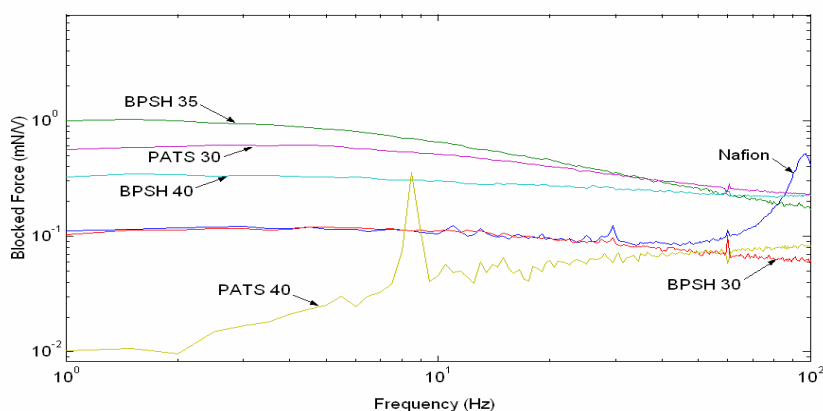


Figure 6.11 Blocked Force Produced Using PATS, BPSH and Nafion Copolymers with Impregnation-Reduction Electrodes

The relationship between performance and capacitance was more closely investigated through the novel electrode plating technique. The hypothesis was to increase the capacitance in a controlled manner which in turn would lead to enhanced performance in free strain response and block force characteristics. Two different metal powders were used to make the directly assembled electrode. Platinum supported on carbon black was used to closely resemble the impregnation reduction electrodes. However, large surface area RuO_2 was found to create the highest performance in both the displacement and force tests. As Figure 6.12 indicates, the platinum based directly assembled MEAs provided lower $\mu\text{strains}$ per volt than the comparable MEAs containing

ruthenium dioxide. This suggested that the capacitance of the RuO₂ metal-polymer interface was higher than the platinum based materials. The weight ratio of metal to polymer in the electrodes was held constant at 2.5:1 with 6 layers of electrode ink painted on the decals before hot pressing. After membrane electrode fabrication, transducers were ion-exchanged into either the proton (H⁺) or the lithium (Li⁺) forms and tested. It was concluded that protons produced enhanced strain response for electrodes based on RuO₂ as compared to lithium cations. It was suggested that the hydration shell on the lithium cations was large enough so as to not penetrate the ruthenium dioxide pores.³¹¹ Therefore, the electric double layer that was produced was not complete across the entire electrode surface thereby decreasing the overall performance.

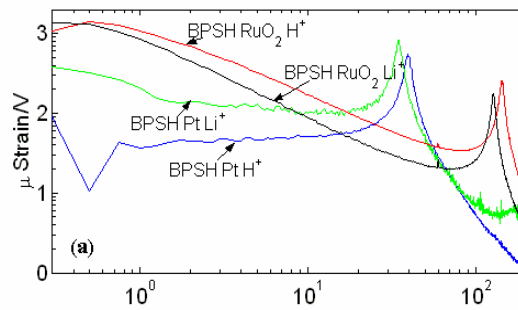


Figure 6.12 BPSH 35 Copolymers with Novel Electrodes Containing Platinum (Pt) or Ruthenium Dioxide (RuO₂) in the Proton (H⁺) and Lithium (Li⁺) Forms

Calculation of the capacitance for the novel electrodes indicated that the ruthenium dioxide metal provided higher values as compared to platinum based MEAs. Figure 6.13 shows the capacitance in mF/cm² on the y-axis and frequency on the x-axis. Both the proton and lithium forms of the platinum based MEAs showed an order of magnitude decrease in the calculated capacitance relative to the RuO₂ materials. This

³¹¹ H.-K. Kim, S.-H. Cho, and T.-Y. Seong, J. Vac. Sci. Technol. B 21(3), pp. 949--952,2003.

further indicated that the electric double layer is more pronounced with RuO₂ materials than Pt materials. It was suggested that RuO₂ introduced a redox coupling effect between two valence states of ruthenium giving higher effective capacitance.³¹²

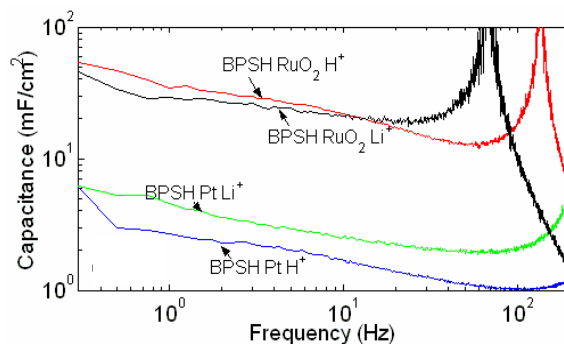


Figure 6.13 Capacitance of BPSH35 Using Platinum and Ruthenium Dioxide Metals along with Proton and Lithium Cations

Another positive characteristic of the novel electrode plating technique was the ability to tailor the thickness and therefore the loadings of the metals in the electrodes. Figure 6.14 (a) and (b) indicate that increases in electrode thickness produced enhanced μ strains per unit volt and furthermore, decreasing membrane thickness from 7 mils to 2 mils produced remarkably higher displacement values. This suggested that both displacement and free strain output of the transducers was increased by enhancing electrode thickness thereby giving larger electrolyte-electrode surface areas. The increase in surface area produced higher capacitance and therefore better performance. It was further observed that the displacement and μ strain were enhanced by decreasing the membrane thickness, however it was assumed that the maximum blocked force would decrease dramatically.

³¹² Winter, M and Brodd, R. J. *Chem. Rev.* 'What Are Batteries, Fuel Cells and Supercapacitors' 2004, 104, 4245-4269.

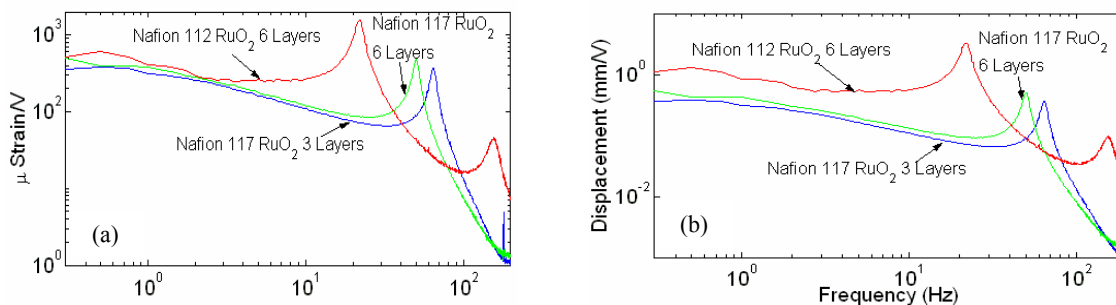


Figure 6.14 Normalized Strain and Displacement for Nafion 117 and 112 MEAs Using 3 and 6 Layers of RuO₂ Ink Painted onto Decals and Hot Pressed

As previously concluded in this paper, enhanced performances were produced using BPSH35 and PATS30 copolymers relative to Nafion. Furthermore, RuO₂ metal composite electrodes produced much higher capacitance and strain relative to platinum based directly assembled MEAs. Therefore, comparisons of the alternative materials with Nafion using the novel electrode plating technique and the impregnation-reduction technique was plotted in Figure 6.15 (a), (b), (c) and (d). Over the entire range of materials and experiments, the direct assembly electrodes performed the best when compared to the impregnation-reduction electrodes at frequencies below 10 Hz. All of the materials were tested in the proton form and were 7 mils thick. The strain at low frequencies was found to increase by five times for the novel electrode plating technique for all the copolymers with PATS30 having the highest values. Free strain measurements in the low frequency range were on the order of 1600 microstrain/V. The normalized force showed a dramatic increase when using the novel electrodes where the PATS30 MEA outperformed all others in the low frequency range. The poor performance of Nafion type transducers in the blocked force experiments was directly related to the low hydrated modulus of the material at 120 MPa.

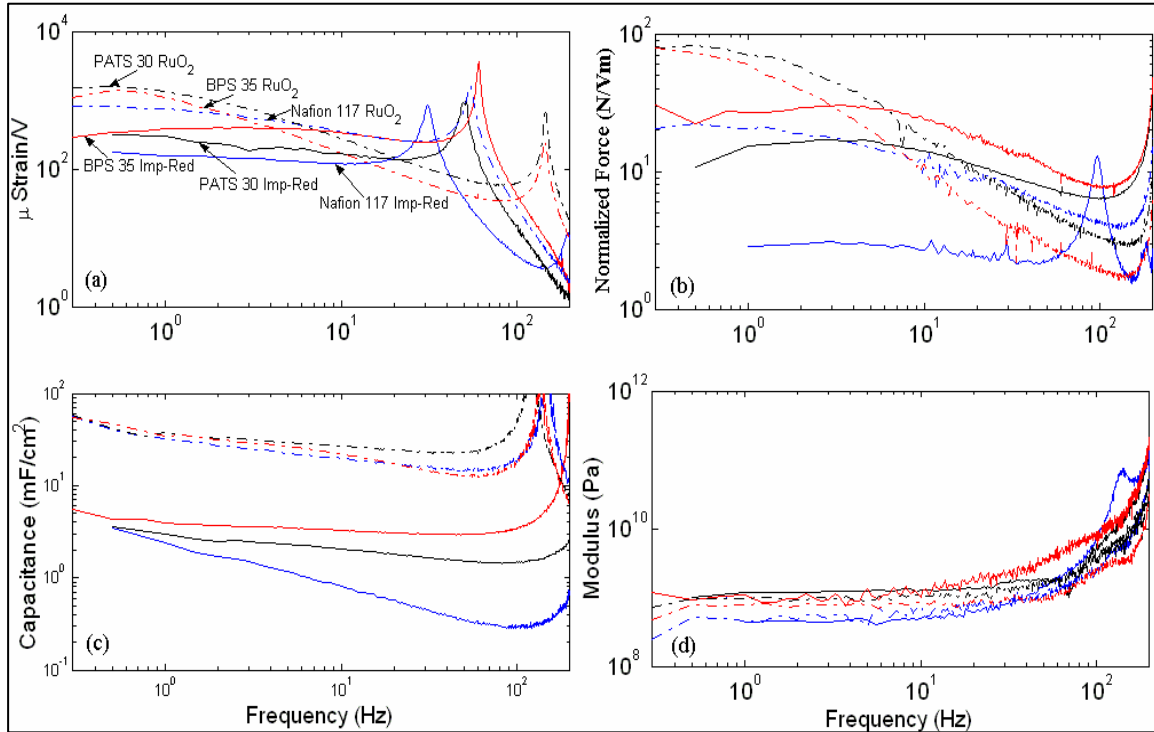


Figure 6.15 Strain (a), Force (b), Capacitance (c) and Modulus (d) Plotted Against Frequency for BPSH35, PATS30 and Nafion 117 Using Impregnation-Reduction and RuO₂ Based Direct Assembly Electrodes

The first order ‘roll-off’ exhibited in the frequency response function of the transducers that was observed for the ruthenium dioxide electrodes at high frequencies could have been due to the previously stated reduction-oxidation reactions that are inherent with RuO₂ metals. Nafion MEAs made with the direct self-assembly did not show the roll-off, therefore suggesting the interfacial resistance associated with the unlike polymers of the membrane (BPSH or PATS) and electrodes (Nafion) was the main cause of the high frequency roll-off. The limitation of diffusion speed of the cations in the transducers at high frequencies for RuO₂ electrodes was slow because of hindered transport through the interface of the electrode and membrane. Therefore, this interface between two unlike polymers blocked the ability of the ions to move freely in and out of

the polymer-electrode interface. It was prominent in the PATS and BPSH materials and not Nafion 117 because Nafion was used in the electrodes.

The capacitance of the materials was calculated using the electrical impedance of the material as determined by measuring the flow of current into the material during the free displacement test. It was observed that the capacitance of the novel electrode plating method increased by an order of magnitude relative to the impregnation-reduction electrodes. This dramatic increase was primarily due to the enhanced electrolyte-metal interfacial area produced by the uniformly dispersed metal in ionomer matrix. The modulus of the materials was found to be a function of the membrane properties and not necessarily due to the electrode properties.

The relationship of performance and capacitance suggested by increasing the capacitance of a material increased the free strain output. Because high capacitance was presumably due to the electric double layer that formed at the electrolyte-metal boundary, an increase in the interfacial area increased the capacitance and thus electromechanical transduction. Ruthenium dioxide could not have been incorporated using the impregnation-reduction electrodes. Therefore, the direct assembly technique allowed controlled loadings and dispersions of various metals. The RuO₂ metal powders had a large surface area per gram relative to the platinum black metal which permitted higher polymer-metal interface areas providing enhanced capacitance and electromechanical actuation.

6.4 Conclusions

The capacitance-performance relationship was presented and indicated that increased capacitance enhanced the blocked force and free strain output of electromechanical transducers. BPSH and PATS based transducers showed enhanced performance using both impregnation-reduction and hot pressed direct assembly electrodes relative to the state of the art Nafion based MEAs. The novel electrode plating method increased the capacitance by an order of magnitude thus enhancing the strain and force relative to the impregnation-reduction electrode plating technique. The metal used in the electrodes had a major effect on performance and ruthenium dioxide was found to perform the best when compared to platinum based electrodes. The novel direct assembly electrode technique was found to be much more compliant by allowing more controllable morphologies and variations in MEA parameters. Further research should include various electrode plating techniques including directly painting ink onto ionomer membranes rather than hot pressing electrode decals; removing the impregnation-reduction steps from the novel electrode plating technique; pressing gold leafs onto the MEAs so as to remove the gold electroplating step. Since these materials must be solvated in order to perform, the operating environments are limited. Ongoing research is focusing on employing ionic liquids that have no measurable vapor pressure as the solvation media rather than water that tends to evaporate after roughly 1000 actuation cycles. Further characterization of partially fluorinated copolymers based on BPSH could possibly allow a decrease in the high frequency roll-off associated with the aromatic copolymers because of enhanced compatibility with perfluorinated Nafion.

6.5 Acknowledgements

The authors would like to thank the Department of Energy and United Technologies Corporation for funding under contract # sub-56844-FMIJOBDOE-99241. The experimental testing was funded by the U. S. Army Research Laboratory and the U. S. Army Research Office under contract # DAAD19-02-1-0275.

CHAPTER 7

DIRECTLY COPOLYMERIZED 45 MOLE PERCENT DISULFONATED POLY(ARYLENE ETHER PHENYL PHOSPHINE OXIDE SULFONE) TERPOLYMERS FOR PEM FUEL CELL SYSTEMS: SYNTHESIS, FABRICATION AND CHARACTERIZATION OF HETEROPOLYACID COMPOSITE MEMBRANES FOR HIGHER TEMPERATURE FUEL CELL APPLICATIONS

K.B. Wiles¹, C. M. de Diego², J. de Abajo² and J.E. McGrath¹

¹Department of Chemistry and Macromolecules and Interfaces Institute

Virginia Polytechnic Institute and State University

Blacksburg, VA 24061

²Departamento de Química Macromolecular

Instituto de Ciencia y Tecnología de Polímeros. CSIC.

Madrid, Spain

Abstract

The synthesis and fabrication of 45 mole percent disulfonated poly(arylene ether phenyl phosphine oxide sulfone) terpolymer-heteropolyacid (HPA) composite membranes and membrane electrode assemblies was investigated. A series of 45 mol% disulfonated biphenol-based poly(arylene ether phenyl phosphine oxide sulfone) terpolymers (BPSH45-PPO) was synthesized by nucleophilic aromatic substitution terpolymerizations. The amounts of 4,4'-diphenyl phenyl phosphine oxide comonomer incorporated into the terpolymer backbone were precisely controlled from 0-50 mole percent, thereby creating a series phosphine oxide containing terpolymers. The disulfonation level was unchanged so as to provide full understanding of PPO incorporation while maintaining the adequate conductivity of 45 mole percent disulfonated copolymers. Phosphine oxide incorporation was monitored by ^1H NMR and Fourier transform infrared spectroscopy (FTIR). Composite membranes were prepared by solution blending the dissolved terpolymers with the dissolved phosphotungstic acid HPA. Fourier transfer infrared spectroscopy was used to evaluate band shifts corresponding to the sulfonic acid moieties on the copolymer backbone hydrogen bonded to the HPA molecules. Phosphorous 31 NMR (^{31}P NMR) was used to monitor hydrogen bonding between the phenyl phosphine oxide moieties and the phosphotungstic acid molecules. The composite BPSH45-PPO membranes exhibited low HPA molecule water extraction after acidification at room temperature and boiling temperatures. The membranes containing HPA indicated improved conductivity at high temperatures and low relative humidities when compared to the pure terpolymer samples. For example, at 120 °C and 45% relative humidity at atmospheric pressure, the conductivity of the

composite BPSH45 sample containing 30 wt% of HPA and 10 mol% BFPPPO was 21 mS/cm while the conductivity of the pure BPSH45 with 10 mol% BFPPPO sample was only 9 mS/cm. The increase of proton conductivity was attributed to the water retention characteristics of the HPA molecules, which allowed enhanced mobility of the protons even at lower humidification levels. The increase in the amount of phenyl phosphine oxide into the terpolymer backbone was however unfavorable to the overall conductivity and hydrogen-air fuel cell performance. This may be due to complex formation between the sulfonic acid and phosphine oxide groups. This extremely strong attraction decreased the sulfonic acid activity towards proton transport mechanisms thereby decreasing conductivity.

Key Words: poly(arylene ether phosphine oxide sulfone), poly(arylene ether sulfone), proton exchange membrane, fuel cell, Nafion, composite membrane, phosphotungstic acid, heteropolyacid

7.1 Introduction

Novel engineering systems based on proton exchange membrane (PEM) fuel cells as an alternate energy source is considered very attractive due to diminishing natural resources, global warming, acid rain and smog producing precursors associated with combustion energy processes. PEM fuel cells directly produce electrical energy from electrochemical reactions by delivering fuel (H_2) to the anode and an oxidizer (O_2) to the cathode. Specific limitations of the fuel cell that is currently hindering mass production include usable temperature ranges, hydrogen storage, fuel efficiency and cost. Polymer electrolyte membranes are presently limited by the liquid water temperature range. Hydrogen ions are transported across the membranes in an aqueous environment and thus above the boiling point of water, the mechanism becomes severely limited. Temperatures above 100 °C would decrease platinum poisoning by carbon monoxide and would increase reaction kinetics.

Phosphine oxide containing polymers based on poly(arylene ether)s and poly(arylene thioether)s have been reported to be stable at high temperatures while also being flame retardant and plasma resistant.^{313,314,315,316} Generally these high performance polymers have been suggested as flame retardant materials that also complex with certain metals to help in dispersion and retention of inorganic/organic additives.³¹⁷ Furthermore, reports on phosphine oxide containing poly(arylene ether)s that have good interactions with a wide variety of thermoplastics and thermosets like phenoxy, epoxy and vinylester resins

³¹³ Smith, C.D.; Grubbs, H.J.; Webster, H.F.; Gungor, A.; Wightman, J.P. and McGrath, J.E., *High Perform. Polym.*, 1991, 4, 211.

³¹⁴ Bhatnager, A.; Liu, Y. N.; Geibel, J. F. and McGrath, J. E. *Polymer Preprints*, 1997, 38(2), 227.

³¹⁵ Riley, D.J.; Gungor, A.; Srinivasan, S.A.; Sankarapandian, M.; Tchatchoua, C.; Muggli, M.W.; Ward, T.C. and McGrath, J.E., *Polym Eng. Sci.*, 1997, 37(9), 1501.

³¹⁶ Ding, Y. and Hay, A. S. *J. Polym. Sci.: Part A: Poly. Chem.*, 1998, 36, 519.

³¹⁷ Hergenrother, P.M., *Angew Chem. Int. Ed. Engl.* 1990, 29, 34.

has recently been described.³¹⁸ It has been proposed that these phosphine oxide containing materials could have an increased interaction with functionalized carbon fibers, glass fibers or inorganic additives due to the very polar phosphine oxide groups. Synthetic procedures to produce phosphine oxide containing polymers has mainly incorporated 4,4'-bis(fluorophenyl) phenyl phosphine oxide (BFPPPO), Figure 7.1, as the electrophile and biphenols or thiobiphenols as the nucleophilic containing monomers.

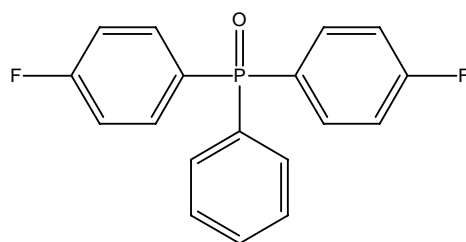


Figure 7.1. Chemical Structure of 4,4'-bis(fluorophenyl) phenyl phosphine oxide

The polymerizations can be carried out in solution or in the melt. The melt polymerizations³¹⁹ followed the silylation route proposed by Kricheldorf.³²⁰ These solventless reactions produced polymers that were free of inorganic salt byproducts and used for reactive extrusion techniques due to their low viscosity in the melt even at high molecular weights (30,000 g/mol). The solution polymerization technique follows the same synthetic procedures as has been described for nucleophilic aromatic substitution

³¹⁸ Wang, S., Zhuang, H., Shobha, H. K., Glass, T. E., Sankarapandian, M., Ji, Q., Shultz, A. R., McGrath, J. E. *Macromolecules* 34(23), 8051-8063, 2001.

³¹⁹ Mecham, S. J.; Hickner, M. A.; Sankarapandian, M.; Grieco, L. M.; McGrath, J. E. *SAMPE* 1999, 16.

³²⁰ Kricheldorf, H. R. and Bier, G. *Polymer*, 1984, 25, 1151.

reactions using potassium carbonate as the base that abstracts the proton from the nucleophilic monomer.

An early report of poly(arylene ether phenyl phosphine oxide) was published by Hashimoto et al³²¹, who obtained only low molecular weight polymeric material. They reacted 4,4'-bis(chlorophenyl) phenyl phosphine oxide (BCPPO) with various bisphenols in different aprotic dipolar solvents. The strong base approach (NaOH) was used because the phosphonyl moiety was described as being less of an electron-withdrawing group as compared to the corresponding sulfone group. Smith et al³²² showed that high molecular weight could be obtained from the use of bis(4-fluorophenyl)phenyl phosphine oxide (BFPPPO) due to the higher reactivity of the fluoro compounds as compared to the chloro compounds. More recently, McGrath et al³²³ have incorporated various architectures into the polymer backbone, such as sulfonyl and carbonyl. The resulting polymeric materials based on BFPPPO monomers were observed to be amorphous, non-coplanar polymers with high T_g s and high thermal stabilities.

Sulfonating the phosphine oxide containing monomer has been reported³²⁴, but produces a polymer that contains only one sulfonic acid moiety per repeat unit (Figure 7.2).

³²¹ Hashimoto, S.; Furukawa, I. and Ueyama, K. *J. Macromol. Sci. Chem*, 1977, A11, 2167.

³²² Smith, C.D.; Grubbs, H.J.; Webster, H.F.; Gungor, A.; Wightman, J.P. and McGrath, J.E., *High Perform. Polym.*, 1991, 4, 211.

³²³ McGrath, J. E.; Mecham, S. J.; Hickner, M. A.; Wang, S.; Shobha, H. B.; Oishi, Y. and Sankarpandian, M. *Polymer Preprints*, 1999, 40(2), 1291.

³²⁴ Shobha H.K.; Smalley, G.R.; Sankarpandian, M. and McGrath, J.E. *Polymer Preprints*, 2000, 41(1), 180.

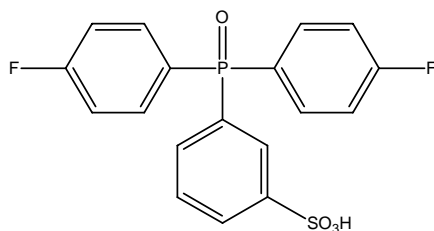


Figure 7.2. Mono-Sulfonated BFPPO

The phosphine oxide containing monomer, BFPPO, was reacted with SO_3 in fuming sulfuric acid to produce a mono-sulfonated pendant phenyl ring. Minor products of di- and tri- substituted monomers were also formed in the reaction, therefore, the mono-substituted species was isolated from the reaction mixture using different recrystallization techniques. The nucleophilic monomer used was 4,4'-biphenol, which gave a wholly aromatic sulfonated copolymer by direct copolymerization. Proton conductivity measurements indicated a lower conductivity relative to the disulfonated sulfone analog due to the lower degree of sulfonation per repeat unit and strong hydrogen bonding between the phosphine oxide moiety and sulfuric acid moiety. The thermogravimetry data indicated a decrease in the 10% weight loss temperature as more of the sulfonated monomer was added probably due to the loss of more sulfonic acid groups as the sulfonation level increased. The ionomeric effect was noted in the increase in intrinsic viscosity as the sulfonation level increased. The ionomeric effect is described as the association or aggregation of the ionic sulfonate groups to produce multiplet structures that can also form higher agglomerations like spheres, clusters and channels.

Improvement of proton conductivity and membrane properties, especially at elevated temperatures, has been a well studied research goal of university and industrial

investigators. Blending of different polymers by physical techniques is a straightforward process to modify characteristics and properties of polymer materials.³²⁵ However, polymer-polymer miscibility is difficult to achieve because most polymers are known to be incompatible.³²⁶ When no specific interactions, like acid-base or hydrogen bonding, between two polymer materials exist, microscopic and macroscopic phase separation is usually observed, which is termed as a negative characteristic, but can still alter polymer properties. In the case of fuel cell membranes, improving membrane properties in the areas of proton conductivity, mechanical strength and water swelling is of utmost importance. For example, many researchers are blending non-sulfonated materials with sulfonated materials in order to produce a membrane that has significantly better mechanical strength and lower water swelling.^{327,328,329} Gore and Associates membranes are composite membranes that are based on Nafion[®] copolymers using GORE TEX[®] as a support.³³⁰ The main advantage of the micro-reinforced Gore-Select membranes was observed in the mechanical strength of very thin films. The thickness of the membranes was allowed to decrease to values lower than the non-supported membranes due to the enhanced physical properties of the blended materials so as to still have mechanical durability for PEM applications. Therefore, this polymer-polymer blend was a good candidate for alternative PEMFCs, however, it still has the limitations associated with Nafion[®] type membranes at elevated temperatures and in direct methanol fuel cells.

³²⁵ Paul, D.R. and Bucknall, C. *Polymer Blends Vol.I. Formulation and Performance*, Wiley & Sons: New York, 2000.

³²⁶ Paul, D. R. and Newman, S., Eds. *Polymer Blends*, Academic Press: New York, 1978.

³²⁷ Wilhelm, F.G.; Punt, I.G.M.; van der Vegt, N.F.; Strathmann, H. and Wessling, M. *J. Membr. Sci.*, 2001, 1, 5138.

³²⁸ Kerres, J.; Ullrich, A., Meier, F. and Haring, T. *Solid State Ionics*, 1999, 125, 243.

³²⁹ Deimede, V.; Voyiatzis, G.A.; Kallitsis, J.K.; Qingfeng, L. and Bjerrum, N.J. *Macromolecules*, 2000, 33, 7610.

³³⁰ Doyle, M. and Rajendran, G. In *Handbook of Fuel Cells*, Vielstich, W.; Lamm, A. and Gasteiger, H. A., Eds.; John Wiley & Sons Ltd.: New York, 2003, 3.

Furthermore, the interfacial issues of the different polymers have not been fully investigated or understood, but could be adversely significant.

Polymers containing high levels of acidification usually show excellent conductivity, but often suffer from high water swelling, which produces decreased mechanical strength that makes it useless for hydrated fuel cells. Therefore, in order to resolve this problem, polymers with high concentrations of ionic groups can be reinforced with a compatible polymer that does not swell and has good mechanical strength. Kerres et al¹⁷² incorporated this idea when they blended sulfonic acid containing polymers with a polymer that contained a basic nitrogen moiety. These two functional groups would help to make two different polymers compatible through acid-base interactions. The sulfonated polymers employed in this study were post-sulfonated poly(ether sulfone) and post-sulfonated poly(ether ether ketone). The basic polymers used were poly(benzimidazole), poly(ethyleneimine) and poly(4-vinylpyridine). Dissolution of the polymers separately in NMP and adding one polymer solution to the other while stirring at a high rate produced good blending of the polymeric materials. Solution casting onto glass substrates showed no visible separation, as would be the case with non-compatible polymers. As the authors described, high proton conductivity was obtained by blending sulfonated poly(sulfone) with diaminated poly(sulfone) to produce a tough ductile film with a conductivity similar to that of Nafion[®] 112. Furthermore, low methanol permeation was observed relative to Nafion[®], which was proposed to be due to the specific interactions between the basic amine groups and the acidic sulfonic groups to produce a membrane with higher acid strength.

Investigations to find PEMs that can be used at temperatures above 100 °C is currently the major thrust in the field of proton exchange membrane hydrogen/air fuel cells. The performance barriers of pure ion containing membranes and polymer/polymer blends are trying to be overcome by the incorporation of inorganic fillers that also are protonically conductive. These inorganic fillers can aid in the enhancement of mechanical properties and water retention at high temperatures. Furthermore, polymers that do not have any proton conductivity could be used as a matrix for ionically conductive inorganic additives that are stable at fuel cell use temperatures for high temperature conductivity. The perfluorinated membranes perform poorly at elevated temperatures (>80 °C) due to dehydration and also presumably due to a thermal transition in the partially hydrated form. At temperatures above the boiling point of water, dehydration of the membranes under ambient conditions occurs dramatically (120 °C @ 45% relative humidity) when a 100% hydrated hydrogen fuel stream is fed into the cell. Therefore, difficulties in high temperature fuel cell usage at ambient pressure are compounded by dehydration and decreased fuel cell performance. The overall ambition of this type of research is to find a membrane that could be used at temperatures above 100 °C and conducts protons at ambient pressure with little water. Therefore, nanocomposite PEMs have developed into a new field of macromolecular science coupled with engineering.

Crystalline forms of inorganic heteropolyacids (HPA) have recently been used for additives in PEMs by blending with dissolved ionic polymeric materials.³³¹ The HPAs, in the crystalline form, are protonically conductive inorganic fillers that usually have a

³³¹ Zaidi, S.M.J.; Mikhailenko, S.D.; Robertson, G.P.; Guiver, M.D. and Kaliaguine, S.J. *J. Membr. Sci.*, 2000, 173, 17.

strong interaction with specific functional groups in the polymeric material. Many HPA possibilities exist, but only a few have been studied. Some of these are phosphotungstic acid, zirconium phosphate and silicotungstic acid. All of these examples contain multiple acid moieties with relatively high proton conduction as compared to other inorganic fillers. The HPA in PEMs presumably give alternative mechanisms to proton transport at temperatures above 100 °C where very little water is present.

Composite membranes based on phosphotungstic acid have recently been shown to have higher conductivities and lower water swelling at elevated temperatures as compared to the pure copolymer membranes. Kim et al³³² described solution blending and film casting using commercially available phosphotungstic acid hydrate (Figure 7.3) and poly(arylene ether sulfone) copolymers, BPSH.

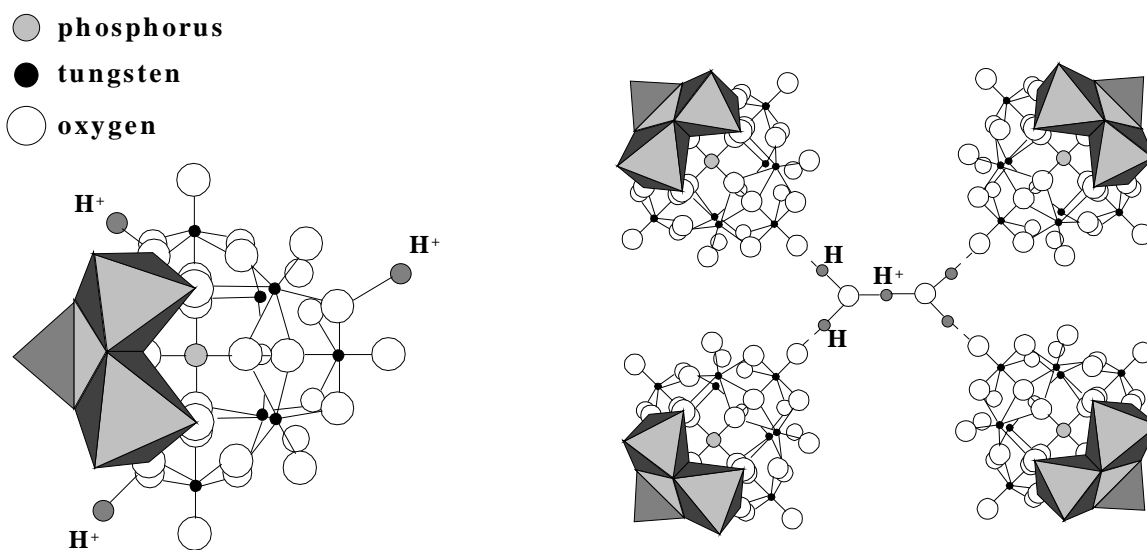


Figure 7.3 Primary Keggin and Secondary Hydrated Structures of Semicrystalline Phosphotungstic Acid

³³² Kim, Y. S., Wang, F., Hickner, M., Zawodzinski, T. and McGrath, J. E. *J. Membr. Sci.* 212, 263, 2003.

The composite membranes showed variable water extraction of the HPA, which is water soluble, after water vapor treatment. Thermalgravimetry data suggested enhanced stability of the sulfonate groups and better mechanical strength with lower water absorption relative to the non-composite membranes. This data, coupled with the FTIR band shifts of the sulfonic acid groups and tungstic oxide groups, indicated a strong specific interaction between the HPA molecules and the sulfonic acid moieties. An increase in proton conductivity for the composite membranes was also observed at elevated temperatures under pressure. A BPSH membrane with 40% disulfonation and 30 weight percent HPA additive produced conductivities of 0.08 S/cm at room temperature and 0.15 S/cm at 130 °C under pressure at 100% relative humidity. For comparison, the unfilled membranes showed conductivities of 0.07 S/cm at room temperature and only 0.09 S/cm at 130 °C in similar conditions. Furthermore, FTIR was used to observe the dehydration of the pure membranes and the composite membranes dynamically at increasing temperatures. It was noted that the composite membranes had an increase in water retention at temperatures from 100 °C to 280 °C. These results suggested that the HPA composite membranes would be good PEMs for high temperature fuel cells operating at 120 °C by aiding in water retention, which is directly responsible for proton conductivity through specific water transport mechanisms.

Polybenzimidazole (PBI) has also been used as the matrix material for phosphotungstic acid filled membranes.³³³ In this research, the PBI was not sulfonated and served primarily as the film-forming host for a PEM. Therefore, the only protonically conductive material in the membrane was the HPA. Since HPA and PBI were soluble in DMAc, solution cast films were produced that had 60 weight percent of

³³³ Staiti, P.; Minutoli, M.; Hocevar, S. *J. Power Sources*, 2000, 90, 231.

HPA. Thermogravimetric analysis indicated very good thermal stability reaching temperatures of 400 °C. The conductivity values were relatively low at 0.0014 S/cm at 150 °C in 100% relative humidity. This low conductivity could be due to a decrease in proton movement across the membrane from HPA to HPA molecule without any sulfonated matrix. If the membrane was to be sulfonated, proton movement would presumably be increased, however, degradation of the PBI could occur due to hydrolysis from the sulfonic acid moieties.

Layered zirconium hydrogen phosphonates incorporated into ionic containing polymers have recently been investigated by Alberti et al³³⁴ in Italy. They have used both sulfonated PEEK and Nafion[®] as the ionically conductive matrix for composite MEAs. These types of inorganic fillers are themselves protonically conductive and are not water soluble. Therefore, the leaching out of the inorganic filler might be decreased in hydrated environments, which would afford better stability and longevity in the fuel cell environment. This research group has also used an inorganic material based on titanium phosphate that has recently been shown to have the highest proton conductivity of all the studied layered phosphonates.^{335,336} It was noted that the incorporation of the inorganic filler showed heterogeneity at values above 20 weight percent filler in Nafion[®] recast membranes. Lower weight percents of the layered titanium fillers were used and showed increased conductivities relative to the unfilled polymers

PEMs based on Nafion[®] are limited to membrane performance below 80 °C presumably due to a thermal transition of the hydrated form and loss of water. The

³³⁴ Alberti, G.; Casciola, M. and Palombari, R. *J. Membr. Sci.*, 2000, 172, 233.

³³⁵ Alberti, G.; Constantino, U.; Casciola, M.; Ferroni, S.; Massinelli, L. and Staiti, P. *Solid State Ionics* 2001, 145, 249.

³³⁶ Alberti, G. and Casciola, M. *Annu. Rev. Mater. Res.*, 2003, 33, 129-154.

polyperfluorinated sulfonic acid membranes are the state-of-the-art PEMs used for both hydrogen and methanol fuel cells.³³⁷ However, some specific limitations exist for Nafion™-type membranes, which include low conductivity at high temperatures and low humidity as well as high methanol permeability that decreases fuel efficiency.³³⁸ A novel approach³³⁹ could involve the use of heteropolyacids (HPA) as an additive for compatible sulfonated hydrocarbon polymers. Many HPAs have high proton conductivities but are also water-soluble. HPA composite membranes based on polymers that have a high affinity for the HPA additive can, in principle, make the HPA complex insoluble in water while still retaining high proton conductivity at elevated temperatures.

This report illustrates the synthesis and characterization of phosphine oxide containing aromatic ether terpolymers and fabrication of composite membranes. By dissolving inorganic heteropolyacids in a dipolar solvent and blending the solution with dissolved ionic polymeric materials, composite membranes that aid in proton conductivity at high temperatures were solution cast. The HPAs, in the crystalline form, were protonically conductive inorganic fillers that have a strong interaction with specific functional groups in the polymeric material. The present research employs phosphotungstic acid hydrate as an inorganic filler incorporated into 45 mol% disulfonated poly(arylene phenyl phosphine oxide ether sulfone) terpolymers synthesized using nucleophilic aromatic substitution reactions for use in PEM fuel cells at temperatures above 100°C. The disulfonation level was held constant at 45 mole percent

³³⁷ M. A. Hickner, H. Ghassemi, Y. S. Kim, B. R. Einsla and J. E. McGrath, *Chem. Rev.* 2004, 104, 4587-4612.

³³⁸ M. Mathias, H. Gasteiger, R. Makharia, S. Kocha, T. Fuller, T. Xie and J. Pisco, Preprints of Symposia - American Chemical Society, Division of Fuel Chemistry 2004, 49(2), 471-474.

³³⁹ Kim, Y.S., Wang, F., Hickner, M., Zawodzinski, T. A. and McGrath, J. E. *J. Membrane Sci.*, 2003, 212, 263-282.

so as to more fully understand the effects of phosphine oxide incorporation while still providing adequate conductivity for fuel cell characterization. The possible specific interactions present in the 45 mol% disulfonated BPSH-PPO/HPA composite films that retain the water-soluble HPA molecules in the organic soluble PEM are shown in Figure 7.4. The specific interactions in the composite membranes aid in decreasing extraction values of the HPA in aqueous environments thus allowing very little, if any, leaching of the ionically conducting HPA.

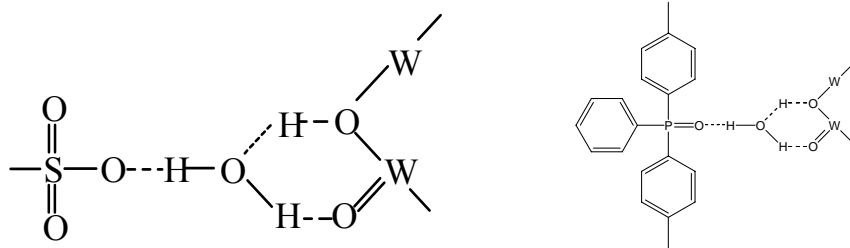


Figure 7.4 Possible Interactions of HPA with Sulfonate and Phosphine Oxide Moieties

7.2 Experimental

7.2.1 Materials

The 4,4'- bis(fluorophenyl) phenyl phosphine oxide (BFPPPO) was synthesized following a reported procedure.³⁴⁰ Anhydrous potassium carbonate and 4, 4' - difluorodiphenylsulfone (DFDPS) were obtained from Aldrich. NMP and toluene (both from Burdick and Jackson) were dried as follows: NMP was dried overnight over calcium hydride with a nitrogen purge and distilled at reduced pressure; toluene was

³⁴⁰ Riley, D. J., *PhD. Dissertation*, VPI & SU, 1997.

dried over molecular sieves. Disulfonation of DFDPS was performed in a similar fashion as previously described to prepare 3,3'-disulfonate-4,4'-difluorodiphenylsulfone.³⁴¹

Phosphotungstic acid hydrate was obtained from Fluka Chemika and dried at 80°C for 24 hours before use.

7.2.2 Synthesis of Disulfonated Poly(arylene ether phenyl phosphine oxide sulfone)

Terpolymers

Typical terpolymerizations of SDFDPS, DFDPS, BFPPPO and biphenol were conducted in a flame dried three-necked flask. The flask was fitted with a nitrogen inlet, thermocouple sensor, over-head stirrer and Dean Stark trap fitted with a condenser. After charging all the monomers and solvents, the reaction flask was heated in an oil bath to 150 °C, and the toluene was allowed to reflux for 4 hours to remove any water present from the hydrated atmosphere or hydrated monomers. The toluene was then removed over a 60-minute time interval. The Dean Stark trap was emptied and the reaction temperature was slowly increased to 180 °C for 16 hours. By the end of the reaction, the solution media became very viscous. The reaction mixture was diluted and hot filtered at 150 °C using a Buchner funnel to remove the by-product (salt, KF). The isolated filtrate was slowly poured into a 50-fold excess of isopropanol to precipitate the copolymer. The fibrous precipitate was collected by filtration and washed with isopropanol and water to aid in the removal of salts. It was dried under vacuum at 80 °C for one hour, then at 100 °C for 15 hours. The degree of phosphine oxide incorporation was controlled by varying the charging ratio of BFPPPO to DFDPS (Figure 7.5).

³⁴¹ Wiles, K. B.; Munoz, C. M. and McGrath, J. E. *Polymer Preprints*, **2004**, 45(1), 724.

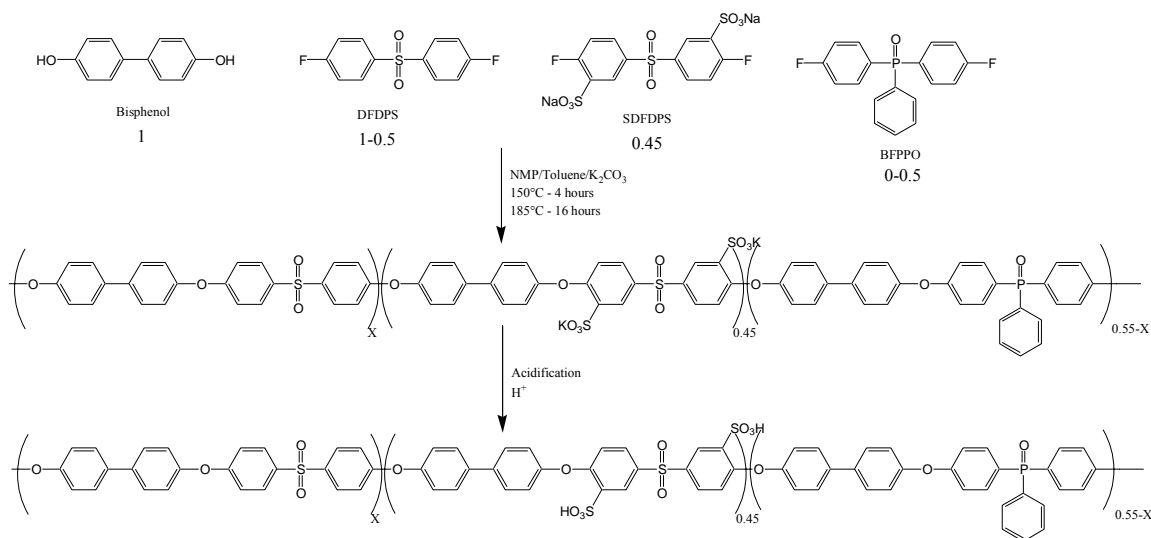


Figure 7.5 Synthesis of Disulfonated Poly(arylene phenyl phosphine oxide ether sulfone) Terpolymers

7.2.3 Membrane Preparation

The potassium salt films were prepared by first redissolving the fibrous copolymer in dimethylacetamide (DMAc) and then by filtering the solution through a 0.45 μm TeflonTM syringe filter thereby directly casting the solution into a glass-casting tray. The glass tray had side-walls so as to aid in membrane thickness control. The copolymer solutions were dried in a vacuum oven by slowly increasing the temperature settings from 50 °C for 4 hours to 80 °C for 4 hours to 100°C for 12 hours and finally for 120 °C for 4 hours. Careful leveling of the glass casting tray provided uniform films. Addition of water to the casting tray swelled the membranes and allowed them to be easily removed. The salt form membranes were then transformed into the acid form using a boiling (~100 °C) technique in 0.5 M sulfuric acid in water for two hours. The residual sulfuric acid was removed by boiling in water for another 2 hours. All the neat

membranes tested were acidified using this high temperature acidification treatment so as to appreciably change the morphological characteristics of the resulting acidified membranes through possible reorganization of the sulfonate moieties producing ion clusters and channels.³⁴²

7.2.4 Composite Membrane Fabrication

Transparent, tough and ductile films were prepared by solution casting the acid form of 45% disulfonated co- and terpolymers (5 wt%) having various amounts of phosphine oxide moieties and the semi-crystalline form of phosphotungstic acid (Fluka Chemicals) dissolved in DMAc and mixed overnight. Prior to dissolution in DMAc, phosphotungstic acid (PTA) was dried at 100 °C in a convection oven for 16 hours (water molecules per HPA ~ 6). The casting conditions were the same as the neat membranes on glass trays as described above. Various phosphine oxide levels of 45% disulfonated terpolymers produced a family of phosphotungstic oxide containing composite membranes (BPSH45-PPO 0-50). The weight ratio of HPA to disulfonated terpolymer was typically 30 weight percent. All the resulting membranes were transparent with a slight yellow color similar to the neat membranes.

³⁴² Y. S. Kim, F. Wang, M. A. Hickner, S. McCartney, Y. T. Hong, W. L. Harrison, T. A. Zowadzinski and J. E. McGrath, *J. Polym. Sci.: Part B: Polym. Phys.* 2003, 41, 2816.

7.2.5 Acidification and HPA Extraction of Composite Membranes

The composite membranes were tested after reacidification using Method 1 or Method 2 acidification techniques. Method 1 reacidification of the composite membranes was performed at room temperature using a 1.5 M sulfuric acid solution in water. The copolymer composite membranes were submersed in the slow stirring solution for 24 hours and then rinsed with deionized (D. I.) water. Residual sulfuric acid was removed from the membranes by allowing them to be submersed in slow stirring D. I. water for another 24 hours while changing the water every 6 hours. A thorough and final rinsing removed the last traces of sulfuric acid. This room temperature reacidification produced what will now be termed Method 1 (M1) composite membranes. Method 2 reacidification of the composite films employed boiling (~100 °C) conditions in 0.5 M sulfuric acid in water for two hours. After a thorough rinsing, the residual sulfuric acid was removed by boiling in water for another 2 hours. A final rinse produced what will now be termed Method 2 (M2) composite membranes. HPA extraction was measured by the difference in weight before and after reacidification of the dry composite membranes divided by the original weight.

7.2.6 Fourier Transform Infrared Spectroscopy (FTIR) and Proton/Phosphorous Nuclear Magnetic Resonance (NMR)

Absorbance mode FTIR spectra of the neat and composite thin films were obtained using a Nicolet Impact 400 FTIR spectrophotometer fitted with a ceramic heating cell. Peak shift experiments were performed using vacuum dried thin films at a

temperature of 120 °C. The resolution of all the spectra was constant at 2 cm⁻¹. The average of 48 scans was reported. Proton and phosphorous NMR spectra were obtained with a JEOL 500 MHz spectrometer using DMSO-d₆ as solvent (5% w/v polymer solutions).

7.2.7 Water Uptake

The water absorption of the composite membranes and neat copolymers was accomplished by using weight-difference calculations. The acidified films were dried in a vacuum oven at 100 °C for 24 hours and weighed. They were then immersed in deionized water at room temperature for 24 hours at which time they were removed from the water, blotted dry and weighed again. A final drying in vacuum at 100 °C for 24 hours was performed at which time the samples were then weighed. Weight gain based on the dry weight was recorded using an average of three membranes per type of film. No measurable loss was observed from the first-dry weight to the second-dry weight, thereby suggesting no HPA extraction for either of the M1 or M2 composite membrane series during water uptake experiments.

7.2.8 Intrinsic Viscosity (IV) Measurements

IV data were calculated using the extrapolated values to zero concentration of the averages of the reduced and inherent viscosities. Characterization of molar mass after

polymerizations was monitored by intrinsic viscosity measurements using NMP at 25 °C and a Cannon Ubbelohde viscometer.

7.2.9 Gel Permeation Chromatography (GPC)

Gel permeation chromatography determined the molecular weights using a Waters 1515 isocratic HPLC pump, Waters Autosampler and Waters 2414 refractive index detector calibrated using narrow molecular weight distribution polystyrene standards. The oven temperature of the column set containing two Styragel HT 6E and one Styragel HT 3 was constant at 60 °C. N-methylpyrrolidone containing 0.05 M LiBr with a 1.0 mL/min flow rate was used as the mobile phase.

7.2.10 Proton Conductivity at High Temperatures and Low Humidities

Ionic conductivity was measured using a Hewlett Packard 4192 Impedance/Gain Phase Analyzer over a frequency range of 10Hz-1MHz.³⁴³ The resistance of the films was taken at the frequency which produced the minimum imaginary response. The ionic conductivity of the membranes was calculated from the measured resistance and the geometry of the cell. High temperature conductivity data was attained in a convection oven fitted with a deionized water humidification steam generator and a hygrometer to measure relative humidity on a dynamic scale (Figure 7.6). The temperature was controlled by an oven thermocouple placed directly next to the conductivity cell. The membranes were allowed to equilibrate for four hours before testing.

³⁴³ T. A. Zawodzinski, M. Neeman, L. O. Sillerud and S. J. Gottesfeld, Phys. Chem. 1991, 95, 6040.

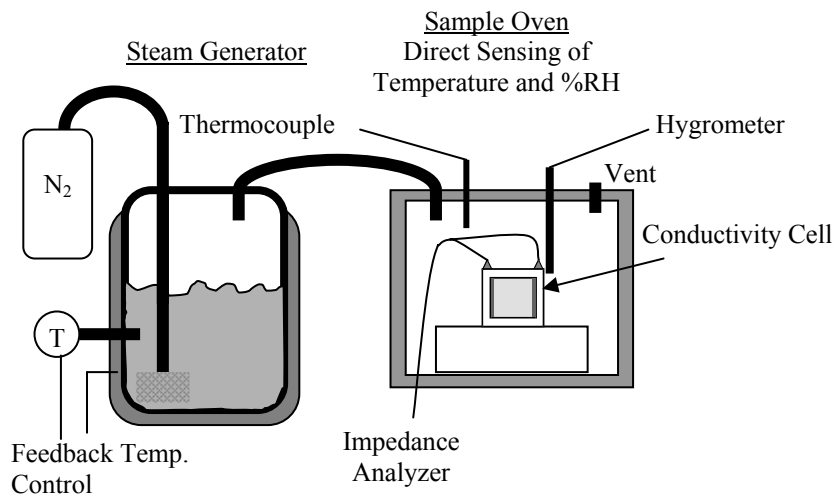


Figure 7.6 Schematic of Conductivity Measurement Apparatus for use at Elevated Temperature and Reduced Relative Humidity at Atmospheric Pressure

7.2.11 Hydrogen/Air Fuel Cell Performance

Fuel cell performance was obtained using a Fuel Cell Technologies Test Station operating up to 10 Volts at 50 Amps and 60 Watts. A Hewlett Packard load box with a computer interface was used to monitor voltage, current and resistance of 5 cm^2 membrane electrode assemblies. Catalyst loadings and weight percent of ionomer were held constant for all samples at 0.2 mg/cm^2 using 20%Pt on Vulcan carbon and 28.5wt% N1100 in both anode and cathode electrodes respectively. Catalyst inks contained Nafion (5% dispersion in alcohols), Glycerol and 20% Pt supported on carbon black. The formulations obtained a 2.5:1 ratio of platinum catalyst to Nafion. The ink was stirred and sonicated to promote even dispersion of the Pt/C particles. The Nafion dispersion and platinum supported on carbon were obtained from Electrochem Inc. and the glycerol

from Aldrich. Electrode decals were fabricated using Teflon reinforced with glass fiber backing layers. The catalyst ink was painted layer-by-layer onto the decals using a high quality brush. Uniform electrodes were dried after every coat of ink at 130 °C for ten minutes. After the correct loadings were obtained by calculating the difference between the decal backing layer and the electrode decal, the prefabricated electrodes were dried overnight at 130 °C to remove any residual glycerol and alcohols. Membrane electrode assemblies (MEAs) were produced by placing a salt form membrane between two electrode decals and hot pressing at 210 °C and 3000 psi for a total of 8 minutes. The MEAs were then acidified using either M1 or M2 acidification techniques. After building the single 5 cm² cell using the Fuel Cell Technologies Inc. hardware, conditioning of the cell was performed using a life time test at 0.5 Volts at 80 °C and 100 %RH. After the current density reached a plateau, voltage-current-resistance experiments were conducted.

7.3 Results and Discussion

7.3.1 Synthesis and Characterization of Phosphine Oxide Containing Terpolymers

The terpolymer synthesis involved condensing a specific amount of disulfonated activated dihalide, non-sulfonated activated dihalide, BFPPPO and biphenol in NMP and toluene, which was used as an azeotroping agent to remove any water.

Terpolymerizations were necessarily conducted using the disulfonated sodium salt form of SDFDPS. However, by using potassium carbonate as the base, ion exchange of the

sodium and the potassium ions occurred, thereby producing potassium salt form terpolymers. The disulfonated potassium salt form polymers were then transformed into the acid form by using the boiling technique described in the experimental section. As expected, a significant increase in water sorption was observed relative to the unsulfonated control type polymers, especially in the acid form.

Molecular weight was determined by intrinsic viscosity in NMP at 25 °C and gel permeation chromatography using NMP+0.5M LiBr at 60 °C relative to narrow molecular weight polystyrene standards. Table 7.1 indicates the molecular weights and intrinsic viscosities for a series of terpolymers that contain 2, 10, 20, 30, 40 and 50 mol% BFPPPO in the terpolymer backbone. The level of disulfonation was held constant at 45 mole percent. BPSH45 was used as the control copolymer containing no phosphine oxide moieties. The number average molecular weights, as determined by GPC, ranged from 53,000-84,000 g/mol indicating appreciable film forming characteristic molecular weights. The polydispersity (PDI) values, which were at or below 2.0, signified good polymerization conditions were obtained relative to typical step growth and condensation reaction PDI values. The intrinsic viscosities ranged from 1.0-1.2 dL/g suggesting similar molecular weights throughout the entire series of polymers.

Table 7.1 Molecular Weight Characterization of BPSH45 and BFPPPO Containing BPSH45

POLYMER	Intrinsic Viscosity (NMP @ 25°C) (dL/g)	GPC (NMP+LiBr); Polystyrene Standards		
		Mn(g/mol)	Mw(g/mol)	PDI
BPSH45	1.01	55K	102K	1.9
BPSH45/2%BFPPPO	1.0	53K	98K	1.9
BPSH45/10%BFPPPO	1.2	69K	120K	1.7
BPSH45/20%BFPPPO	1.0	67K	125K	1.9
BPSH45/30%BFPPPO	1.01	84K	171K	2.0
BPSH45/40%BFPPPO	1.0	83K	156K	1.9
BPSH45/50%BFPPPO	1.02	84K	161K	1.9

7.3.2 Monitoring Polymerizations Using FTIR and NMR

Fourier transform infrared spectroscopy was used to monitor the reaction products to identify the increasing amounts of phosphine oxide incorporation. Figure 7.7 indicates the FTIR spectra of a series of thin film terpolymers as compared to BPSH45. It was observed that the peak at 1115 cm^{-1} corresponded to the pendant phenyl ring stretching that was covalently bound to the phosphorous atom in the backbone. As the amount of BFPPPO increased in the reaction solution, the isolated terpolymer peak intensity at 1115 cm^{-1} increased. Synthetically, BFPPPO monomer replaced the DFDPS monomer in the reaction mixture thereby decreasing the amount of DFDPS as the amount of BFPPPO increased. This was observed in the thin film FTIR spectra for the peak at 1150 cm^{-1} that corresponded to the sulfone peak in the non-disulfonated repeat units. As the amount of BFPPPO increased from 0% to 50%, the peak intensity of the non-disulfonated sulfone

monomer decreased. The increase and decrease of the phenyl phosphine oxide and non-disulfonated sulfone moieties indicated good incorporation of the BFPPPO monomer in the backbone of the terpolymers.

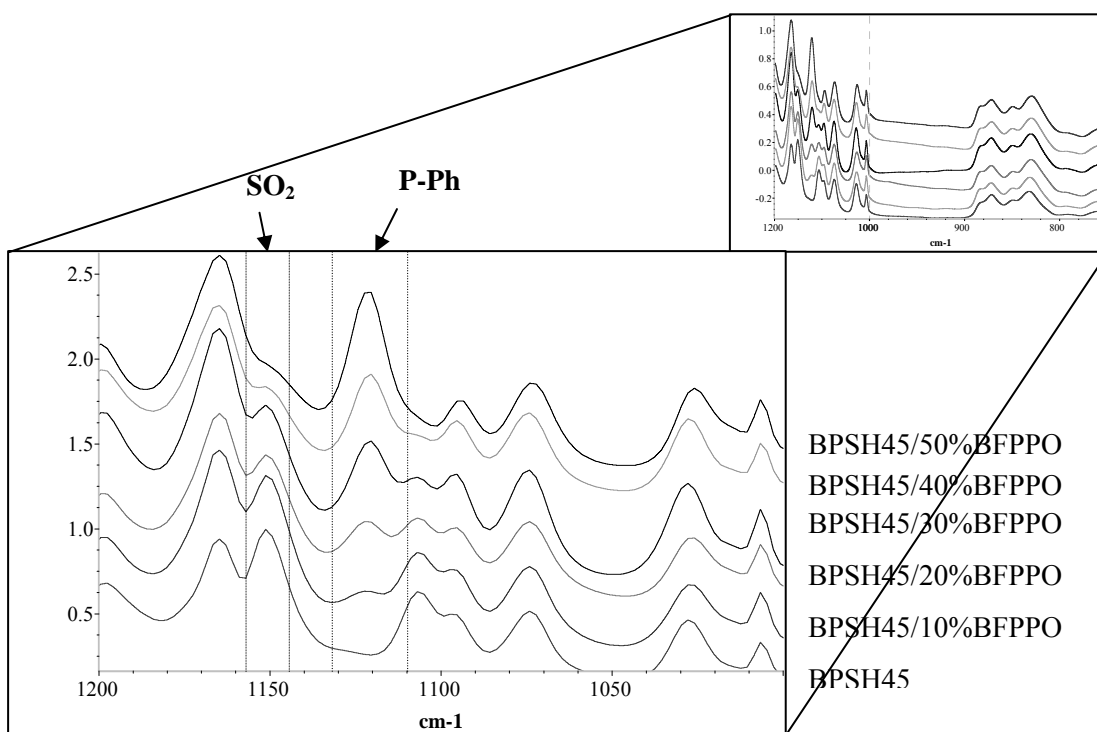


Figure 7.7 Thin Film FTIR of Poly(arylene ether phenyl phosphine oxide sulfone) Terpolymers and BPSH45

Proton nuclear magnetic resonance was used to further characterize the incorporation of BFPPPO in the backbone architecture. Figure 7.8 indicates the ^1H NMR spectra of a series of terpolymers containing increasing amounts of BFPPPO monomer incorporated into the polymer architecture. Characteristic peaks at 7.6 and 7.7 ppm indicated the increasing amounts of protons associated with the phenyl pendant ring and aryl rings next to the phosphorous atom respectively as the amount of BFPPPO increased in the reaction solution. The loss in peak intensity at 7.9 ppm was determined to be

associated with the protons on the phenyl rings next to the non-disulfonated sulfone repeat unit. Coupling these observations with the FTIR observations revealed successful incorporation of the BFPPPO monomer while at the same time decreasing the amount of non-sulfonated sulfone monomer in the backbone architecture.

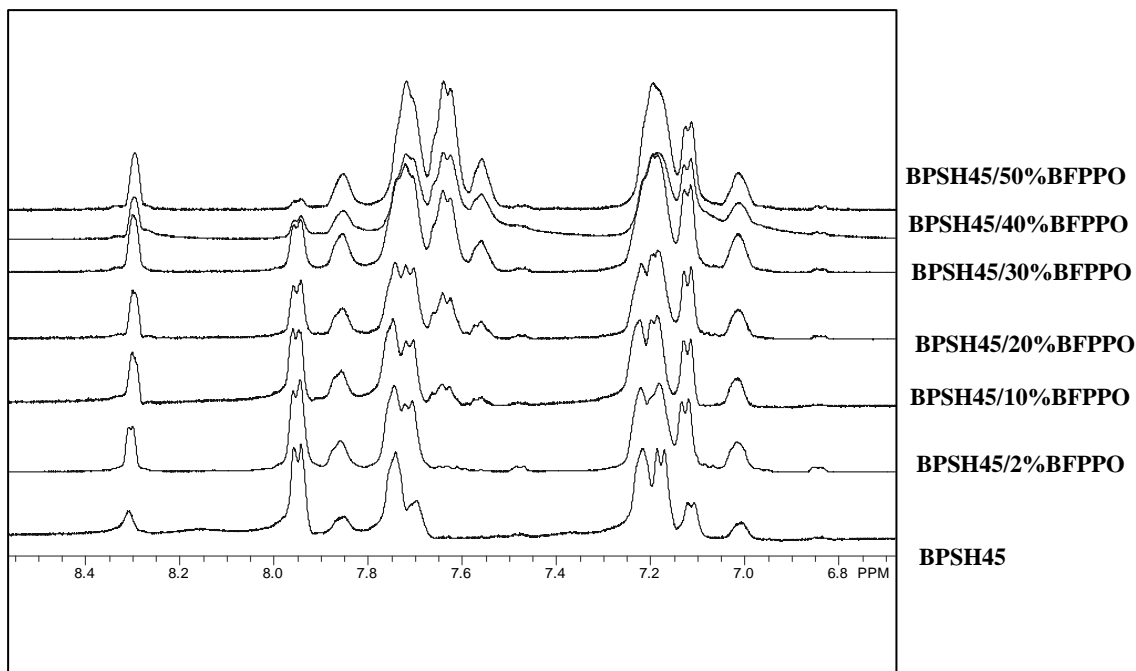


Figure 7.8 Proton NMR of Poly(arylene ether phenyl phosphine oxide sulfone) Terpolymers and BPSH45

7.3.3 Water Uptake Measurements of BFPPPO Containing Terpolymers

After careful drying to remove residual solvent, the cast membranes were transformed into the acid form by a high temperature, boiling method for two hours using 0.5 M sulfuric acid in water (Method 2) or a room temperature method using 1.5M sulfuric acid for 24 hours (Method 1). After acidification, the Method 2 membranes were

boiled in deionized water for two hours, while the Method 1 membranes were slowly stirred in deionized water for 24 hours to remove any residual acid and rinsed thoroughly. Water was removed from the membranes using a vacuum oven for 24 hours at 100 °C. The dry membranes were weighed and then immersed in water for 24 hours to allow water sorption equilibration and then weighed again. The difference in weight from the dry form to the hydrated form divided by the dry weight determined the percent water uptake. Figure 7.9 indicates the water uptake percentages as a function of the amount of BFPPO incorporation into the backbone architecture for both acidification techniques. The initial rise in water sorption was assumed to be due to an affinity of the phenyl phosphine oxide (PPO) moieties for water, while the drop in water sorption at higher amounts of PPO moieties was due to the complex formation of the phosphine oxide groups with the sulfonate moieties.

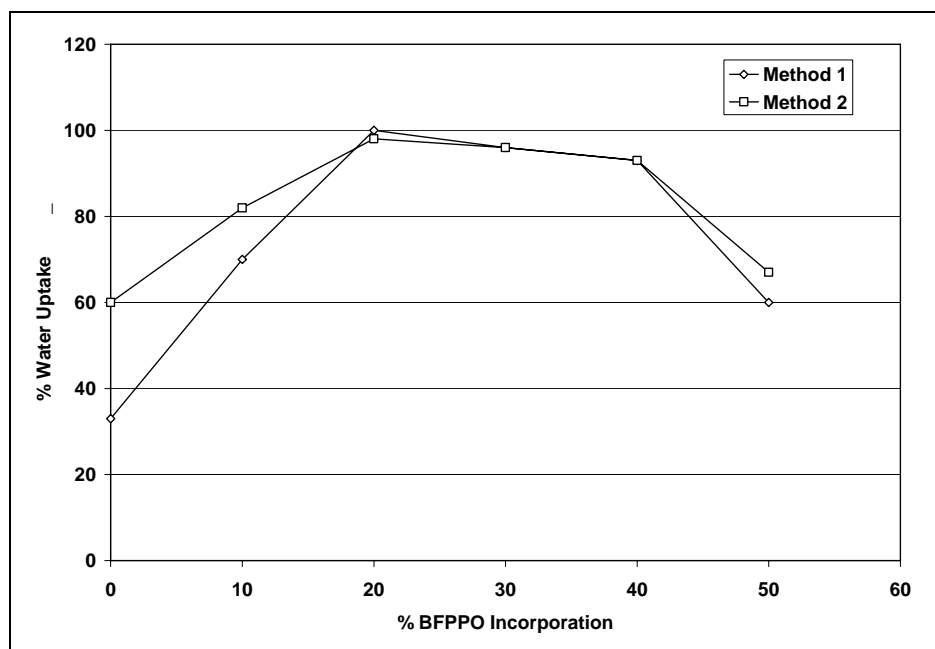


Figure 7.9 Water Uptake of M1 and M2 Series of PPO Containing Terpolymers

7.3.4 Specific Interactions of Phosphine Oxide and Heteropolyacid

Composite membranes were solution cast from high molecular weight acid form BPSH45 and BPSH45-PPO co- and terpolymers and 30 weight percent of phosphotungstic acid (PTA) inorganic filler. The acid form rather than the salt form terpolymers were used to promote proper hydrogen bonding and polar interactions between the sulfonate and acid groups on the PTA molecules. Specific interactions in the disulfonated terpolymer-PTA composite membranes are extremely important so as to positively influence the dispersion and miscibility of the PTA particles in the copolymer matrix. The extremely polar phosphine oxide moieties also allowed specific interactions through dipole complex formation. The complex of PTA particles to the polymer

backbone and pendant sulfonate groups aids in retaining the water soluble inorganic additive in humidified conditions. The composite membranes were removed from the glass trays reacidified using M1 or M2.

The proposed interactions were characterized using thin film FTIR spectroscopy that focused on one specific frequency range. The 1020-1090 cm^{-1} range contained the symmetric stretching regions of the SO_3 moieties and the sulfonated aryl rings. Figure 7.10 displays the spectral regions of the neat and composite membranes using a representative BPSH45 copolymer, BPSH45-50%PPO and BPPO45-50%PPO containing 30, 45 and 60 wt% PTA. All of the FTIR spectra were recorded at 120 °C after drying the films in vacuum at 100 °C for 24 hours so as to remove the possibility of dissociated water molecules at lower temperatures affecting the characteristic bands. The region from 1110-1130 cm^{-1} was assigned to the phosphine-phenyl moieties, which seemed to be unaffected by the incorporation of PTA. The symmetric stretching of SO_3 was observed at 1029 cm^{-1} in pure BPSH45 and shifted to 1025 cm^{-1} for the PPO containing thin films. This red shift of the sulfonate band indicated an attraction of the sulfonate with the PPO groups. The affect of chain architecture on the addition of PTA was observed by the shift in the peak of BPSH45-50%PPO at 1025 cm^{-1} to 1031 cm^{-1} in the composite membrane containing 60 wt% PTA. The gradual peak shift that was observed for the increasing amounts of PTA molecules was determined to be due to the complex formation of the sulfonate groups with the acid moieties on the PTA. Further evidence for sulfonate-PTA complex formation was noted at 1075 cm^{-1} . Peak shifts from 1075 cm^{-1} to 1082 cm^{-1} for the symmetric stretching of the aryl ring covalently bound to the

sulfonate group further indicated the change in polymer architecture by complex formation.

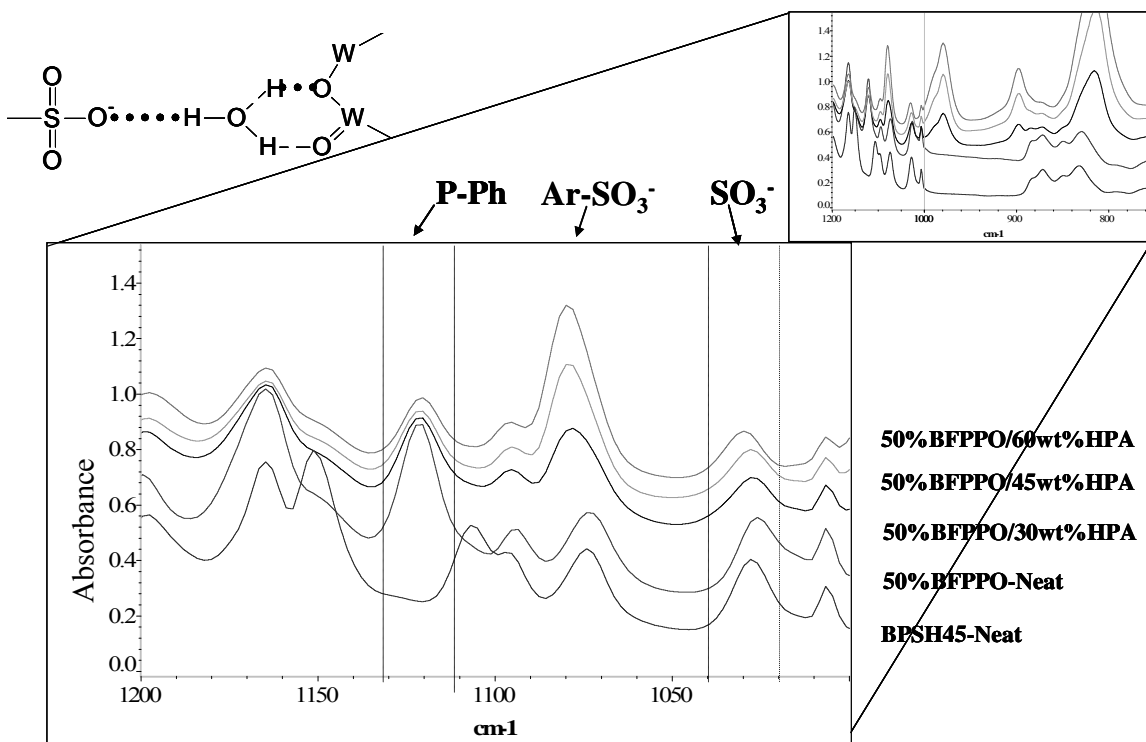


Figure 7.10 FTIR Spectra Indicating Band Shifts Associated with Sulfonate-PTA Complex

Complex formation of the PTA molecules with the phosphine oxide moieties was probed using ^{31}P NMR. Figure 7.11 indicates the phosphorous peak at 24.75 ppm associated with neat terpolymer material (BPSH45+50%PPO) and a peak shift to 24.88 for the composite materials containing 30, 45 and 60 wt% PTA. This phosphorous peak shift indicated strong interactions associated with the PTA molecules and PPO moieties for all levels of PTA incorporation. This strong PTA-PPO complex formation was hypothesized to retain the water soluble PTA particles in fully hydrated environments similar to those in a proton exchange membrane fuel cell.

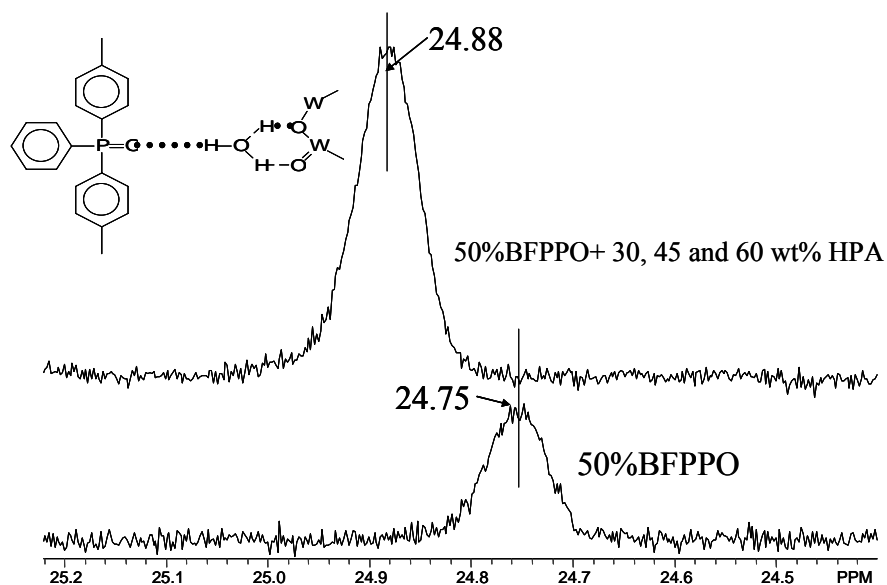


Figure 7.11 Phosphorous 31 NMR Indicating Peak Shift of Backbone Phosphorous Moiety with 30, 45 and 60 wt% PTA Inorganic Additive

7.3.5 Water Uptake of Composite Membranes Using Various Acidification Techniques

The water uptake is generally known to play an important role on proton conductivity and mechanical properties in a fuel cell environment.³⁴⁴ As the water uptake increases, the solvation state of the sulfonate groups also increases, which, in turn, produces high proton conductivity. However, enhanced water uptake produces poor mechanical strength materials when cycled through high and low relative humidity environments. Some materials loose all physical properties due to hydragel formation. Others contain stresses that are produced between the electrodes and membrane that

³⁴⁴ Zawodzinski, T. A., Springer, T. E., Davey, J., Jestel, R., Lopez, C., Valeria, J. and Gottsfeld, S. J. *Electrochem. Soc.* 140, 1981, 1993.

become large with increasing water sorption thereby producing delamination and performance loss. As can be observed in Figure 7.12 that shows water uptake versus mole percent BFPPPO content for composite membranes containing 30 wt% PTA, water sorption of the reacidified films using method 2 acidification obtained the highest water uptake values. The composite films that were reacidified using M1 or M2 and having more than 10%PPO moieties indicated water management was enhanced in the composite films relative to the neat films as shown in Figure 7.9. The membranes that contained less than 10%PPO groups had higher water uptakes relative to the neat membranes presumably due to the PTA extraction that occurred during reacidification; extraction will be probed in the following section. Interestingly, these results suggested that the PTA in the composite films decreased the overall water sorption. This is interpreted as being due to two different mechanisms. First, the membranes were dried in a vacuum oven after submersion in liquid water where, presumably all the water was removed. However, it was believed that the removal of the strongly hydrogen bonded water molecules in the composite membrane was incomplete due to the strong interactions with the sulfonate, PPO and PTA molecules. Second, since the number of water absorption sites decreased in the composite membranes due to the strong complex formation of sulfonic acid groups with the PTA molecules and PPO moieties, lower water amounts were reversibly absorbed. The initial rise in water uptake of the PTA composite membranes was primarily due to an affinity of the phenyl phosphine oxide (PPO) moieties for water, while the drop in water sorption at higher amounts of PPO moieties was due to the complex formation of the phosphine oxide groups with the sulfonate moieties and PTA molecules.

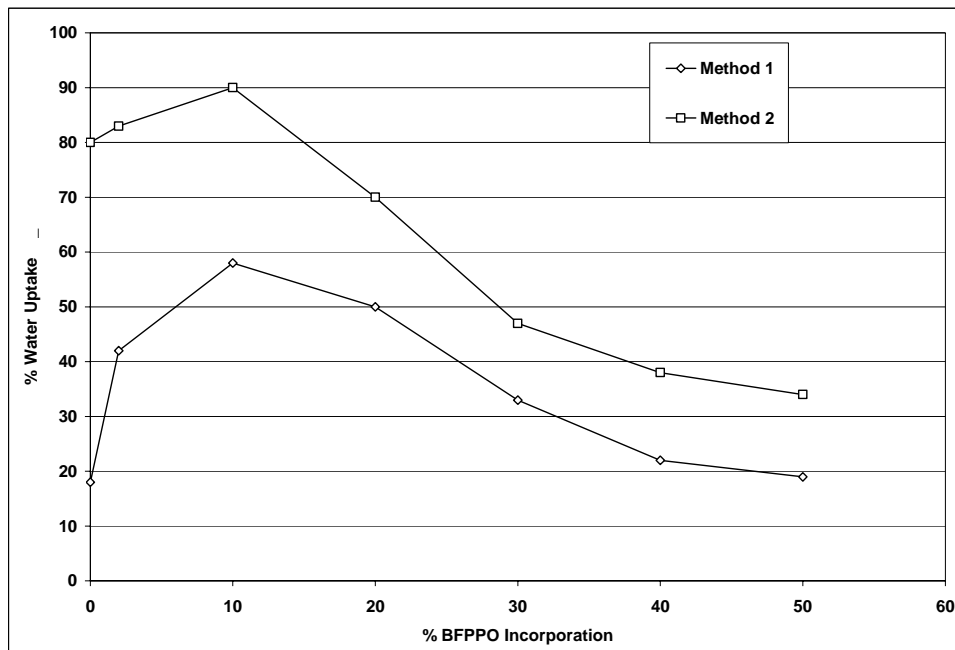


Figure 7.12 Influences of PPO Content and PTA Inorganic Filler (30 wt%) on Water Uptake of Composite Membranes

7.3.6 Extraction of the PTA in Composite Membranes

Retention of the PTA inorganic particles was presumed to be one of the primary parameters that control chemical properties leading to good conductivity values and durable lifetimes. If low affinity between the PTA and disulfonated copolymers was a characteristic of the composite membrane, the PTA material, which is water soluble, would be easily extracted from the film in the presence of water. This would undoubtedly decrease the proton conductivity and durability by creating voids and possibly pin-holes in the membrane. Figure 7.13 indicates the extraction of the inorganic filler in the composite membranes that were loaded with 30 weight % PTA before reacidification. The difference in weight from before and after reacidification was

divided by the total weight of PTA before extraction. The M2 reacidification technique extracted the largest amount of PTA while the room temperature extraction of the M1 films indicated that very little PTA was removed. The rigorous environment at boiling temperatures and the increase in water swelling using M2 acidification were the primary reasons for the loss of PTA molecules during the M2 reacidification technique. At these temperatures, the thermal energy available for PTA dissolution from the complex with the sulfonate and phosphine oxide moieties was high enough so as to extract the water soluble additive. This created porous structures indicative of foam sponges which increases water sorption for the lower %PPO containing materials thereby extracting the highest amounts of filler. However, at higher levels of PPO content (20-50%PPO), PTA extraction was lowered due to the strong interactions of the PPO groups and PTA molecules. This is evidenced by the decrease in PTA extraction as the percent of phosphine oxide incorporated into the terpolymer structure was increased from 10% to 50%.

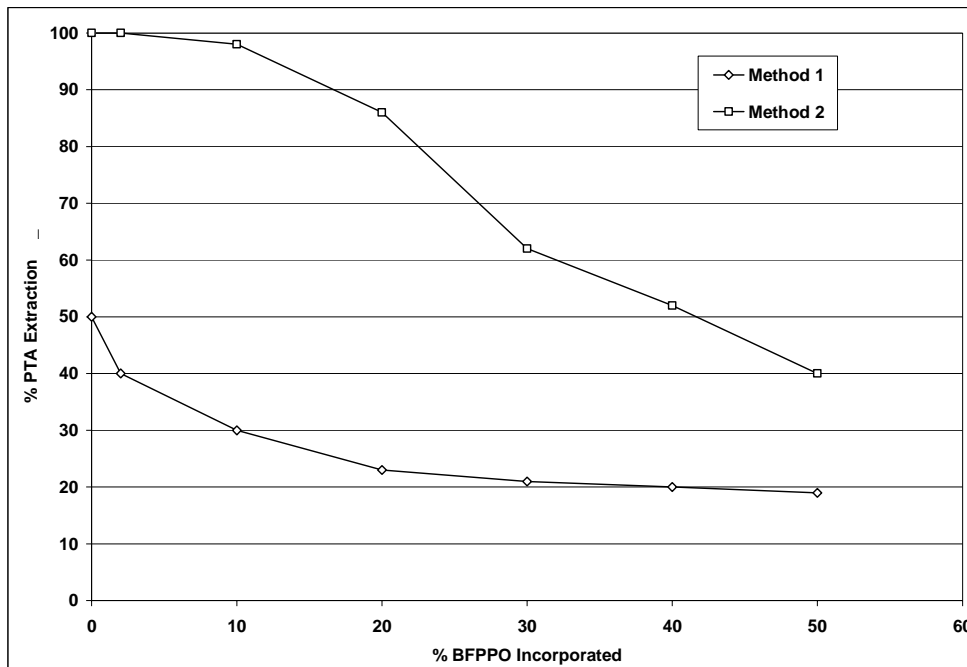


Figure 7.13 Extraction of Phosphotungstic Acid as a Function of Reacidification Technique and BFPPPO Content

7.3.7 Proton Conductivity at 120 °C in 45% Relative Humidity

Proton conductivity experiments were performed in an apparatus similar to the one shown in Figure 7.6 after equilibration for four hours. Table 7.2 indicates the conductivity performance at 120 °C in 45% relative humidity under atmospheric pressure for the neat and composite membranes. These experiments were meant to imitate a fuel cell environment where humidified gases and low hydration due to atmospheric pressure and high temperatures create rigorous conditions. At all levels of BFPPPO content, the M1 composite membranes containing an initial charging of 30 weight percent of PTA showed enhanced proton conductivity relative to neat polymers at temperatures above the boiling point of water where little relative humidity was present. This increase in

conductivity performance relative to the pure unfilled copolymers suggested higher amounts of water retention at temperatures above the boiling point of water than the pure copolymers that would rapidly dehydrate, thereby decreasing proton transport characteristics.

Table 7.2 Conductivity at 120°C and 45% R.H. and Water Uptake of Neat and Composite Membranes as Compared to 45mol% Copolymer Control Containing No PPO Moieties

Membrane	M2 Conductivity (mS/cm) Neat Polymer	% H ₂ O Uptake Neat Polymer	M1 Conductivity (mS/cm) With 30wt%HPA	%H ₂ O Uptake of Composite M1
BPSH 45	11	50	14	35
10% PPO	9	80	21	58
20%PPO	3.3	95	20	50
30%PPO	3.1	90	15	35
40%PPO	3	88	10	28
50%PPO	2.9	65	7	20

7.3.8 Hydrogen/Air Fuel Cell Performance

Membrane electrode assemblies were fabricated using electrode decals containing Nafion 1100 ionomer. The Pt loadings and the weight percent Nafion ionomer in the anode and cathode electrodes were held constant at 0.2 mg/cm² and 28.5% respectively. The 3 mil (75 micron) thick membranes were hot pressed at 210 °C using 3000 psi of pressure for eight minutes. The membrane electrode assemblies were then assembled into a single cell having 5 cm² of active catalyst area. Conditioning and wet-up of the cell was performed at 0.5V until the current density leveled, typically around 4 hours.

Series of voltage- current-resistance curves were performed at 80 °C in 100 % RH and 20 psig and at 120 °C in 50% RH and 20 psig.

The fuel cell performance of BPSH45, BPSH45+20%PPO and BPSH45+50%PPO membrane electrode assemblies at 80 °C, 100% RH and 20 psig are shown in Figure 7.14. These sets of experiments were designed to mimic the actual fuel cell conditions of stationary power applications used for private residence and business applications. The kinetic region of the curve (1-0.8V) indicated the electrode performance, which is dominated by electrode kinetics. The performance of the electrodes was best for BPSH45 where the phosphine oxide containing membranes showed a decrease in current densities at any give voltage. This was presumed to be due to the possible complex that was associated with the Pt-PPO moieties thereby decreasing the number of active catalyst sites at the interface of the electrode and membrane. Another explanation for the loss of performance in the kinetic region of these voltage current curves is the aptitude of the membrane to transport hydrogen and oxygen thereby creating a back-flux of protons that ultimately work against the system. The hydrogen crossover was thought to be higher for the PPO containing membranes thus allowing larger amounts of protons to be created at the cathode. The ohmic region of the voltage current curves (0.8-0.4 V) is indicative of the membrane conductivity and resistance. At voltage values of 0.5 V, BPSH45 had a current density of 1045 mA/cm² where the 20%PPO and 50%PPO membranes showed only 624 and 404 mA/cm² respectively. The dramatic loss in MEA performance was presumably due to the complex formation of the PPO groups with the sulfonic acid moieties thereby decreasing the number of active proton transport sites across the membrane.

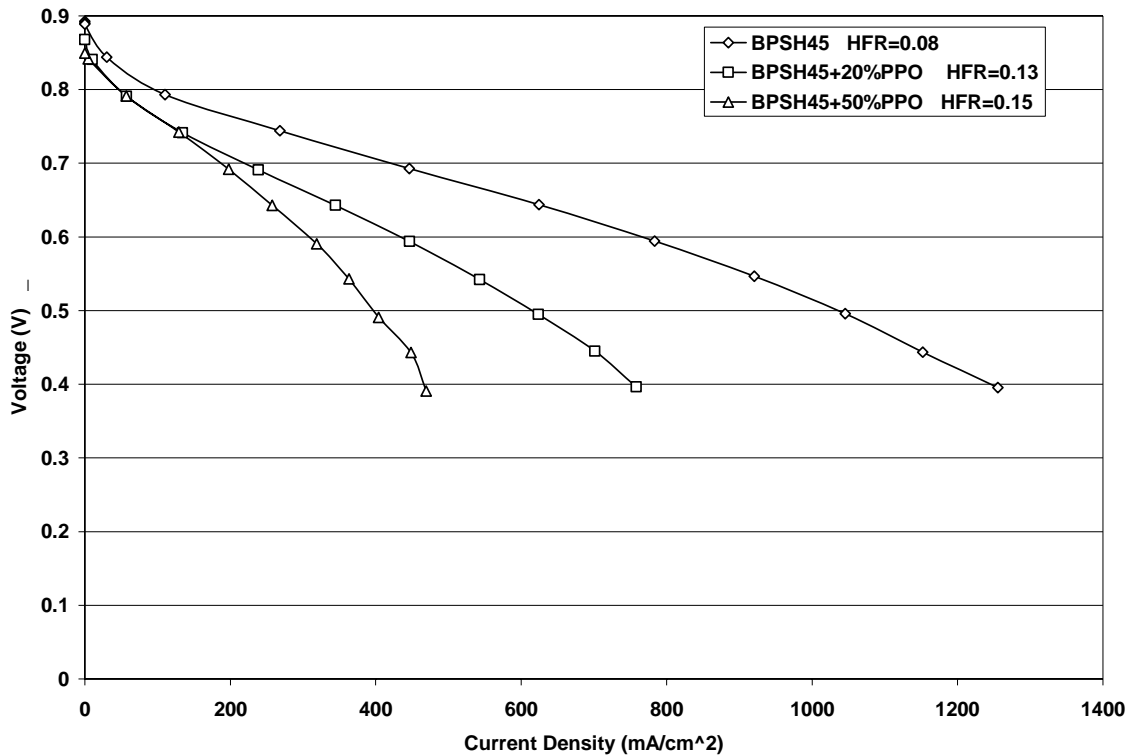


Figure 7.14 Fuel Cell Performance at 80 °C at 100% RH and 20 psig for Neat Terpolymer Membrane Electrode Assemblies

The performance of PTA containing composite membrane electrode assemblies at 80 °C in 100 %RH and 20 psig is shown in Figure 7.15. All the MEAs were reacidified using the room temperature M1 technique to minimize the amount of PTA extraction. As noted previously, BPSH 45 had the highest amount of PTA extraction at 50% while the 20%PPO and 50%PPO membranes had only 23% and 19% respectively. By coupling the extraction data with the fuel cell performance data, two different processes were determined to provide the interesting characteristic fuel cell results. The first was the PTA extraction. The BPSH copolymer had the highest amount of extraction thereby

producing large voids and sponge-like characteristics. The morphology that was produced presumably caused non-continuous sulfonate phases that hindered proton transport and fuel cell performance. The second process was complex formation between the PPO, sulfonate and PTA moieties. At high levels of PPO content (50%PPO), the complex formation of PPO with both PTA and sulfonic acid was so extreme that the proton transport was limited due to loss of acid sites through hydrogen bonding with the PPO moieties. However, at lower levels (20%PPO), the PPO complex formation with PTA allowed retention in water environments while not removing all sulfonate and PTA moieties from the proton transport processes. Therefore, the best performance of the composite membranes was from the 20%PPO terpolymer that had very high PTA retention while still allowing sulfonic acid proton transport. The kinetic region of the curves suggested that high levels of hydrogen crossover were produced for the BPSH45 sample that originally had 30 wt% PTA filler. After reacidification, much of the inorganic filler was extracted (50%) causing voids that increased crossover through pinhole formation and a back-flux of protons from hydrogen that reacted at cathode.

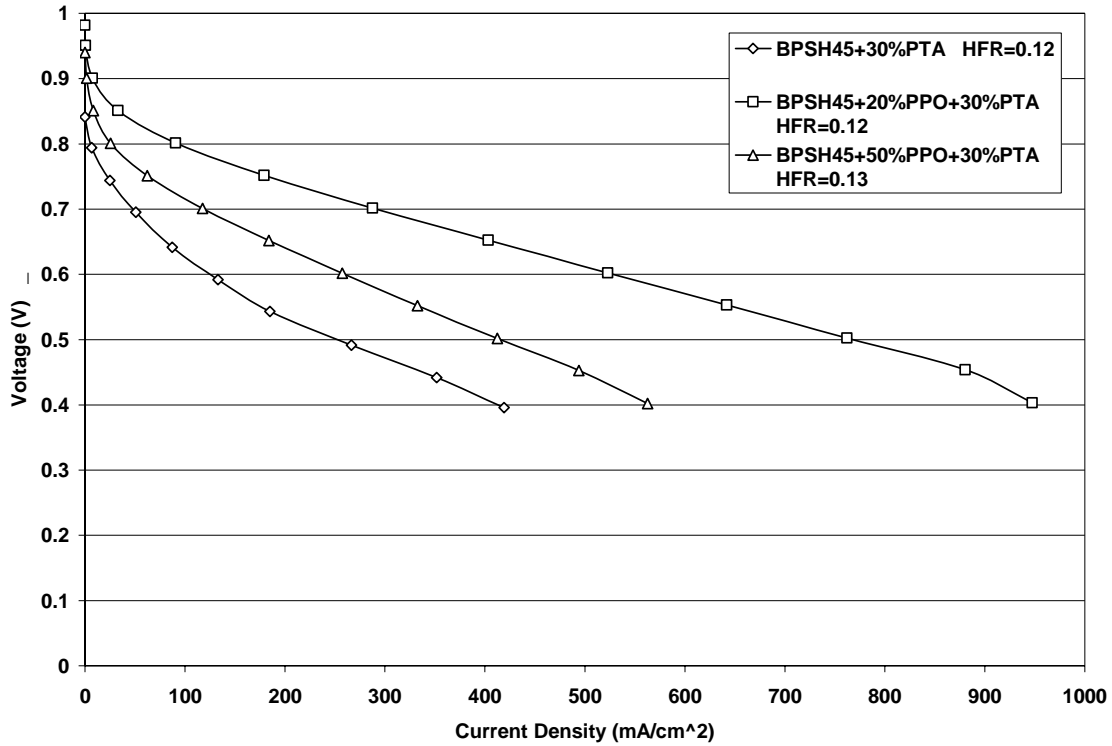


Figure 7.15 Voltage Current Curve at 80 °C at 100% RH and 20 psig for 30 wt% PTA Composite Membrane Electrode Assemblies

The performance of the pure BPSH45+20%PPO MEA and the composite BPSH45+20%PPO MEA at 120 °C, 50% RH and 20 psig was plotted in Figure 7.16. These sets of experiments were used to assess actual fuel cell conditions that have been outlined by The Department of Energy for automotive applications. The performance in the electrode active area of the curves indicated the neat terpolymer had high hydrogen crossover presumably due to the permeability of the PPO containing material, however, further characterization must be performed. The ohmic region of the curves showed that the composite material performed better than the neat material. At 0.5V, the current density of the composite MEA was 220 mA/cm² while the neat membrane showed only 198 mA/cm². The gain of 22 mA/cm² was presumably due to greater water retention at

temperatures above the boiling point of water in a 50% relative humidity environment. As compared to BPSH45 copolymers, the 20%PPO material showed very high levels of PTA retention, which accounted for high proton conductivity at elevated temperatures and low relative humidities.

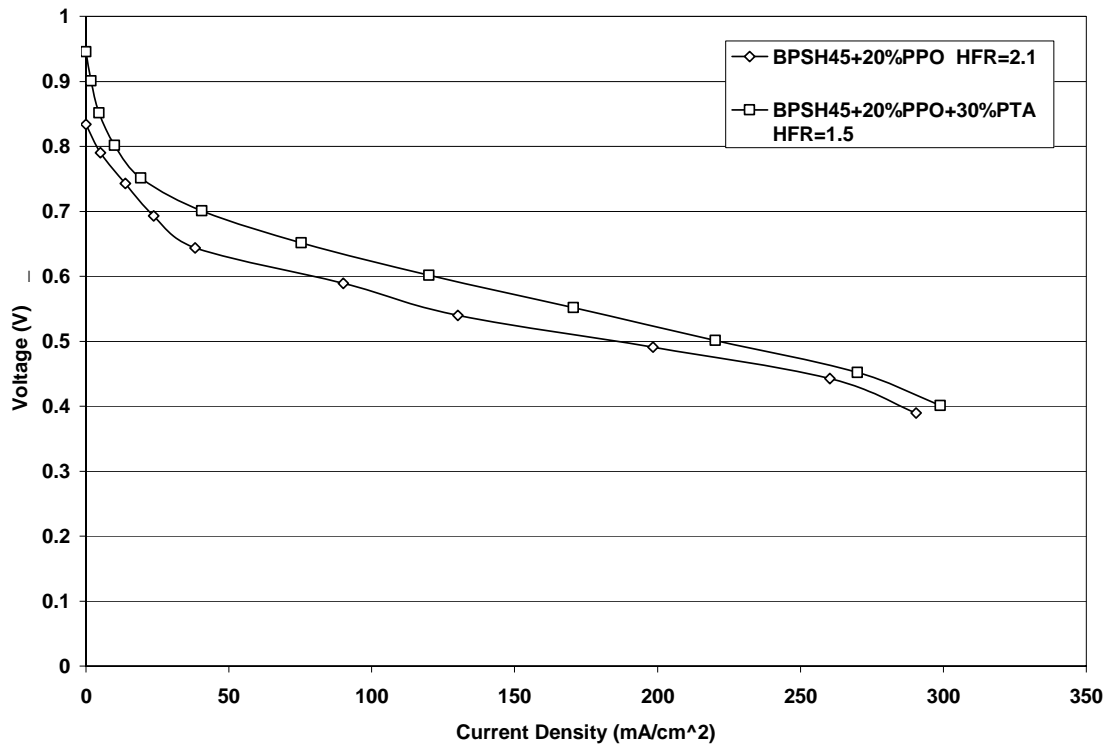


Figure 7.16 Fuel Cell Performance at 120 °C at 50% RH and 20 psig for BPSH45+20%PPO Neat and 30 wt% PTA Composite Terpolymer

7.4 Conclusions

Specific characteristics and interactions of the PPO effects on the sulfonic acid moieties and PTA molecules were thoroughly probed using FTIR, ^{31}P NMR, water uptake, proton conductivity and fuel cell analyses. Polymer synthesis using highly reactive difluoro monomers created a family of poly(arylene ether phenyl phosphine oxide sulfone) terpolymers having various levels of phosphine oxide ranging from 0-50 mole percent. Molecular weight characterization using intrinsic viscosity and gel permeation chromatography indicated high degrees of polymerization were obtained providing high number average and weight average molecular weights. The incorporation of phosphine oxide into the terpolymer structure was monitored using FTIR and ^1H NMR. Phosphine oxide incorporation was found to be quantitative relative to the amount of BFPPPO charged into the reaction. Water uptake experiments indicated complex formation of the PPO and sulfonate groups. The initial rise in water sorption was determined to be due to an affinity of the PPO moieties for water, while the drop in water sorption at higher amounts of PPO was due to the complex formation of the phosphine oxide groups with the sulfonate groups. When solution mixed with PTA dissolute, composite membranes were found to be tough and transparent indicating good dispersion of the PTA molecules. The specific interactions were first observed using FTIR experiments. The data indicated strong interaction and complex formation occurred at the sulfonate-PTA molecule interface. Interactions between the PPO groups and PTA particles were observed using ^{31}P NMR that showed a band shift assigned to the phosphorous atom incorporated into the terpolymer backbone. This was indicative of

hydrogen bonding and complex formation through polar interactions of the PPO and PTA molecules. The water uptake data of the composite membranes showed further evidence of the specific interactions. The composite membranes showed lower water uptake relative to the pure terpolymer membranes suggesting better water management and smaller dimensional swelling. The materials with the highest water sorption were found to be the composite terpolymers that were acidified by M2. The M1 composite membranes showed only fractional amounts of water sorption when compared to the pure copolymers. It was concluded that the specific interactions of the PTA particles with the sulfonate groups and PPO moieties on the terpolymer backbone removed the water sorption sites from the overall mechanism thus not absorbing extreme amounts of water. Extraction of the PTA particles during the reacidification was calculated with respect to the original amount of PTA molecules incorporated into the material. It was noted that the high temperature and harsh conditions of the M2 reacidification technique extracted most of the PTA particles in the low PPO containing membranes indicating low overall affinity. It was concluded that the specific interactions between the PTA, PPO and sulfonate groups were lost in this high energy environment thereby extracting the water soluble molecules. At higher levels of PPO (20-50%), the affinity for the PTA molecules was high enough so as to decrease the extraction levels thereby enhancing PTA retention. Proton conductivity was determined at 120 °C in 45% relative humidity for both the neat and composite membranes. The 120 °C conductivity was dominated by the composite membranes reacidified using M1 and having PPO contents around 20%. This enhancement of conductivity at elevated temperatures was presumably due to the greater water retention due to the PTA particle retention and low amounts of sulfonate complex

formation. Hydrogen-air fuel cell performance at both 80 °C and 120 °C was performed on neat MEAs and on composite MEAs containing 30 weight percent PTA. The voltage-current curves at 80 °C of the neat membranes indicated strong interactions of the PPO with the sulfonic acid sites that hindered the proton transport mechanism thereby decreasing the overall performance for PPO containing membranes. The performance curves of the composite membranes showed a tradeoff between PTA retention and PTA-PPO-sulfonate complex formation. When no PPO was present (BPSH45), the PTA extraction was high producing voids and pinholes in the membrane thus decreasing fuel cell performance. When large amounts of PPO were present in the terpolymer backbone (50%), complex formation permitted very little of the PTA to be extracted, however, the large amount also permitted enhanced complex formation between the PPO and sulfonate groups thereby decreasing the number of active transport sites. It was found that the composite terpolymer containing 20%PPO provided the lowest extraction with the highest possible conductivity at 120 °C. The fuel cell performance further indicated these findings by showing the best overall performance at 120 °C and 50%RH. It is concluded that highly polar phosphine oxide containing disulfonated copolymers increased the affinity for the PTA molecules, which increased particle retention in water environments even at high temperatures. A series of copolymers containing increasing amounts of phosphine oxide groups were used to determine the optimal amount of chain polarity so as to retain as much PTA as possible yet still allowing free acid sites for proton transport mechanisms.

Acknowledgments

The authors would like to thank the Department of Energy and United Technologies Corporation for funding under contracts: sub-56844-FMIJOBDOE-99241 and #DE-FC36-01G011086. Further appreciation is extended to OMNOVA Solutions Signature University Award for their generous fellowship and Sandia National Laboratories for their kind guidance and support.

CHAPTER 8

DIRECTLY COPOLYMERIZED 45 MOLE PERCENT PARTIALLY FLUORINATED DISULFONATED POLY(ARYLENE ETHER SULFONE) COPOLYMERS FOR PEM FUEL CELL SYSTEMS: SYNTHESIS, FABRICATION AND CHARACTERIZATION OF MEMBRANES AND MEMBRANE ELECTRODE ASSEMBLIES FOR FUEL CELL APPLICATIONS

K.B. Wiles¹, C. M. de Diego², J. de Abajo² and J.E. McGrath¹

¹Department of Chemistry and Macromolecules and Interfaces Institute
Virginia Polytechnic Institute and State University
Blacksburg, VA 24061

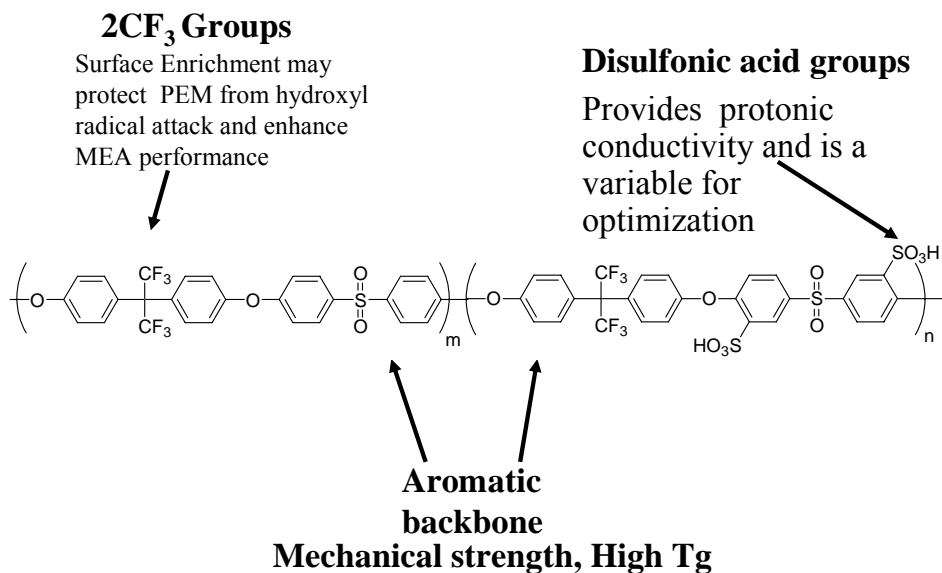
²Departamento de Química Macromolecular
Instituto de Ciencia y Tecnología de Polímeros. CSIC.
Madrid, Spain

Graphical Abstract

The effect of hexafluoroisopropylidene bisphenol incorporation into 45 mol% poly(arylene ether sulfone) copolymers was investigated. The novel series of directly disulfonated poly(arylene ether sulfone) copolymers with various mole ratios of fluorination were synthesized following traditional nucleophilic aromatic substitution

polycondensation reactions. The levels of fluorination within the statistically random copolymer architecture was varied from 0-100 mole percent using hexafluoroisopropylidene bisphenol (6FBP) and the correct stoichiometric amount of 4,4'-biphenol. The mole percent of disulfonation was held constant at 45%, which corresponded to a mole ratio of 3,3'-disulfonated-4,4'-difluorodiphenol sulfone (SDFDPS) to 4,4'-difluorodiphenol sulfone (DFPDS) of 0.45:0.55. The constant disulfonation afforded precise understanding of the effects that partial fluorination had on the polymeric system while allowing for enhanced proton conductivity associated with 45 mole percent disulfonated copolymers. Solution cast transparent membranes were characterized using intrinsic viscosity, gel permeation chromatography, Fourier transform infrared spectroscopy (FTIR), proton nuclear magnetic resonance (^1H NMR), x-ray photoelectron spectroscopy (XPS), water uptake, ionic conductivity and hydrogen/air fuel cell experiments. High molecular weight copolymers were obtained based on intrinsic viscosity and gel permeation chromatography experiments. Quantitative incorporation of the 6F-BP monomer into the backbone architecture was monitored using FTIR and NMR analyses. Self assembly of the fluorination groups to the surface of the membranes was observed using XPS analysis and indicated that the fluorine atoms preferentially arranged onto the air surface of the solution cast membranes presumably due to the lower surface energy environment. Water uptake was found to decrease with increasing incorporation of the 6FBP monomer into the polymer backbone. This suggested that the hydrophobic partially fluorinated material aided in water management of the system. Proton conductivity was found to decrease slightly as the amount of fluorination increased presumably due to the decrease in the ion-exchange capacity as the milli-equivalents of

sulfonic acid moieties per gram of polymer decreased due to the larger molar weight of the 6FBP repeat unit. High temperature hydrogen/air fuel cell experiments indicated better Nafion-bonded electrode adhesion for the partially fluorinated materials, as depicted by high frequency resistance experiments.



Chemical Structure of Partially Fluorinated Poly(arylene ether sulfone) Copolymer Indicating Disulfonic Acid Moieties, Aromatic Backbone and Fluorine Containing Linkages

Keywords: Sulfonated Copolymer, Poly(arylene ether sulfone), Direct

Copolymerization, Fluorinated Copolymers, proton exchange membrane, fuel cell,

Nafion

8.1 Introduction

Alternative power sources based on proton exchange membrane fuel cells has gained renewed international interest by offering a mode of electricity that is not based on fossil fuels that are produced in few places of the world. These green energy devices convert chemical energy directly to electrical energy by the catalyzed conversion of hydrogen to protons and electrons. The proton exchange membrane (PEM) is an electronic insulator and a proton conductor thereby allowing proton transport through the membrane. The protons then catalytically react with the electrons and oxygen available on the cathode side of the cell to form water as the byproduct. As an alternative to internal combustion engines, hydrogen fuel cells avoid noisy combustion reactions that in-turn produce high emissions of smog (NO_x) and acid rain (SO_x) precursors. The cell design versatility allows various fuels based on hydrogen and dilute aqueous methanol to be applied to small portable electronic devices, such as cell phones, as well as engineering of large stacks for automotive and stationary power applications.

Alternative proton exchange membranes must possess properties that are, at the least, comparable to the poly(perfluorinated) copolymers that are employed as the state-of-the-art fuel cell membranes. The advantages of Nafion[®]-type membranes include good proton conductance, great durability at temperatures between 20-80 °C and good chemical resistance due to the semicrystallinity of the fluorocarbon backbone. However, these poly(perfluorinated) copolymer membranes do not possess sufficient properties for all fuel cell conditions. When employed in direct methanol fuel cells, Nafion[®] membranes suffer from high methanol permeability which leads to loss of fuel efficiency

and a back-flux of protons that are produced at the cathode rather than at the anode. Furthermore, at operation temperatures above 80 °C in a hydrogen/air fuel cell, the membrane lacks physical and mechanical durability that decreases long-term stability. These deficiencies have produced many alternative polyelectrolyte membranes for use in both direct methanol and hydrogen fuel cells. The majority of the successful alternative membranes are based on high performance polymeric backbones containing sulfonic acid pendant groups. The hydrophobic backbones enhance physical properties and the sulfonic acid pendant groups provide ionic conductance. Many reports have described the advances in alternative proton exchange membranes employing high performance polymer such as polysulfone,^{345,346,347,348} polyimide,^{349,350,351} polybenzimidazole³⁵² and polyketone³⁵³.

An important procedure to produce alternative proton conducting membranes has been to post-sulfonate aromatic engineering thermoplastic materials. Typically, sulfonic pendant moieties are attached using either fuming sulfuric acid or chloro-sulfonic acid to the arylene containing polymer backbone following electrophilic aromatic substitution processes.³⁵⁴ One advantage of this technique is the relative ease of producing an entire family of proton exchange membranes by averting the intricate polymerization reactions.

³⁴⁵ Hickner, M. A., Ghassemi, H., Kim, Y. S., Einsla B. R. and McGrath, J. E. *Chem. Rev.* 104, 4587-4612, 2004.

³⁴⁶ Wang, F., Hickner, M. A., Kim, Y., Zawadzinski, T. and McGrath, J. E. *J. Membr. Sci.* 197, 231-242, 2002.

³⁴⁷ Nolte, R., Ledjeff, K., Bauer, M. and Muhaupt, R. *J. Membr. Sci.* 83, 211, 1993.

³⁴⁸ Koter, S., Piotrowski, P. and Kerres, J. *J. Membr. Sci.* 153, 83-90, 1999.

³⁴⁹ Einsla, B., Y.T. Hong, Y.S. Kim, F. Wang, N. Gunduz and J.E. McGrath, *J. Poly. Sci., Part A: Polymer Chemistry* 44, 862-874, 2004.

³⁵⁰ Gunduz, N., Inan, T. Y., Yidez, E. and McGrath, J. E. *Polymeric Mat. Sci. Eng.* 84, 911, 2001.

³⁵¹ Genies, C., Mercier, R., Sillion, B., Cornet, N., Gebel, G. and Pineri, M. *Polymer* 42, 359, 2001.

³⁵² Kim, Y.J., B.R. Einsla, C.N. Tchatchoua and J.E. McGrath, *High Performance Polymers*, 2005, *submitted*.

³⁵³ Alberti, G., Casciola, M., Massinelli, L. and Bauer, B. *J. Membr. Sci.* 185, 73, 2001.

³⁵⁴ Poppe, D., Frey, H., Kreuer, K., Heinzl, R. and Mulhaupt, R. *Macromolecules* 35, 7936, 2002.

The main disadvantage of this post-ionization process is the inability to reproduce and control the degree of sulfonation that is thought to produce only one pendant sulfonate group per repeat unit.

A viable alternative to post-ionization is synthesizing ion-containing copolymers via direct polymerization of sulfonated monomers. This process produces sulfonate containing copolymers that can be synthetically tailored to produce extremely high molecular weights providing two acid groups per repeat unit. Directly copolymerized sulfonated polyimides were reportedly produced from 9,9'-bis(4-aminophenyl)fluorine-2,7-disulfonic acid after careful synthesis.³⁵⁵ Various sulfonated polyimide architectures have been reported for use in fuel cell systems that employed systematic studies of direct copolymerization of sulfonated monomers.^{356,357,358} Aromatic ether copolymers have been thoroughly investigated by incorporation of various bisphenol structures in disulfonated poly(arylene ether sulfone) copolymers.³⁵⁹ The influence of structure variations on the copolymer architecture was shown to provide defined structure property relationships. The water uptake, morphology and glass transition temperatures were shown to be functions of bisphenol structures at similar degrees of disulfonation. However, the proton conductivity was determined to be directly correlated to the ion-exchange capacity (IEC) on a milli-equivalents of acid groups per gram of polymer scale.

Long-term stability of membrane electrode assemblies is one of the most critical requirements for the successful large-scale production and application of proton exchange

³⁵⁵ Guo, X.; Fang, J., Watari, T., Tanaka, K., Kita, H., Okamoto, K. *Macromol.* 35, 6707, 2002.

³⁵⁶ Kim, H.; Litt, M. *Polym. Prepr. Am. Chem. Soc., Div. Polym. Chem* 42 (2), 486, 2001.

³⁵⁷ Genies, C.; Mercier, R.; Sillion, B.; Cornet, N.; Gebel, G.; Pineri, M. *Polymer* 42, 359, 2001.

³⁵⁸ B.R. Einsla, Y.T. Hong, Y.S. Kim, F. Wang, N. Gunduz, J.E. McGrath, *J. Poly. Sci.: Part A: Polymer Chemistry* 44, 862-874, 2004.

³⁵⁹ W. L. Harrison, F. Wang, J. B. Mecham, M. Hill, V. A. Bhanu, Y. S. Kim and J.E. McGrath, *J. Polym. Sci.; Part A: Polymer Chemistry* 41, 2264, 2003.

membrane fuel cell technology. Fuel cell life time requirements for hydrogen/air membrane electrode assemblies have been reported to be in excess of 10,000 hours.³⁶⁰ The main degradation of stable energy conversion over time for alternative materials to Nafion-based copolymers has been observed to be delamination and high interfacial resistance associated with membranes employing Nafion-bonded electrodes. The chemical incompatibility and the resulting high interfacial resistance of alternative materials with perfluorinated electrode matrices has provided various research avenues to develop novel materials for proton exchange membranes as well as for electrode matrices. Membrane-electrode delamination failure and high cell resistances have been noted for unlike polymers where Nafion-bonded electrodes were employed.^{361,362} Possible techniques to reduce the interfacial tension and delamination that is associated with two dissimilar polymers are to either make the electrode more like the membrane or to synthetically make the membrane more like the electrode.³⁶³ The latter has been chosen for this report where Nafion 1100 has been used as a matrix binder for the electrode decals and alternative partially fluorinated poly(arylene ether sulfone) copolymers have been employed as the proton exchange membrane.

This paper reports the synthesis and characterization of disulfonated partially fluorinated poly(arylene ether sulfone) copolymer materials in which the chemical architecture was tailored to provide better compatibility with Nafion 1100 electrode materials. The modification of structural architecture relative to the previously reported poly(arylene ether sulfone) copolymers to enhance compatibility with perfluorinated

³⁶⁰ Fuel Cell Report to Congress, (ESECS EE-1973), US Department of Energy, Feb. (2003).

³⁶¹ Jorissen, L., Gogel, V., Kerres, J. and Garcke, J. *J. Power Sources* 105, 267, 2002.

³⁶² Scott, K., Taama, W. M. and Argyropoulos, P. *J. Membr. Sci.* 171, 119, 2000.

³⁶³ Zhang, L., Ma, C. and Mukerjee, S. *Electrochim. Acta.* 48, 1845, 2003.

Nafion materials is shown in Figure 8.1. The chemical structure was modified by synthetically incorporating hexafluoroisopropylidene bisphenol (6F-BP) into the repeat units thereby subsequently replacing biphenol. The mole percent of disulfonation was held constant at a stoichiometric ratio of 45 mole percent so as to provide adequate conductivity and allow for a more complete understanding of the effects that partial fluorination had on the polymeric system. Characterization techniques included intrinsic viscosity, gel permeation chromatography, Fourier transform infrared spectroscopy (FTIR), nuclear magnetic resonance (NMR), x-ray photoelectron spectroscopy (XPS), water uptake, ionic conductivity and hydrogen/air fuel cell experiments. Membrane electrode assemblies were fabricated by hot pressing prefabricated electrode decals containing a Nafion 1100 ionomer matrix and Pt supported on Vulcan carbon black. The partially fluorinated copolymers were compared to poly(arylene ether sulfone) copolymer membrane electrode assemblies in a hydrogen/air fuel cell test station.

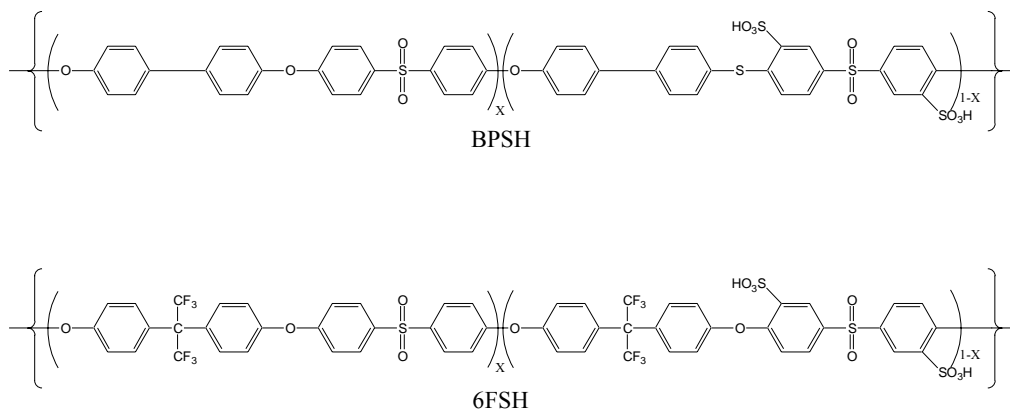


Figure 8.1 Chemical Structure of Biphenol Based Poly(arylene ether sulfone) Copolymers (BPSH) and Hexafluoroisopropylidene Bisphenol Based Poly(arylene ether sulfone) Copolymers (6FSH)

8.2 Experimental

8.2.1 Materials

Hexafluoroisopropylidene bisphenol (6FBP) was obtained from DuPont in monomer grade and used as received. Anhydrous potassium carbonate, 4,4'-biphenol (BP) and 4, 4' - difluorodiphenylsulfone (DFDPS) were obtained from Aldrich. NMP and toluene (both from Burdick and Jackson) were dried as follows: NMP was dried overnight over calcium hydride with a nitrogen purge and distilled at reduced pressure; toluene was dried over molecular sieves. Disulfonation of DFDPS was performed in a similar fashion as previously described to prepare 3,3'-disulfonate-4,4'-difluorodiphenylsulfone (SDFDPS).³⁶⁴

8.2.2 Synthesis of 45 Mole Percent Disulfonated Partially Fluorinated Poly(arylene ether sulfone) Co- and Terpolymers

Typical polymerizations of SDFDPS, DFDPS, BP and 6FBP were conducted in a flame dried three-necked flask. The flask was fitted with a nitrogen inlet, thermocouple sensor, over-head stirrer and Dean Stark trap fitted with a condenser. After charging all the monomers and solvents, the reaction flask was heated in an oil bath to 150 °C while the toluene was allowed to reflux for 4 hours to remove any water present from the hydrated atmosphere or hydrated monomers. The volume of toluene was 50% the

³⁶⁴ Wiles, K. B.; Munoz, C. M. and McGrath, J. E. *Polymer Preprints*, **2004**, 45(1), 724.

amount of NMP used to allow for 20% solids. The toluene was then removed over a 60-minute time interval. The Dean Stark trap was emptied and the reaction temperature was slowly increased to 180 °C for 16 hours. The resulting solution media became very viscous. The reaction mixture was diluted and hot filtered at 150 °C using a Buchner funnel to remove any by-products (salt, KF). The isolated filtrate was slowly poured into a 50-fold excess of isopropanol to precipitate the terpolymer. The fibrous precipitate was collected by filtration and washed with isopropanol and water to aid in the removal of salts. It was dried under vacuum at 80 °C for one hour, then at 100 °C for 15 hours. The degree of 6FBP incorporation was controlled by varying the charging ratio of BP to 6FBP (Figure 8.2).

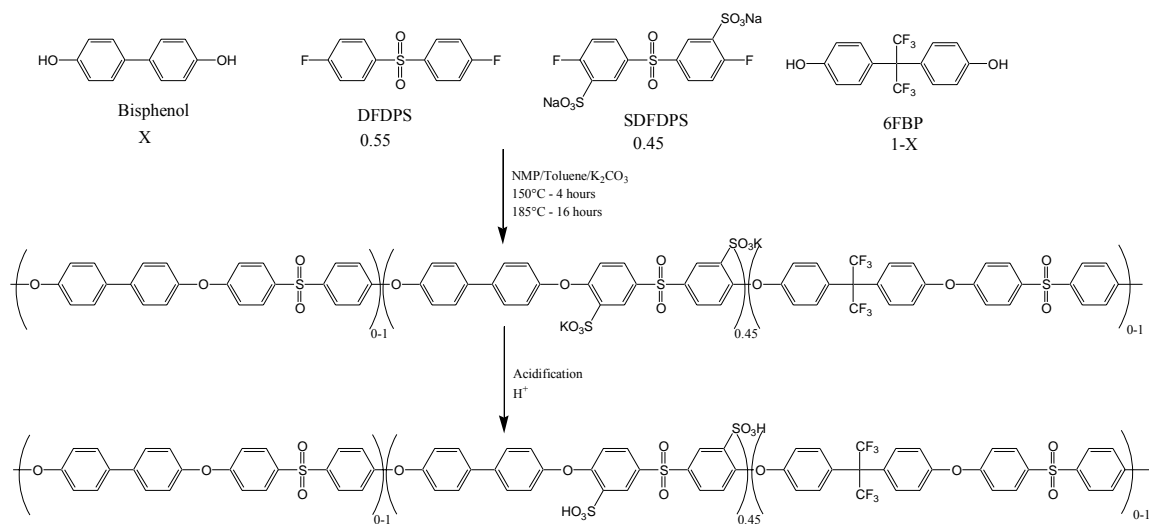


Figure 8.2 Synthesis of 45 Mole Percent Disulfonated Partially Fluorinated Poly(arylene ether sulfone) Co- and Terpolymers

8.2.3 Membrane Preparation

The potassium salt films were prepared by first redissolving the fibrous copolymer in dimethylacetamide (DMAc) and then by filtering the solution through a 0.45 μm Teflon[™] syringe filter thereby directly casting the solution into a glass-casting tray. The glass tray had side-walls so as to aid in membrane thickness control. The copolymer solutions were dried in a vacuum oven by slowly increasing the temperature settings from 50 °C for 4 hours to 80 °C for 4 hours to 100°C for 12 hours and finally for 120 °C for 4 hours. Careful leveling of the glass casting tray provided uniform films. Addition of water to the casting tray swelled the membranes and allowed them to be easily removed. The salt form membranes were then transformed into the acid form using a boiling (~100 °C) technique in 0.5 M sulfuric acid in water for two hours. The residual sulfuric acid was removed by boiling in water for another 2 hours. All the membranes tested were acidified using this high temperature acidification treatment so as to appreciably change the morphological characteristics of the resulting acidified membranes through possible reorganization of the sulfonate moieties producing ion clusters and channels.³⁶⁵

8.2.4 Characterization

Absorbance mode FTIR spectra of thin films were obtained using a Nicolet Impact 400 FTIR spectrophotometer. The resolution of all the spectra was constant at 2

³⁶⁵ Y. S. Kim, F. Wang, M. A. Hickner, S. McCartney, Y. T. Hong, W. L. Harrison, T. A. Zowadzinski and J. E. McGrath, *J. Polym. Sci.: Part B: Polym. Phys.* 2003, 41, 2816.

cm⁻¹. The average of 48 scans was reported. Proton NMR spectra were obtained with a JEOL 500 MHz spectrometer using DMSO-d₆ as solvent (5% w/v polymer solutions). The water absorption was calculated by using weight-difference calculations. The acidified films were dried in a vacuum oven at 100 °C for 24 hours and weighed. They were then immersed in deionized water at room temperature for 24 hours at which time they were removed from the water, blotted dry and weighed again. A final drying in vacuum at 100 °C for 24 hours was performed at which time the samples were weighed again. Weight gain based on the dry weight was recorded using an average of three membranes per membrane type. Intrinsic viscosity (IV) data were calculated using the extrapolated values to zero concentration of the averages of the reduced and inherent viscosities. Characterization of molar mass after polymerizations was monitored by intrinsic viscosity measurements using NMP+0.05 M LiBr at 25 °C and a Cannon Ubbelohde viscometer. Gel permeation chromatography determined the number average molecular weights using a Waters 1515 isocratic HPLC pump, Waters Autosampler and Waters 2414 refractive index detector calibrated using narrow molecular weight distribution polystyrene standards. The oven temperature of the column set containing two Styragel HT 6E and one Styragel HT 3 was constant at 60 °C. N-methylpyrrolidone containing 0.05 M LiBr with a 1.0 mL/min flow rate was used as the mobile phase. Proton conductivity was measured in liquid water at 25 °C and 80 °C using a Hewlett Packard 4192 Impedance/Gain Phase Analyzer over a frequency range of 10Hz-1MHz.³⁶⁶ The resistance of the films was taken at the frequency which produced the minimum imaginary response. The ionic conductivity of the membranes was calculated from the measured resistance and the geometry of the cell. Atomic surface fluorine compositions

³⁶⁶ T. A. Zawodzinski, M. Neeman, L. O. Sillerud and S. J. Gottesfeld, Phys. Chem. 1991, 95, 6040.

were measured by an X-ray photoelectron spectrometer (XPS) using a Perkin-Elmer physical electronic model 5400 with a hemispherical electron analyzer and position sensitive indicator. The X-ray source was an Mg K α operated at 15 kV and 20 mA. The vacuum in the sample chamber was constant at 10⁻⁸ Torr while the take off angles were invariable at 10° corresponding to a sampling depth of less than 1 nm. Introduction of the acid groups was classified by the calculated ion exchange capacity (IEC). When determining the theoretical amount of acid equivalents per gram of polymer, the calculations involve the following for disulfonated copolymers:

$$\text{IEC} = \frac{(2 * \text{mol fraction of disulfonation})}{((\text{MW}_{\text{repeat}} * \text{mol fraction } y) + (\text{MW}_{\text{sulf. repeat}} * \text{mol fraction } z))}$$

Where the value 2 in the numerator corresponds to two sulfonate moieties on the sulfonated repeat units, y is the mole fraction of the unsulfonated monomer/repeat units, z is the mole fraction of the sulfonated monomer/repeat units, MW_{repeat} is the molecular weight of the unsulfonated repeats units and MW_{sulf. repeat} is the molecular weight of the sulfonated repeat units. This equation calculates the equivalents of acid moieties per gram of polymer.

8.2.6 Hydrogen/Air Fuel Cell Performance

H₂/Air fuel cell performance was determined using a Fuel Cell Technologies Test Station with a Hewlett Packard load box. A computer interface was used to monitor

voltage, current and resistance of 5 cm² membrane electrode assemblies. Catalyst loadings and weight percent of ionomer were held constant for all samples at 0.2 mg/cm² using 20wt% Pt on Vulcan carbon black and 28.5wt% Nafion 1100 in both anode and cathode electrodes. Catalyst inks contained Nafion (5% dispersion in alcohols), Glycerol and 20% Pt supported on carbon black. The formulations obtained a 2.5:1 ratio of platinum catalyst to Nafion. The ink was stirred and sonicated to promote even dispersion of the Pt/C particles. The Nafion dispersion and platinum supported on carbon were obtained from Electrochem Inc. and the glycerol from Aldrich. Electrode decals were fabricated using Teflon reinforced with glass fiber backing layers. The catalyst ink was painted layer-by-layer onto the decals using a high quality brush. Uniform electrodes were dried after every coat of ink at 130 °C for ten minutes. After the correct loadings were obtained by calculating the difference between the decal backing layer and the electrode decal, the prefabricated electrodes were dried overnight at 130 °C to remove any residual glycerol and alcohols. Membrane electrode assemblies (MEAs) were fabricated by placing a salt form membrane between two electrode decals and hot pressing at 210 °C and 3000 psi for a total of 8 minutes. The MEAs were then acidified using the high temperature boiling technique discussed previously. After building the single 5 cm² cell using the Fuel Cell Technologies Inc. hardware, E-Tek single sided gas diffusion layers and Teflon gaskets, conditioning of the cell was performed using a life time test at 0.5 Volts at 80 °C and 100 %RH. After the current density reached a plateau, voltage-current-resistance experiments were performed.

8.3 Results and Discussion

8.3.1 Synthesis and Characterization of Partially Fluorinated 45 Mole Percent Co- and Terpolymers

Poly(arylene ether sulfone) polymerizations were conducted by condensing 45 mole percent of disulfonated activated dihalides (SDFDPS) with activated dihalides (DFDPS), BP and 6FBP (Figure 7.2). The constant disulfonation afforded precise understanding of the effects that partial fluorination had on the polymeric system while allowing for enhanced proton conductivity associated with 45 mole percent disulfonated copolymers. The reactions were performed in NMP as the polar organic solution using toluene as a refluxing agent to aid in removal of residual water through azeotropic mechanisms. By using potassium carbonate as the base, ion exchange of the sodium and the potassium ions occurred, thereby producing potassium salt form copolymers. As noted above, the activated dihalide was 4,4'-difluorodiphenol sulfone (DFDPS). Similarly, the disulfonated activated dihalide employed was 3,3'-disulfonate-4,4'-difluorodiphenylsulfone (SDFDPS). It is well known that halogen atoms ortho- or para- to a strongly electron-withdrawing substituent undergoes nucleophilic aromatic substitution readily which produced high molecular weight polymeric materials. Table 7.1 summarizes the calculated ion-exchange capacities, intrinsic viscosities and weight average molecular weights for BPSH45 and partially fluorinated 45 mole% disulfonated polymers. The IEC was calculated and found to decrease with increasing amounts of 6FBP incorporation because of the larger molecular weight of the 6FBP monomer relative to the BP monomer. The intrinsic viscosity values ranged from 0.5-0.9 dL/g.

This indicated that small variations in hydrodynamic volume was present, however, all the values were consistent with tough, film forming characteristics. Gel permeation chromatography, based on polystyrene standards, probed the weight average molecular weight with good accuracy, however, the number average molecular weight was observed to be skewed due to ionomer effects. The weight average molecular weights ranged from 34,000 g/mol for BPSH45 to 92,000 g/mol for BPSH45+30%6FBP. All the weight average molecular weights were indicative of appreciable film forming characteristics. All of the polymer membranes when completely dried showed no signs of cracking or brittleness that is typical when low molecular weight polymer were produced.

Table 8.1 Calculated Ion Exchange Capacity and Molecular Weight Characterization of BPSH45 and Partially Fluorinated BPSH45 Co- and Terpolymers

	IEC meq/g	Intrinsic Viscosity (NMP+0.05M LiBr @ 25°C) dL/g	GPC (NMP+LiBr) Mw
BPSH45	1.9	0.54	34K
BPSH45-6F10	1.8	0.73	65K
BPSH45-6F30	1.7	0.81	92K
BPSH45-6F50	1.6	0.50	52K
BPSH45-6F70	1.5	0.90	86K
6FSH45	1.4	0.66	65K

The incorporation of 6FBP into the BPSH45 architecture was monitored using ¹H NMR. The NMR spectra of BPSH45 and partially fluorinated materials are shown in Figure 8.3. The observed loss of the two peaks at 7.0 and 7.7 ppm was assigned to the

decreasing amounts of the biphenol structure, namely the two types of hydrogen atoms associated with the biphenol aryl rings. As the incorporation of 6FBP was increased, the amount of BP charged into the reaction mixture was decreased so as to replace the BP structure with the 6FBP structure. The gain in intensity of the peak at 7.4 ppm corresponded to the increase in 6FBP architecture that was polymerized into the BPSH45 backbone structure. For the 6FSH copolymer, no biphenol was evident in the NMR spectra thereby qualitatively determining good incorporation of the 6FBP monomer when coupling these observations to the molecular weights and product yields.

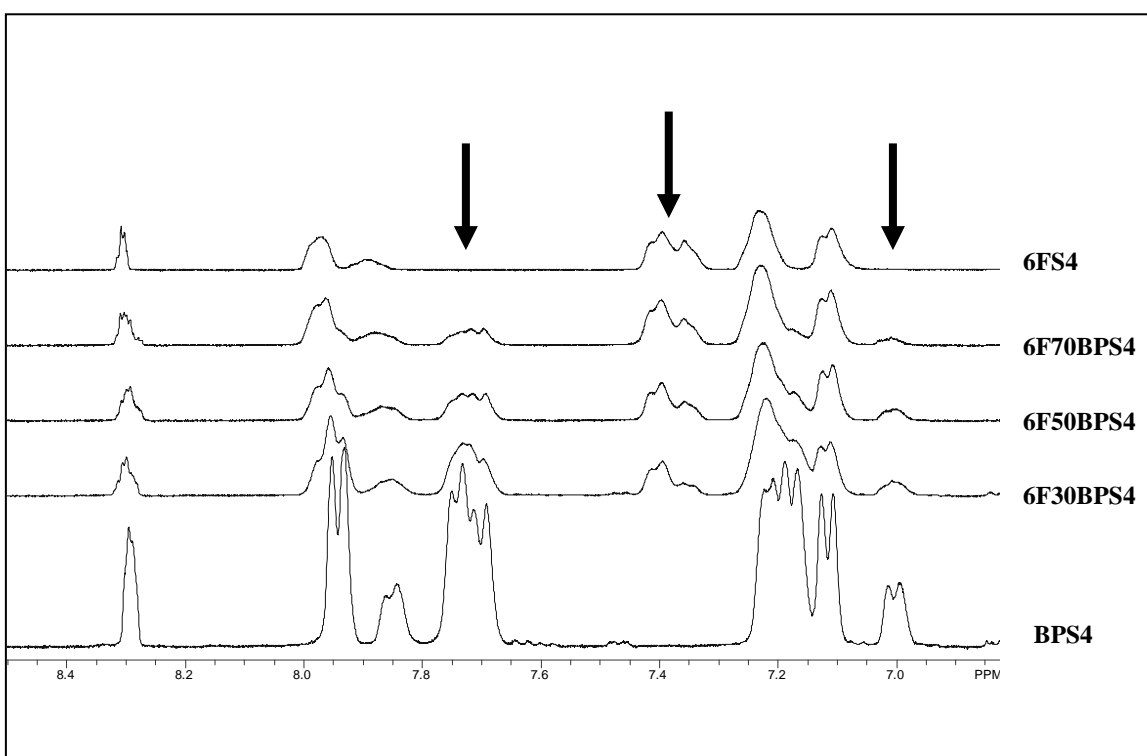


Figure 8.3 Incorporation Effect of 6FBP on ^1H NMR Peaks Indicating Loss of BP and Gain of 6FBP Moieties

Incorporation of 6FBP was also monitored by Fourier transform infrared spectroscopy. The FTIR spectra are shown in Figure 8.4 and indicate the gain in

intensity of peaks at 950 and 1550 cm^{-1} . The peaks ranging from 900-1000 cm^{-1} were determined to be the carbon to fluorine stretching (C-F) associated with the 6FBP monomer structure. The peak at 1550 cm^{-1} was assigned to the asymmetric stretching of the arylene rings attached to the hexafluoroisopropylidene moiety. These FTIR spectra were used to determine the qualitative and quantitative incorporation of the 6FBP repeat unit. The FTIR peak at 1008 cm^{-1} was indicative of the diphenyl ether absorption (AR-O-AR) which was used as the standard for normalizing the spectra. By monitoring the incorporation of the 6FBP architecture by FTIR and NMR, qualitative and quantitative analysis indicated excellent incorporation of the 6FBP moiety into the polymer backbone.

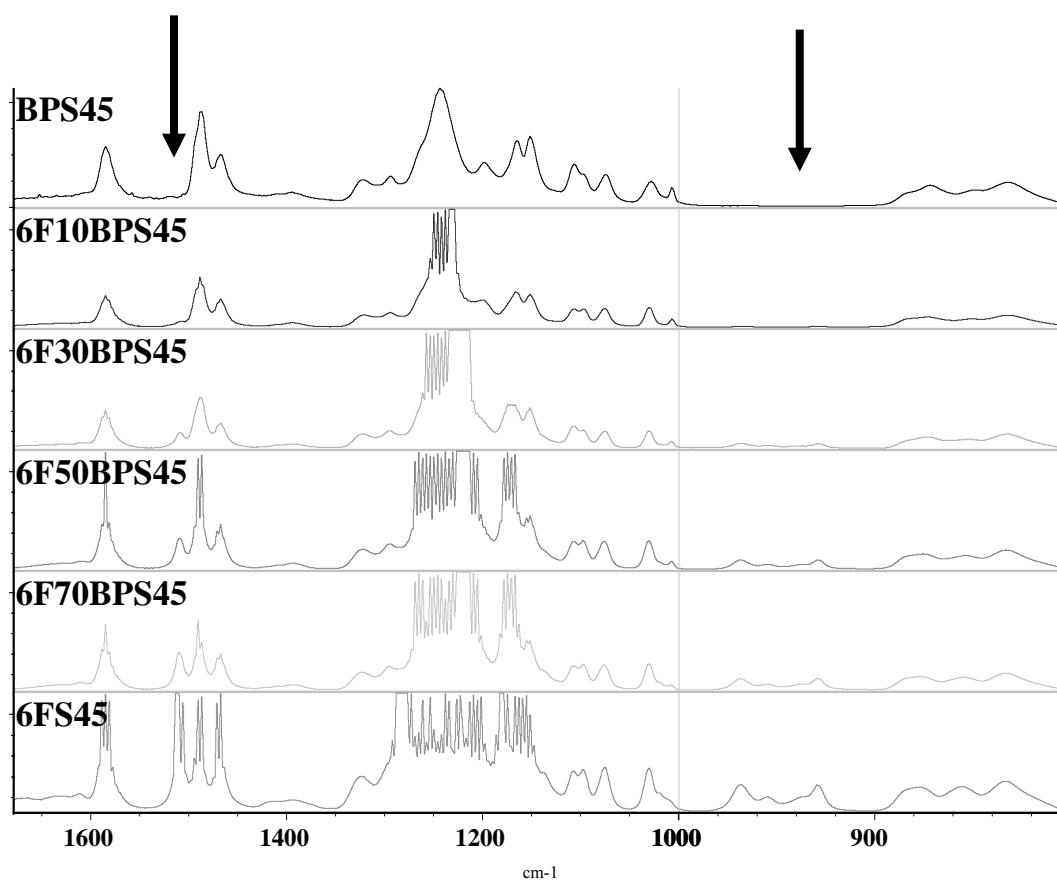


Figure 8.4 FTIR Spectra of Salt Form Thin Films Indicating the Incorporation of 6FBP Monomer Into the Polymer Backbone

8.3.2 X-Ray Photoelectron Spectroscopy (XPS) Surface Analysis of 6FBP Containing Polymers

Surface analysis of the partially fluorinated co- and terpolymers was recorded using an X-ray photoelectron spectrophotometer. Atomic percentages of fluorine on the surface (less than 1 nm deep) are reported in Table 8.2. All the membranes were tested in the acid form after high temperature acidification. The glass side refers to the side of the solution cast membrane that was in direct contact with the glass casting substrate. The air side refers to the membrane that was in contact with air rather than with glass. Relative to the calculated bulk values, the atomic fluorine percentages were found to be enhanced on the surfaces of both the glass and air sides. These data correspond to a self assembly phenomenon that preferentially assembles the fluorine atoms to the lower surface energy interface. Therefore, the fluorine in the bulk migrated to the vacuum interface during casting and thus accounted for the enhanced fluorine content at the membrane-vacuum interface. This could have ramifications to the adhesion of the Nafion containing electrodes. Nafion is perfluorinated and thus contains large amounts of fluorine atoms on the surface. While fabricating membrane electrode assemblies, it is hypothesized that the fluorine content in the 6FBP containing materials would reduce water swelling and aid in the adhesion of the Nafion electrodes to the alternative proton exchange membrane. The tailoring of the poly(arylene ether sulfone) copolymer architecture to provide more chemical compatibility with Nafion electrodes presumably allows more durable MEAs and lower high frequency resistances, which is a measure of membrane-electrode compatibility.

Table 8.2 Calculated Bulk Fluorine and Experimental Surface Fluorine Percentages Measured at Depths of Less Than 1 nm

Copolymer Composition	Air side %F	Glass side %F	Calculated %F
6FS45	14.9	12.7	10.3
6F70BPSH45	8.8	7.5	7.2
6F50BPSH45	6.6	6.0	5.1
6F10BPSH45	3.8	1.9	1.3

8.3.3 Percent Water Uptake of Salt and Acid Form Membranes as a Function of Fluorine Content

Water uptake was determined using both the potassium salt and high temperature acidified form membranes in liquid water at room temperature. Figure 8.5 indicates the water uptake of potassium salt membranes decreased as the amount of 6FBP polymerized into the chemical architecture increased from 0% to 100%. The water sorption of BPS45 was found to be 21% while the uptake of 6FS45 was only 6%. The decrease in water sorption suggested that the hydrophobic fluorine atoms associated with the 6FBP moieties played a key role in the overall physical uptake properties. The hydrophobicity of the 6FBP architecture was also observed in the water uptake of the acidified membranes as shown in Figure 8.6. A similar trend was observed for the acidified membranes relative to the potassium form membranes in that the water uptake of BPSH45 was 95% while the uptake of 6FSH45 was only 42%. Because the intrinsic viscosity measurements and the ion exchange capacities were relatively similar, the main

variable was determined to be the amount of fluorine in the material. If IEC was the dominant factor, water uptake would have linearly decreased as the amount of 6FBP incorporation increased. However, it was observed that the water uptake leveled at 30 mole percent incorporation of 6FBP indicating a lower effect of IEC. As the amount of fluorination increased, the amount of water sorption was found to decrease. This suggested that the hydrophobicity of the 6FBP moieties tend to repel water. As the amount of fluorination increased, the water repulsion characteristics tended to decrease the physical water uptake of both the salt and acid form membranes. This is hypothesized to have positive ramifications on electrode adhesion as well as durability. As the water uptake of the material becomes more similar to Nafion (~30wt%), the differences in physical dimensional swelling becomes less, thereby decreasing the electrode-membrane interfacial stresses associated with delamination processes. This corresponds to better long-term performance and durability of the membrane-electrode assembly system. By coupling the XPS data, that indicated surface fluorine enrichment, and the water uptake measurements, the high frequency resistance is hypothesized to be lower for the 6FBP containing MEAs.

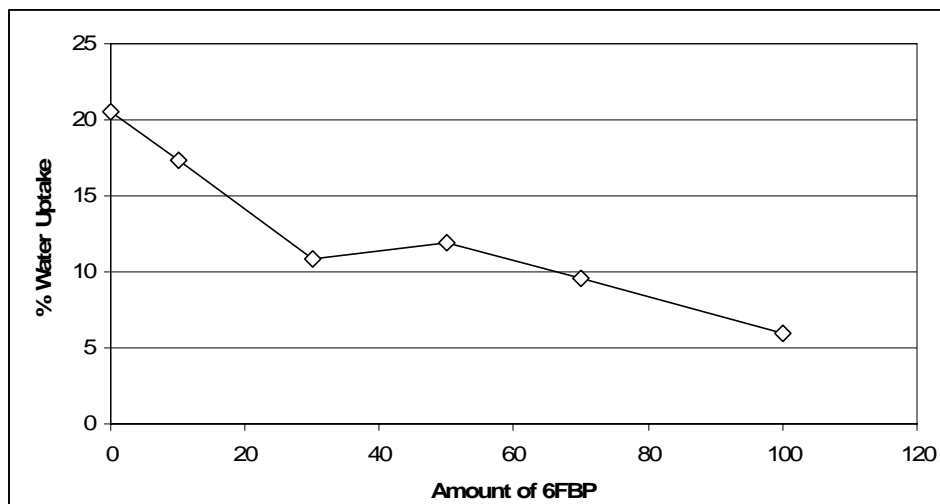


Figure 8.5 Percent Water Uptake of Potassium Salt Form Membranes as a Function of Fluorine Content

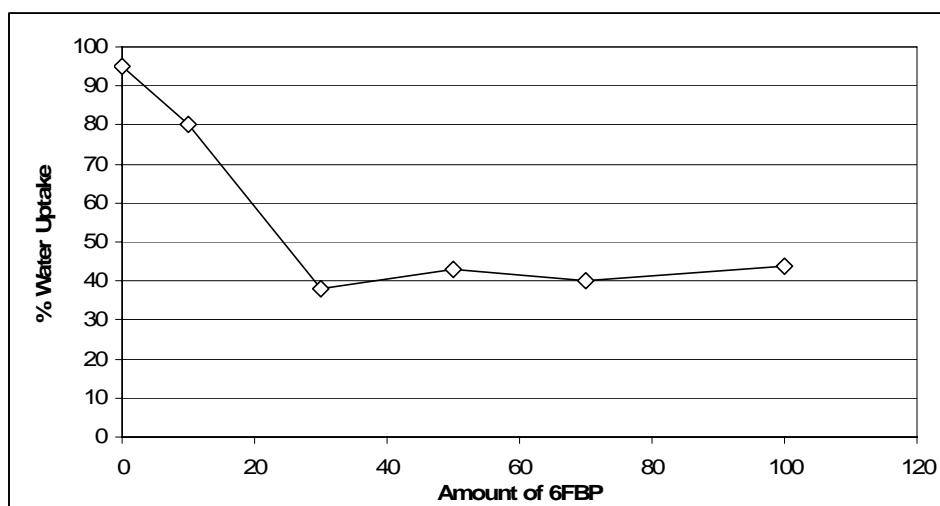


Figure 8.6 Water Uptake of Acid Form Membranes as a Function of 6FBP Content Measured at Room Temperature in Liquid Water

8.3.4 Proton Conductivity at Room Temperature and 80 °C in Liquid Water

The ionic conductivity was measured using thin films (2 mil thick) that were fully hydrated and equilibrated in liquid water at room temperature and 80 °C. Table 8.3 indicates that the ionic conductivity at both room temperature and 80 °C decreased with increasing amounts of 6FBP. Relative to the ion exchange capacities, the proton conductivities were determined to follow a similar trend. As the IEC decreased, the proton conductivity decreased. When comparing these results to the water uptake that leveled off at 30%6FBP incorporation, the conductivity is suggested to be more reliant on the IEC than the amount of fluorine in the chemical architecture. It was also noted that as the temperature of the fully hydrated environment increased, the proton conductivity increased. This is presumably due to better reaction kinetics increasing the ion transport from one sulfonic acid site to the next.

Table 8.3 Ionic Conductivity at Room Temperature and 80 °C for Partially Fluorinated and BPSH45 Co- and Terpolymers

	IEC meq/g	Conductivity at RT (mS/cm)	Conductivity at 80°C (mS/cm)
BPSH45	1.9	110	230
6F10BPSH45	1.8	94	210
6F30BPSH45	1.7	74	200
6F50BPSH45	1.6	67	200
6F70BPSH45	1.5	64	190
6FSH45	1.4	60	160

8.3.5 Hydrogen/Air Fuel Cell Performance as Measured by Polarization Curves and High Frequency Resistances

Hydrogen/air fuel cell performance was examined on a 5 cm² active catalyst area MEA using 0.2 mg Pt/cm² on both anode and cathode electrodes. The amount of Nafion ionomer in the electrodes was held constant at 28.5 weight percent while the thickness of all the membranes was 2 mils. Figure 8.7 indicates voltage-current-resistance data for BPSH45 and 6F30BPSH45 at 80 °C and 100% relative humidity at 20 psig. These sets of experiments were designed to imitate the actual fuel cell conditions of stationary power applications used for private residence and business applications. The 6F30BPSH45 terpolymer was chosen because of its low water swelling and high proton conductivity relative to BPSH45. By coupling the water uptake and conductivity data, it was suggested that BPSH 45 should have better performance in the ohmic resistance area (0.8-0.4 V) of the fuel cell curve. The ohmic resistance area of the performance curves is indicative of membrane conductivity and MEA resistances. The kinetic electrode activity (1.0-0.8 V) and high frequency resistance were found to be comparable for both MEAs; suggesting that the fully humidified environment allows for possible differences in water swelling characteristics. At 0.5 Volts, the current density of BPSH45 was 1200 mA/cm² while 6F30BPSH45 was only 1100 mA/cm². The 100 mA/cm² drop in performance was found to mainly be due to the difference in proton conductivity. BPSH45 had a higher measurable proton conductivity at 80 °C (230 mS/cm) than 6F30BPSH45 (210 mS/cm) thereby allowing proton transport to be more facile and efficient giving enhanced performance under fully humidified conditions.

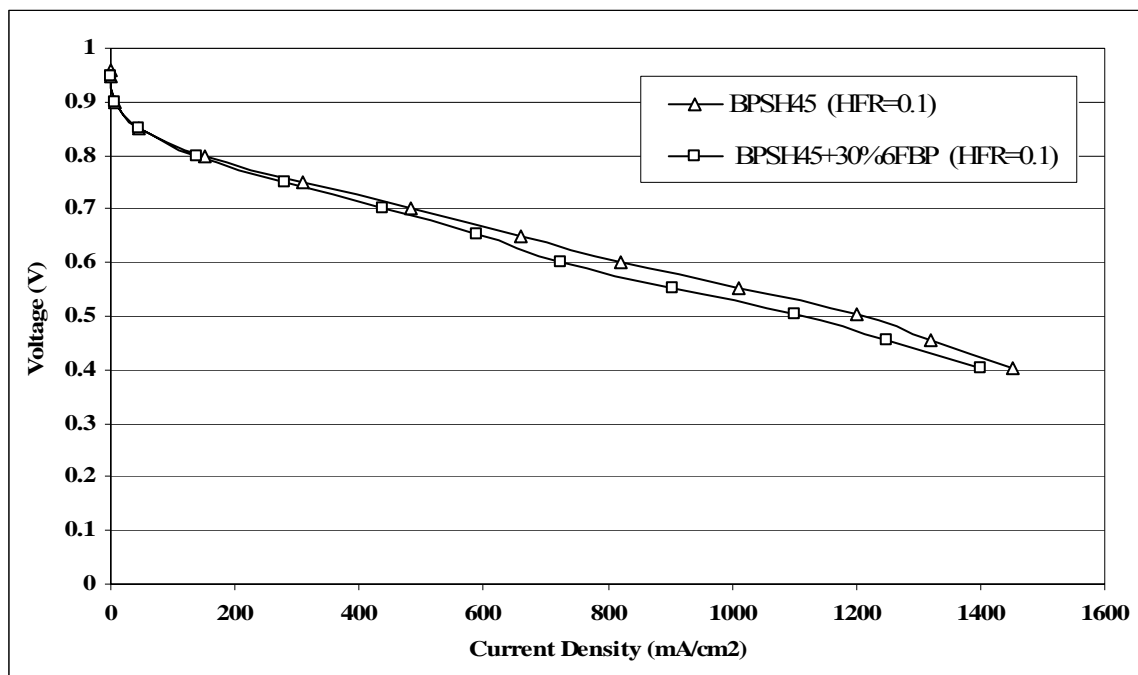


Figure 8.7 Initial Voltage-Current Curves and High Frequency Resistances at 80 °C and 100% Relative Humidity at 20 psig for BPSH45 (IEC = 1.9) and 6F30BPSH45 (IEC = 1.7) Co- and Terpolymers Using 0.2 mg/cm² of Platinum

The performance of BPSH45 and 6F30BPSH45 membrane electrode assemblies at 120 °C and 50% relative humidity at 20 psig is shown in Figure 8.8. These sets of experiments were used to understand fuel cell conditions that have been outlined by The Department of Energy for high temperature, low humidity automotive applications. At this temperature and low humidity, water swelling is not as much of a factor as membrane-electrode adhesion because the MEAs are already partially dehumidified therefore allowing better measurements of true membrane-electrode compatibility. The performance in the electrode active area of the curves indicated similar characteristics, however, a slight increase in current density was observed for 6F30BPSH45 (330 mA/cm²) relative to BPSH45 (305 mA/cm²) in the ohmic region of the curve at 0.5 Volts.

The increase in performance of 25 mA/cm² for the partially fluorinated material suggested that the slight decrease in conductivity at 80 °C in water was overcome by better electrode adhesion and chemical compatibility. The high frequency resistance (HFR) of BPSH45 was found to be 0.86 ohm*cm² while the partially fluorinated material showed only 0.81 ohm*cm². The lower resistance associated with this measurement was primarily due to the better adhesion and chemical compatibility of the Nafion electrode to the 6F30BPSH45 material. This tended to overcome the slight conductivity difference and thus produced better fuel cell performance at low relative humidities. It was hypothesized that the long-term durability of the MEA would be enhanced due to better chemical adhesion and similar water swelling characteristics relative to the Nafion electrodes; however, more experiments, including open circuit voltage at 100 °C and 25% RH, must be performed to more fully understand the MEA durability.

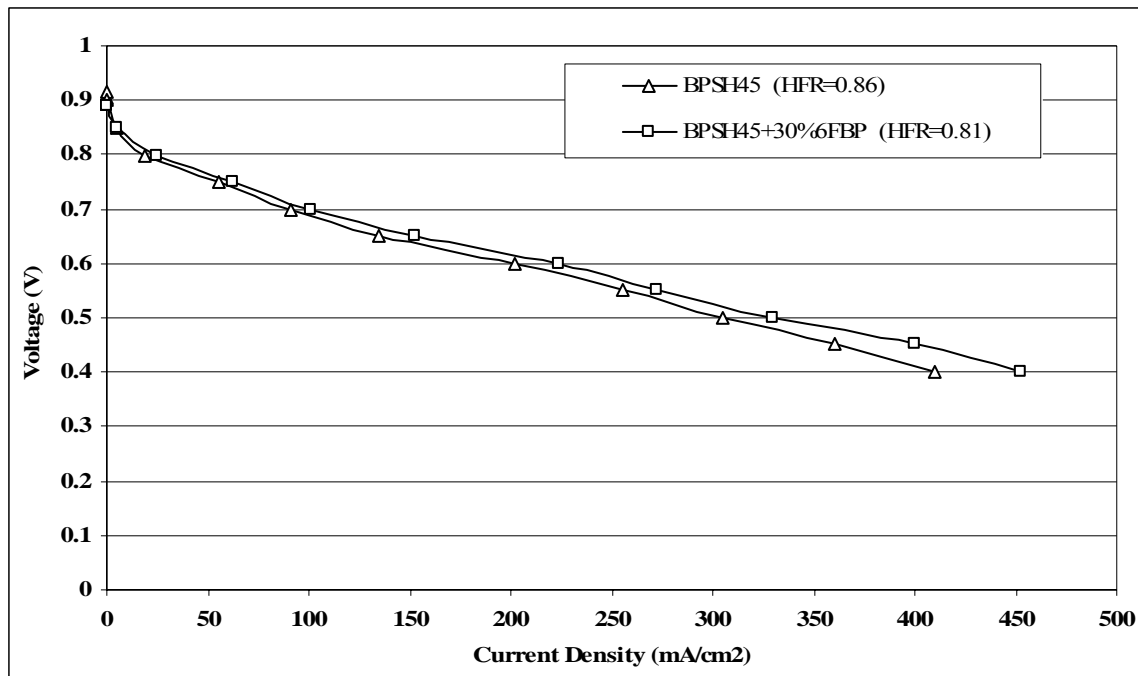


Figure 8.8 Fuel Cell Performance of BPSH45 (IEC = 1.9) and 6F30BPSH45 (IEC = 1.7) at 120 °C and 50% Relative Humidity at 20 psig Using 0.2 mg/cm² of Platinum

8.4 Conclusions

Successful synthesis of partially fluorinated poly(arylene ether sulfone) co- and terpolymers was performed by directly copolymerizing hexafluoroisopropylidene bisphenol, 4,4'-biphenol, 4, 4' - difluorodiphenylsulfone and 3,3'-disulfonate-4,4'-difluorodiphenylsulfone using nucleophilic aromatic polycondensation techniques. The intrinsic viscosity and gel permeation chromatography molecular weight values indicated successful polymerization conditions as well as good film forming characteristics. Fluorinated monomer incorporation was monitored by FTIR and ¹H NMR and indicated quantitative polymerizations of 6FBP monomer architecture into the backbone while the BP structure was observed to decrease as it was replaced with 6FBP. Surface analysis using XPS indicated that self assembly occurred during membrane casting providing enhanced fluorine concentration on the surface of the membrane relative to the bulk calculations. This phenomenon accounted for better chemical compatibility to the Nafion containing electrodes thereby decreasing the high frequency resistance in the fuel cell experiments. Water uptake was found to decrease for increasing amounts of 6FBP monomer polymerized into the backbone architecture. It was suggested that the molecular weights and IEC calculations were relatively similar thereby indicating that the fluorination amount directly accounted for the decrease in water sorption. As more hydrophobic monomer was incorporated into the backbone architecture, the water sorption was decreased due to the water repelling characteristics of fluorinated materials. Proton conductivity was found to decrease with decreasing IEC, however, as the

temperature was increased from room temperature to 80 °C, the conductivity increased. Hydrogen/air fuel cell performance at 80 °C showed enhanced performance in the ohmic region of the curves for BPSH45 that had a higher water uptake and conductivity values as compared to the 6F30BPSH45 material. However, at 120 °C and 50% relative humidity, the fuel cell performance in the ohmic region of the curve was found to be slightly better for the 6F30BPSH45 MEA. Furthermore, the high frequency resistance was found to be lower for the partially fluorinated material indicating better electrode-membrane adhesion and compatibility. This suggested that the overall fuel cell performance was more of a function of the membrane electrode assembly characteristics rather than the membrane characteristics alone.

Acknowledgments

The authors would like to thank the Department of Energy and United Technologies Corporation for funding under contracts: DE-FC36-01G011086 and sub-56844-FMIJOBDOE-99241. Further appreciation is extended to OMNOVA Solutions Signature University Award for their generous fellowship.

CHAPTER 9

Overall Dissertation Conclusions

Successful synthesis of poly(arylene thioether sulfone) copolymers was performed by directly copolymerizing either disulfonated chloro- or fluoro- activated dihalide monomers using nucleophilic aromatic polycondensation techniques. Successful synthesis of SDFDPS was achieved using electrophilic aromatic substitution with fuming sulfuric acid. The rates of reactions were faster with the fluorinated monomer and thus it was easier to prepare high molecular weight copolymers. Morphological studies using AFM phase imaging indicated a phase inversion from hydrophobic to hydrophilic continuity in the range of 35-40 mole percent disulfonation for the PATS system. Coupling these findings with water uptake further characterized the percolation threshold to a dramatic increase of water sorption from 35 to 40 mole percent disulfonation. Enhanced proton conductivity was obtained with increasing mole percent of disulfonation reaching levels of 0.16 S/cm for PATS 50.

Synthetically controlling the molecular weight of disulfonated PATS copolymers using differences in the reactivity of the monomers allowed a systematically detailed study of the effect of molecular weight on PATS fuel cell membranes in fuel cell environments. Many properties of proton exchange membranes have been determined to be directly related to molecular weight. The physical properties that were analyzed include water uptake, conductivity, methanol permeation, relative selectivity to Nafion[®] and hydrated storage modulus. Assessment of proton conductivity indicated that the molecular weight range that was studied had very little effect. However, the water uptake and lambda values were determined to change drastically with changes in molecular weight. For the low MW series of PATS copolymers, the water uptake and the lambda values (number of water molecules per sulfonic acid group) were much higher than the high MW series that showed similar conductivity values. The low MW series indicated enhanced methanol permeability, which would lead to low fuel efficiency and a reverse flux of proton transport. The low MW samples were concluded to have fewer chain

entanglements thereby allowing higher amounts of water and methanol to be adsorbed and transported into and through the membrane.

Specific characteristics and interactions of the PTA-PATS composite membranes was thoroughly probed using FTIR, TGA, TEM, water uptake, conductivity and fuel cell analyses. When solution mixed with PTA, composite membranes were found to be tough and transparent indicating good dispersion of the PTA molecules. The specific interactions were first observed using FTIR experiments. The data indicated strong interaction and complex formation occurring at the sulfonate on the copolymer backbone and the bridging oxygen atoms on the PTA molecules. It was concluded that the water retention characteristics of the composite films were enhanced due to the specific interactions with the polymer backbone and the secondary hydrated structure of the PTA molecule. The composite membranes showed lower water uptake relative to the pure copolymer membranes suggesting better water management and smaller dimensional swelling. It was concluded that the specific interactions of the PTA particles with the sulfonate groups on the copolymer backbone removed the water sorption sites from the overall mechanism thus not absorbing excess amounts of water. The water extraction of the M1 composite membranes indicated moderate loss of the PTA material. The enhancement of conductivity at elevated temperatures was presumably due to the greater water retention and increase in acidity of the composite membranes. Hydrogen-air fuel cell performance at both 80 °C and 120 °C was performed on a pure PATS 30 MEA and a PATS 30 composite MEA containing 30 weight percent PTA. The voltage-current curve at 80 °C indicated possible pinhole formation during equilibration that was due to the extraction of PTA particles. It was concluded that the data reaffirmed the hypothesis that PTA particles were abstracted creating voids and increasing the interfacial resistance between the membrane and electrodes.

Electromechanical transducer research for actuator and sensor applications indicated that increased capacitance enhanced the blocked force and free strain output performances. BPSH and PATS based transducers showed enhanced performance using both impregnation-reduction and hot pressed direct assembly electrodes relative to the state of the art Nafion based MEAs. The novel electrode plating method increased the capacitance by an order of magnitude thus enhancing the strain and force relative to the

impregnation-reduction electrode plating technique. The metal used in the electrodes had a major effect on performance and ruthenium dioxide was found to perform the best when compared to platinum based electrodes. The novel direct assembly electrode technique was found to be much more compliant by allowing more controllable morphologies and variations in MEA parameters.

Successful synthesis of poly(arylene ether phenyl phosphine oxide sulfone) terpolymers was followed by NMR and FTIR techniques. Highly polar phosphine oxide moieties were incorporated to allow for enhanced interactions between the polymer backbone and PTA molecules to aid in retention of the inorganic additive. Specific characteristics and interactions of the PPO effects on the sulfonic acid moieties and PTA molecules were thoroughly probed using FTIR, ^{31}P NMR, water uptake, proton conductivity and fuel cell analyses. When solution mixed with PTA, composite membranes were found to be tough and transparent indicating great dispersion of the PTA molecules. The FTIR data indicated strong interaction and complex formation occurred at the sulfonate-PTA molecule interface. Interactions between the PPO groups and PTA particles were observed using ^{31}P NMR that showed a band shift assigned to the phosphorous atom incorporated into the terpolymer backbone. This was indicative of hydrogen bonding and complex formation through polar interactions of the PPO and PTA molecules. The M1 composite membranes showed only fractional amounts of water sorption when compared to the pure copolymers. It was concluded that the specific interactions of the PTA particles with the sulfonate groups and PPO moieties on the terpolymer backbone removed the water sorption sites from the overall mechanism. At higher levels of PPO (20-50%), the affinity for the PTA molecules was high enough so as to decrease the extraction amounts thereby enhancing PTA retention. The 120 °C conductivity was enhanced by the composite membranes reacidified using M1 and having PPO contents around 20%. This enhancement of conductivity at elevated temperatures was presumably due to the greater water retention due to the PTA particle retention and low amounts of sulfonate complex formation. Hydrogen-air fuel cell performance at both 80 °C and 120 °C was performed on neat MEAs and on composite MEAs containing 30 weight percent PTA. It was found that the composite terpolymer containing 20%PPO provided the lowest extraction with the highest possible conductivity

at 120 °C. The fuel cell performance further indicated these findings by showing the best overall performance at 120 °C and 50%RH. It is concluded that highly polar phosphine oxide containing disulfonated copolymers increased the affinity for the PTA molecules, which increased particle retention in water environments. A series of copolymers containing increasing amounts of phosphine oxide groups were used to determine the optimal amount of chain polarity so as to retain as much PTA as possible yet still allowing free acid sites for proton transport mechanisms.

Successful synthesis of partially fluorinated poly(arylene ether sulfone) co- and terpolymers was performed by directly copolymerizing hexafluoroisopropylidene bisphenol (6FBP) into the BPSH45 backbone. The 6FBP monomer was introduced to decrease the water swelling and increase the bonding characteristics of the membrane with Nafion electrodes. Fluorinated monomer incorporation was monitored by FTIR and ¹H NMR and indicated quantitative polymerizations of 6FBP monomer architecture into the backbone while the BP structure was observed to decrease as it was replaced with 6FBP. Surface analysis using XPS indicated that self assembly occurred during membrane casting providing enhanced fluorine concentration on the surface of the membrane relative to the bulk calculations. Water uptake was found to decrease for increasing amounts of 6FBP monomer polymerized into the backbone architecture suggesting the hydrophobic fluorination amount directly accounted for the decrease in water sorption. As more hydrophobic monomer was incorporated into the backbone architecture, the water sorption was decreased due to the water repelling characteristics of fluorinated materials. Hydrogen/air fuel cell performance at 120 °C and 50% relative humidity was found to be slightly better for the 6F30BPSH45 MEA. Furthermore, the high frequency resistance was found to be lower for the partially fluorinated material indicating better electrode-membrane adhesion and compatibility. This suggested that the overall fuel cell performance was more of a function of the membrane electrode assembly characteristics rather than the membrane characteristics alone.

Vitae

Kenton Broyhill Wiles

PROFILE

Ph.D. dissertation includes synthesis, characterization and engineering of various poly(arylene sulfone) copolymers as candidates for proton exchange membrane fuel cells and actuator/sensor applications. Masters thesis concentrated on melt processable carbon fiber precursors utilizing acrylonitrile-methyl acrylate copolymers synthesized via free radical copolymerizations.

EDUCATION

VIRGINIA POLYTECHNIC INSTITUTE & STATE UNIVERSITY

Doctor of Philosophy Candidate in Macromolecular Science and Engineering, Blacksburg, Virginia May, 2005

Major: Macromolecular Synthetic Chemistry and Engineering; GPA 3.6

Dissertation Title: Disulfonated Poly(arylene thioether sulfone) Copolymers, Poly(arylene ether sulfone) Copolymers and Poly(arylene ether phosphine oxide sulfone) Terpolymers as Candidates for Proton Exchange Membranes for Fuel Cell and Ionic Polymer Transducer Applications.

Research Advisor: James E. McGrath

Masters of Science in Chemistry, Blacksburg, Virginia August 2002

Major: Physical Organic Polymer Chemistry

Thesis Title: Determination of Reactivity Ratios for Acrylonitrile/Methyl Acrylate Free Radical Copolymerization via Nonlinear Methodologies Using Real Time FTIR Spectroscopy.

Research Advisor: James E. McGrath

Selected Coursework: Synthetic Macromolecular Chemistry, Polymer Morphology of the Rubber and Crystalline State, Polymer Processing, Polymeric Degradation, Rheology of Polymer Materials, Macromolecular Fundamentals with Laboratories, Technical Presentations and ACS Technical Writing.

INDIANA UNIVERSITY

December 1998

Bachelor of Arts, College of Arts and Sciences, Bloomington, Indiana

Major: Chemistry. Major GPA: 3.2

RESEARCH AND TEACHING EXPERIENCE

VIRGINIA TECH, Blacksburg, VA

August 1999 - Present

Graduate Research Assistant

- Systematically studied proton exchange membrane and sulfonated monomer synthesis for fuel cell systems.
- Applied the principles and tools of polymer chemistry and engineering to the synthesis of novel polymeric transducers for actuator, sensor and supercapacitor applications.
- Fostered interdisciplinary research encompassing chemistry, chemical engineering and mechanical engineering.
- Interfaced with industrial companies and government laboratories interested in joint research and commercialization efforts.

- Developed characterization methods to screen novel fuel cell membrane candidates.
- Coordinated fuel cell test stand operation and construction with hydrogen and methanol fuels.
- Characterized polymers by GPC, FTIR, NMR, Fiber Spinning, Adhesion Lap Shear, TGA, DSC, DMA, SEM, TEM, AFM, Methanol Permeability, Titration, Intrinsic Viscosity and AC Impedance.
- Applied research emphasizing melt processable carbon fiber precursors and kinetic studies on free radical solution polymerizations using insitu FTIR and ¹H NMR techniques.
- Conducted investigations with various synthetic strategies including free radical, emulsion, solution, suspension, step growth, condensation and catalyst coupling polymerizations.

VIRGINIA TECH, Blacksburg, VA

August 1999 – Present

Graduate Teaching Assistant

- Teaching Assistant for Organic Laboratories from 1999-2000.
- Organic Chemistry Recitation Instructor, Fall Semester 2001.
- Laboratory Instructor for ACS Principles of Polymer Chemistry Short Courses, 1999-Present.
- Undergraduate and graduate student mentor for membrane synthesis and electrode engineering.
- Summer Undergraduate Research Program (SURP) mentor.

UNITED TECHNOLOGY CORPORATION FUEL CELLS, South Windsor, CT

March 2005

Visiting Scientist

- Systematically conducted various electrochemistry characterization techniques, which included accelerated performance tests, durability cycling, cyclic voltometry and hydrogen pump manipulations, on novel fuel cell membranes and membrane electrode assemblies.
- Enabled a more specific characterization of both membrane and membrane-electrode performances that facilitated a better understanding of the relationship between chemical structure and physical functions of fuel cell systems.
- Fundamentally characterized various electrode techniques focused on proper membrane-electrode adhesion.

SANDIA NATIONAL LABS, Albuquerque, NM

June 2004

Visiting Scientist

- Systematically conducted fuel cell testing of novel proton exchange membranes and membrane electrode assemblies.
- Devised and standardized various characterization methodologies for screening novel membrane candidates in high temperature hydrogen/air fuel cells.
- Used the principles and tools of electrochemistry in order to evaluate the effects of reduced ohmic resistances on fuel cell performance, which enabled modification of electrode structure development techniques to optimize fuel cell characteristics.

REILLY INDUSTRIES INC., Indianapolis, IN
1999

May - August

Bench Chemist in Research and Development Laboratory

- Systematically studied dye inhibiting copolymers by free radical gaseous polymerization techniques and led characterization efforts using NMR, FTIR, GC and titration analyses.
- Outlined high-temperature and high-pressure pilot scale procedures for synthesis of dye inhibiting copolymers.

Peer Reviewed Publications and Future Manuscripts

K.B. Wiles, V.A. Bhanu, A.J. Pasquale, T.E. Long and J.E. McGrath, 'Monomer Reactivity Ratios for Acrylonitrile-Methyl Acrylate Free-Radical Copolymerizations,' *J. Poly. Sci.: Part A: Polymer Chemistry*, 42(12), 2994-3001, 2004.

K.B. Wiles, F. Wang and J.E. McGrath, 'Directly Copolymerized Poly(arylene sulfide sulfone) Disulfonated Copolymers for PEM-Based Fuel Cell Systems I: Synthesis and Characterization,' *J. Poly. Sci.: Part A: Polymer Chemistry*, Accepted, 2005.

K.B. Wiles, M. A. Hickner and J.E. McGrath, 'Directly Copolymerized Poly(arylene sulfide sulfone) Disulfonated Copolymers for PEM-Based Fuel Cell Systems II: Effect of Molecular Weight on Transport and Mechanical Properties,' *J. Poly. Sci.: Part A: Polymer Chemistry*, In Press, 2005.

K.B. Wiles and J.E. McGrath, 'Directly Copolymerized Poly(arylene sulfide sulfone) Disulfonated Copolymers for PEM-Based Fuel Cell Systems III: Fabrication and Characterization of Heteropolyacid Composite Membranes for Higher Temperature Fuel Cell Applications,' *J. Poly. Sci.: Part A: Polymer Chemistry*, In Press, 2005.

K.B. Wiles, C. M. de Diego, J. de Abajo and J.E. McGrath, 'Partially Fluorinated Disulfonated Poly(arylene ether sulfone) Copolymers for PEM Fuel Cell Systems,' *Journal of Membrane Science*, In Press, 2005.

K.B. Wiles, C. M. de Diego, J. de Abajo and J.E. McGrath, 'Synthesis and Characterization of Phosphotungstic Acid Composite Membranes Using Directly Copolymerized Disulfonated Poly(arylene ether phenyl phosphine oxide sulfone) Terpolymers,' *Macromolecules*, In Press, 2005.

K. B. Wiles, B.J. Akle, D.J. Leo and J.E. McGrath, 'Directly Copolymerized Poly(arylene sulfide sulfone) and Poly(arylene ether sulfone) Disulfonated Copolymers for Use In Ionic Polymer Transducers,' *Journal of the Electrochemical Society*, In Press, 2005.

V.A. Bhanu, **K.B. Wiles**, P. Rangarajan, T.E. Glass, D.G. Baird, G.L. Wilkes and J.E. McGrath, 'Melt Processable Carbon Fiber Precursors Based on Acrylonitrile Copolymers' *Polymer*, 2002, 43, 4841.

B.J. Akle; **K. B. Wiles**, D.J. Leo and J.E. McGrath, 'Effects of Electrode Morphology on the Performance of BPSH and PATS Ionic Transducers,' *Proceedings of the International Society for Optical Engineering (SPIE)*, Paper 385-73, San Diego, CA, 2004.

K.B. Wiles, M.S. Thesis, Chemistry, Virginia Polytechnic Institute and State University, Blacksburg, VA, 2002, <http://scholar.lib.vt.edu/theses/available/etd-09022002-112751/>.

First Author Preprint Publications and Presentations

K.B. Wiles, B.J. Akle, D.J. Leo and J. E. McGrath, 'Performance Characterization on Various Electrode Morphologies of Ionic Polymer Transducers,' *Proceedings of Electrochemical Society*, Presentation at the 206th Meeting of The Electrochemical Society, Honolulu, HI, 2004.

K.B. Wiles, J.E. McGrath, 'Ionomer Membrane-Ionic Liquid Composites for High Temperature Proton Exchange in Fuel Cell Applications,' *Proceedings of Electrochemical Society*, Presentation at the 206th Meeting of The Electrochemical Society, Honolulu, HI, 2004.

K. B. Wiles, C. M. de Diego and J. E. McGrath, 'Disulfonated Poly(arylene ether phenyl phosphine oxide sulfone) Terpolymers for PEM Fuel Cell Systems,' *Preprints of Symposia - American Chemical Society, Division of Fuel Chemistry (2004)*, 49(2), 538-540, presented at the National ACS Conference in Philadelphia, PA.

K.B. Wiles, C. M. de Diego and J.E. McGrath, 'Poly(arylene sulfide sulfone) Copolymer Composites for Proton Exchange Membrane Fuel Cell Systems: Extraction and Conductivity,' *Polymer Preprints*, 2004, 45(1), 724, presented at the National ACS Conference in Anaheim, CA.

K.B. Wiles, V.A. Bhanu, F. Wang, M. A. Hickner and J.E. McGrath, 'Poly(arylene thioether sulfone) Copolymers for PEM Based Fuel Cell Systems,' *Polymer Preprints*, 2003, 44(1), 1089, presented at the National ACS Conference in New Orleans.

K.B. Wiles, V.A. Bhanu, F. Wang, and J.E. McGrath, 'Synthesis and Characterization of Disulfonated Poly(arylene sulfide sulfone) Copolymers as Candidates for Proton Exchange Membranes,' Polymer Preprints, 2002, 43(2), 993, presented at the National ACS Conference in Boston.

K.B. Wiles, V.A. Bhanu, T.E. Long and J.E. McGrath, 'Determination of Reactivity Ratios for Acrylonitrile/Methyl Acrylate Free-Radical Copolymerization Via Nonlinear Methodologies Using Real Time FTIR,' Polymer Preprints, 2001, 42(2), 608, presented at the National ACS Conference in Chicago.

AWARDS AND FELLOWSHIPS

- Macromolecular Science and Engineering Program Fellowship for Outstanding Graduate Research, 2004.
- Chevron-Phillips Chemical Company and Macromolecular Science and Engineering Travel Grant Award, 2004.
- Graduate Research Development Project Grant, Fall 2003.
- OMNOVA Solutions Signature University Award Fellowship for Outstanding Research, 2002.

PROFESSIONAL ACTIVITIES AND AFFILIATIONS

- Member of American Chemical Society since 1998.
- Member of ACS Polymer Division (POLY) since 2001.
- Member of ACS Polymeric Materials Science and Engineering Division (PMSE) since 2001.
- Member of Electrochemical Society since 2003.
- Professional presentation at Plug Power Inc. Seminar Series, December 2004.
- Professional consultant for Battelle focusing on ionic-polymer synthesis and fuel cell engineering, 2002-Present.

REFERENCES

Dr. James E. McGrath

University Distinguished Professor, Chemistry Department
Virginia Tech, Blacksburg, VA
540-231-5976, jmcgrath@vt.edu

Dr. Garth L. Wilkes

University Distinguished Professor, Chemical Engineering
Virginia Tech, Blacksburg, VA
540-231-5498, gwilkes@vt.edu

Dr. Timothy E. Long

University Professor, Chemistry Department
Virginia Tech, Blacksburg, VA
540-231-2480, telong@vt.edu

Dr. Judy S. Riffle

University Professor, Chemistry Department
Virginia Tech, Blacksburg, VA
540-231-8214, jriffle@vt.edu

Dr. Donald G. Baird

Harry C. Wyatt Professor of Chemical Engineering
Virginia Tech, Blacksburg, VA
540-231-5998, dbaird@vt.edu